Properties and Performance of Polymer Blends

10

S. F. Xavier

Contents

The Sect. 10.4, "Miscibility and Solubility" is authored by R. Arunima[1], V. P. Poornima[2], Sabu Thomas[1,2]
[1]Centre for Nanoscience and Nanotechnology
[2]School of Chemical Sciences, Mahatma Gandhi University, Priyadarshini Hills, Kottayam, Kerala-686560, India

S.F. Xavier
Parul Innovation Center, Parul Institute of Technology, Vadodara, Gujarat, India

Formerly at Research Center, Indian Petrochemicals Corporation Ltd., Vadodara, Gujarat, India
e-mail: dr.sfxavier@gmail.com; francis1951@yahoo.com

L.A. Utracki, C.A. Wilkie (eds.), *Polymer Blends Handbook*,
DOI 10.1007/978-94-007-6064-6_12,

Abstract

This chapter presents an overview of properties and performance of polymer blends. It is structured into nine sections dealing with aspects required for assessing the performance of a polymer blend. These are mechanical properties comprising of both low-speed and high-speed popularly studied properties; chemical and solvent effects; thermal and thermodynamic properties; flammability; electrical, optical, and sound transmission properties; and some special test methods which assumed prominence recently because of their utility.

Each section opens up with standard test methods such as ASTM, BS, DIN, and ISO for each property evaluation and is summarized. Since presentation of all test methods for each property is beyond the scope of this chapter, one popular test method is described in detail while others are discussed with reference to it. The factors controlling each property are also examined. Each section concludes with an outline of the state of the art pertinent to the aspect in focus. Definitions of all terms from each section are grouped together in Table 10.36.

Toughening plays an important role in designing polymer blends. Due emphasis has been given to this aspect by presenting the different methods of determining blend toughness, specially using ductile fracture mechanics; the mechanisms of toughening; and also the factors influencing toughness. Flammability aspect assumed a great deal of interest ever since the US Federal Trade Commission's (FTC) action in 1972. Commercial exploitation of a polymer blend is regulated, since then, by its flammability characteristics. A brief review on factors affecting flammability is presented, and a list of fire-retardant chemicals is provided in Table 10.37.

The recent advances in optical properties, sound transmission properties, and certain "special testing methods" are presented at the closing of the chapter. These "special test methods" are not yet matured into international test methods but, nevertheless, are popularly used for meeting the requirements of certain applications. Hence, awareness of these methods is considered to be essential. The chapter concludes with perspectives for the future developments.

10.1 Introduction

Modern technology thrusts challenging demands on the performance capabilities of materials, including polymers and their blends. A new approach to the science and technology of polymer blends has emerged recently, i.e., polymer blends by design rather than by availability. These polymeric materials must perform under strenuous mechanical, chemical, thermal, and electrical conditions imposed by the requirements of a specific application. Service in these applications usually involves several criteria to be fulfilled without a loss of economic advantage. Indeed, performance requirements of polymer blends are often at the limit of the properties that can be achieved. Moreover, these materials are expected to endure complex environmental conditions for extended time. All these factors stress the need for in-depth studies of the properties and performance of polymer blends.

There are three aspects to material properties and performance:

1. The origin – identification of the mechanisms responsible for given performance characteristics
2. Methods of determination – the most reliable way that the properties should be measured
3. The numerical values of the characteristic parameters of the material

In principle, the entire handbook is dedicated to discussion of these three aspects. For example, in ▶ Chap. 2, "Thermodynamics of Polymer Blends," the molecular aspects of polymer–polymer interactions, the methods of

characterization, as well as the numerical values of the thermodynamic parameters are given. Similarly, in ▶ Chap. 3, "Crystallization, Morphological Structure, and Melting of Polymer Blends," the three aspects vis-à-vis nucleation, melting, etc., are presented. In ▶ Chap. 7, "Rheology of Polymer alloys and Blends," flow, generation of flow-imposed lamellar morphology was discussed. This morphology has been used to control permeability through polymeric membranes.

Another important aspect of the material performance characteristics that is growing in significance is the balance of properties – for many applications it is not so important what is the value of a single parameter, but how well the material combines a number of characteristic properties. Take, for example, the use of polymer alloys for automobile fenders. Here the general requirements (viz., weight reduction, part consolidation, cost, design flexibility, increased impact, crashworthiness) translate into requirements for stiffness, strength, impact resistance, low coefficient of linear thermal expansion, weight reduction, chemical, corrosion and heat resistance, finish, oven paintability, and cost. These aspects are well presented in ▶ Chap. 15, "Applications of Polymer Blends."

The third aspect of the properties, the numerical values of measured parameters, represents enormous challenge to authors of a chapter such as this ▶ Chap. 12, "Broadband Dielectric Spectroscopy on Polymer Blends". The polymer blend industry produces well over 500 generic name blends, each in dozens of grades (Utracki 1994, 1998). Physically, it is impossible and practically useless to attempt reproducing the data sheets of these thousands of blends. Furthermore, the industry is dynamic, continuously adding and/or removing grades from the market. The modern source of the numerical information must also be active, changing along with the variability of materials, viz., the Internet. Most of the major resin producers' offer updated data sheets on the Internet, for example, www.allied.com, www.amoco.com, www.basf.com, www.dow.com, www.dupont.com, www.eastman.com, www.ge.com, www.hoechst.com, www.solutia.com, etc.

This chapter presents an overview of properties and performance of polymer blends, focusing on these aspects that are outside the main domain of the other chapters in this handbook. Such properties as mechanical, chemical, and solvent effects and thermal, flame retardancy, electrical, and optical properties are discussed. Further, the developments in sound transmission, certain special test methods in aroma barrier, permeability test for liquids, and environment stress cracking are included in the second edition of this handbook. In addition, the data is updated and upgraded. And, finally, the relevant and useful websites for additional information are also provided towards the end of this chapter.

The response of a polymer blend to tensile, compressive, and flexural stresses is examined in the initial section. Its rigidity, fatigue, and failure characteristics are also studied. The toughened polymers have enhanced the status of polymer blends, thus the toughening mechanisms have received considerable attention from researchers. The fracture mechanics approach of testing and the fascinating toughening mechanisms prevailing in these wonderful materials are also examined.

Insufficient chemical resistance of a blend at times leads to its rejection for use in an aggressive chemical environment, although it possesses an excellent combination

of mechanical properties. Thus, chemical and solvent effects on polymer blends are important factors that frequently determine blends' applicability. Attention has been given to chemical resistance of blends starting from the fundamental concept of the solubility parameters. Apart from the chemical and environmental restrictions, thermal resistance of a polymer blend is often a major criterion for its applicability. Thus, the thermal conductivity, heat capacity, and heat deflection temperature of polymeric materials are discussed in separate sections.

In this second edition of handbook, discussions regarding low-temperature brittle point, Vicat softening point, oxidative induction time, melt and crystallization parameters using DSC, and thermal degradation using TGA are added in order to bring around completion of comprehension on thermal properties of polymers and blends.

Flame resistance has become a legal requirement for commercial utilization of polymers and their blends in many applications. Innumerable test methods for flammability have been developed in different countries, and several books and handbooks are exclusively dealing with this subject. Discussion of the test methods that are *en vogue* in various countries is beyond the scope of this chapter; thus only the most popular test methods are discussed. The fire-retardant chemicals and their suppliers are tabulated in Table 10.37.

The use of polymer blends in electrical as well as electronic applications has been increasing rapidly. The electrical insulation properties of these materials cannot be ignored. Moreover, conducting polymers are likely to make an industrial breakthrough. These types of blends are also briefly discussed.

In addition, oxidative induction time, an exclusive test method popularly engaged in checking the suitability of an insulation material for cables, is added in the second edition.

Optical clarity has received considerable attention from the research community, as well as industry, especially, since transparent ABS was introduced to the market. Although success in this area has been limited, nevertheless this property is pertinent when considering blend suitability to a particular application. Few significant innovations have come up in photoluminescence and thermoluminescence, but the subject is, however, not mature enough to make a comprehensive story of the subject.

Some special test methods which have illuminated the applications of polymer blends are grouped together towards the end, viz., aroma barrier test, permeation test for liquids, and environmental stress cracking, which are special in nature but not really obtained the status of ASTM or BS methods. Nevertheless, they are used in industry as they meet the special application requirements of these wonderful materials. The chapter concludes with a discussion of these aspects.

10.2 Low-Speed Mechanical Properties

10.2.1 Tensile Strength, Tensile Modulus, and Elongation

The tensile stress–strain test is most widely used. Owing to the viscoelastic nature of polymers, the test is only a rough guide to how a polymer will behave in

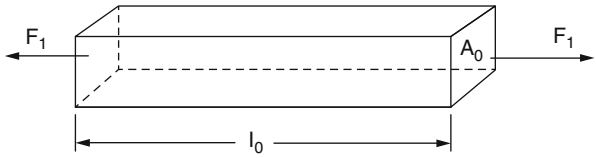

Fig. 10.1 Material in tension

a finished product. Often, results of a single test conducted at one temperature and speed of testing are published. To get a clear understanding of a polymer, it is required to have the tests at several temperatures, rates of testing, and other conditions (Dukes 1966).

There is no universally accepted set of definitions with regard to the tensile tests. The terms listed in Appendix 2 have been taken from the widely accepted norms (ISO/DIS 527; **BS 2782 Methods 320A to F; ASTM D638-95).

The most frequently applied stress–strain measurements are made in tension by stretching the specimen as shown in Fig. 10.1. A tensile stress can thus be defined as

$$\sigma_1 = \frac{F_1}{A_o} \tag{10.1}$$

where σ_1 is the tensile stress, F_1 is the tensile force, and A_o the cross-sectional area of the specimen. If the tensile stress stretches the specimen to length l_1, the tensile strain, ε_1, is defined as

$$\varepsilon_1 = \frac{(l_1 - l_o)}{l_o} = \frac{kt}{l_o} \tag{10.2}$$

where l_o is the initial length of the specimen, k is the rate of extension, and t is the time. Continuing the stressing operation to the ultimate, i.e., measuring the force until the material breaks, tensile strength, known as the ultimate tensile stress:

$$\sigma = \frac{F}{A} \tag{10.3}$$

where F is the force at failure and A is the cross section at failure.

During the process of stretching, the specimen's dimensions orthogonal to the axis of applied force decrease, and thus the area of cross section decreases. For experimental convenience, however, tensile strengths are usually based on the original cross section (A_o) which is easily measured at the beginning of the experiment:

$$\text{Elongation at break } (\%) = 100\ \frac{(l - l_o)}{l_o} \tag{10.4}$$

From the point of view of mechanical performance, four types of materials have been identified. They are best discussed in terms of the stress–strain dependence:

1. Brittle, showing proportionality between stress and strain up to the point of rupture. Here, the modulus, $E = \sigma/\varepsilon$, is constant, independent of strain, ε.

2. Semi-ductile, showing decreasing proportionality between stress and strain up to the point of rupture. Here, the modulus, $E = \sigma/\varepsilon$, decreases with strain, ε.
3. Ductile, initially showing similar relationship between stress and strain as the semi-ductile materials. However, these materials deform further, causing the stress pass through a maximum (yield). The rupture takes place at lower values than the yield stress.
4. Ductile with flow. These materials show still greater deformability than the typical ductile materials. Initially, the stress–strain dependence resembles that described for ductile resin, but before the rupture, there is a zone of deformation where the stress remains about constant. Within this zone there is "flow" of material that usually leads to molecular alignment and/or to changes to the crystalline structure (viz., deformation of polyolefins).

10.2.1.1 Methods of Measurement

Stress–strain measurements for polymer blends can be conducted in one of two modes: using a constant rate of loading or a constant rate of stretching. The first method is very often used in adhesives testing. The latter method is the most extensively employed in polymer and blend testing. In tensile testers, a sample is clamped between grips or jaws that are pulled apart at constant strain rates varying from 0.5 to 500 mm/min. The stress on the sample is monitored with the load cells ranging between 2 g and 5,000 kg or more. The elongation must avoid errors arising out of sample slippage from the grips. There are a variety of jaws that can hold different samples. A review of grip systems is presented in "Handbook of Plastics Test Methods" (Brown 1981). Jaw design and specimen shape and preparation are selected so as to minimize the introduction of extraneous stress or strain.

Tensile tests on different polymer blends employ specimens of different sizes. To conduct a tensile test, a specimen capable of being gripped at both ends is required. The basic types of dumbbell configurations and dimensions recommended by ISO are illustrated in Fig. 10.2. The American specifications differ only in number of dimensional details and are based essentially on imperial units. In case of rigid polymer blends (such as engineering blends), the specimen can be molded, machined on a lathe, or simply cut out from thin, flat sheets.

The dumbbell specimen with narrow waist (Fig. 10.2a) is generally preferred in testing rubbers and their blends with thermoplastics. The dumbbell specimen with broad waist (Fig. 10.2b) is used for polymers and blends exhibiting low-to-moderate elongation at break. Dog-bone test specimens (Fig. 10.2c) are used for polymer blends that do not allow any elongation measurement to be made. The parallel strip specimens (Fig. 10.2d) are used for reinforced thermoplastics or blends. In order to avoid the problem of sample fracturing near the grips, the end pieces of the grips are normally bonded.

10.2.1.2 Standard Test Methods for Tensile Properties

The standard test methods for tensile properties are listed in Table 10.1 and the recommended test speeds in Table 10.2.

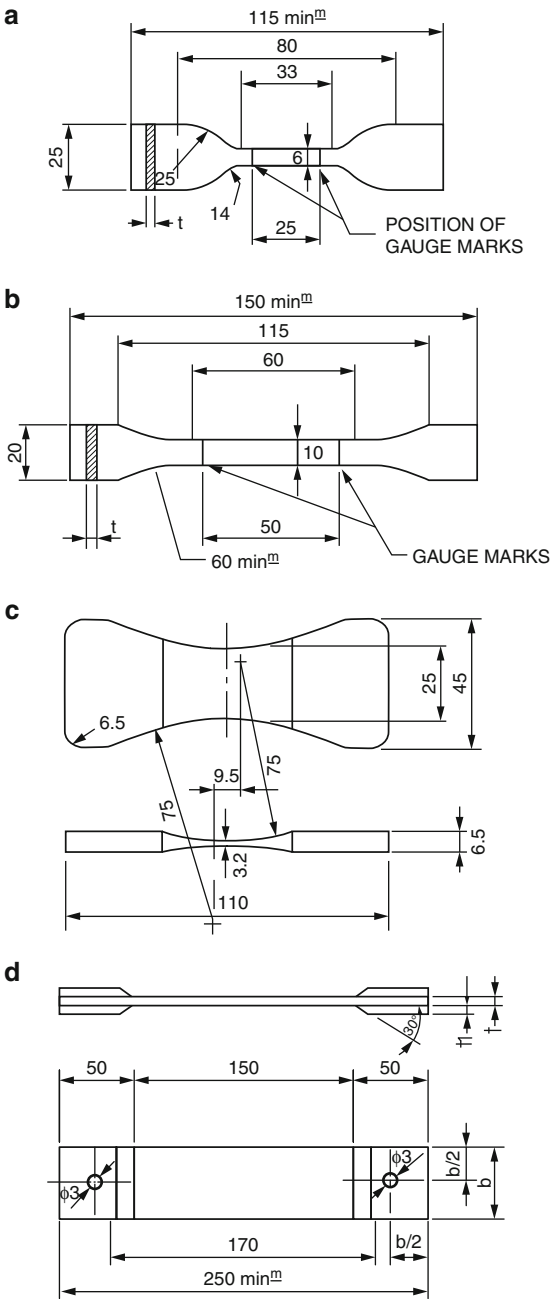

Fig. 10.2 (**a**) Tensile test specimen: Narrow-waisted dumbbell (ISO/DIS 527 Type A). (**b**) Tensile test specimen: Broad-waisted dumbbell (ISO/DIS 527 Type B). (**c**) Tensile test specimen: Dog-bone dumbbell (ISO/DIS 527 Type C). (**d**) Tensile test specimen: Parallel-sided strip (ISO/DIS 527 Type D)

Table 10.1 Standard test methods for the determination of the tensile properties of polymers

Test method	Materials	Specimen	Test speeds
ISO R527	Plastics	1 mm thick	See Table 10.2
ISO R1184		<1 mm thick	
BS 2782			
Method 320A	Flexible plastic sheets blends, filled or reinforced	Stamped from sheets	500 mm/min
Method 320B	Composites	Injection molded	1, 5, 25, 50 and 100 mm/min
Method 320C	Rigid thermoplastic, thermosets	Machined from sheets	As in Method-A

Table 10.2 Recommended test speeds according to DIS 527 (ISO/DIS 527)

Speed A	1 mm/min	±50 %
Speed Al	2 mm/min	±20 %
Speed B	5 mm/min	±20 %
Speed C	10 mm/min	±20 %
Speed D[a]	20 or 25 mm/min	±10 %
Speed E	50 mm/min	±10 %
Speed F	100 mm/min	±10 %
Speed G[a]	200 or 250 mm/min	±10 %
Speed H	500 mm/min	±10 %

[a]Both the mentioned speeds are allowed because they are popularly used throughout the world

Measurements of "Apparent" Strain

The elongation of specimen is followed by using gauge marks and measuring the distance between them preferably continuously or by making use of clip-on type of extensometer. In the case of blends exhibiting strains in excess of 50 %, optical extensometers are to be used. The merits and demerits involved in different methods of strain measurements are discussed in detail elsewhere (Brown 1981).

Measurement of Modulus

The standard test methods calculate the tensile modulus by drawing a tangent to the initial linear part of the stress–strain curve and calculating the slope of the line. In cases where no clearly defined linear portion exists, the "secant modulus" should be determined.

10.2.2 Compressive Strength

Stress–strain curves developed during tensile, flexural, and compression tests may be quite different from each other. The moduli determined in compression are generally higher than those determined in tension. Flaws and submicroscopic cracks significantly influence the tensile properties of brittle polymeric materials.

However, they do not play such an important role in compression tests as the stresses tend to close the cracks rather than open them. Thus, while tension tests are more characteristic of the defects in the material, compression tests are indicators of the material content of the specimen used. The ratio of compressive strength to tensile strength in the case of polymers is in the range 1.5–4 (Dukes 1966).

10.2.2.1 Standard Methods for Compressive Tests

The standard methods for compressive tests are listed in Table 10.3. For example, the ISO Standard 604 allows four types of test specimens: (1) the right square prism, (2) the right rectangular prism, (3) the right cylinder, and (4) the right circular crown tube. The test specifies for each of these test specimens, the load-bearing surfaces be parallel to each other within 0.1 % of the height of the test piece.

10.2.2.2 Plane-Strain Compression Test

Williams and Ford developed "plane-strain compression test" which was initially applied to metals (Williams and Ford 1964). It was based on the fact that strain is easier to measure in compression test. The same test method may be used for polymer blends to obtain total deformation curves up to high levels of strain that may be encountered in engineering applications. Williams had further explained the application of this technique to polymers (Williams 1964).

10.2.3 Flexural Strength and Flexural Modulus

Flexural tests may be carried out in tensile or compression test machines. In standard tests, three-point bending test is preferred, although it develops maximum stress localized opposite the center point (support). If the material in this region is not representative of the whole, this may lead to some errors. Four-point test offers equal stress distribution over the whole of the span between the inner two supports (points) and gives more realistic results for polymer blends (Fig. 10.3). Expressions for the calculation of flexural strength and modulus for differently shaped specimens are given in Table 10.4.

Standard test methods for flexural properties are listed in Table 10.5. They may be carried out in tensile or compression test machines. Three-point bending is often used. Four-point test offers equal stress distribution over the whole of the span between the inner two supports (points), and it is preferred for polymer blends. The curvature of the bearing rods is also important as too sharply curved rods lead to fracture of the specimen.

10.2.4 Rigidity and Rockwell Hardness

"Hardness" is not a fundamental property. Its measurement is subjected to the effects of temperature, time, and other test variables. Hardness measurement of

Table 10.3 Standard test methods for compressive tests

No.	Test method	Specimen	Materials
1.	ISO 604 (1973)	(1) The right square prism, (2) the right rectangular prism, (3) the right cylinder, and (4) the right circular crown tube	The load-bearing faces are to be parallel to each other within 0.1 % of the test piece height
2.	British standard BS 2782, Method 345A		
	Type 1	For sheets of thickness not less than 12 mm	Thermoplastics, including polymer blends and thermosets
	Type 2	For sheets of thickness less than 12 mm (for sheets of thickness >12 mm, the test piece is machined only on one face so as to reduce the thickness to 12 mm)	Thermoplastics, including polymer blends, and thermosets
	Type 3	For casting and lamination resin systems without fibrous reinforcement	
	Type 4	Test pieces are identical to ISO 604	Neat resins
	Type 5	For flat injection-molded or compression-molded thin sheets materials	Glass fiber-reinforced laminates
3.	USA standards ASTM D695-10[a]	For a right prism the preferred dimensions are 12.7 mm square by 25.4 mm height	For rod slenderness ratio should be in the range 11–15:1
	The method is the same as in BS, but specimen dimensions differ		
4.	German standards DIN 53454 (1971)	Similar to British Standards in the form as well as dimensions of test specimens	

[a]ASTM standard test methods are available on web: http://enterprise.astm.org/

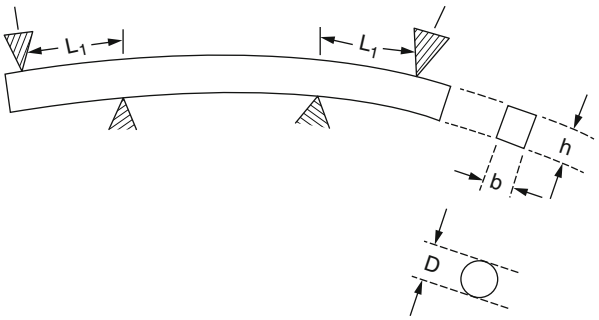

Fig. 10.3 Four point bending

Table 10.4 Expressions for calculation of flexural strength and modulus

No.	Geometry	Strength (MPa)	Modulus (MPa)	Comments
1.	**Four-point bending**			P = Load (N) at the moment of break
				P_Y = Maximum load (N) at yield or break
	ASTM D6109-97 (load span = 1/3 support span)	$S = PL/bd^2$	$E = 0.21\ L^3m/bd^3$	L = Support span (mm)
				B = Width of beam (mm)
				d = depth of beam (mm)
	ASTM D6272-98 (load span = 1/2 support span)	$S = 3PL/4bd^2$	$E = 0.17\ L^3m/bd^3$	m = slope of the secant (N/mm)
				For Unreinforced and reinforced plastics
2.	**Two-point bending**			For fiber-reinforced pultruded rods use ASTM D4476-97
	ASTM D790-99 (support span-to-depth ratio < 16:1)	$S = 3P_Y\ L/2bd^2$	$E = L^3m/4bd^3$	

plastics is similar to the traditional methods applied to metals. It usually employs a standard indenter (often a hardened steel ball), forcing it under known load into a flat surface of the plastic and then measuring the resultant degree of indentation.

Unlike other Rockwell scales, Rockwell R_α parameter correlates with the hardness as determined by ball indentation. Fett (1972) has shown that

$$H = \left[\frac{441.4}{(150\text{-}R_\alpha)}\right]^{1.23} \tag{10.5}$$

where H is the hardness by ball indentation and R_α is the Rockwell hardness parameter.

The standard test methods for determining Rockwell hardness are listed in Table 10.6, and the Rockwell scales are given in Table 10.7. For example, ISO 2039 employs a hardened steel ball, 5 mm diameter. The ball is pressed into the specimen under a specified load selected to give an indentation between 0.07 and 0.10 mm (Method A) or between 0.15 and 0.35 mm (Method B). The recommended thickness of the specimen is 4 mm and the suggested time of application of the load is 30 s before the depth reading is taken.

10.2.5 Fatigue Characteristics

Fatigue failure may occur when a specimen fractured into two parts was softened and/or its stiffness significantly reduced by thermal heating or cracking. Sometimes, for different reasons, a large number of cycles elapses from the first formation of microscopic cracks to complete fracture. In this case, the fatigue failure is

Table 10.5 Standard test methods for flexural properties

No.	Test method	Specimen	Material
1.	ISO standards	Standard test specimen dimensions: $80 \times 10 \pm 0.5 \times 4 \pm 0.2$ mm	For single-phase materials
	ISO 178	Length is 20 times the thickness and width is between l0 and 25 mm	For materials containing fillers
		Length is 20 times the thickness and width is between 20 and 50 mm	
2.	British standards BS 2782 Method 335A Method 336B	Identical to ISO 178.	
		It employs cantilever-bending mode. Standard test specimen (molded) dimensions are $70 \times 25.4 \times 1.5$ mm. A hole of diameter 2.0–2.02 mm is to be drilled centrally	
3.	USA standards ASTM[a] D790 Method I Procedure-A Procedure-B Method II Procedure A Procedure B	Three-point loading system	Procedure-A is for materials that fracture at small deflections
		Test specimen dimensions and rate of cross-head motion are to be selected based on support span-to-depth ratios (1/d = 16 to 1, 32 to 1, 40 to 1 or 60 to 1)	
		Four-point loading system. Recommended test specimen dimensions and rate of crosshead motion are given based on support span-to depth ratios	Procedure-B is for materials that undergo large deflections
4.	German standards DIN 53452 DIN 53435	Similar to three-point loading for ISO 178 For four-point loading (using Dynstat apparatus)	

[a]ASTM standard test methods are available on web: http://enterprise.astm.org/

arbitrarily defined as having occurred when the specimen can no longer support the applied load within the deflection limits of the apparatus.

Plastics, including polymer blends, are relatively high damping and low thermal conductivity materials. Thus, repeated straining of an article leads to a temperature rise within and throughout its body. Rapid stress–strain cycling can significantly heat up the article and thereby induce thermal failure – the phenomenon is frequency dependent. Where the thermal effect is to be a minimized, much lower frequency, of the order of a few Hz, should be employed.

Fatigue data are usually presented in the form of S–N curves, in which stress amplitude S is plotted versus log N_f, where N_f is the number of cycles to fracture an unnotched specimen, either in bending or in tension. A typical example of such a curve is shown in Fig. 10.4. Here, the S–N curve for rubber-toughened PMMA provides the "endurance limit," which is defined as the lowest stress amplitude at which fracture occurs. In general, most S–N curves flatten out at $N_f = 10^7$. Rubber toughening, in the case of styrene polymers, is found to reduce fatigue resistance and causes a decrease in the endurance limit (Sauer and Chen 1983, 1984). This is due to promotion of crazing and reduction of stresses by the rubber particles. The cyclic loading then degrades the crazes into cracks.

Table 10.6 Standard test methods for determining Rockwell hardness

No.	Test method	Specimen	Indentation
1.	ISO standards: ISO 2039 Method A Method B Revised procedure follows that of ASTM D785-98.	4 mm thick specimen	Between 0.07 and 0.10 mm Between 0. 15 and 0.35 mm Time of load application is 30 s
2.	British standards	8 to 1 0 mm thickness	
	BS 2782	For "Softness Number"	
	Method 365A	As ISO 2039	
	Method 365D	As ASTM D2583-95	
	Method 1001	Measures Rockwell	
	Part 3 (Method 365C)	Hardness	
3.	USA standards ASTM D785-98[a]	Uses Rockwell hardness tester, and scales (see Table 10.7)	Minor load is applied for 10 s, then major load for 15 s; the hardness reading is taken off the scale 15 s after the major load is removed
	Procedure A	6 mm thick specimen	Indentation is recorded 15 s after application of major load, but with minor load still on
	Procedure B		
4.	German standards DIN 53456	As in ISO 2039	Same as ISO 2039 except the major load must be selected from 49 N, 132 N, 358 N and 96IN, with a minor load of 9.81 N in all cases

[a]See: http://enterprise.astm.org/

Table 10.7 Rockwell scales (ASTM D785-98 (http://enterprise.astm.org/))

Rockwell hardness	Minor load (kg)	Major load (kg)	Indenter diameter (in.)	Indenter diameter (mm)
R	10	60	0.5000 ± 0.0001	12.7000 ± 0.0025
L	10	60	0.2500 ± 0.0001	6.3500 ± 0.0025
M	10	100	0.2500 ± 0.0001	6.3500 ± 0.0025
E	10	100	0.1250 ± 0.0001	3.1750 ± 0.0025
K	10	150	0.1250 ± 0.0001	3.1750 ± 0.0025

Fatigue-induced deformation mechanisms can be studied by measuring the volume changes. Another sensitive method is to monitor the hysteresis loops under tension–compression loading. This is illustrated in Fig. 10.5. All specimens initially show a small elliptical loop, indicating the viscoelastic response of the polymer (Bucknall and Stevens 1980; Sauer and Chen 1984; Bucknall and Marchetti 1983). Plots of tensile versus compressive loop area reflect the proportions of shear yielding and crazing. This method has been used to detect the onset of crazing in fatigue tests

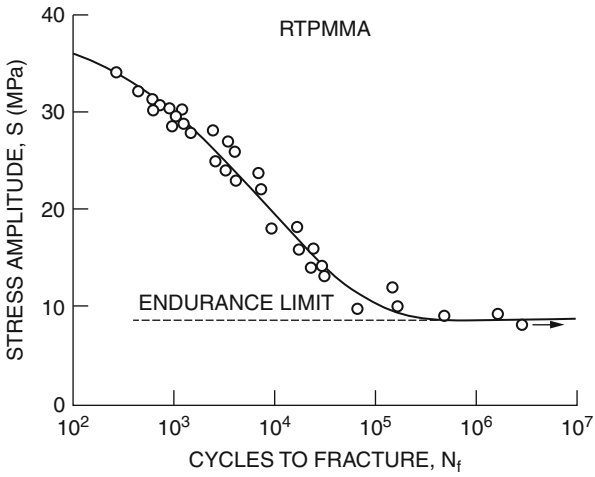

Fig. 10.4 S-N curve for rubber-toughened PMMA (Bucknall 1988)

on ABS. Following the trend in metallurgy, fracture mechanics techniques are now widely used to study fatigue in polymers.

Standard test methods for fatigue testing are listed in Table 10.8. As an example, ASTM D671 makes use of the constant amplitude of force approach (Satake 1970). Two dumbbell-type test pieces, both of triangular form, are described. They are to be selected according to the thickness and stress range over which the measurements are to be made. The apparatus described operates only at a fixed frequency of 30 ± 5 % Hz.

10.2.6 Review of Low-Speed Mechanical Properties of Blends

The low-speed stress–strain dependence for PS and HIPS is shown in Fig. 10.6. These data well illustrate the change induced by incorporation of elastomeric particles into PS matrix. As shown, upon toughening, PS brittle behavior changes into ductile with flow.

The low-speed mechanical properties of polymer blends have been frequently used to discriminate between different formulations or methods of preparation. These tests have been often described in the literature. Examples of the results can be found in the references listed in Table 10.9. Measurements of tensile stress–strain behavior of polymer blends are essential (Borders et al. 1946; Satake 1970; Holden et al. 1969; Charrier and Ranchouse 1971). The rubber-modified polymer absorbs considerably more energy; thus higher extension to break can be achieved. By contrast, an addition of rigid resin to ductile polymer enhances the modulus and the heat deflection temperature. These effects are best determined measuring the stress–strain dependence.

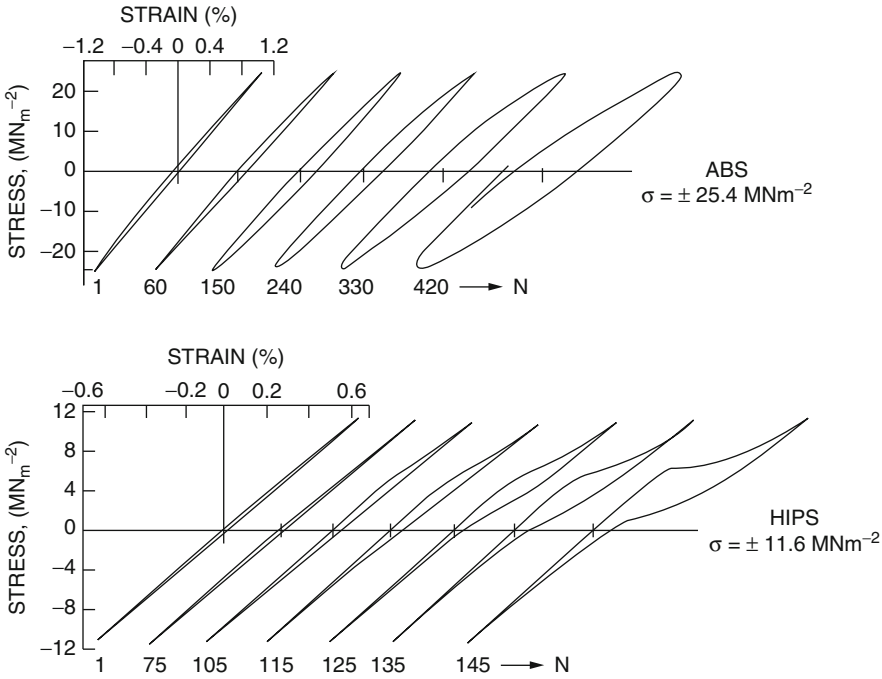

Fig. 10.5 Hysteresis loops developed during fatigue tests of ABS and HIPS (Bucknall 1988)

Table 10.8 Standard methods for fatigue testing

No.	Test method	Approach	Specimen	Frequency of testing
1.	USA standards ASTM D671-93[a]	Constant amplitude of force	Two specimens of triangular form with rectangular cross section	Fixed frequency of 30 Hz
2.	German standards DIN 53442	Constant amplitude of deformation	Dumbbell shaped (tensile dumbbell) test specimens	Variable frequency

[a]See: http://enterprise.astm.org/

10.3 High-Speed Mechanical Properties

The subject of impact strength of plastics has received considerable attention in official standards, material data sheets, and literature at large. The result of an impact test is basically no more than one point on the general curve of studying strength properties as a function of speed of testing. One advantage an impact test can offer is a ready measure of the actual energy required to break a test piece, which information can also be calculated from stress–strain diagrams in tensile or flexural tests with some effort.

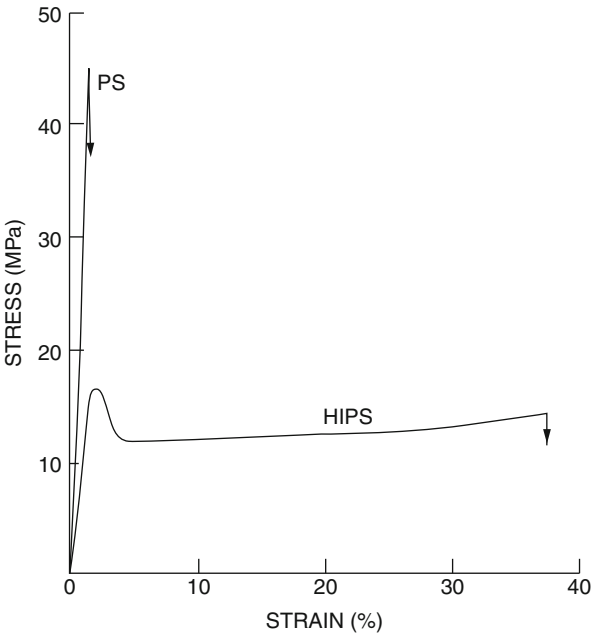

Fig. 10.6 Tensile stress–strain curves for PS and HIPS (Bucknall 1988)

All materials tend to fracture if stressed severely enough. Some materials fracture more easily than others and are thereby said to be "brittle." Brittleness is the property of a material manifested by fracture without appreciable prior plastic deformation. In ductile fracture significant plastic flow occurs before fracture. Strain at fracture is more than a few per cent, unlike brittle fracture, and may be several hundred per cent. However, a sharp distinction cannot be made between brittle and ductile fracture since even in glassy materials some deformations take place. Further, a given material will fail in a brittle manner under some conditions and a ductile manner under other conditions. Thus, brittle fracture is favored by the low temperature and fast loading and when the state of stress approaches a uniform, i.e., triaxial or dilatational, state. Materials with low T_g are more likely to suffer ductile fracture, but the mode of fracture also depends on the fracture conditions. Furthermore, any structural feature that raises T_g, such as bulky side groups or cross-linking, promotes brittle fracture. In a given material fracture may undergo brittle/ductile transition, depending upon the testing temperature. At this transition temperature, the mode of fracture changes from brittle to ductile fracture (Kinloch and Young 1983).

10.3.1 Impact Strength

In many applications a satisfactory resistance to impact loading is an important performance requirement, and, indeed, impact toughness is often the deciding

Table 10.9 Sources for low-speed mechanical property data of polymer blends, Examples:

Blend	Test	Results	References
HIPS	Tensile stress–strain	See Fig. 10.6	Bucknall 1988
HDPE/PP	Tensile properties		Robertson and Paul 1973; Deanin and Sansone 1978; Greco et al. 1980; Dumoulin 1988
HDPE/PP/EPR		EPR acts as a compatibilizer	Nolley et al. 1980; Utracki 1995
HDPE/PP + two EPR's	Tensile properties for different compositions	Stress–strain curves, strength, modulus, yield stress, etc.	D'Orazio et al. 1983
PP/Cross-linked rubber		Tensile yield strength, tensile modulus etc.	Dao 1982
PC/SAN	Tensile properties of different compositions	Effect of blend composition on mechanical properties	Keitz, et al. 1984; Kurauchi and Ohta 1984; Koo et al. 1985; Weber and Schoeps 1985; Gregory et al. 1987; Chiang and Hwung 1987; Skochdopole et al. 1987; Quintens and Groeninckx 1990
PC/HDPE, PC/LDPE and PC/PS	Tensile properties	Mechanical properties of. immiscible/miscible blends	Kunori and Geil 1980
PC/ABS	Tensile properties	Tensile strength, modulus and elongation at break	Suarez et al. 1984; Chiang and Hwung 1987
PA/PE/ionomer	Mechanical properties	Reduction in particle size of dispersed phase	Fisa 1991; Fairley 1990; Fairley and Prud'homme 1987; Chuang and Han 1984, 1985; Macknight et al. 1985; Han and Chuang 1985
Polymers/blends	Fatigue behavior	Review of fatigue behavior	Takemori 1984; Radon 1980; Hertzberg and Manson 1980; Saur and Richardson 1980; Andrews 1969
Rubber-toughened PMMA	Fatigue behavior	Fig. 10.4	Bucknall 1988
Rubber-toughened PS	Fatigue behavior	Rubber toughening reduced the fatigue resistance and endurance limit	Sauer and Chen 1983, 1984
HDPE/LCP	Mechanical properties	Increased tensile strength, modulus and HDT. Decreased elongation at break, and impact strength	Yamaoka et al. 1989

(*continued*)

Table 10.9 (continued)

Blend	Test	Results	References
PP/LCP, PVC/LCP	Tensile and impact properties	Mechanical properties varied with interphase adhesion and orientation of LCP domains	Seppala et al. 1992; Lee 1988
PA-6/LCP	Mechanical properties	Changes in mechanical explained in terms of morphology	La Mantia et al. 1989
PA-12/LCP	Mechanical properties	Mechanical properties correlated with morphology	Kiss 1987; Ramanathan et al. 1987; Blizard and Baird 1986
Amorphous PA/LCP	Mechanical properties	Tensile strength and flexural modulus increased with increasing LCP content	Siegmann et al. 1985
PC/LCP	Tensile and other mechanical properties	Tensile properties improved	Isayev and Modic 1987; Kiss 1987; Weiss et al. 1989; Blizard and Baird 1986a, b; Malik et al. 1989; Blizard et al. 1990; Zhuang et al. 1988; Shin and Chung 1989
PET/LCP	Flexural properties	Flexural modulus increased with LCP content	Zhuang et al. 1988; Amano and Nakagawa 1987; Brostow et al. 1988; Joseph et al. 1984; Sukhadia et al. 1990; Seppala et al. 1992
PET/LCP, PBT/LCP	Tensile properties	PET-LCP copolymer as compatibilizer was used	Poli et al. 1996
PES/LCP	Flexural properties	Increasing LCP content increased modulus, but decreased strength	Kiss 1987; Cogswell et al. 1981; Yazaki et al. 1994
PPS/LCP	Tensile and impact properties	Mechanical properties depended on miscibility, LCP orientation, etc	Ramanathan et al. 1988; Seppala et al. 1992; Nobile et al. 1990
PSU/LCP	Mechanical properties		Nobile et al. 1990
PEI/LCP	Mechanical properties		Blizard et al. 1990; Nobile et al. 1990; Kiss 1987
PEEK/LCP	Tensile and impact properties	Properties varied with anisotropy due to LCP content	Kiss 1987; Cogswell 1981; Mehta and Isayev 1991
PP/Olefinic Elastomer	Mechanical properties and morphology	Elastomer enhanced the toughness of blends but reduced stiffness	Lotti et al. 2000

(*continued*)

Table 10.9 (continued)

Blend	Test	Results	References
EPR/PP, peroxide cross-linked	Tensile, elongation, elastic modulus, Izod, hardness, Vicat softening point, HDT	Microstructure (DSC, SEM) found to influence mechanical properties	Tasdemir and Topsakaloglu 2007
NBR and E-MA toughened PA6 nanocomposites	Tensile, Young's modulus	Finely dispersed nonreactive polar elastomers provided best balanced mechanical properties	Kelnar et al. 2006
PA6/4 % MMT/ SEBS-g-MA	Fracture toughness, tensile properties, impact properties	SEBS-g-MA enhanced fracture toughness of PA6/4 % MMT	Tjong and Bao 2005
PP/Elastomer; PP/Calcium carbonate	Toughness	PP toughness higher with elastomer compared to calcium carbonate	Zhang et al. 2004
NanoCaCO$_3$/PPE/ SBS	Toughness, impact strength	Synergistic toughening occurred with nanoCaCO$_3$ and SBS in PPE matrix	Chen et al. 2004
PP/EOR	Tensile, impact strength	EOR with high octane content and high molecular wt provide blends of high impact strength	Premphet and Paecharoenchai 2002
PA6/VLDPE, PA6/VLDPE-g-MA, PA6/VLDPE-g-DEM	Fracture toughness, impact strength	Compatibilized blends behaved different and better way	Lazzeri et al. 1999
PA6/LDPE-g-MAH	Tensile, flexural, Izod impact	Izod impact strength increased with LDPE-g-MAH was 20 %	Sandeep 2006
PA6/PP-g-ITA, PA6/HDPE-g-ITA, PA6/PP-g-(ITA-St), PA6/HDPE-g-(ITA-St)	Tensile, impact strength	Impact strength increased up to 70 % after using PP-g-ITA and HDPE-g-ITA as compatibilizer	Liu 2007
PA6/UHMWPE using HDPE-g-MAH as compatibilizer	Mechanical properties	HDPE-g-MA improved mechanical properties of blends	Zhao 2005
PA6/LDPE, PA6/LDPE using Na-EMAA as compatibilizer	Mechanical properties	Mechanical properties of compatibilized blends were improved	Canfora 2004; Lahor 2004; Pakeyangkoon 2005
Nano-PA6/ABS using POE-g-MA	Impact strength, HDT	Impact strength increased with addition of compatibilizer (POE-g-MA0)	Lai 2006

(*continued*)

Table 10.9 (continued)

Blend	Test	Results	References
HDPE/PA6 + Electron Beam Irradiation	Mechanical properties	Mechanical properties of electron beam irradiated blends were improved	Lian 2004
PP/EPDM with Nano-SiO_2	Izod impact strength	Izod impact strength of ternary blends improved two to three times compared to binary blends	Hong et al. 2007
PTT/LCP(Vectra A950)	Mechanical properties	LCP improved tensile modulus, slightly reduced tensile strength and drastically reduced elongation compared to PTT	Pisitsak and Magaraphan 2009

factor in materials selection (Vincent 1971; Bucknall et al. 1972; Turner 1973; Bucknall 1977; Reed 1979; Kinloch and Young 1983; Savadori 1985; Brostow and Corneliussen 1986; Havriliak et al. 1996). For the past several decades, ductile grades of usually brittle polymers, such as PS, PMMA, PVC, or PA, have been used. The most widely used test for impact assessment is the notched Izod impact test. A single operator can run up to 150,000 tests in a year (Havriliak et al. 1996).

The test is also an important material or product specification for toughness – it is often one of few material constants specified as a product development objective. It appears that the earliest reference to the subject of impact testing was in 1734 by Swedenborg who wrote that iron bars were tested by throwing them against a sharp edge (Lethersich 1948). If the blow marks the bar without breaking any part of it, this was a sign of tenacity. Further, experimental and theoretical works pointed out the dependence of the resistance of metals on the test speed and notches. Two devices were introduced by Charpy (in 1901) and by Izod (in 1903) for analyzing the impact performance of materials (see Fig. 10.7). The impact resistance is evaluated in energy terms, i.e., by evaluating the difference between the potential energy before and after impact, the energy absorbed by the specimen during the impact process is obtained.

From the physical point of view, the Izod equipment is equivalent to that of Charpy. However, the main differences between the two are the clamping system, the notch, the hammer speed, and its weight. Charpy adopted the keyhole form of notch. At such an early stage in the history of impact testing, Charpy found that correlations between static and dynamic tests were obtainable provided a notched bar was used. In 1925, the Izod and Charpy tests were extended to plastic materials, and many results on plastics were published a year later (Werring 1926).

The growth of fracture mechanics has placed greater emphasis on tests that use sharply notched specimens. These results were found to provide more fundamental information. Instrumented impact testing is a recent development that provides information on force – deflection curves. In addition to these notched bar tests, extensive use of falling dart tests is also being made. However, interpretation of the

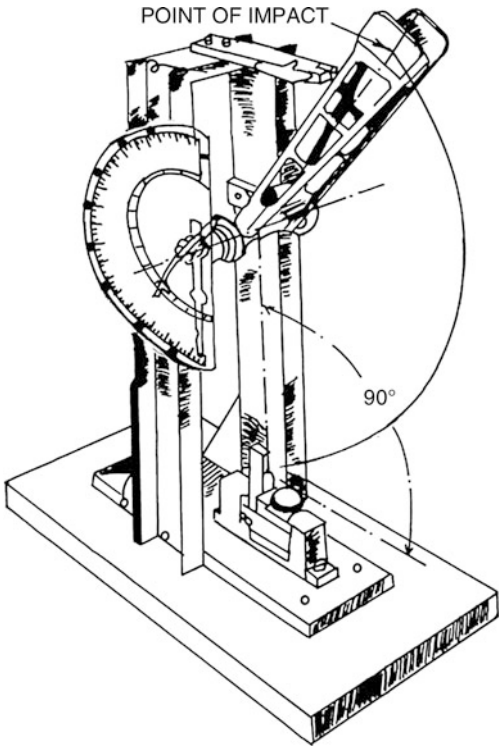

Fig. 10.7 Cantilever beam (Izod type) impact machine (ASTM D256)

data from the latter is far from straightforward. The impact strength is not a fundamental material property. The results depend on the specimen geometry, test method, and the employed parameters. Thus, it is difficult to correlate the results obtained from different test techniques and extremely difficult to correlate the results from impact tests on specimens of the material to the impact performance of the manufactured article.

Correlation of results from one test to another for a given material becomes difficult because of different stress states of the specimen and the associated strain rates in different tests. In the tensile-impact test, the stress state is uniaxial and it measures the tensile property at a high strain rate. In Izod and Charpy tests, the presence of notch gives a triaxial state of stress. The falling-weight test is always in the forefront of high-speed testing for evaluating the strain rate sensitivity of materials. In this case, the stress is biaxial. Several attempts were made to relate fracture mechanics theories to impact test results (Brown 1973; Marshall et al. 1973; Plati and Williams 1975). The topic was also reviewed (Kinloch and Young 1983; Brostow and Corneliussen 1986).

10.3.1.1 Izod Impact

One of the most often used tests for impact assessment is the notched Izod impact test. The basic principle of the test is to allow a pendulum of known mass to fall

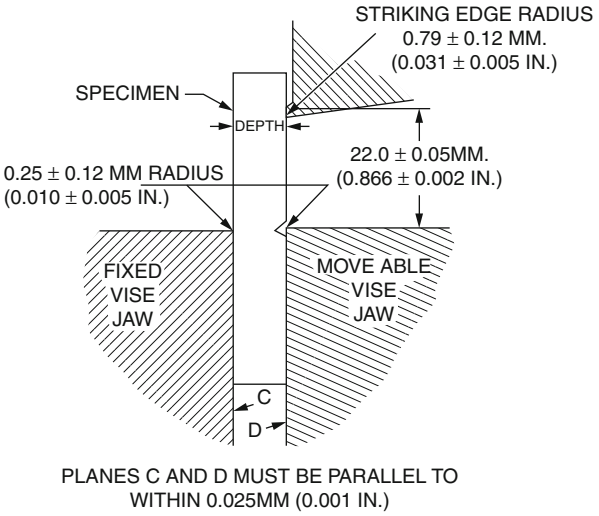

Fig. 10.8 Relationship of vise, specimen and striking edge to each other for Izod test methods A and C (ASTM D256)

from a known height and strike a standard specimen at the lowest point of its swing, and to record the height to which the pendulum continues its swing (see Fig. 10.7). If the striking edge of the pendulum coincides with the center of the percussion of the pendulum, the bearings of the pendulum are frictionless, and there is no loss of energy to windage, then the product of the mass of the pendulum and the difference between the fall distance and the height it reaches after impacting the test specimen is the impact strength of the latter.

The test may be carried out on plane rectangular bars, but most often a carefully defined notch is molded or machined into the face to be struck (Fig. 10.8). The impact tests are often regarded as a means of assessing the resistance of a material to shock where notches or "stress raisers" generally are present. The ratio of impact strength of unnotched to that of notched specimen is sometimes regarded as a measure of the notch sensitivity of a material.

Despite the popularity of the test, it is still poorly understood in terms of generating an actual "material" property. The test reveals little about molecular dynamics and is not related to molecular structure. It is often criticized by fracture mechanics experts because of uncertainties about gauge length, complex state of stress, its dependence on thickness as well as a wide range of shear rates during the experiment, and the relationship of these factors to real situations (Havriliak 1996).

The test, nevertheless, does have several important features. First, it is accepted by a large technical audience and is in common use. Second, it is a reproducible test, mostly because of the work of the ASTM. Finally, the impact results for various materials are spread over two orders of magnitude. When this spread is compared with the signal-to-noise ratio, the material range is impressive. Attempts are made to set up this ubiquitous test method on a firm platform based on the principles of fracture mechanics.

Table 10.10 Standard test methods for the determination of Izod impact strength

No.	Test method	Impact energies	Test specimen	Notch
1.	ISO R180	1.0, 2.75, 5.5, 11.0 and 22.0 J	Four types permitted. Type 4 is preferred (80 ± 2 × 10 ± 0.2 × 4 ± 0.2 mm)	Two types of cut notches allowed
2.	BS 2782 Method 306 A	1.36, 4.07 and 13.6 J	(63.5 ± 2 × 12.7 ± 0.2 × 12.7.0 ± 0.3 mm) or (63.5 ± 2 × l2.7 ± 0.2 × 6.4 ± 0.3 mm)	Molded notch allowed in Type A. Cut notches allowed in Type B and C
3.	ASTM D 256-00	A range of pendulum energies from 2.710 to 21.680	Length: 63.50 mm (max.), 60.30 mm (min) Width: 12.7 mm (max), 3.00 mm (min). Breadth: 12.70 ± 0.15 mm	Cut notches allowed

Standard test methods for the determination of Izod impact strength are listed in Table 10.10. For example, ISO R180 normalizes the notch length. The velocity of the striker on impact has been standardized at 3.5 ± 10 % m/s with impact energies of 1.0, 2.75, 5.5, 11.0, and 22.0 J. Four types of test pieces are permitted.

10.3.1.2 Charpy Impact

The Charpy test is similar to the Izod impact test. In both the tests, flexural impact takes place by a pendulum (Fig. 10.9) striking a bar-shaped test piece (Fig. 10.10). However, as described before, there are quite significant differences between them, and no general correlation relating the data obtained from each have been developed.

Standard test methods for the determination of Charpy impact strength are listed in Table 10.11. For example, BS 2782 (Method 351A) uses a rectangular, notched or unnotched, bar supported at both ends in such a position that the pendulum strikes it in the center, directly behind the notch. The energy absorbed in the impact is read directly by means of a pointer from a scale calibrated to allow for frictional and windage errors. Three standard test pieces are defined – the preferred being 120 × 15 × 10 mm with a span of 70 mm. The standard impact energies are 0.5, 1, 4, 15, and 50 J.

10.3.2 Fracture Mechanics

Griffith (1920) showed that brittle solid materials fail at lower strengths because of the presence of flaws acting as stress concentrators. The hypothesis has become the basis of "fracture mechanics," used to interpret the fracture of many solids, including polymers and their blends. The theoretical background is presented in standard texts (Kinloch and Young 1983; Williams 1984; Broek 1986; Brostow and Corneliussen 1986).

Linear elastic fracture mechanics (LEFM), which has grown out of the work of Griffith, provides the most satisfactory basis for characterizing the fracture process

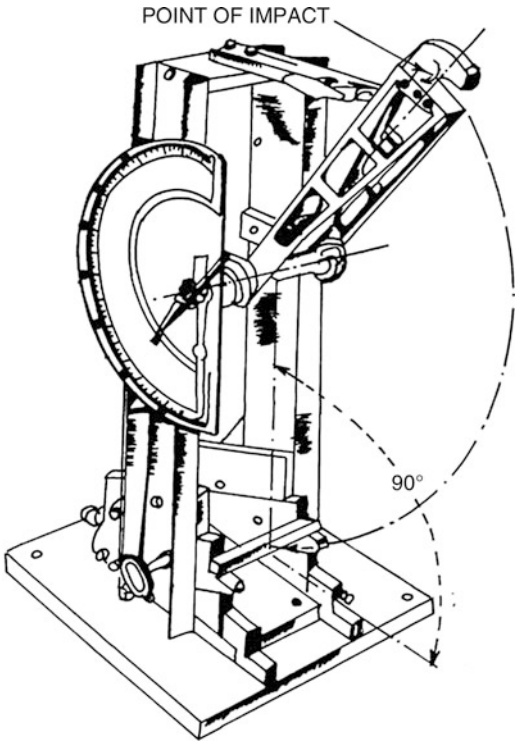

Fig. 10.9 Simple beam (Charpy-Type) impact machine (ASTM D6110-97)

of polymer composites and multiphase polymers. It enables each of the factors contributing to fracture to be considered separately. Results obtained from the fracture mechanics analyses have thrown considerable light upon the behavior of polymers under tensile, impact, and fatigue loading. Unfortunately, the conditions of LEFM are very severe and require that the fracture process is nearly totally elastic. Only under such conditions the data can be used for large scale predictions. However, elastic behavior cannot always be obtained in a laboratory-scale test and some experimental or theoretical tools need to be available to help in predicting the brittleness of large-scale article. Furthermore, in case of rubber-toughened plastics, extensive yielding usually precedes fracture even in the presence of a sharp crack, so that LEFM techniques are Unsuitable.

A crack in a solid may be stressed in three different modes (Kinloch and Young 1983; Brostow and Corneliussen 1986). The cleavage or tensile-opening mode (Mode I) is technically the most important one since it is commonly encountered and usually results in failure. Two closely related approaches have been used (Williams 1984):

1. The first is an energy criterion that supposes that fracture takes place when sufficient energy is released (from the stress field) during crack growth to supply the energy requirements of the new fracture surfaces created (Orowan 1948).

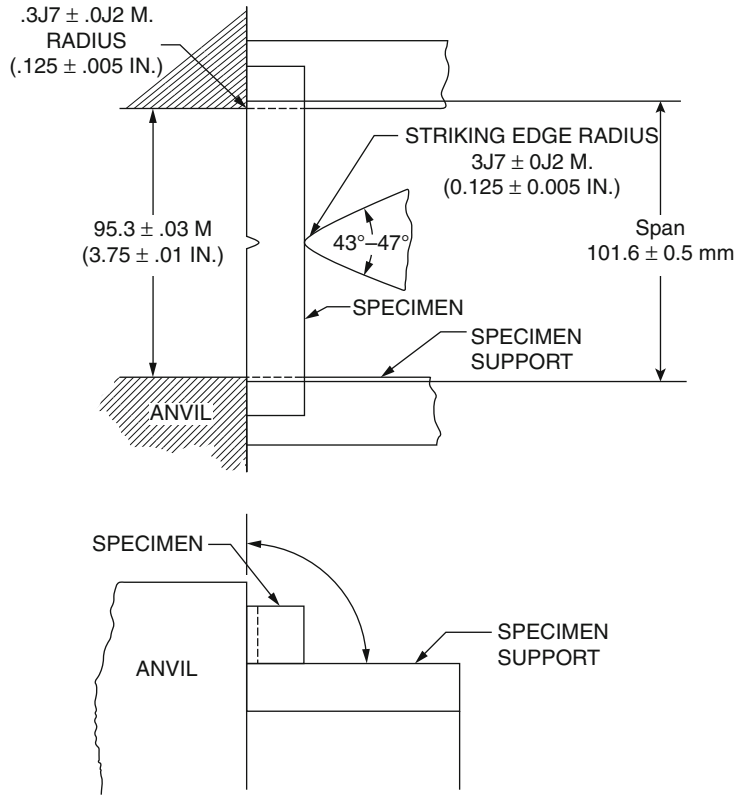

Fig. 10.10 Relationship of anvil, specimen and striking edge to each other for Charpy test method (ASTM D6110-97)

The fracture of a material is thereby characterized by the material property G_c known as the "strain energy release rate" or "fracture energy" (Kinloch and Young 1983; Brostow and Corneliussen 1986).

2. Rivlin and Thomas (1953) developed the second approach. They showed that the stress field around a sharp crack in an elastic material could be uniquely defined by a parameter known as the "stress intensity factor," K. When K reaches a critical value K_c (which is a material property often called the "fracture toughness"), fracture takes place.

The criterion for crack propagation is that $K_I > K_{Ic}$. For plane strain in Mode I, values of G_{Ic} and K_{Ic} are related:

$$K_{Ic}^2 = \frac{E\, G_{Ic}}{(1-\nu^2)} \tag{10.6}$$

where E is Young's modulus and ν is Poisson's ratio. In SI units, K_{Ic} is usually given in $MPa.m^{0.5}$ and G_{Ic} in kJ m^{-2}. To make valid fracture mechanics

Table 10.11 Standard test methods for the determination of Charpy impact strength

No.	Test method	Impact energies	Test specimen	Notch
1.	BS 2782, Method 351 A	0.5, 1, 4, 15, and 50 J	Preferred test dimensions are 120 × 15 × 10 mm	Type A (standard), square section, 2 mm wide and one-third specimen thickness in depth. Type B and C are V-shaped with base radii 0.25 mm and 1.00 mm respectively. The depth of these notches is set to one-fifth thickness
2.	ISO R179	Two striking energy levels	Four types of test pieces are allowed. First three are as in British standards. Fourth type is 125 mm long by 13 mm square	Same notch types as above. Molded notches are permitted. Machined notches are preferred
3.	DIN 53453 (Similar to BS Method)	As in BS Method	As in BS Method	Type A as given in BS Method (Type B-and C are not specified)
4.	ASTM D6110-97	2.710 ± 0.135 J	(127.00 to 124.50) × (12.70 ± 0.15) × (12.70 to 3.00 mm)	The included angle of the notch is 45 ± 1°, with a radius of curvature at the apex of 0.25 ± 0.05 mm

[a]ASTM standard test methods are available on web: http://enterprise.astm.org/

measurements, it is necessary to ensure that specimen dimensions are large in comparison with the plastic zone surrounding the crack tip. For metals, according to ASTM E399,

$$(w - a),\ a,\ B\ >\ 2.5\left(\frac{K_{Ic}}{\sigma_y}\right)^2 \tag{10.7}$$

where w is the width of the specimen, a is the crack length, B is the thickness, and σ_y is the uniaxial yield stress of the specimen. In the case of polymer blends, it is preferable to experimentally determine the effects of specimen dimensions upon G_c and K_c rather than rely upon the applicability of the above conditions.

The main experimental problem is to prepare specimens in which the plane-strain/plane-stress conditions are satisfied (Williams 1984; Kinloch and Young 1983). Apparent toughness values of K_c and G_c are higher in thin specimens than in thick ones. Measurements on several rubber-toughened plastics have shown a decrease in K_{Ic} with increasing thickness, B. The minimum value of B required, in the case of HIPS, for a valid determination of K_{Ic} at 296 K appears to be about four times higher than that given by Eq. 10.7 (Yap et al. 1983). Unfortunately, there is no reliable criterion for crazing under plane strain, and therefore it is difficult to suggest an alternative to the standard approach that has been used successfully for metals.

The toughness observed for rubber-toughened plastics is determined by the mechanism of deformation created by the plane strain at the tip of a sharp crack. There are two factors to be considered:

1. The fall in yield stress that occurs in ductile polymers as the temperature increases or the strain rate reduces. This fall results in a plane-strain to plane-stress transition, as indicated in Eq. 10.7 and therefore an increase in fracture resistance.
2. The release of constraint that results from cavitation in the matrix or void formation in the rubber particles (Bucknall 1988; Young 1988).

Linear elastic fracture mechanics studies on toughened brittle plastics at room temperature concentrated on thermosetting resins, which have sufficiently high yield stresses to meet the requirements of Eq. 10.7. There has been increasing emphasis on ductile fracture mechanics in testing the toughened thermoplastics. An alternative approach is to determine the parameter, J_{Ic}, which is the quantity corresponding to G_{Ic} in linear elastic fracture mechanics, as discussed below.

10.3.3 Fracture Mechanics Testing

10.3.3.1 Determination of G_c

The ductile fracture mechanics is gaining importance in testing polymer blends, especially the toughened thermoplastics. Some of the types of specimen which have been used to study the failure of ductile polymers whose deformation is elastic (but nonlinear) are shown in Fig. 10.11 (Kinloch and Young 1983). Formulae have been developed to determine G_c for these specimens, and examples are given in Table 10.12. Again, the parameter defining the fracture process G_c, is a function of applied load, crack length, and geometrical factor (Young 1988). Typical values of G_c and K_c are listed in Table 10.13.

The problem of defining conditions for crack propagation becomes more difficult when the material is sufficiently ductile to form a large plastic zone at the crack tip. The problem is encountered particularly while testing rubber-modified plastics. Two ductile fracture criteria have been developed for metals, one based on crack-tip opening displacement (CTOD) and the other upon the energy line integral (J-integral) around the crack tip. The crack-opening displacement (COD) criterion has been applied to a number of polymers and blends, but the J-integral method is receiving more attention. Physically, COD is measured between the outer edges of the crack whereas CTOD is defined as the distance between two crack walls at the end of the fatigue crack. Thus, while COD is easy to measure, the determination of CTOD is not simple.

The CTOD δ is the relative displacement of the two fracture surfaces at the crack tip. Critical values of CTOD δ_c may be measured by means of a mechanical clip gauge or recorded photographically. Furthermore, a cine camera may be used to follow the crack initiation and propagation as in HIPS (at 293 K) (Ferguson et al. 1973). The authors reported that both LEFM and CTOD criteria were applicable at different stages of the fracture. On application of load to the specimen, the crack began to extend at a fixed value of K_I, to give a value of K_{Ic}, for crack initiation. Then, at the crack tip, began to form a stress-whitened yield zone. The load on the

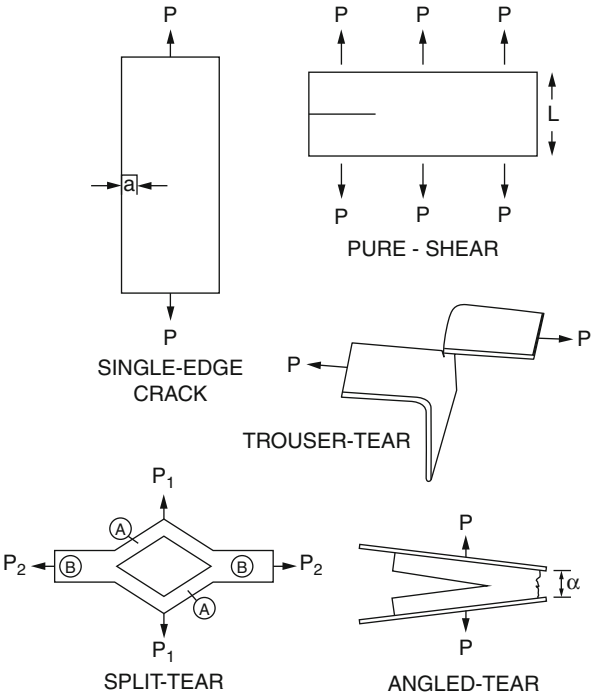

Fig. 10.11 Schematic diagrams of various specimens used for fracture mechanics testing of flexible polymeric materials. P = Applied load (Young 1988)

specimen continued to increase as both crack and yield zone extended, and a load maximum was observed at a fixed value of CTOD.

Precise determination of CTOD is often difficult. Furthermore, these measurements are unsuitable for use in design. For these reasons, models that enable CTOD to be calculated in terms of stresses have been developed (Dugdale 1960). In a wide plate with a central crack of length 2a with a narrow planar plastic zone of length L, extending from each of the crack tips, the applied stress σ is given by (Bucknall 1978)

$$\sigma = \frac{a}{(a+L)} = \cos\left(\frac{\pi\sigma}{2\,\sigma_y}\right) \tag{10.8}$$

The CTOD δ can be expressed as

$$\delta = \left[\frac{8\;\sigma_y\, a}{(\pi E)}\right] \ln\;\sec\;\left(\frac{\pi\sigma}{2\;\sigma_y}\right) \tag{10.9}$$

For small values of applied stress ($\sigma < 0.3\;\sigma_y$), the plastic zone size is small compared with the crack length and Eq. 10.9 can be simplified to read

Table 10.12 Expressions for G_C for fracture mechanics of crack growth in flexible polymers (Kinloch and Young 1983)

Geometry (see Fig. 10.11)	Expressions for G_C	Comments	References
Single-edge crack	$G_C = 2k_1 a W_C$	λ_c = extension ratio at onset of crack growth	Rivlin and Thomas 1953; Greensmith 1963; Lake 1979
	$k_1 = \pi\lambda_c^{-1/2}$	W_C = critical stored elastic strain energy density	
Pure shear	$G_c = lW_C$	1 = initial length	Rivlin and Thomas 1953
Trouser tear	$G_C = (2P_C\lambda_C/b) - 2wW_C$ when $\lambda_C = 1$ $G_C = 2P_C/b$	P_C = load at onset of crack growth	Rivlin and Thomas 1953
		w = width of specimen arms	
		λ_C = critical extension ratio in arms	
		W_C = strain-energy density in arms	
		b = specimen thickness	
Split tear	$G_C = \frac{\lambda_C^A + \lambda_C^B}{2b}\left(\sqrt{P_{1C}^2 + P_{2C}^2} - P_{2C}\right)$	λ_C^A and λ_C^B are critical extension ratios in regions A and B respectively; P_1 and P_2 are loads respectively transverse and in the split direction	Lake 1979
Angled tear	$G_C = (2P_C/b)\sin(\alpha/2)$		Thomas 1960

Table 10.13 Typical values of the fracture energy G_c and the fracture toughness K_c. for various materials (Kinloch and Young 1983)

Material	Young's modulus E (GPa)	G_c (kJm^{-2})	K_C ($MNm^{-3/2}$)
Rubber	0.001	13	–
Polyethylene	0.15	20	–
Polystyrene	3.0	0.4	1.1
High-impact polystyrene	2.1	15.8	–
PMMA	2.5	0.5	1.1
Epoxy	2.8	0.1	0.5
Rubber-toughened epoxy	2.4	2.0	2.2
Glass-reinforced thermoset	7.0	7.0	7.0
Glass	70	0.007	0.7
Wood	2.1	0.12	0.5
Aluminum alloy	68	20	37
Steel mild	210	12	50
Steel alloy	210	107	150

$$\delta = \pi\sigma^2 \frac{a}{(E\sigma_y)} \tag{10.10}$$

Under these conditions, LEFM analysis is applicable to the specimen.

In the case of a brittle fracture in a wide and thick plate containing an edge crack of length a, the critical applied stress at fracture σ_c is related to the Young's modulus E, the Poisson's ratio ν, and the fracture surface energy G_{Ic}; the critical stress can be expressed from the Griffith equation as

$$\sigma_c^2 = \frac{E\ G_{Ic}}{\pi a\ (1-\nu^2)} \tag{10.11}$$

From Eqs. 10.10 and 10.11, for plane-strain deformation,

$$G_{Ic} = \sigma_y\ \delta_c\ \left(1-\nu^2\right) \tag{10.12}$$

Tests are conducted, in normal practice, on compact tension specimens rather than wide center-notched plates. Some allowance must be made for geometrical effects, including the finite width of the specimen, the difference between edge and center notches, and any rotations occurring at the grips.

In general, it is not possible to measure CTOD, but rather the crack-opening displacement (COD). The latter quantity can be determined at the outer end of the notch with a suitable clip gauge. Thus, for a notched three-point-bend specimen, it was shown that a "plastic hinge" can form around the tip of the crack (Brostow and Corneliussen 1986). If the center of rotation is known, the CTOD can be calculated from the measured COD. A standard has been published (BS 5762).

10.3.3.2 J-Integral Techniques

Single-Specimen Method

If there is extensive plasticity in a material under tension, it gives rise to a relatively large size of the crack-tip plastic zone, and solutions for elastic–plastic behavior are not readily available. J-integral provides a means of determining the energy release rate for such cases. This integral was applied to crack problems (Cherepynov 1967; Rice 1968). Rice showed that J-integral describes the flow of energy into the crack-tip region and that the dominant term in the description of stress and strain singularities at the crack tip could also be written in terms of J. He demonstrated that the value of J was independent of the integration path. In practice, J can be determined from changes in load displacement diagram with changes in crack length (ASTM E813). This method has been reviewed (Williams 1984; Landes and Begley 1979; Pascoe 1986). The J-integral is given by (Kinloch and Young 1983).

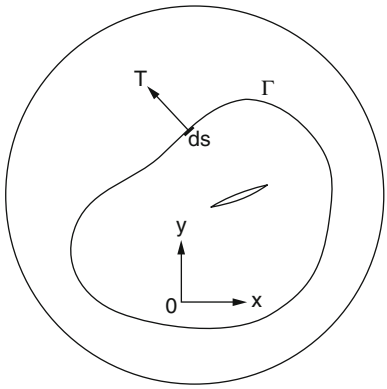

Fig. 10.12 Contour for definition of J-integral (Brostow and Corneliussen 1986)

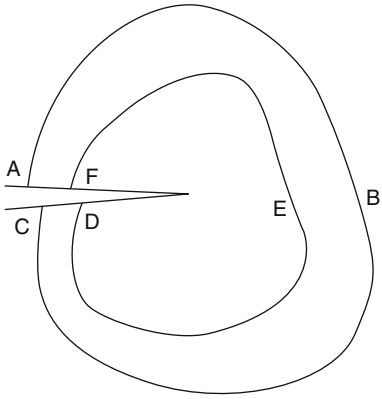

Fig. 10.13 Contour surrounding crack-tip (Brostow and Corneliussen 1986)

$$J = \int_{\Gamma} \left\{ Z\partial y - T\left(\frac{\partial u}{\partial x}\right) ds \right\} \tag{10.13}$$

where Γ is a closed contour in a stressed solid (Fig. 10.12), T is the tension vector perpendicular to the contour in an outward direction, u is the component of displacement of the contour in x-direction, ds is an element of the contour Γ, and Z is the strain energy (plastic and elastic) per unit volume.

In Fig. 10.13, a closed contour is taken as two curves surrounding the tip of the crack, one DEF inside the other ABC which are joined by two portions of the crack surface AF and CD. The integral around the contour is zero. Along the parts AF and CD which lie parallel to the x-axis and which have no normal stress on them, $T = 0$ and $dy = 0$. Therefore, the integral along ABC is equal and opposite in sign to that along DEF. For outward directed vectors, T, therefore, the integral is path independent. The J-integral method (ASTM E813) of

fracture toughness measurement has been applied to a variety of polymers (Theuer et al. 1988; Rimnac et al. 1988) and rubber-toughened polymers (Huang and Williams 1987; Huang 1988; Huang and Wang 1989; Hashemi and Williams 1985; Takemori and Narisawa 1989).

The multi-specimen J-integral technique (ASTM E813) also provides a method for determination of J_{Ic}, a measure of fracture toughness. A critical evaluation of ASTM E813-81 and E813-87 has been published (Narisawa and Takemori 1989; Huang and Wang 1989; Huang et al. 1990).

Multiple-Specimen Method

A major problem often encountered in the above described "single-specimen method" is that the crack growth measured from a side view may not be accurate, as the crack front may vary from the central region to the sides. A "multiple-specimen method" was developed to bypass this problem.

The method has been applied to numerous ductile polymeric materials (Begley and Landes 1972; Landes and Begley 1974). The critical J values obtained by using single-specimen method were greater than those obtained from the standard multiple-specimen method (Westerlind et al. 1991). Many workers have used the ASTM standards of E813-87 to characterize the fracture toughness of polymers (Chan and Williams 1981, 1983; Hashemi and Williams 1986; So and Broutman 1986; Huang and Williams 1987; Narisawa 1987; Rimnac et al. 1988; Narisawa and Takemori 1989; Huang and Williams 1990; Huang 1990; Moskala and Tant 1990).

Hysteresis Energy Method

When a pre-cracked specimen of a toughened polymer is under load, viscoelastic and inelastic micro-mechanisms such as crazing, cavitation, debonding, and shear yielding are expected to take place mainly around the crack tip. These micro-mechanisms occur during the process of crack-tip blunting (pre-crack) and during crack propagation. A portion of the storage energy is therefore consumed, and a relatively large crack-tip plastic zone is formed, which can be quantified by the corresponding hysteresis energy. For rubber-toughened polymeric materials, the crack tends to propagate within the plastic zone. A new J-integral method based on hysteresis properties of polymeric materials was proposed (Lee and Chang 1992; Lee et al. 1992).

In case of a cracked specimen, the material surrounding the crack tip can be divided into three parts: (1) the first plastic zone, (2) the second plastic zone, and (3) the elastic fracture surface (Lu et al. 1996). The specific energy balance equation for a cracked specimen can be expressed as

$$\left(\frac{1}{B}\right)\left(\frac{dU}{da} - \frac{dU_e}{da} - \frac{dU_k}{da}\right) = \left(\frac{1}{B}\right)\left(\frac{dU_p{}^{ppz}}{da} + \frac{dU_p{}^{spz}}{da}\right) + 2\,\gamma_s \quad (10.14)$$

where U is the input energy at different displacements, U_e is the elastic energy, U_k is the kinetic energy, $U_p{}^{ppz}$ is the plastic energy for the primary plastic zone, $U_p{}^{spz}$ is the

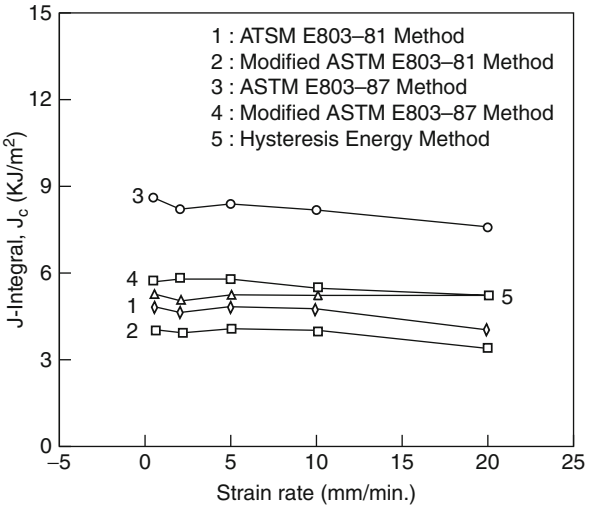

Fig. 10.14 Plots of critical J_{IC} value versus the strain rate (Lu et al. 1996)

plastic energy for the secondary plastic zone, and γ_s is the fracture surface energy and a is the initial crack length. The energy dissipated of the system is given by

$$\left(\frac{1}{B}\right)\frac{d(HE)}{da} = \left(\frac{1}{B}\right)\left(\frac{dU_p{}^{ppz}}{da} + \frac{dU_p{}^{spz}}{da}\right) + 2\,\gamma_s \qquad (10.15)$$

where HE is the hysteresis energy.

This approach assumes that there is a region surrounding the crack tip with local energy dissipation. This arises from viscoelasticity, plasticity, and bond rupture and can be considered the characteristic of the fracture process. For polymers the characteristic of this localized energy dissipation is considered to be independent of geometries.

The J_{Ic} values obtained based on hysteresis energy method were close to these obtained using E813-81 method, but significantly lower than those from E813-87 method. Experimentally the hysteresis energy method is relatively simple, because the tedious measurement of crack growth length is not necessary. Figure 10.14 shows variations of J_c values for PC/ABS blends obtained using different J-integral methods – as shown, the spread is ±40 % (Lu et al. 1996).

The J-integral by hysteresis energy method was applied to elastomer modified PC (Lee and Chang 1992; Lee et al. 1992), HIPS (Lee et al. 1992, 1993), ABS (Lu et al. 1995), PC/ABS blend (Lu and Chang 1995; Lu et al. 1996), and PC/PBT blend (Lu and Chang 1995).

Essential Work of Fracture Method

The theoretical analysis of J-integral is well established (Rice 1968; Begley and Landes 1972), and the experimental procedure is standardized (ASTM E813-89). However, some aspects of the method still remain controversial (Hashemi and

Williams 1986; Huang and Williams 1987, 1990; Narisawa and Takemori 1989, 1990; Swei et al. 1991). For example, the procedure for J–R curve construction restricts the application of the J-integral method to only static loading tests. J-integral method is usually difficult and expensive (Bramuzzo 1989). The specimen size required by the J-integral method makes it impossible to characterize the toughness of polymeric thin films. It is also well recognized that using a blunting line to define the critical value of J-integral may not be proper for some ductile polymers (Hashemi and Williams 1986; Narisawa and Takemori 1989). The J-integral analysis based mainly on metals is not fully appropriate to polymers. This is particularly true when the heterogeneous and toughened polymer blends are involved.

To overcome the above drawbacks, a new method based on "essential work of fracture" concept was introduced (Broberg 1971, 1975). In this method, it is proposed that when a cracked ductile solid, such as a toughened polymer blend, is loaded, the fracture process and the plastic deformation take place in two different regions, viz., the inner process zone and the outer plastic zone. Much of the fracture work during crack propagation, dissipated in the plastic zone, is not directly associated with the fracture process. Only that work that goes into the fracture process zone is a material constant. Hence, the total fracture work, W_f, should be separated into two parts, i.e., the essential work of fracture (i.e., the work required to create two new fracture surfaces, W_e) and a nonessential work of fracture (W_p):

$$W_f = W_e + W_p \tag{10.16}$$

W_e is essentially a surface energy, and for a given thickness it is proportional to ligament length ($l = W - a$), while W_p is a volume energy and proportional to l^2. Thus, the total fracture work is rewritten as

$$W_f = w_e tl + \beta w_p tl^2 \tag{10.17}$$

where w_e and w_p are the specific essential work of fracture and nonessential work of fracture (or specific plastic work), respectively; β is the plastic zone shape factor; while t, W, and a are thickness, width, and initial crack length, respectively. Then, the specific total fracture work, w_f, is

$$w_f = \frac{W_f}{tl} = w_e + \beta w_p l \tag{10.18}$$

There are two kinds of specific essential work of fracture available, according to the stress state of the ligament area, viz., plane-stress-specific essential work of fracture (w_e) and plane-strain-specific essential work of fracture (w_{Ic}) (Wu and Mai 1996).

The w_e can be obtained if l/t ratio is large enough to ensure plane-stress condition in the ligament area, and it is proved to be a material constant for a given sheet thickness (Mai and Cotterell 1986a, b; Mai et al. 1987; Mai and Powell 1991). With a reduction of l/t ratio, plastic constraint increases and the plane-stress/plane-strain fracture transition may occur at a certain l/t ratio. Theoretical analysis shows that the specific essential work of fracture method is equivalent to the J-integral method for all three fracture modes (Mai and Powell 1991; Mai 1993).

The essential work of fracture approach has been applied to characterize the fracture properties of toughened polymer blends, such as PBT/PC/IM (where IM is the impact modifier) and ABS/PC. It is successfully used to determine the fracture toughness of a ductile LLDPE film (Wu and Mai 1996), and single-edge and double-edge notched different polymeric films (Hashemi 1993; Hashemi and Yuan 1994; Chan and Williams 1994; Karger-Kocsis and Czigany 1996; Karger-Kocsis and Varga 1996). It is also applied to study the effect of specimen size, geometry, and rate of tests in case of PBT/PC blends (Hashemi 1997).

10.3.4 Mechanisms of Toughening

Early investigations of the fracture of solids assumed that fracture involved only the creation of new surfaces (Griffith 1920; Kinloch and Young 1983). However, since measured values of G_c were well in excess of the surface energy of the material, it was soon realized that significant amounts of energy were also dissipated through other processes such as localized plastic deformation in the vicinity of the crack (Kinloch and Young 1983). In general, two mechanisms are responsible for this plastic deformation in rigid polymers, namely, "crazing" (Kausch 1983; Kambour 1973) and "shear yielding" (Ward 1983). The two mechanisms are not mutually exclusive. Under certain conditions both operate simultaneously.

10.3.4.1 Crazing

Crazing is an important source of toughness in rubber-modified thermoplastics. A craze can be described as a layer of polymer a nanometer to a few micrometers thick, which has undergone plastic deformation approximately in the direction normal to the craze plane as a response to tension applied in this direction (Kambour 1986). Crazing occurs without lateral contraction. As a result, the polymer volume fraction in the craze is proportional to $1/\lambda$, where λ is the draw ratio in the craze. The reduction in density occurs on such a small scale that the refractive index is markedly reduced, which accounts for the reflectivity of the craze (Kramer 1983).

Several methods of studies have been developed. Osmium-staining technique, pioneered by Kato (1967), is one of the most successful methods for observing crazing in rubber-toughened plastics. It depends upon a reaction between osmium tetroxide, OsO_4, and double bonds in PBD and other unsaturated polymers. But, it is not suitable for saturated rubbers.

Ruthenium tetroxide, RuO_4, is more reactive staining agent that can be used to differentiate between rubber and matrix when the former is essentially saturated. For example, clean glass slides (50 × 10 mm) were dipped in 2 wt% solutions of polymer, and the solvent was subsequently evaporated under vacuum at 50 °C (323 K) for 24 h. The films were removed from the glass substrate by immersing the slides in distilled water and then lifting the floating film from the water surface onto copper microscope grids. A 0.5 wt% solution of RuO_4 in distilled deionized water was used for staining. The aqueous solution (golden yellow when fresh) was found to

be effective for a considerable time (up to 6 months if kept in a firmly sealed glass container in a freezer). Film-covered grids were vapor stained in a glass-covered dish (Trent et al. 1981, 1983). Transmission electron micrographs, TEM, can be taken to illustrate detailed morphological features (at an accelerating voltage of 80 KV).

Recently, methods have been developed to characterize the relative amount of crazing and non-crazing that occurs in rubber-toughened glassy polymers, using the invariant obtained from small-angle X-ray scattering (SAXS) analysis. SAXS not only overcomes the disadvantages of transmission electron microscopy (e.g., the use of ultrathin samples), but the use of high intensity synchrotron radiation permits in situ deformation studies (Paredes and Fischer 1979; Brown and Kramer 1981). The new method of SAXS analysis leads to quantification of the contribution from crazing and non-crazing to the total deformation (He et al. 1998).

10.3.4.2 Shear Yielding

Yielding is a mechanism, in which a thin layer of polymer deforms in shear at constant volume. It is characterized by regions of sheared polymer oriented approximately at 45° to the tensile or compression stress. Unlike crazing, shear flow is essentially a process continuous in space, i.e., one that may spread through a much greater volume fraction of the stressed body and thus consume much more energy in total. Shear yielding is much less sensitive to environmental effects. In short, shear deformation is better than crazing, but crazing is better than no deformation at all (Kambour 1986).

Shear bands are highly birefringent and are most clearly observed in transmitted polarized light (Bucknall 1977). They are also visible as reflecting planes in ordinary transmitted light at glancing incidence, owing to refractive index differences between the band and the adjacent undeformed polymer (Kramer 1974, 1975). Both crazing and shear yielding involve the absorption of energy, and most methods of toughening polymers involve modifying the polymer such that more crazing and shear yielding take place. The rubber-modified polymer absorbs considerably more energy in a tensile test because of its higher extension to break, which can be achieved only as a result of yielding in the matrix. The rubber particles play only a secondary role but, nevertheless, a vital one.

Firstly, they accelerate yielding by acting as stress concentrators initiating deformation in the matrix; secondly, they respond to the hydrostatic component of stress by cavitating and increasing in volume, thus allowing the strain in the matrix to increase; and thirdly, in their cavitated and extended state, they stabilize the yielded polymer by carrying a share of the applied stress (Bucknall 1988). All three functions appear to be necessary for effective toughening, although their relative importance varies, depending upon the mechanisms contributing to toughening, and the kinetics of deformation, which in turn depend upon the material and the type of loading. Various types of response of the rubber particles have been observed experimentally as the polymer yields. They include (a) debonding between rubber and matrix (Haward and Bucknall 1976), (b) cavitation within the particle (Breuer et al. 1977; Kinloch 1985; Yee and Pearson 1986), (c) craze like fibrillation of the rubber

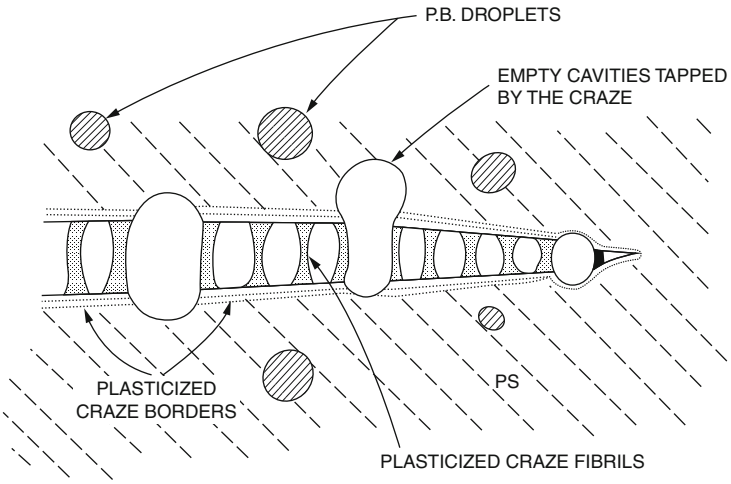

Fig. 10.15 Schematic rendering of craze moving in a field of encapsulated PB pools draining their content onto the craze surfaces when tapped by the advancing craze (Argon et al. 1990)

phase (Beahan et al. 1976; Donald and Kramer 1982), and (d) crazing within sub-inclusions (Seward 1970). Many polymers are toughened by blending or copolymerizing with a rubber (Kinloch and Young 1983; Bucknall 1977). This method of toughening is now well established for many thermoplastics, thermosets, and even adhesives.

10.3.4.3 Other Mechanisms

A new route for achieving a substantial lowering of stresses for craze growth without relying on potent craze initiators involves controlled local plasticization of a polymer by a low molecular weight diluent, distributed in a heterogeneous fashion throughout the material (Gebizlioglu et al. 1990; Argon and Cohen 1990). This mechanism is schematically shown in Fig. 10.15.

The advancing craze, nucleated from free surfaces or other occasional imperfections, cuts into the dispersed population of PB-2.76 K pools (which at this low molecular weight acts like a relatively low viscosity liquid) and drains the contents of these pools onto the surfaces of the craze. Although the solubility of the PB 2.76 K into PS under standard conditions of room temperature and atmospheric pressure is negligibly small (of the order of 4×10^{-3}), this should increase greatly in the presence of a negative pressure (Argon and Cohen 1990). The plasticization due to the increased sorption of the low molecular weight PB diluent into the craze surfaces is a highly interactive and complex process. The new mechanism offers considerable promise for practical industrial applications as only very small quantities of the plasticizing substance are needed, and thus subsidiary properties such as optical transparency and tensile modulus are less affected compared to the other methods of toughening.

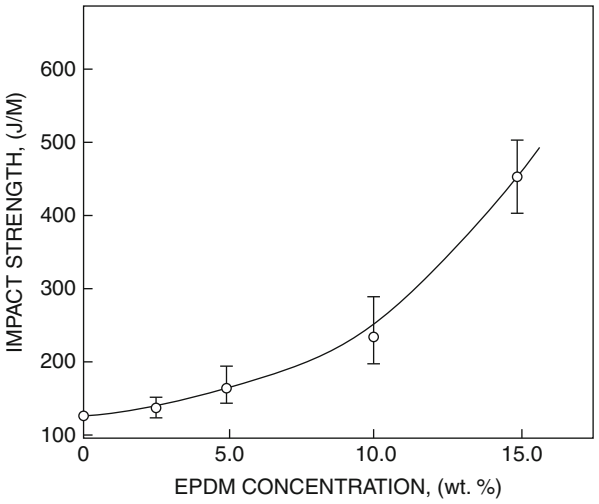

Fig. 10.16 Influence of EPDM concentration on Izod impact strength of PPBC-EPDM blends

10.3.5 Factors Affecting Blend Toughness

Rubber toughening is the most often used method of improving the impact resistance of polymers (Bucknall 1977). The impact modified materials are usually the blends of a rigid matrix polymer with an elastomer. The composition of the constituents, their miscibility, and the morphology influence the deformation and failure mechanism in the blend. Particle size of the elastomer, its dispersion, and its adhesion with matrix are also the important factors determining the toughness.

10.3.5.1 Composition

The composition of individual constituents of a blend plays an important role in modifying the impact strength of the blend. The impact strength of polypropylene block copolymer (PPBC) blends with different concentrations of EPDM is shown in Fig. 10.16 (Xavier et al. 1994). Upon incorporation of the elastomer, the impact strength increases. EPDM was found to reduce the crystallinity of PPBC and significantly influence its failure mechanism. Both crazing and shear yielding were found to be responsible for the observed increase in impact strength. As shown in Fig. 10.16, above 10 wt% of EPDM, the increase in impact strength is more prominent. However, it was observed that such significant rise in impact strength adversely affected the other mechanical properties, such as flexural and tensile moduli of the blends.

In the case of PVC/ABS blend, the addition of ABS improved the impact strength of the blend (Sharma et al. 1988). At low concentrations of ABS, a small number of rubber particles (i.e., the butadiene particles in ABS) are insufficient to significantly improve the impact strength (Fig. 10.17). Increasing ABS concentration up to 50 wt% increased impact strength. The maximum impact strength obtained at the optimum blend composition is considerably higher than that of neat ABS itself. Since the particle size (Kulshreshtha et al. 1989) of the dispersed

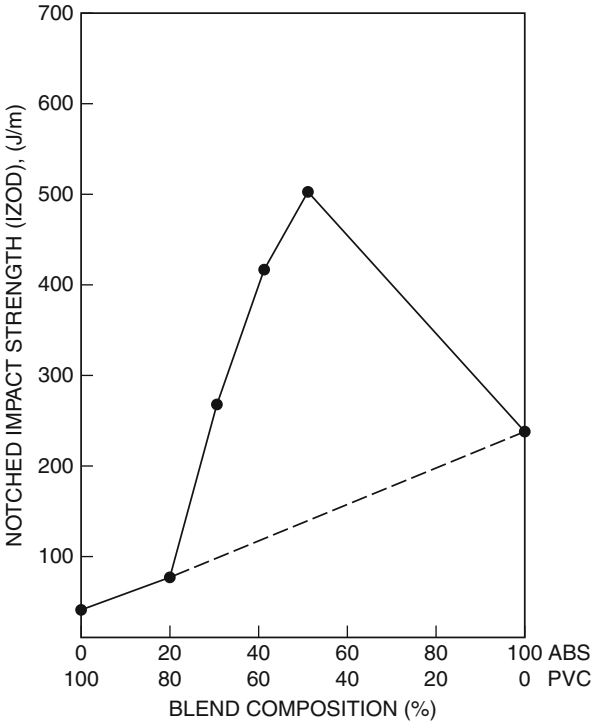

Fig. 10.17 Influence of PVC/ABS blend composition on Izod impact strength

PBD (of ABS) phase is unlikely to change with blend composition, it is evident that there exists a critical volume fraction of rubber phase necessary for the maximum improvement in impact strength. When this critical concentration of rubber (or ABS) is exceeded, impact strength drops.

10.3.5.2 Morphology

The performance characteristics of a blend depend on its morphology, which in turn depends on the thermodynamic and rheological properties of the components (Plochocki 1983; Karger-Kocsis et al. 1984; Howe and Wolkowicz 1987; Wu 1987; Utracki 1989). However, due to nonequilibrium nature of the highly viscous polymer mixtures, often the processing conditions strongly influence the product morphology. The topic is discussed in the last part of Sect. 10.3.6: Low-Speed Mechanical Properties of Blends. Further details of the morphology-processing conditions can be found in ▶ Chap. 7, "Rheology of Polymer Alloys and Blends"; ▶ Chap. 8, "Morphology of Polymer Blends"; and ▶ Chap. 9, "Compounding Polymer Blends."

The properties of PPBC/EPDM blends strongly depend on the crystalline micromorphology of PPBC, as well as on the particle size and degree of dispersion of EPDM (Xavier et al. 1994). The DSC cooling thermograms indicated that the degree of crystallinity in PPBC decreased with increasing concentration of EPDM (Table 10.14 and Fig. 10.18).

Table 10.14 Crystallinity indices (A/m values) from DSC (Xavier et al. 1994)

No.	Blend	A/m (arbitrary units)
1.	PPBC (neat polymer)	232
2.	PPBC + EPDM (2.5 wt%)	216
3.	PPBC + EPDM (5.0 wt%)	208
4.	PPBC + EPDM (10.0 wt%)	206
5.	PPBC + EPDM (15.0 wt%)	197

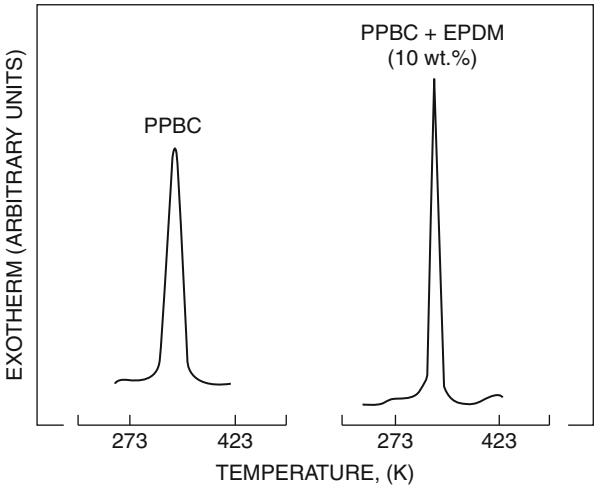

Fig. 10.18 DSC thermograms recorded during cooling cycle for PPBC and its blends with EPDM (10 wt%)

As observed under optical microscope with crossed polarizers, incorporation of up to 10 wt% EPDM into PPBC does not affect the nucleation density or ultimate size of PPBC spherulites (Fig. 10.19). The EPDM particles act as inert inclusions, constituting geometrical obstacles to the PPBC spherulites' growth, thus changing their morphology. Nevertheless, some interfacial interactions are observed in the case of a blend with 10 wt% EPDM. The spherulites of PPBC are found to nucleate from the interface with EPDM (Fig. 10.19c). This resembles the transcrystalline structure observed in several glass or carbon fibers reinforced, semicrystalline polymers, such as PP, PE, PA-6, etc. (Xavier 1991). Such a structure was considered an indication of good interfacial interaction between the two constituents.

The EPDM particles were found either to initiate crazes or to terminate them, depending on the interfacial bonding, the particle size, the concentration, and the interparticle distances. The variation of notched Izod impact strength of PPBC blends with different EPDM concentrations is shown in Fig. 10.16. The fracture surface of a blend with 10 wt% EPDM, as examined under SEM, is shown in Fig. 10.20. The hemispherical embeddings and hollows (representing the removed EPDM particles) are clearly visible on the fracture surface. The ribbonlike structures visible on the fractured surfaces are probably the micro-shear bands in the blends.

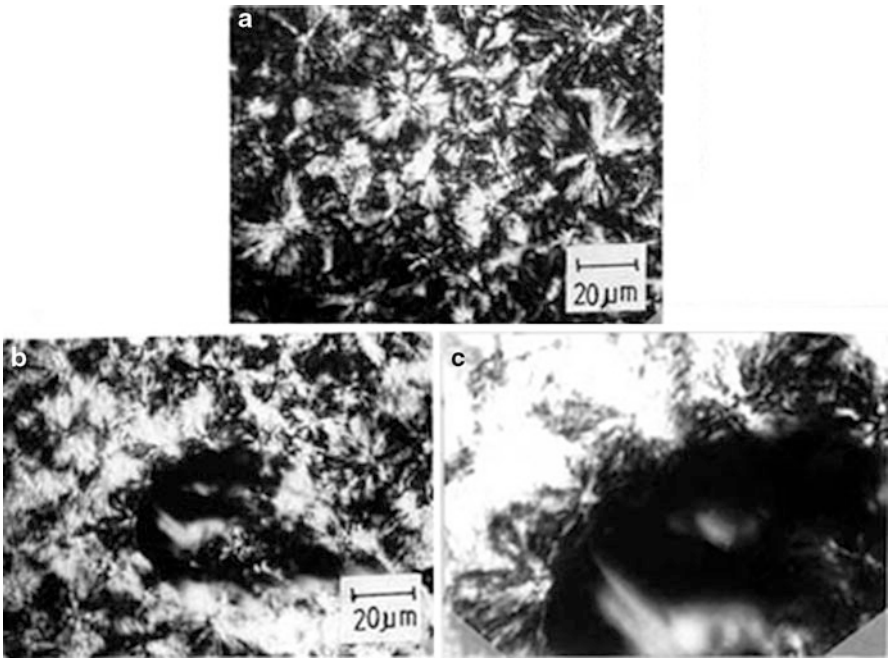

Fig. 10.19 Optical micrographs of (**a**) PPBS spherulites, (**b**) PPBC spherulites in the presence of EPDM and (**c**) PPBC spherulites nucleating from interface with EPDM

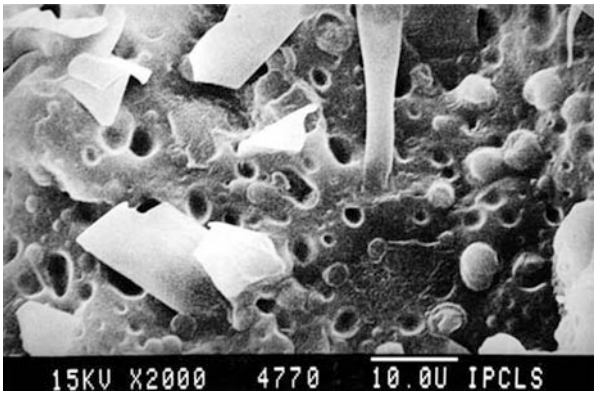

Fig. 10.20 SEM micrograph of PPBC + EPDM (10 wt%) blend fracture surface

Approximate ranges of the experimental techniques to study different blend morphologies are summarized in Table 10.15. See also ▶ Chap. 8, "Morphology of Polymer Blends" in this handbook.

10.3.5.3 Elastomer Particle Size

Elastomeric particle size plays a prominent role in controlling the toughening mechanisms of a polymer. It has been shown that particle size of an elastomer

Table 10.15 Approximate ranges of experimental techniques to study blend morphology of (1) interatomic; (2) molecular, spherulites; (3) Filler aggregates, compatibilized blends; (4) reinforcements, immiscible blends; (5) Voids (Utracki 1989)

Domain Size	1	2		3		4	5
Scale (μm)	10^{-4}	10^{-3}	10^{-2}	10^{-1}	10^{0}	10^{1}	10^{2}
Microscopy						Optical	
					SEM		
				TEM			
Spectroscopy		IR					
Thermal			DSC				
Mechanical			TMA				
Dielectric			DS				
Diffraction	WAXS						
			SAXS				
					SANS		
						Light	

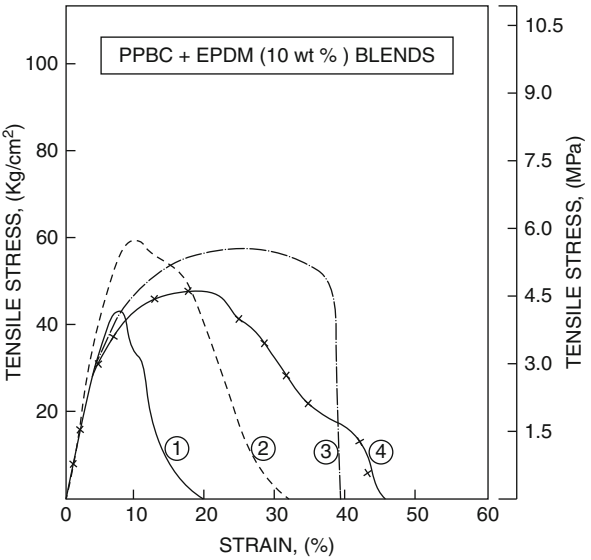

Fig. 10.21 Infl uence of EPDM particle size on tensile stress–strain curves of PPBC blends. EPDM particle sizes (*1*) 0.60 mm, (*2*) 3.45 mm, (*3*) 4.35 mm, (*4*) 5.50 mm

significantly influences the deformation and failure processes: small particles favor shear yielding, while coarser dispersions promote crazing (Jang et al. 1985). There is an optimal particle size resulting in maximum impact resistance (Speri and Patrick 1975; Stehling et al. 1981; Karger-Kocsis et al. 1981).

The tensile stress–strain curves of PPBC and its blends with EPDM of different particle sizes (for concentration equal 10 wt%) are shown in Fig. 10.21 (Xavier et al. 1994). The particle size of EPDM has considerably affected the post-yield behavior of the blends. Although the yield stress initially increases with reduction

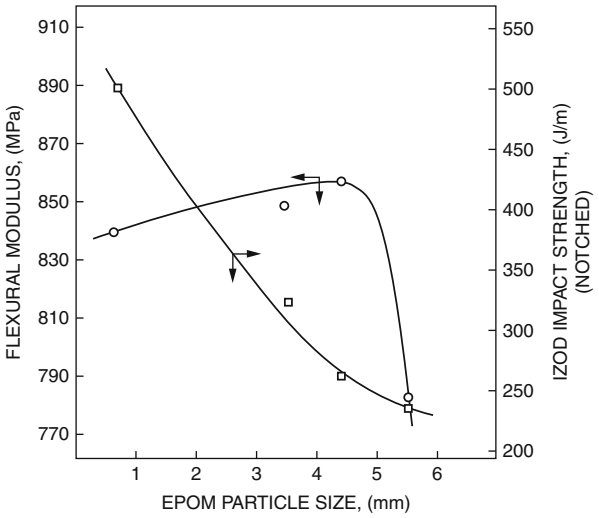

Fig. 10.22 Influence of EPDM particle size on flexural modulus and Izod impact strenght of PPBC/EPDM (10 wt%)

of EPDM particle size (from 4.35 to 3.45 μm), with further reduction of size (to 0.60 μm), it decreases. Earlier studies of the tensile properties of heterogeneous polymer blends have shown that Young's modulus poorly reflects morphological changes (Pukanszky et al. 1989; Pukanszky and Tudos 1990). Accordingly, the particle size dependence of Young's modulus is weak.

By contrast (see Fig. 10.22), in the case of PPBC blend with EPDM, the flexural modulus was found to significantly decrease when large EPDM particles ($d \geq 4$ mm) were used. The notched Izod impact strength was strongly affected by the particle size. As usually it is the case, reducing it caused the impact strength to increase. With the reduction in EPDM particle size, the number of particles has increased and the interparticle distance was reduced. Thus, multiple crazing in the blend was enhanced further with increased number of rubber particles and also reduced particle size.

The shear yielding also is influenced with change in particle size resulting in increased impact strength. The notched Izod impact fracture surfaces examined under SEM are shown in Fig. 10.23. Change in EPDM particle size had significantly changed the fracture morphology. The fibrous sheets like structures are probably the micro-shear bands in the blends. The number of these bands increases with reduction of the rubber particle size as the smallest particle (at constant loading) corresponds to their maximum number. The formation and break down of the micro-shear bands absorb enormous energy, and hence it increases the Izod impact strength.

Both principal fracture mechanisms, shear yielding and crazing, are influenced by the particle size. In PPBC matrix, where spherical elastomeric particles are chemically bonded, the energy absorption takes place mainly by deformation of the matrix. In such systems, a large amount of shear yielding is to be expected. The shear yielding becomes more prominent upon increasing the concentration of EPDM as well as reduction of their particle size. The micro-shear bands in the fracture surface (Fig. 10.23e) clearly support these expectations.

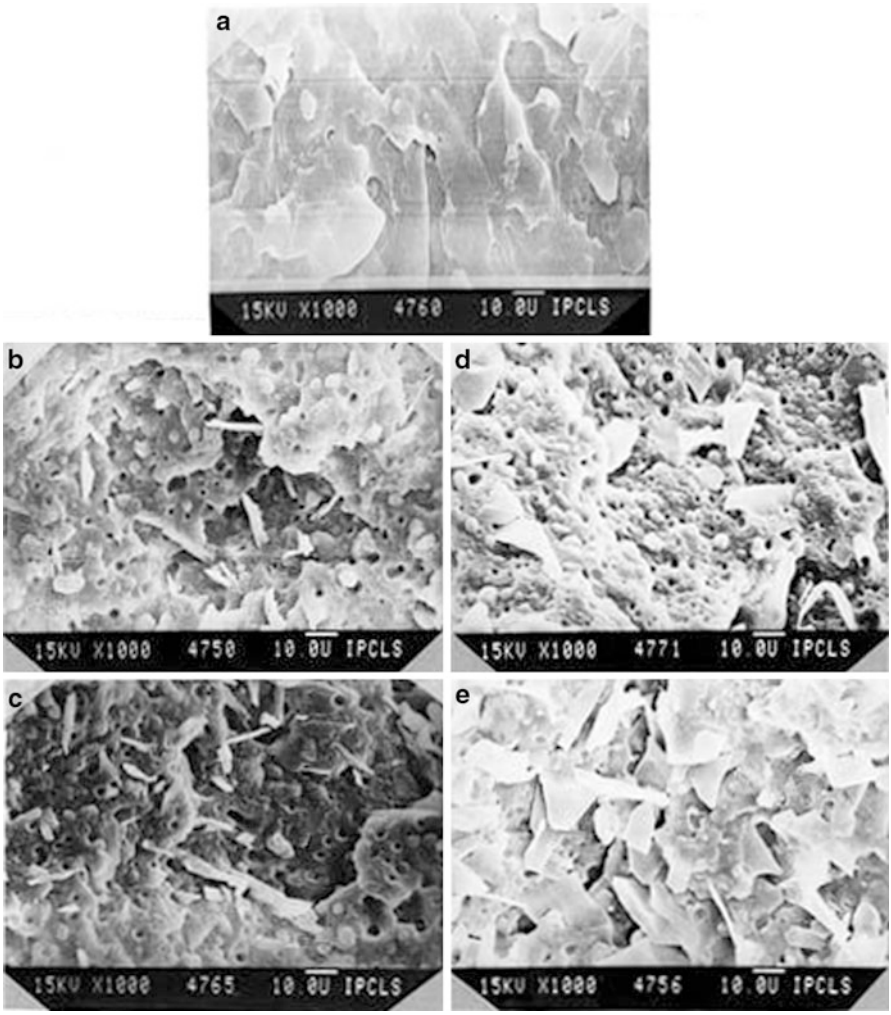

Fig. 10.23 SEM micrographs of the impact fracture surfaces of (**a**) PPBC and its blends with EPDM (10 wt%) with different (**b**) 5.50 mm, (**c**) 4.35 mm, (**d**) 3.45 mm and (**e**) 0.60 mm particle sizes

10.3.5.4 Miscibility

The notion of polymer miscibility implies intimate mixing on the segmental level. A miscible blend is expected to have a homogeneous composition throughout. The understanding of chemical principles in polymer miscibility is getting refined as a result of the appearance of several reviews and books on the topic (Krause 1972; Olabisi et al. 1979; Paul and Barlow 1980; Paul 1982; Ottenbrite et al. 1987; Utracki 1989). The level of molecular mixing existing in polymer blends that exhibit macroscopic properties indicative of single-phase behavior is commanding

considerable attention. More detailed information on this topic can be found in ▶ Chap. 2, "Thermodynamics of Polymer Blends" in this handbook.

The best commercial advantages of a polymer blend can best be summarized by the word "versatility" (Olabisi et al. 1979). Unfortunately, miscible polymer–polymer blends usually show additivity of the component polymers properties, thus their versatility is limited. Furthermore, like any other single-phase resin, for most applications miscible blends need to be toughened and/or reinforced. Thus, with the exception of PMMA/PVDF blends (primarily used for coatings), there are no miscible blends on the market. The interest in miscible polymer blends is for the purpose of compatibilization and judicious selection of the processing conditions that may lead to the spinodal decomposition-type morphology (see ▶ Chap. 8, "Morphology of Polymer Blends" in this handbook).

Immiscibility dominates polymer blends. It reveals itself as opacity, delamination, double glass transition, or combination of these properties. Most immiscible polymer blends require compatibilization and toughening.

Owing to low values of the combinatorial entropy mixing, miscibility in polymer–polymer systems requires the existence of strong specific interactions between the components, such as hydrogen bonding (Olabisi et al. 1979; Solc 1982; Walsh and Rostami 1985; Utracki 1989). The thermodynamic characterization of the interactions in miscible polymer blends has been the subject of extensive studies (Deshpande et al. 1974; Olabisi 1975; Mandal et al. 1989; Lezcano et al. 1992, 1995, 1996; Farooque and Deshpande 1992; Juana et al. 1994).

Based on the Huggins–Flory theory, the polymer–polymer interaction parameter, χ_{12}, has been used to describe interactions between the two components. As a consequence, this "parameter" takes into account the enthalpic and non-combinatorial entropy of mixing contributions. Calorimetry, differential scanning calorimetry (DSC), Fourier transform infrared spectroscopy (FTIR), inverse gas chromatography, microscopy, etc., are used to investigate the miscibility and morphology of the blends (Zhong and Guo 1998; Lezcano et al. 1998). Comprehensive surveys of miscible polymer systems along with various methods of miscibility determination have been published (Olabisi et al. 1979; Utracki 1989; Coleman et al. 1991).

10.3.5.5 Other Factors

Temperature strongly influences the impact behavior of toughened plastics. Charpy impact energy measurements at different temperatures in the case of HIPS containing various concentrations of PBD showed two transitions, at 233 and 273 K (Bucknall 1988). At these temperatures, the material exhibited transitions from brittle to semi-ductile and then to ductile.

Newman and Williams (1978) carried out sharp-notch Charpy tests for ABS at $193 \leq T(K) \leq 333$ and showed that linear elastic fracture mechanics was applicable only up to 233 K. Above 273 K, the energy absorbed in impact was proportional to the fracture area and correlated well with the volume of the whitened zone. Mixed behavior occurred at the intermediate temperatures. More detailed study of the notched Izod impact behavior of ABS was carried out using instrumented

tests (Rink et al. 1978). The authors found that the force at peak load, F_m, decreased slowly with increasing temperature from 133 to 353 K; increased by a factor of two between 193 and 273 K; and then decreased again.

Because of the oxidative degradation of the main-chain double bonds, the plastics toughened by diene-type elastomers (e.g., PBD or other rubbers) are susceptible to aging. The UV radiation breaks the chemical bonds, initiating chain reactions in which the polymer is attacked by the atmospheric oxygen, becoming cross-linked or chemically degraded. Embrittlement of the surface has a similar effect to the introduction of a sharp crack. The effects are clearly seen in Charpy and Izod impact tests. Although the subsurface polymer is unaffected by the aging, a crack initiated at the surface can accelerate throughout the degraded layer and cause low-energy fracture of the specimen (see ▶ Chap. 14, "Degradation, Stabilization, and Flammability of Polymer Blends").

Geometry of a toughened plastic specimen also influences the impact strength and its mode of failure. The specimen's length, width, and thickness may affect the fracture behavior. Whether the specimen is notched or not, as well as the dimensions of the notch, may also influence the impact behavior (Kinloch and Young 1983). As discussed above in Sect. 10.3.3, "Fracture Mechanics Testing" – it is important to determine the material parameters (the initiation and the propagation energies) using the specimen geometry that reduces the effects of geometry to an acceptable level.

10.4 Miscibility and Solubility

10.4.1 Miscibility in Polymer Blends

Since physical properties of polymer blends are influenced strongly by blending conditions and processes that, in turn, affect the level of mixing of the blends, there is a growing interest in studying the miscibility and phase behavior of polymer blends. The most important factor leading to miscibility in low molecular weight materials is the combinatorial entropy contribution which is very large compared to high molecular weight polymers. For miscibility to occur, ΔG_m must be smaller than 0.

The properties of polymer blends are determined mainly by the miscibility of the components and structure. The miscibility of polymer blends is generally believed to originate from the specific interactions between polymers. The miscibility has been widely used to describe multicomponent polymer blends whose behavior is similar to that expected of a single-phase system. Many attempts have been made for the understanding of the miscibility of polymer blends, in which the determination of the crystallization behavior and the thermodynamic interaction between polymers are of central importance. Usually thermodynamic miscibility and homogeneity can be attained when the free energy of mixing, ΔG_m, is negative. (A more detailed discussion is available in ▶ Chap. 2, "Thermodynamics of Polymer Blends.")

The term ΔG_H has been used to describe all types of specific interactions (hydrogen bonding, ion–ion, ion–dipole, charge transfer, electron interactions, etc.) that provide negative contribution to the free energy of mixing. The interactions of

the van der Waals type are accounted for by the $\chi'_{12}\phi_1\phi_2 \geq 0$ term with χ'_{12} given by Hildebrand's solubility parameter (Hildebrand 1964).

Hildebrand pointed out that the order of solubility of a given solute in a series of solvents is determined by the internal pressures of the solvents. Later, Scatchard introduced the concept of "cohesive energy density" into Hildebrand's theories. The solubility parameter is a numerical value that indicates the relative solvency behavior of a specific solvent. It is derived from the **cohesive energy density** of the solvent, which in turn is derived from the **heat of vaporization.** In 1936 Joel, H. Hildebrand proposed the square root of the cohesive energy density as a numerical value indicating the solvency behavior of a specific solvent:

$$\delta = \sqrt{c} = \left(\frac{\Delta H - RT}{V_m}\right)^{\frac{1}{2}} \tag{10.19}$$

Hildebrand and Scott and Scatchard proposed that the enthalpy of mixing is given by

$$\Delta H_{\mathrm{m}} = V_{\mathrm{mix}}\left[\left(\frac{\Delta E_1^{\mathrm{V}}}{V_1}\right)^{\frac{1}{2}} - \left(\frac{\Delta E_2^{\mathrm{V}}}{V_2}\right)^{\frac{1}{2}}\right]^2 \Phi_1\Phi_2 \tag{10.20}$$

where V_{mix} is the volume of the mixture, ΔE_i^{V} is the energy of vaporization of species i, V_i is the molar volume of species i, and Φ_i is the volume fraction of i in the mixture. $\Delta E_{\ 1}^{\ V}$, i is the energy change upon isothermal vaporization of the saturated liquid to the ideal gas state at infinite volume.

The heat of mixing must be smaller than the entropic term ΔGm for polymer–solvent miscibility ($\Delta Gm \leq 0$). Therefore, the difference in solubility parameters (∂_1–∂_2) must be small for miscibility or dissolution over the entire volume fraction range (Grulke et al. 1999).

The effect of polymer–polymer interactions on the miscibility and macroscopic properties of PVC/PMMA, PVC/PS, and PMMA/PS blends were studied and the miscibility of the components was characterized by the Flory–Huggins interaction parameter or by quantities related to it by Fekete et al. (Fekete et al. 2005). The comparison of interaction parameters determined by different methods indicates that PVC and PMMA are nearly miscible, while PS is immiscible either with PMMA or with PVC at all compositions. Flory–Huggins interaction parameters calculated from equilibrium methanol uptake (χ'_{12}) are plotted as a function of composition in Fig. 10.24. The negative values obtained for the PVC/PMMA blends hint at complete miscibility, although χ'_{12} depends on composition which indicates limited miscibility. The positive interaction parameters determined for the PVC/PS and PMMA/PS blends suggest immiscibility.

The influence of chemicals and solvents on a polymer blend depends on the nature of solvent and the blend components, as well as on morphology of the blends. The chemical/solvent resistance of an amorphous polymer is improved by the presence of semicrystalline polymer(s). For the best solvent resistance, the latter

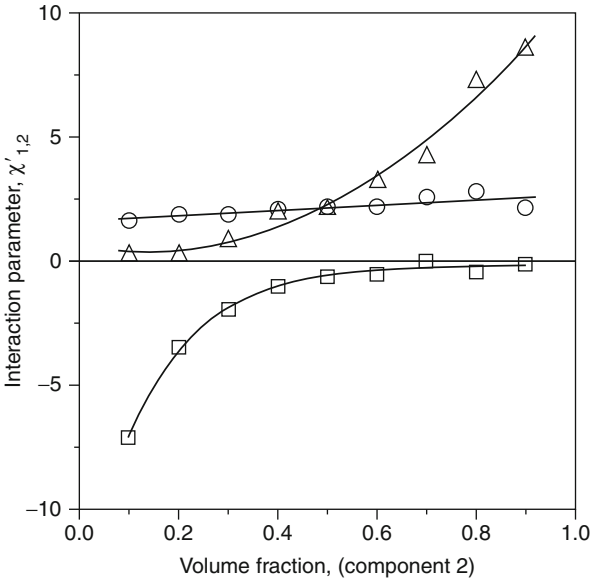

Fig. 10.24 Relationship between composition and the Flory–Huggins interaction parameter determined from equilibrium solvent uptake; (□) PVC/PMMA, (○) PMMA/PS, (Δ) PVC/PS; component 2: PMMA in PVC/PMMA, PS in PMMA/PS, and PVC/PS blends (Fekete et al. 2005)

polymers should be the matrix. The semicrystalline polymers such as PA, POM, PBT, or PET contribute to the solvent and chemical resistance, high processability, and rigidity, while amorphous polymers (ABS, PC, and PSF) provide impact strength and elongation and often the cost reduction.

10.4.2 Solubility Parameter/Prediction of Miscibility

According to the solubility parameter approach at predicting compatibility, two polymers mix well if the difference in the pure component solubility parameter is small. In polymer systems where the interactions are dominated by the van der Waals forces, solubility is favored by chemical similarity of solvent and polymer. Molecular weight, chain branching, and cross-linking of individual polymers slightly influence the solubility parameter (for more details see ▶ Chap. 2, "Thermodynamics of Polymer Blends," Sect. 2.6.2.3).

For polymer molecules, the solubility parameter (δ) is best calculated using the table of molar attraction coefficients. Here, E is given as

$$\delta = e \Sigma \frac{E}{M} \tag{10.21}$$

where E is summed over the structural units of the polymer, M the "polymer" molecular weight, and "e" is the density.

In coating and in rubber industry, the solubility approach is used respectively to select the solvent or to study swelling of the cured rubber by solvents. The

approach was also useful in calculating the effects of pressure and temperature on free energy of mixing. However, the predictions with the Hildebrand solubility parameters are made in the absence of any specific interactions, especially hydrogen bonds. They also do not account for the effects of morphology (crystallinity) and cross-linking. In addition, there may be (non-ideal) changes with changes in temperature and, in many cases, with changes in concentration. Polymer blends with specific interaction include PMMA/PEO, PVAc/PEO, etc.

In a strict sense, the molecular interactions should be nonspecific, without forming associations or orientation, hence not of the hydrogen or polar type.

The solubility parameter approach is applicable to amorphous polymer systems. Highly crystalline polymers, viz., PE or PTFE, are insoluble at room temperature, but they obey the solubility principles at $T \geq 0.9\ T_m$, i.e., at temperatures not more than 10 % (in Kelvin) above their melting temperature.

The biggest drawback of the solubility parameter approach has been the omission of the specific and entropic interactions effects.

10.4.3 Binary Interaction Parameters

The binary interaction generally refers to the interactions between polymer–polymer and polymer–solvent. The nature of solvent–polymer interaction plays an important role in the miscibility of blends. Many thermodynamic properties of polymer solutions such as solubility, swelling behavior, etc., depend on the polymer–solvent interaction parameter (χ). The quantity was introduced by Flory and Huggins. Discussions of polymer miscibility usually start with Flory–Huggins equation for free energy of mixing of a blend (refer to ▶ Chap. 2, "Thermodynamics of Polymer Blends").

The Flory–Huggins theory is widely used still and has been successful, largely, in describing thermodynamics of polymer solutions.

It is also important to note that the Flory–Huggins is a mean-field theory (for the use of the formulation of the change in internal energy due to mixing).

The miscibility of ethylene–styrene copolymer blend was studied by the help of interaction parameters by Chen et al. (2001). They proposed that the interaction parameter for a blend of copolymers is a linear combination of the individual parameters. The nature of the polymer–solvent interaction plays an important role in deciding the influence of chemical and solvent effect on blends. For a compatible amorphous/crystalline blend, the Nishi–Wang equation (Nishi and Wang 1975) is commonly used to determine the polymer–polymer interaction parameter from the melting point depression experiments. Nishi and Wang equation is based on Flory–Huggins theory. The method involves a comparison of the equilibrium melting point of a neat semicrystalline polymer to that of the same polymer in blends of different compositions. For a binary mixture of two relatively high molecular weight polymers, one semicrystalline and one noncrystalline, Nishi and Wang showed that

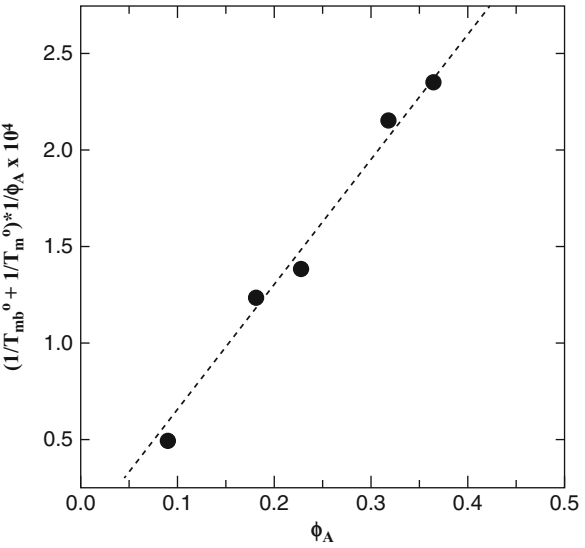

Fig. 10.25 Nishi–Wang plot for semicrystalline PSMA14/PCL blends (Gouveia et al. 2011)

$$\frac{1}{T_{mb}^{0}} - \frac{1}{T_{m}^{0}} = -\frac{RV_{Bu}}{\Delta H_{f}^{0} V_{Au}} \chi_{AB} \phi_{A}^{2} \tag{10.22}$$

where T^{0}_{m} and T^{0}_{mb} are, respectively, the equilibrium melting points of the neat semicrystalline component and of the blend containing a volume fraction of amorphous component f. R is the universal gas constant, ΔH^{0}_{f} is the molar heat of fusion, V_{Au} and V are the molar volumes of the amorphous and crystalline units, respectively.

PSMA/PCL blends were analyzed by Gouveia et al. (2011) using Nishi–Wang equation. They plotted $(1/T^{0}_{mb} - 1/T^{0}_{m})$ against ϕ^{2}_{A} and resulted in a straight line with slope proportional to χ_{AB} and zero y-intercept (Fig. 10.25).

10.4.4 Phase Separation Process

In polymer solutions and polymer blends, LCST, UCST, combined UCST and LCST, hourglass, and closed-loop shaped phase diagrams have been found experimentally. These five types of phase diagrams are the most commonly observed phase diagrams in polymer systems. An important role is played by temperature in the phase diagrams according to the equation:

$$T^{*} = \frac{d_1}{d_2} \tag{10.23}$$

Here d_1, d_2 are constant for a particular system. If the signs of d_1 and d_2 are opposite, then T^* is negative, and all miscibility gaps are of one type, for

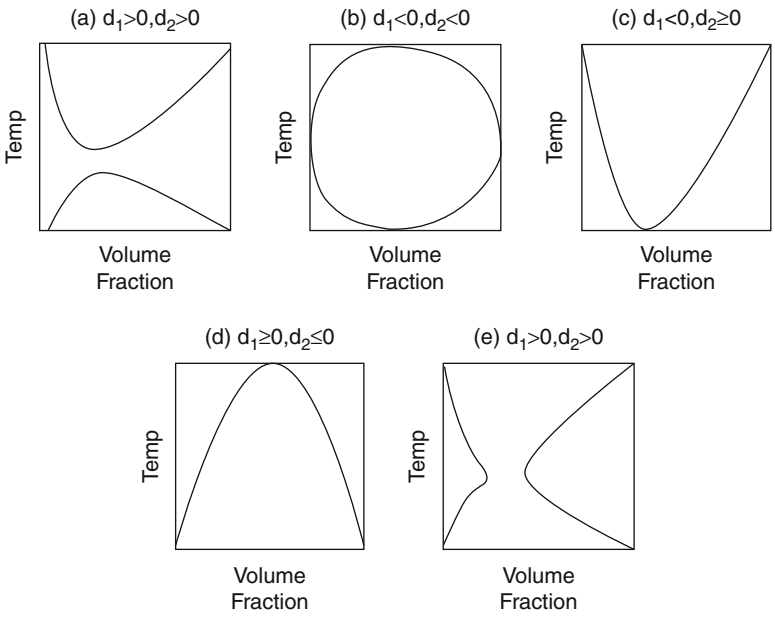

Fig. 10.26 Schematic illustration of types of possible polymer blend phase diagrams, for binary blends where additional complications that can be introduced by competing processes (such as crystallization of a component) are absent. The coefficients d_1 and d_2 refer to a general functional form (as a function of temperature and component volume fractions) of the binary interaction parameter that quantifies deviations from ideal mixing (Courtesy: *Online resources*)

$d_1 > 0$, $d_2 < 0$ yielding exclusively the UCST type. In the opposite case of $d_1 < 0$ and $d_2 > 0$, leading exclusively to the LCST type. However, in the remaining cases where both the coefficients possess the same sign, the temperature T^* is physically important – with $d_1 > 0$ and $d_2 > 0$ (LCST type) for $T > T^*$ but changes to (UCST type) for $T < T^*$, resulting in an hourglass type of phase diagram for lower molecular weights. Finally, for $d_1 < 0$ and $d_2 < 0$, the pattern is switched and the diagram has the form of a closed loop. A simple schematic representation is given above (Fig. 10.26).

Diblock copolymers formed from polystyrene covalently linked to poly(*n*-pentylmethacrylate), P(S-b-*n*PMA), which have only weak segmental interactions, are shown to exhibit closed-loop phase behavior over a narrow range of molecular weight.

Liquid–liquid phase separation of a miscible blend system can occur either during heating (LCST type) or during cooling (UCST type) (Fig. 10.27). A detailed discussion on phase diagrams is presented in ▶ Chap. 2, "Thermodynamics of Polymer Blends."

Phase separation in polymer solutions may proceed either by nucleation and growth (NG) or by spinodal decomposition (SD). Spinodal decomposition is also of interest from a more practical standpoint, as it provides a means of producing a very

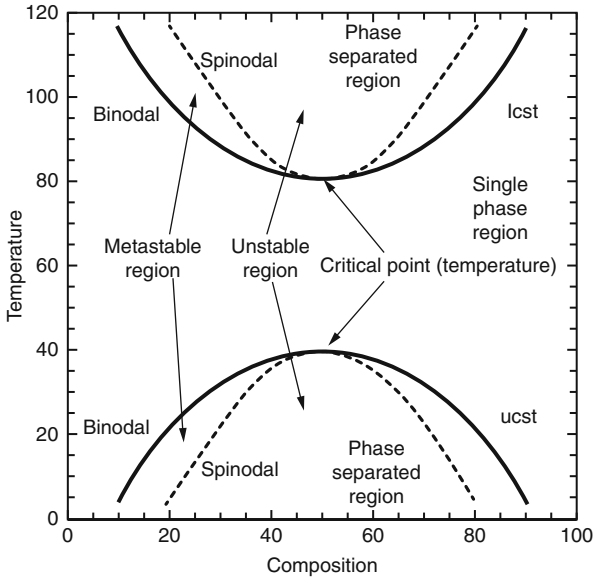

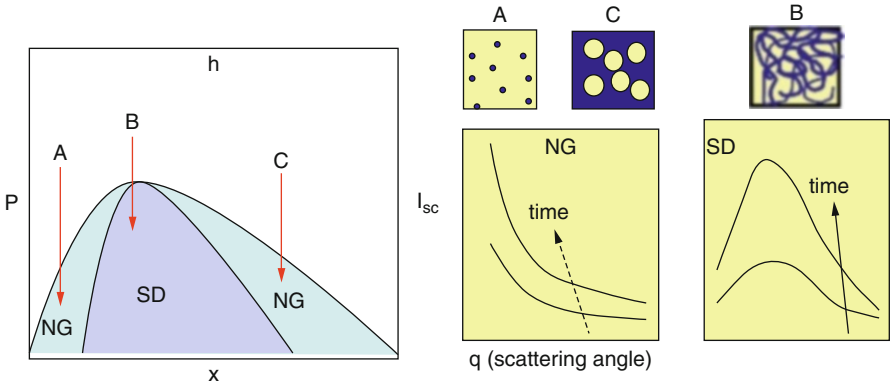

Fig. 10.27 Phase diagram showing LCST and UCST behavior for polymer blends (Courtesy: *Online resources*)

Fig. 10.28 Schematic illustration of the metastable (nucleation and growth) and unstable (spinodal decomposition) domains in polymer solutions and consequences of pressure quench at different polymer concentrations (Courtesy: *Online resources*)

finely dispersed microstructure that can significantly enhance the physical properties of the material. Nucleation and growth is the phase separation mechanism in the metastable regions which are schematically illustrated in Fig. 10.28 which shows the phase boundaries for a polymer solution in term of the miscibility pressures (or demixing pressures) at a given polymer concentration x.

A simple representation of the two mechanisms is given in Fig. 10.29.

The phase boundaries and the kinetics of phase separation of polymer blends are very rich areas of investigation, with, additionally, important technological applications.

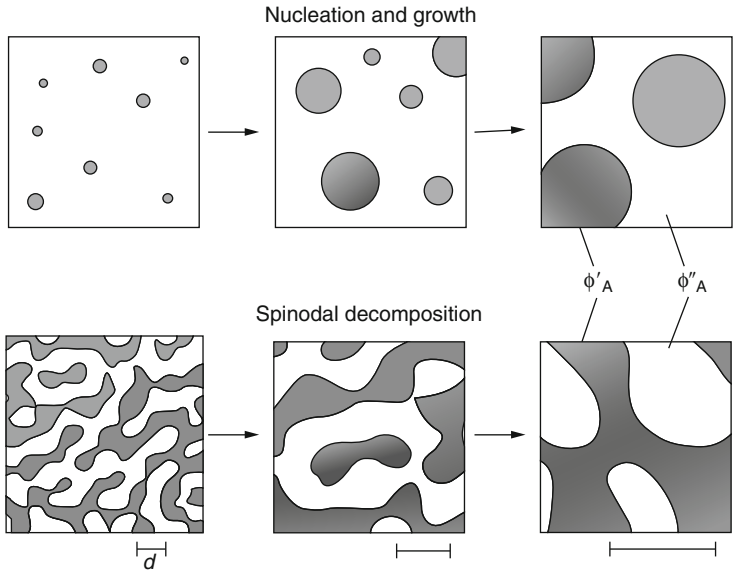

Fig. 10.29 Nucleation and growth and spinodal decomposition patterns in binary blends (Longjian Xue et al. 2012)

Figure 10.30 shows schematically the variation of the free energy of mixing, ΔG_m, with composition for a typical high molecular weight binary polymer blend and the corresponding phase diagram. The binodal denotes the limits of miscibility and is determined by the points of common tangent to the free energy curve, where the chemical potentials of the two coexisting phases will be equal. The spinodal denotes the limits of metastability of the system where the curvature changes from positive to negative and the second derivative of ΔG_m is zero. Inside the spinodal, the system is unstable to all concentration fluctuations and the blend spontaneously separates into coexisting phases via the process known as spinodal decomposition.

When mixing, most of the polymer mixtures get phase separated. Consider the example of polystyrene and polybutadiene. Mixing these two polymers results in an immiscible blend. When polystyrene is mixed with a small amount of polybutadiene, the two polymers will not blend; instead the polybutadiene will separate from the PS into little spherical blobs.

The determination of phase separation in partially miscible polymer blends by means of thermal analysis is often difficult because of the small demixing enthalpy and the slow rate of the diffusion-controlled process. Dreezen et al. (2001) studied the phase separation of PEO/PES and PEO/Aramid blends by optical microscopy, conventional DSC and MTDSC. The onset of phase separation from optical microscopy corresponds very well to the onset of a small stepwise increase in the MTDSC heat capacity (Fig. 10.31).

Phase separation process takes place in a number of ways. It may be thermally induced, reaction induced, crystallization induced, etc. Thermally induced phase

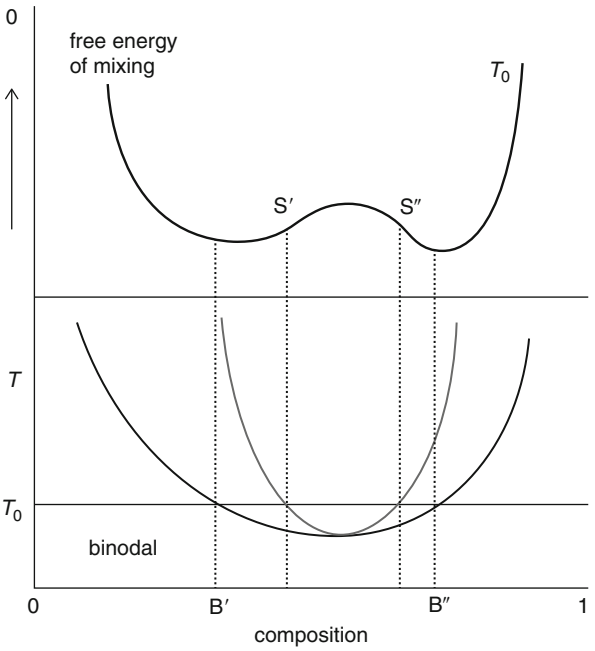

Fig. 10.30 Schematic showing the Gibbs free energy of mixing as a function of composition at a chosen temperature T_0 (*upper panel*). Given in the *lower panel* is the corresponding phase diagram showing the binodal (*outer*, *dark grey*) and spinodal (*inner*, *light grey*) curves; marked are the binodal and spinodal compositions at T_0 (B′, B″ and S′, S″) which are related to the features) (Courtesy: *Online resources*)

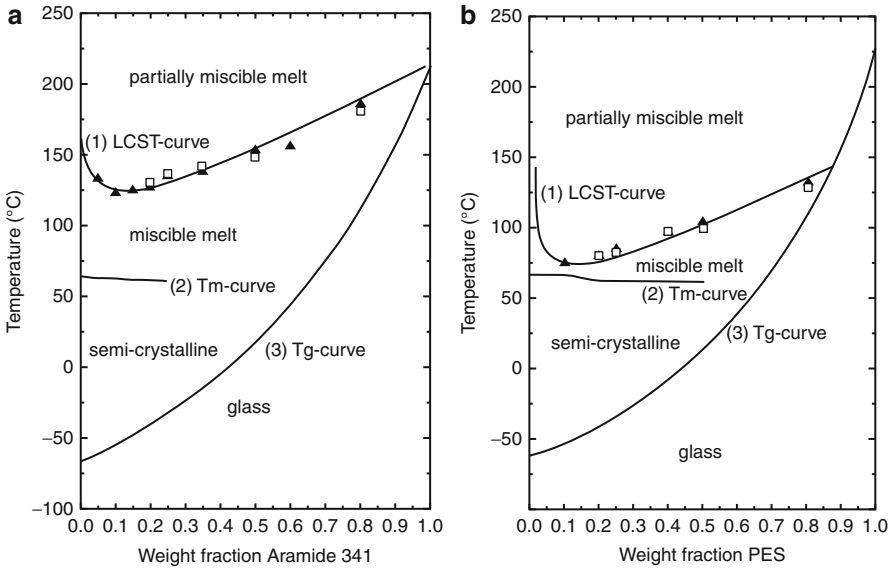

Fig. 10.31 Phase diagram of (**a**) PEO/Aramid and (**b**) PEO/PES blend system (▲) cloud point determined by optical microscopy, (□) onset of demixing obtained by modulated differential scanning calorimetry (Dreezen et al. 2001)

separation process is based on the phenomena that the solvent quality usually decreases when temperature is decreased. After demixing is induced, the solvent is removed by extraction, evaporation, or freeze-drying. The reaction-induced phase separation can be investigated by different observation techniques such as time-resolved small-angle light scattering (TRSALS), optical microscopy (OM), differential scanning calorimetry (DSC), digital image analysis (DIA), etc.

The phase separation process of blends has been studied by a number of researchers. Chaleat et al. investigated the phase separation of plasticized starch/PVA blends (Chaleat 2012) blends of vinylidene fluoride/trifluoroethylene copolymer and poly(1, 4-butylene adipate) was studied by Kap Jin Kim and Kyu (Kim and Kyu 1999). Fully biodegradable blends of poly(butylene succinate) and poly (butylene carbonate) and its phase behavior were studied by Wang (2012).

10.4.5 Factors Affecting Miscibility and Solubility

Miscibility can be influenced by various factors such as crystalline phase, intermolecular interaction, and reduction of surface tension.

10.4.5.1 Effect of Crystallinity

Growing numbers of commercial materials are blends of two or more polymers in which at least one of the components is a crystalline polymer. The crystallization in miscible blends is restricted to temperatures between the blend glass transition temperature and the equilibrium melting point, $T_{m,e}$, i.e., to the crystallization temperature, $T_c < T_{m,e}$. The difference, $D_c = T_{m,e} - T_c$, depends on the cooling rate and the nucleation process. There are three mechanisms of the crystallization nucleation (Utracki 1989):

1. Spontaneous, homogeneous nucleation – it rarely occurs in the supercooled homogeneous melt.
2. Orientation-induced nucleation, caused by alignment of macromolecules, e.g., in extensional flow field.
3. Heterogeneous nucleation on the surface of a foreign phase.

In thermoplastic blends (2) and (3) are most important mechanisms.

Miscible crystalline/amorphous polymer blends such as PLA/PVC blends have been widely investigated, and oriented crystallization has also been applied to some miscible crystalline/amorphous polymer blends. For miscible blends containing semicrystalline polymers, analysis of the melting point depression is widely used to estimate the Flory–Huggins interaction parameter (χ).

It has been known for more than a century that impurities reduce the melting point. This observation has been used to determine the molecular weight of the contaminant by Raoult. Nearly a hundred years later, this concept was used to calculate the thermodynamic binary interaction parameter $\boldsymbol{\chi}_{12}$ from a melting point depression of a crystalline polymer in miscible blend with low concentration of another polymer. The relation is popularly used in the simplified form for very high molecular weight components (Nishi and Wang 1977):

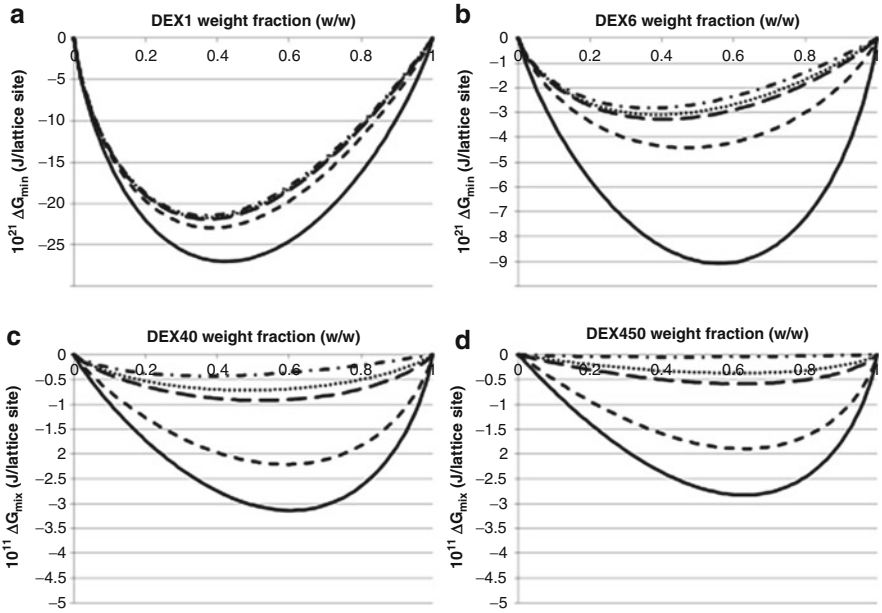

Fig. 10.32 Entropic part of the free energy of mixing per lattice site as a function of DEX weight fraction (w/w): (**a**) DEX1 systems, (**b**) DEX6 systems, (**c**) DEX40 systems, and (**d**) DEX450 systems. Key: PVP12 (*solid*), PVP 17 (*short dash*), PVP25 (*long dash*), PVP30 (*dotted*), and PVP90 (*dash-dot*) (van Eerdebbrugh et al. 2012)

$$\frac{T_m}{T_{m,n}} = 1 + \left(\frac{\chi_{12}\,RT}{V_1}\right)\left(\frac{V_2}{\Delta H_m}\right)\phi^2 \tag{10.24}$$

where T_m is the melting point of crystalline polymer in miscible blend, $T_{m,n}$ is melting point of crystals of neat polymer, V_i is molar volume, and ΔH_m is the heat of fusion. But the determination of the experimental melting points using DSC or optical microscopy and substituting those values in the above equation gives erroneous values for χ.

10.4.5.2 Effect of Molecular Weight

It is well known that polymer molecular weight is a key factor that influences miscibility. Thus, by changing molecular weights of the polymers, systems with variable miscibility characteristics but virtually constant chemical composition potentially can be obtained. Bernard Van and Lynne Taylor applied this to their study and they took dextran and Maltodextrin with PVP (van Eerdebbrugh et al. 2012). Depending on the molecular weights used to prepare DEX-PVP blends, miscibility can vary from completely miscible to virtually immiscible. The higher the combined polymer molecular weight, the lower the miscibility of the resultant blends (Fig. 10.32).

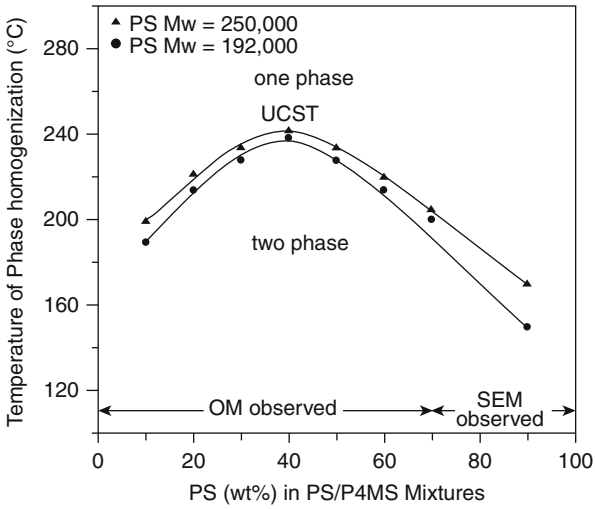

Fig. 10.33 Phase homogenization temperature of the PS/P4MS blend system of (I) PS Mw = 192,000, (II) 250,000 g/mol, both as a function of composition. UCST (*critical point*) is also indicated (Chang and Woo 2001)

Polymer blends (like low molecular weight solvents) can exhibit miscibility or phase separation and various levels of mixing in between the extremes (e.g., partial miscibility). The most important factor leading to miscibility in low molecular weight materials is the combinatorial entropy contribution which is very large compared to high molecular weight polymers. This contribution is the reason that solvent–solvent mixtures offer a much broader range of miscibility than polymer–solvent combinations. The range of miscible combinations involving polymer–polymer mixtures is even much smaller. As an example compare the miscibility of hexane–ethanol mixtures with their high molecular weight analogs of polyolefins and poly(vinyl alcohol). The former is miscible, whereas the latter is highly immiscible.

Phase behavior of blends of polystyrene with poly(4-methylstyrene) has been studied by Chang and Woo (2001). Their study clearly indicates that an increase of molecular weight leads to a reduction in the entropic contribution to the Gibbs free energy of mixing, which is less favorable for miscibility (Fig. 10.33).

10.4.5.3 Effect of Copolymerization

In blends of random copolymers, or in blends of a polymer with random copolymer, the presence of repulsive forces among segments (other than specific interactions discussed before) may lead to miscibility (Wang et al. 2006). The effect of ethylene–styrene content on the miscibility and cocrystallization was studied extensively by Chen (2001). They showed that the miscibility of the system depends only on the comonomer content with composition expressed as weight fraction. Based on the experimental observations, they constructed a miscibility map for binary blends (Fig. 10.34).

The transition from miscibility to immiscibility occurs over a very small change in styrene content; which (difference from 9 to 11 wt%) is sufficient to change the system from miscible to immiscible for copolymers of this molecular weight.

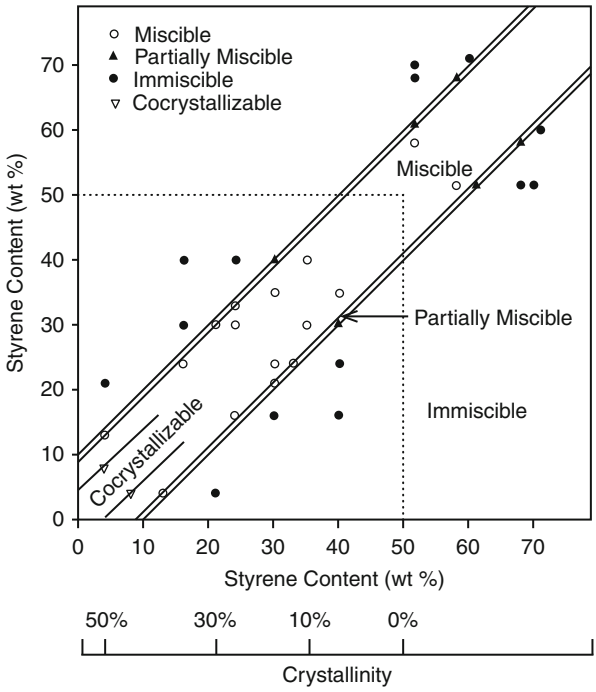

Fig. 10.34 Miscibility map of ethylene–styrene copolymer blends (Chen 2001)

It has been found in the study of PVME and SBS triblock copolymer that solubility of PVME in PS block copolymer domains is larger than in PS homopolymer. This may indicate that the mixing enthalpy has an effect on the blend miscibility. The behavior has been attributed to the effect of PB segments in SBS. The phase equilibriums and miscibility in polymer blends containing random or block copolymer were reviewed. The solubility and miscibility of homopolymer/copolymer blends has been studied by Jiang and Xie (1991). They proposed that when increasing the amount of homopolymer A to the ordered state of block copolymer AB, initially the homopolymer will be dissolved in the microdomains of the block A of the copolymer until the solubility limit is reached beyond which macroscopic phase separation occurs. Results show that the solubility limit depends upon the relative lengths of the block copolymer and the corresponding homopolymer. The dependence of copolymer content on the miscibility of PMMA/SAN blend showed that the transition from miscibility to immiscibility increases with increase in AN copolymer content (Cameron 2002).

10.4.5.4 Effect of Solvents

The solvent effects on polymer blends can be estimated using the solubility parameter δ. The concept was originally used to characterize the strength of interactions in simple liquids, but later it was extended to polymer/polymer as well as polymer/solvent systems. Certain factors, such as structure, composition, and nature of the

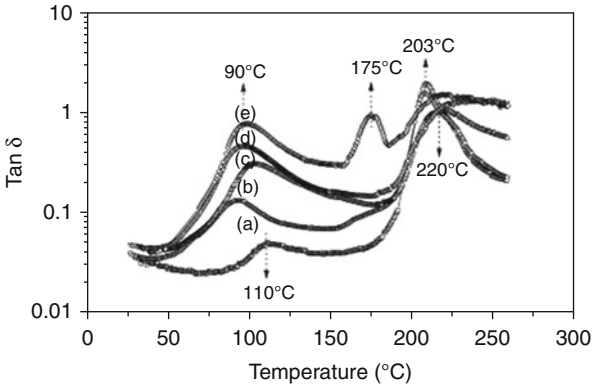

Fig. 10.35 Tan δ of SF/PVA blend films cast from aqueous solution of various blend ratios: (**a**) 100/0, (**b**) 70/30, (**c**) 50/50, (**d**) 30/70, and (**e**) 0/100 (Um and Park 2007)

copolymer, influence the solvent effect. Chemical structure of polymers constituting the blend determines its solvent resistance. The polymers, having the backbone linkages involving oxygen, sulfur, and silicone exhibited enhanced chemical and solvent resistance. Thus, enhanced chemical and solvent resistance has been reported for polymer blends that comprise polymers with ether, thioether, oxymethylene linkages, siloxane and/or imide groups, fluorine, certain block polymers, etc.

The structure of repeat units of individual polymers constituting a blend and the nature of interactions between polymers in a blend are the factors that influence solubility characteristics of a blend. Thus, solubility is affected by cross-linking, hydrogen bonding, formation of donor–acceptor complexes, dipole–dipole interactions, ion–dipole interactions, ion–ion interactions, and segmental interactions.

The effect of casting solvent on the miscibility behavior of silk fibroin/PVF blends was investigated by Um et al. SF/PVA blend films cast from aqueous and formic acid solution. The β-sheet conformation of SF formed by formic acid casting was retained for all SF blends regardless of blend ratio. SF/PVA blends from aqueous solution exhibited a phase-separated morphology and immiscibility by SEM observation and DMTA (Dynamic Mechanical Thermal Analysis) measurement (Um and Park 2007) (Figs. 10.35 and 10.36).

Wu et al. (1997) used the DSC method to study the crystallization behavior of the PVAc/PEO blends using two solvents of chloroform and benzene. They observed that the crystallization of PEO was more suppressed in benzene (Fig. 10.37).

10.4.5.5 Effects of Compatibilizers and Interface Modification

A common method to enhance poor miscibility of two components in a blend is to add a third component to the blend that will have a favorable interaction with the precursor polymers. This third component, often termed a compatibilizer, is designed with the hope it will favorably affect the blend system by potentially changing a miscibility window, strengthening phase-separated domains, or by affecting the kinetics of phase separation thus causing a change in the phase-separated morphology.

A compatible blend is mixture of polymers with low repulsive forces between phases. Compatibilization is referred to any physical or chemical method that

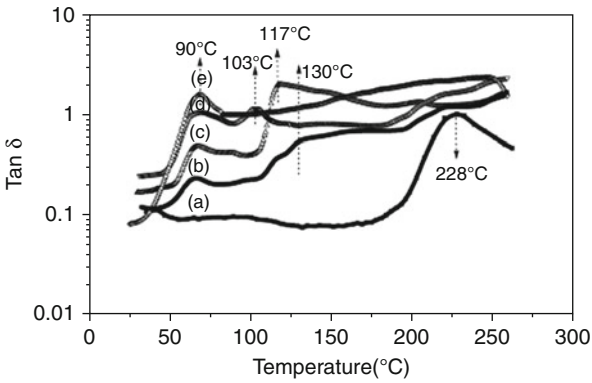

Fig. 10.36 Tan δ of SF/PVA blend films cast from formic acid solution of various blend ratios: (**a**) 100/0, (**b**) 70/30, (**c**) 50/50, (**d**)30/70, and (**e**) 0/100 (Um and Park 2007)

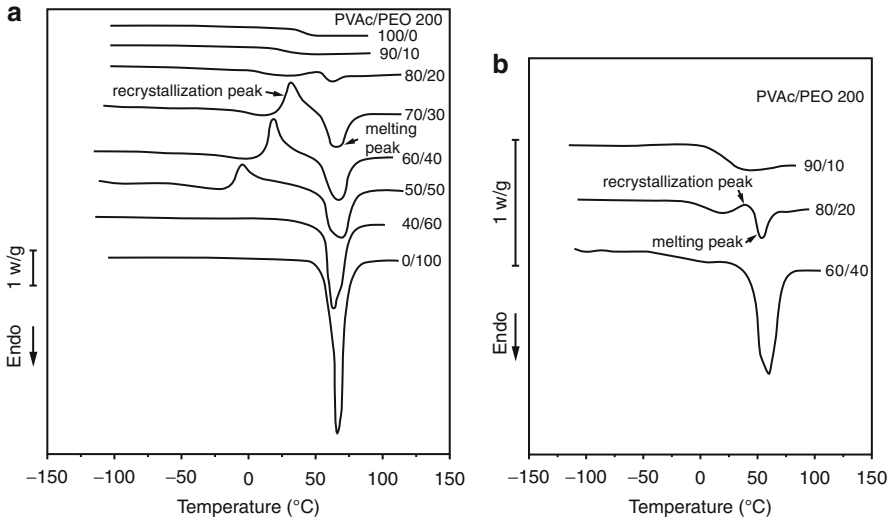

Fig. 10.37 DSC thermograms of (**a**) PVAc/PEO200 blends cast from chloroform and (**b**) benzene (Wu et al. 1997)

results in stabilization (prevention to separate) of polymer blends morphology and properties. Polymer blends are used to change impact or flex properties, chemical resistance, thermoformability, and printability, for example. Some properties of the compatibilized blend exceed that of either component alone. Compatibilizers act through a chemical reaction (reactive compatibilization) or through intermolecular forces of attraction such as van der Waals, hydrogen bonding, based on polarity of the materials (nonreactive compatibilization). In addition, a compatibilizer may function by more or less the same mechanism as a surfactant does to stabilize oil/water mixture, i.e., by being soluble in one or both major

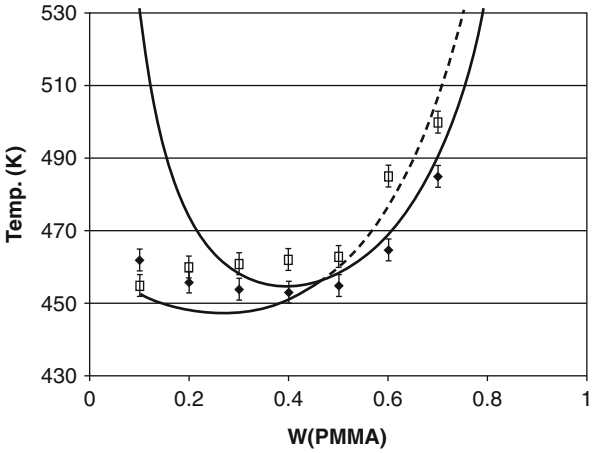

Fig. 10.38 Qualitative comparison between the theory and the experimental phase diagram (*cloud points*) for the PVA/PMMA polymer blend without fillers (*filled diamonds*) and with 10 wt% fumed silica (*open squares*). The *two curves* correspond to the spinodals calculated using equations. It is assumed that both PVA and PMMA had degrees of polymerization (N) 1,000 and that (øN) a + bT, with (a)-10.0, (b) 0.026374. Finally, assumed that (F) 0.65. For the filled system, we took nanoparticle loading of 14 vol%, with the dimensionless particle radius (R) 20 (corresponding to the [a]real[o] particle radius of 10 nm) (Ginzburg 2005)

components of the blend. One such mechanism is by attaching itself to one of the blend components through chemical grafting and leaving a polymeric "tail" that is soluble in the other component.

Most polymers are not miscible and those having closely similar solubility parameter values are likely to be compatible. Two incompatible polymers can be compatibilized by the presence of a third component, which results in a good improvement in the physical and mechanical properties of the blend. The effect of the polyacrylonitrile compatibilizer, on the miscibility and properties of NBR/SBR blends, has been studied by Darwish et al. (2005).

Nowadays, nanoparticles have been widely used as fillers and compatibilizers. They exert certain effect on the miscibility of blends. Ginzburg applied a simple theory to study the effect of nanoparticles on the miscibility of PVA/PMMA blends and compared theoretical and experimental results for the same system with fillers and without fillers (Ginzburg 2005) when nanoparticle radius is smaller than polymer radius of gyration, the addition of nanoparticles increases the critical value of χ_N and stabilizes the homogeneity (Fig. 10.38).

Phase separation of poly(methyl methacrylate)/poly(styrene-co-acrylonitrile) blends in the presence of silica nanoparticles was studied by rheological method by Jianping Gao (2012). Rheology is a frequently used method to determine the phase separation temperature. However, unlike the optical method which can show the phase-separated morphology directly, no visual information can be obtained from rheology (Fig. 10.39).

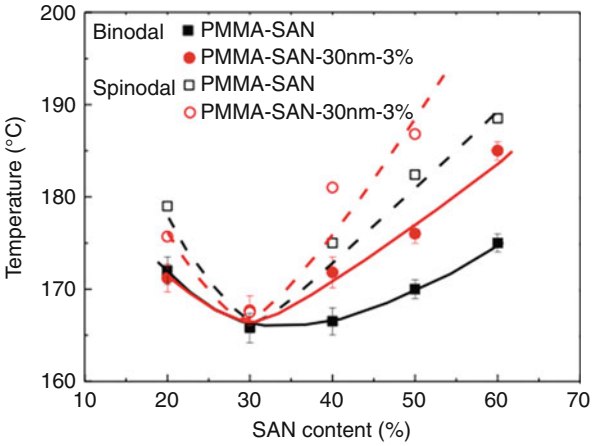

Fig. 10.39 The binodal phase diagram of PMMA/SAN (*solid circles*) and PMMA/SAN/SiO (*solid squares*) by combining the gel-like method and Cole–Cole plot. The spinodal points of PMMA/SAN (*hollow circles*) and PMMA/SAN/SiO (*hollow squares*) are also shown. The *lines* are drawn to guide the eyes (Gao 2012)

10.4.6 Standard Methods of Evaluation of Miscibility, Solubility, and Interaction Parameter

The miscibility behavior of the blends can be determined by various techniques. Glass transition temperature (T_g)-based analysis using differential scanning calorimetry, dynamic mechanical analysis, spectroscopic techniques such as Fourier transform infrared (FTIR) spectroscopy and solid-state nuclear magnetic resonance (NMR), fluorescence spectroscopy, scattering techniques such as small-angle light scattering (SALS) and small-angle X-ray scattering (SAXS), morphology determination by transmission electron microscopy (TEM), scanning electron microscopy (SEM), etc., are the commonly used techniques for the miscibility studies in polymer blends. Each method has its own standard and sensitivity. The specific method used to determine the solubility and miscibility behavior is inverse gas chromatography (IGC); the effect of crystallinity is studied by DSC. The optical microscopy is used to study the spherulitic superstructure of polymer crystals from the melt and explain the relationship between morphology and crystal growth rate. In addition, small-angle light scattering (SALS) and small-angle X-ray scattering (SAXS) are used to study the morphology of crystalline/amorphous polymer blends.

10.4.6.1 Glass Transition Temperature (T_g) Analysis

Thermal methods are useful to study modern polymeric material, usually blends or composites with complex morphologies that are crucial to determining their material properties. The miscibility of polymer blends is often assessed by the measurement of a single glass transition temperature (T_g) as a function of composition. Two T_gs in a DSC thermogram indicates a two-phase system, and a single composition-dependent T_g is often taken as evidence of the formation of a miscible blend.

The differential scanning calorimetry (DSC) is the thermal analysis mainly used to determine a first-order transition (melting) and a second-order endothermic transition (glass transition). DSC has been extensively used for the characterization

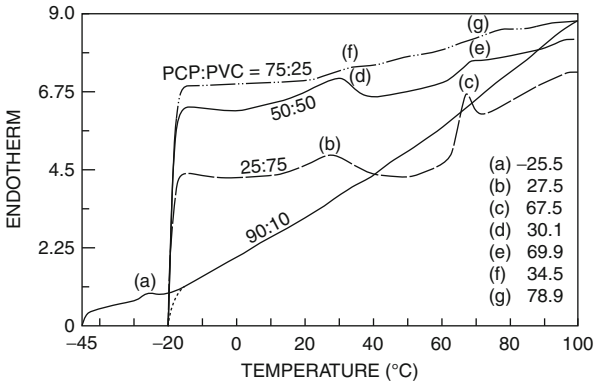

Fig. 10.40 DSC *curves* of PCP–PVC blends of different composition. (*a*)–(*g*) represent T_g of the blends (Saha 2001)

of interchange reactions. Experimentally, the least ambiguous criterion for polymer miscibility is the detection of a single glass transition temperature (T_g), which is intermediate between those corresponding to the two component polymers. Phase separation is judged by the existence of two distinct glass transition temperatures.

The effect of transesterification on the miscibility of the PC–PET blends was studied by Zheng et al. using DSC (Zheng 2004). The binary interaction energies of completely miscible binary pairs that do not phase separate like PPO/PS are studied by small-angle neutron scattering (SANS). The miscibility of PEOx and PVPh blends was investigated by Wang et al. (2001) using FTIR, DSC, high-resolution solid-state NMR, etc. Compatibility of PCP–PVC blends was studied by DSC by Saha (2001). He concluded that the compatibility increases with increase in PCP content (Fig. 10.40). The difference in peaks gradually decreases and at 90 % PCP content merges into single peak.

The phase behavior of blends of TMOS and SAN was investigated by means of optical cloud point measurements and DSC by Pfefferkorn et al. (2012). The blends display partial miscibility with an upper critical solution temperature (UCST). Moreover, the SAN/TMOS blends show pronounced miscibility-window behavior, i.e., the UCST depends strongly on SAN copolymer composition.

DSC technique was used to study polybenzoxazine/poly(ε-caprolactone) blends (Huang 2005), poly([2-oxo-1,3-dioxolan-4-yl]methyl vinyl ether-co-acrylonitrile)/poly(vinyl chloride) blend (Ha et al. 2002), polypropylene/polyethylene binary blends (Wong et al. 2002), etc.

DMA is another technique, which is widely used for the determination of miscibility of polymer blends. Generally for an immiscible blend, the tanδ curves show the presence of two damping peaks corresponding to the T_gs of individual polymers. For a highly miscible blend, the curves show only a single peak in between the transition temperatures of the component polymers, whereas broadening of the transition occurs in the case of partially miscible systems. In the case of miscible or partially miscible blends, the T_gs are shifted to higher or lower temperatures as a function of composition. Perera et al. (2001) studied the miscibility of polyvinyl chloride (PVC)/nitrile butadiene rubber (NBR) and PVC/epoxidized

natural rubber (ENR) blends using DMA. The tanδ curve for PVC/NBR and PVC/ENR blends appeared in between the respective homopolymers, indicating miscibility. The tanδ peaks for the blends were broader than the two homopolymer curves due to some degree of dynamic heterogeneity in the blend. In other words, the blends appeared to be miscible but had a wide range of relaxation times as a result of molecular proximity of the unlike chains.

10.4.6.2 Microscopic Measurements

The liquid–liquid decomposition of a blend of polycarbonate(PC)/polyethylene oxide(PEO) taking place via spinodal decomposition has been studied by optical microscope (Tsuburaya 2004) in Fig. 10.41.

Phase separation may proceed either by nucleation or growth or by spinodal decomposition when the changes in the conditions take the solution into metastable or unstable domains, respectively. Kiran (2009) studied solutions of poly(ε-caprolactone) in acetone/carbon dioxide fluid mixtures.

The structural morphology of a blend is a product of compositional variations formed in the micro-/nanoscales. Atomic force microscopy produces high-resolution images of the sample topography by monitoring the physical displacement of a cantilever interacting with a sample surface. Phase separation is observable in immiscible or partially miscible blends. High-resolution imaging provides useful information pertaining to the domain size and morphological character.

10.4.6.3 Scattering Techniques

Various light-scattering and optical techniques have been investigated as potential candidates for characterization of multiphase polymeric materials. Kinetics of phase separation and dissolution (demixing) of polymer blends, stress whitening process, photon migration in polymer composites, etc., are examined using light-scattering techniques. A light-scattering theory known as the Rayleigh–Gans theory was developed to extend Rayleigh theory to particles that are not optically small. The correction method involves extrapolation techniques that extrapolate light-scattering intensity to zero-scattering angle. This correction technique is important for analyzing results on polymer solutions.

The assessment of miscibility and phase separation conditions is relatively easy and is carried out in many laboratories employing view cells that allow visual or optical observations as phase separation is accompanied by a change in the transmitted light intensity. The assessment of phase separation needs special techniques that allow measurement of the scattered light intensities as a function of the scattering angle and time.

A pattern like the following one is observed after the liquid–liquid phase boundary. The scattered light intensities become brighter in time at all angles (Fig. 10.42).

Direct information on the χ value between blends can be obtained from small-angle neutron scattering (SANS). SANS studies usually involve studies on multiple pairs of deuterated samples, so the effect of deuteration on the interaction parameter can be evaluated quantitatively. Light-scattering techniques can be used to determine the miscibility of PE blends by slowly cooling or heating the blend from the

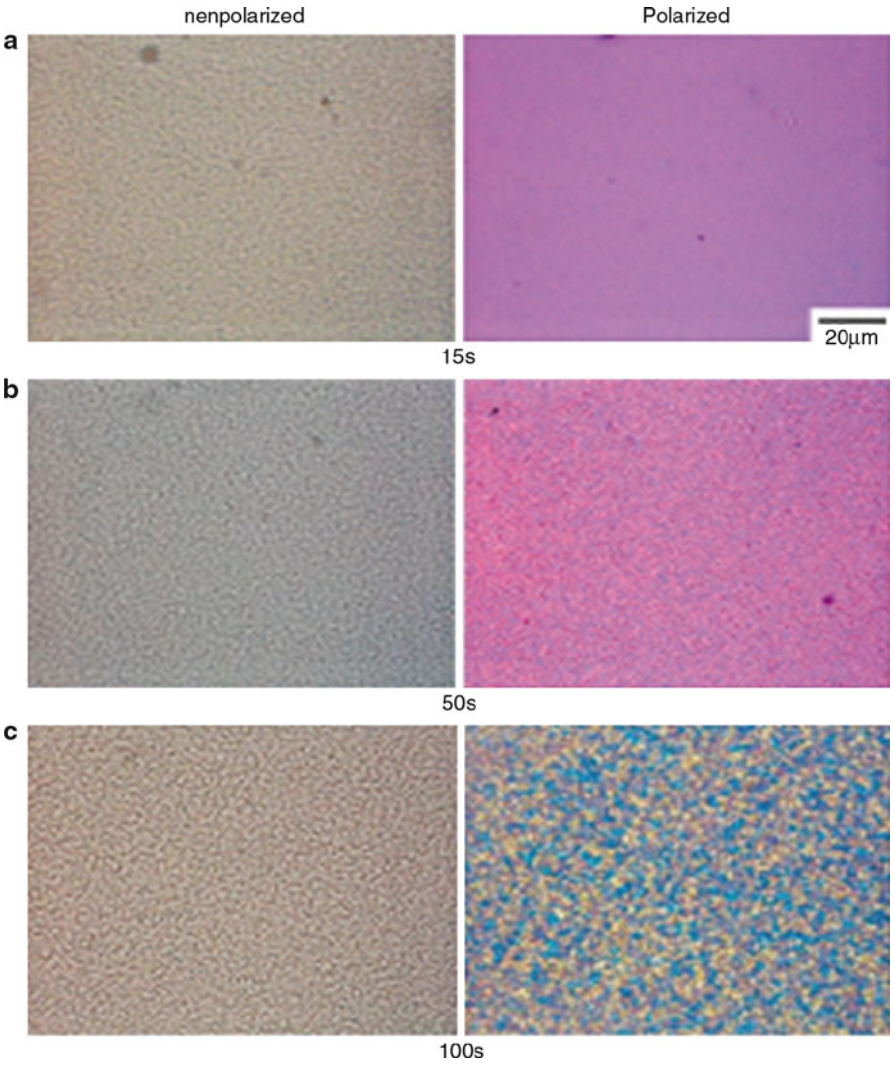

Fig. 10.41 Microscopic observation of the structural development in the 70/30 PC/HM-PEO blend during isothermal annealing at 180 °C. *Left*: unpolarized light. *Right*: polarized light (Tsuburaya 2004)

one-phase region. We can observe the cloud point at which the forward-scattered light intensity increases, indicating the onset of liquid–liquid phase separation.

Akpalu and Ping Peng (Akpalu et al. 2005) studied the melt miscibility of a commercial linear polyethylene and LLDPE system using SANS.

A similar technique called SAXS (small-angle X-ray scattering) is also used to study polymer blends. Small-angle X-ray scattering (SAXS) is a nondestructive scattering technique that records elastic scattering of X-rays at scattering angles

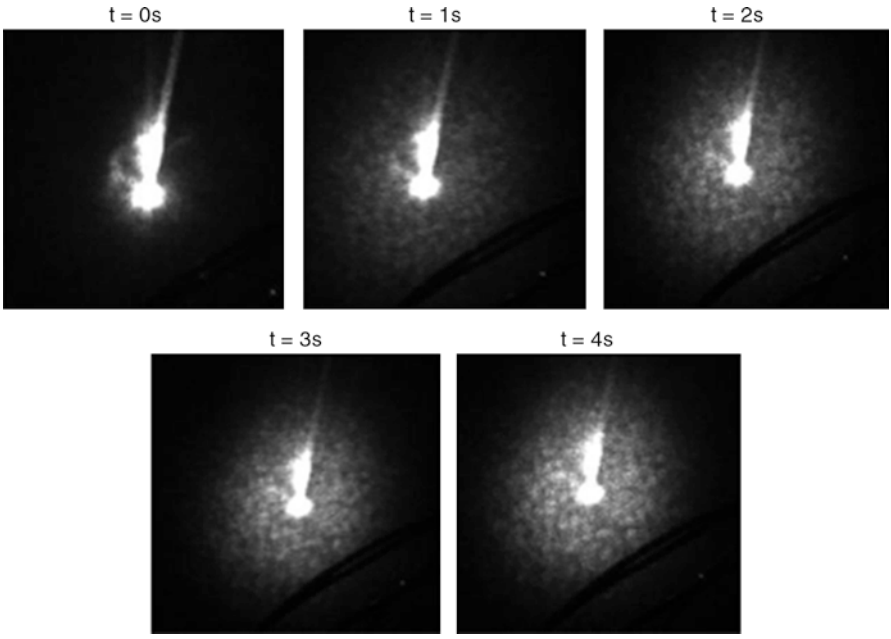

Fig. 10.42 Liquid–liquid phase boundary of blend observed in light-scattering experiment (Courtesy: *Online resources*)

close to the direction of the incident beam. SAXS, due to its q range, often proves useful to study the large structures in binary or ternary blends where one or more components crystallize. Mickiewicz studied extensively the application of SAXS with binary blends of four different high molecular weight poly(styrene-b-isoprene) diblock copolymers with a low molecular weight poly(styrene-b-isoprene-b-styrene) triblock copolymer (Mickiewicz et al. 2008).

Polymerization-induced binodal phase separation in rubber-modified epoxy system containing DGEBA and HTBN during curing was studied using time-resolved SANS. The following figure (Fig. 10.43) shows the pattern during polymerization-induced phase separation (PIPS). The PIPS at 160 °C is much higher (Zhang et al. 1999).

The quantitative analysis of the spectrum is also given. As the time passes from 9 to 11 min, the minimum appeared become closer to the second maxima and finally merged into one to give a broad peak, Fig. 10.44.

The phase separation behaviors of PMMA/SAN blends with and without fumed silica (SiO_2) have been investigated using time-resolved small-angle light-scattering and dynamic rheological measurements. It is found that the effect of SiO_2 on the phase separation behavior of PMMA/SAN blend obviously depends on the composition of the blend matrix (Du et al. 2013).

In the case of polymer blends, refractometric and viscometric methods are used to study the polymer–solvent and polymer–polymer miscibility. It is clear that

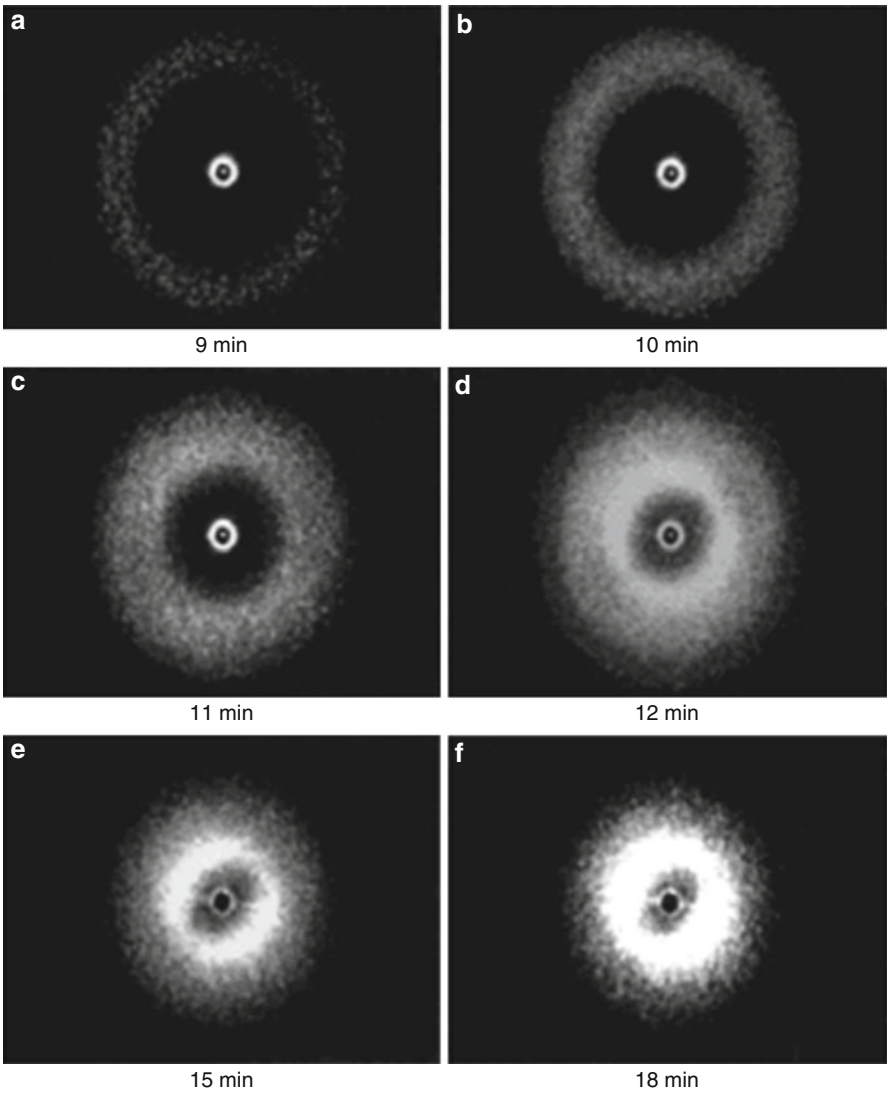

Fig. 10.43 Evolution of light-scattering pattern for the epoxy system cured at 160 °C. HTBN/E-51/MeTHPA/BDMA 5 40/90/70/0.056; (**a**) 9 min, (**b**) 10 min, (**c**) 11 min, (**d**) 12 min, (**e**) 15 min, (**f**) 18 min (Zhang et al. 1999)

behavior of viscosity and refractive index with blend composition is linear for the miscible blends and nonlinear for partially and immiscible blends.

Radhakrishnan and Venkatachalapathy (Radhakrishnan et al. 1996) used the X-ray diffraction to study the crystallization, the PMMA/PEO blends cast from three solvents. The solvent effect is demonstrated from the large differences in the crystallinity values.

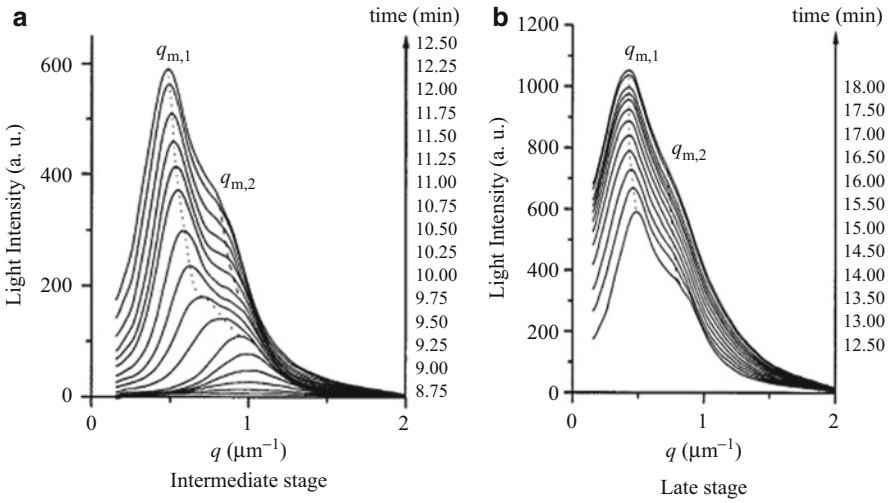

Fig. 10.44 Evolution of light-scattering profile for the epoxy system cured at 160 °C. HTBN/E-1/MeTHPA/BDMA 5 40/90/70/0.056; (**a**) intermediate stage, (**b**) late stage (Zhang et al. 1999)

10.4.6.4 Rheological Measurements

Rheological methods have been frequently used to study the phase separation behavior of partially miscible polymer blends. Rheology is generally sensitive to morphological changes during phase separation. Like optical methods rheological methods are not affected by the transparency of the blend. This method is strongly related to viscoelastic properties of the blend. It is said to have more resolution depending upon the applied oscillatory frequency. Rheological methods are used to get the phase diagram and to study the kinetics and mechanism of phase separation using some empirical rules.

The rheological properties of miscible blends under different temperatures can be obtained from some theoretical models. One such model is the double reptation self-concentration. The DRSC (double reptation self-concentration) model actually includes the temperature dependency and concentration dependency through a complex mixing rule given by the double reptation model and self-concentration model, which helps to exclude the complex contribution from miscible components under different temperatures in the experimental data and only illustrate the effect of the concentration fluctuation and interface formation. This model is applied to study PMMA/SMA (Wei 2011).

The frequency dependent apparent bimodal temperature is shown in Fig. 10.45. In this study, they showed that the storage modulus starts to deviate at the point of phase separation.

The rheological study was also done by Ceren Ozdilek et al. to investigate the thermally induced phase separation of PαMSAN/PMMA blends in presence of functionalized multiwall carbon nanotubes (Ozdilek 2011).

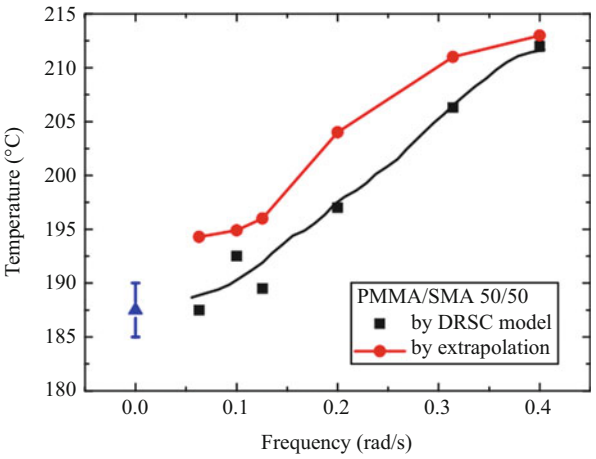

Fig. 10.45 Transition temperature as a function of oscillatory frequency during temperature ramp with a rate 1 °C/min. The triangle point at zero frequency is the transition temperature determined from isothermal frequency sweep (Wei et al. 2011)

10.4.6.5 Inverse Gas Chromatography

Inverse gas chromatography (I_{GC}) has been proven to be useful for the characterization of polymer blends in terms of polymer–polymer interaction parameters, polymer–solute interaction parameters, solubility parameters, molar heat of sorption and mixing, melting point depression as an indicator of miscibility, contact energy parameters, and surface characterization. I_{GC} has the capability of glass transition temperatures as a function of relative humidity. The technique involves creating within a column a stationary phase of the solid material of interest and determining its different physicochemical properties. The glass transition and polymer–polymer interactions are also studied using I_{GC}. Using the T_g detection by I_{GC}, Aouak and Alarifi showed the ability of this technique to study and confirm the miscibility of PBMA/PEO blends (Aouak and Alarifi 2009). It is well known that miscible blends have only one T_g, while immiscible blends have two or more T_g. Retention diagrams are constructed by two probes (solutes): chloroform as a common solvent and heptanes as a common nonsolvent to PBMA and PEO.

The miscibility of binary mixtures of poly(ether imide) (Ultem^{TM}) and a copolyester of bisphenol-A with terephthalic and isophthalic acids (50/50) (Ardel^{TM}) in three compositions (25/50, 50/50, and 75/25) was studied by F. Cakar et al. (2012).

10.4.6.6 Spectroscopic Analysis

Infrared spectroscopy has been widely used to investigate specific interactions in polymer blends in which the miscibility driving force is hydrogen bonding between components. Possibility of hydrogen bonding between hydroxyl groups of PVPh and carbonyl groups of PLLA in the blends of poly(L-lactide) with poly(vinylphenol) was reported by Meaurio et al. (2005). The miscibility and formation of hydrogen bond in the PMMA/CAB blends were studied. The carbonyl frequency of pure PMMA at 1,750 cm^{-1} is reduced to 1,740 cm^{-1} in the 50/50 blend indicating the formation of hydrogen bonding between the component polymers which contribute to the

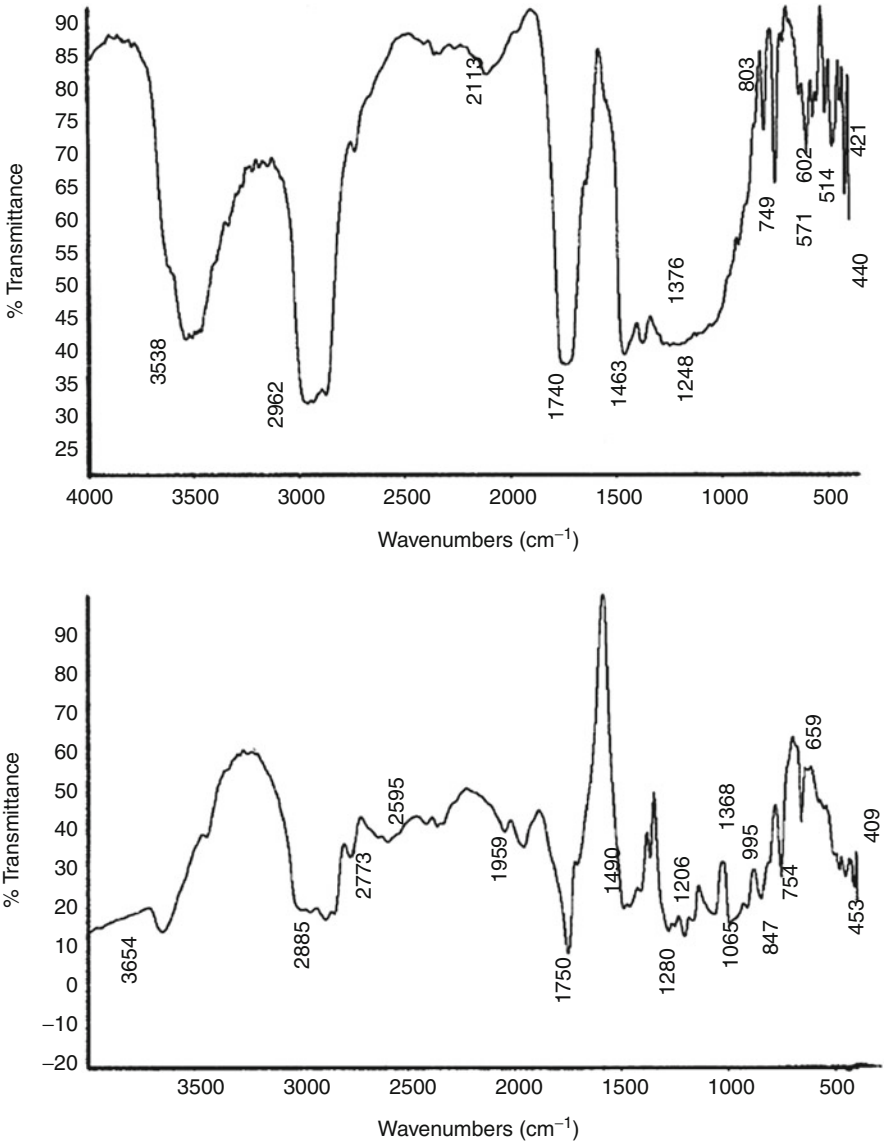

Fig. 10.46 FTIR spectra of Pure PMMA and blend of PMMA/CAB of 50/50 composition (Meaurio et al. 2005)

miscibility of the blends. The FTIR data (Fig. 10.46) also compliments the solution techniques (Selvakumar et al. 2008).

The complete miscibility of the PMMA/DGEBA epoxy blends was confirmed by FTIR spectroscopy by Ritzenthaler et al. Increasing the heating time does not induce any shift or modification of the O–CH_3 (2,850–2,950 cm^{-1}) and the

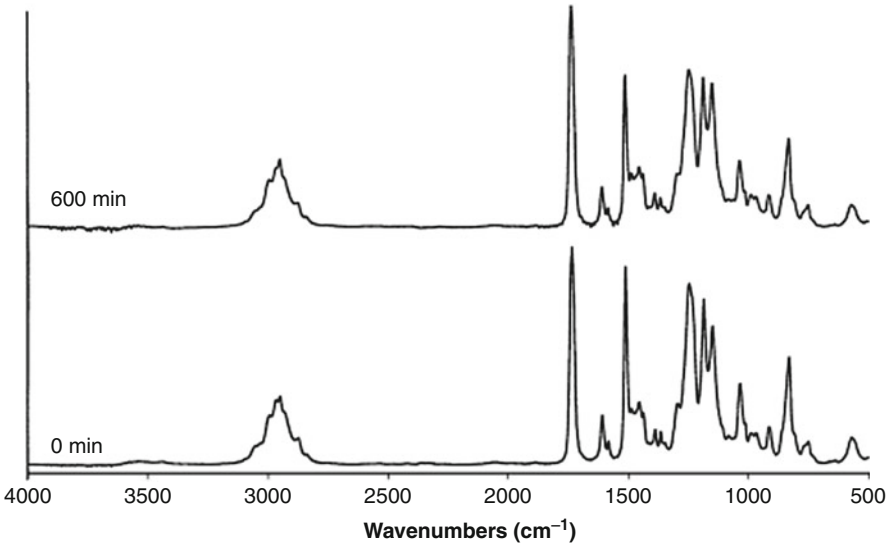

Fig. 10.47 FT-IR spectra of DGEBA 30 wt% PMMA blend at 135 °C (Ritzenthaler et al. 2000)

C = O (1,725 cm^{-1}) peaks of PMMA. The results also confirm that there is no specific interaction between the PMMA and the thermoset components during curing (Fig. 10.47) (Ritzenthaler, et al. 2000).

^{1}H NMR was used to characterize the structure of the reactive and physical blend products of poly(lactic acid) and poly(ε-caprolactone) system by Wang et al. (1998). The investigation of EVA reject/phenolic resin from cashew nut shell liquid (CNSL) blends, using combined NE techniques at solid state, showed the range of compatibility as well as the domain structure present in the microdomains (Martins et al. 1996). The miscibility of poly(styrene-*co*-vinylphenol) containing 5 % vinylphenol monomer units (MPS-5) with syndiotactic poly(methyl methacrylate) (PMMA-s) and with isotactic poly(methyl methacrylate) (PMMA-i) was studied with ^{13}C solid-state n.m.r. complemented with cloud point and differential scanning calorimetry measurements (Lei Jong et al. 1993).

10.4.7 Influence of Miscibility on Final Properties of Blends

In general, a miscible blend of two polymers is likely to have properties somewhere between those of the two unblended polymers. The relative miscibility of polymers controls their phase behavior, which is of crucial importance for final properties. Polymer–polymer miscibility depends on a variety of independent variables, viz., composition, molecular weight, temperature, pressure, etc.

Jong-Han Chun studied the synergistic effect of impact strength and miscibility in polycarbonate PC/ABS blends (Chun et al. 1991). Positive deviations of the modulus

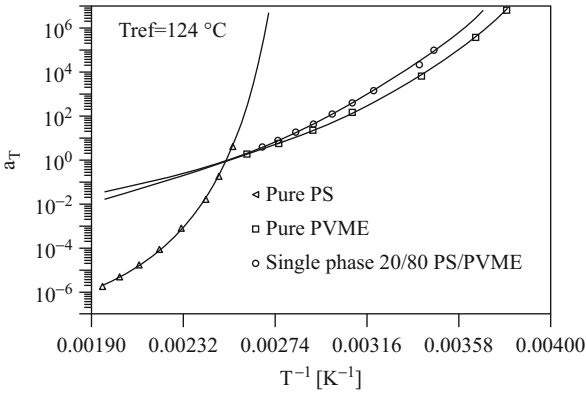

Fig. 10.48 Horizontal shift factors for the pure components and the single-phase 20/80 PS/PVME blend at a reference temperature of 1 °C (Polios 1997)

E_b and yield strength S of polymer blends consisting of partially miscible polymers are analyzed by combining models for miscible and immiscible blends by Jan Kolarík (2000). Several heterogeneous blends of partially miscible polymers, such as polycarbonate (PC)/poly(styrene-co-acrylonitrile) (PSAN) (Kolarik et al. 1997), poly(ether sulfone)/phenoxy (An et al. 1996a, b), and poly(ether-imide)/polyarylate, PC/poly(acrylonitrile-butadiene-styrene) (ABS), PC/PS, polyamide-6/ABS, and PC/poly(ether sulfone) (An et al. 1996) were found to show modulus E_b and/or yield strength S higher than predicted by the rule of mixing (additivity).

In the case of PS/PVME blends studied by Polis et al., the phase separation results initially in a large increase in the low-frequency complex moduli which is attributed to the highly interconnected PVME-rich and PS-rich phases, formed during the spinodal decomposition. The subsequent decrease is the result of the loss of interconnectivity between the two phases due to the breakup and coarsening of the phase-separated domains (Fig. 10.48) (Polios 1997).

The influence of miscibility on the transport properties of polymer electrolyte blends composed of a proton conductor and an insulator was investigated by Jeffrey, Gasa, Weiss, and Montgomery Shaw (2006). The proton conductive component in the blends was SPEKK, while the nonconductive component was either PEI or PES. The phase behavior of PEI–SPEKK blends was strongly influenced by the sulfonation level of the SPEKK. At low sulfonation levels (ion-exchange capacity (IEC) = 0.8 meq/g), the blends were miscible, while at a slightly higher level (IEC = 1.1 meq/g), they were only partially miscible, and for IEC = 1.4 meq/g, they were effectively immiscible over the entire composition range. The PES–SPEKK blends were miscible over the entire range of SPEKK IEC considered in this study (0.8–2.2 meq/g). Poly(ether ketone ketone) (PEKK) itself is a relatively new engineering thermoplastic that has high-temperature stability, excellent chemical and solvent resistance, and excellent mechanical properties. The effect of compatibilization on the miscibility and final effect on the mechanical properties of PA/PPO blend have been studied by Cao et al. (2011). They used graphite oxide as a compatibilizer. Figure 10.49 represents the stress behavior and tensile strength data of the uncompatibilized and GO sheet compatibilized blends. They observed that the tensile strength of the blends increased by 87 %.

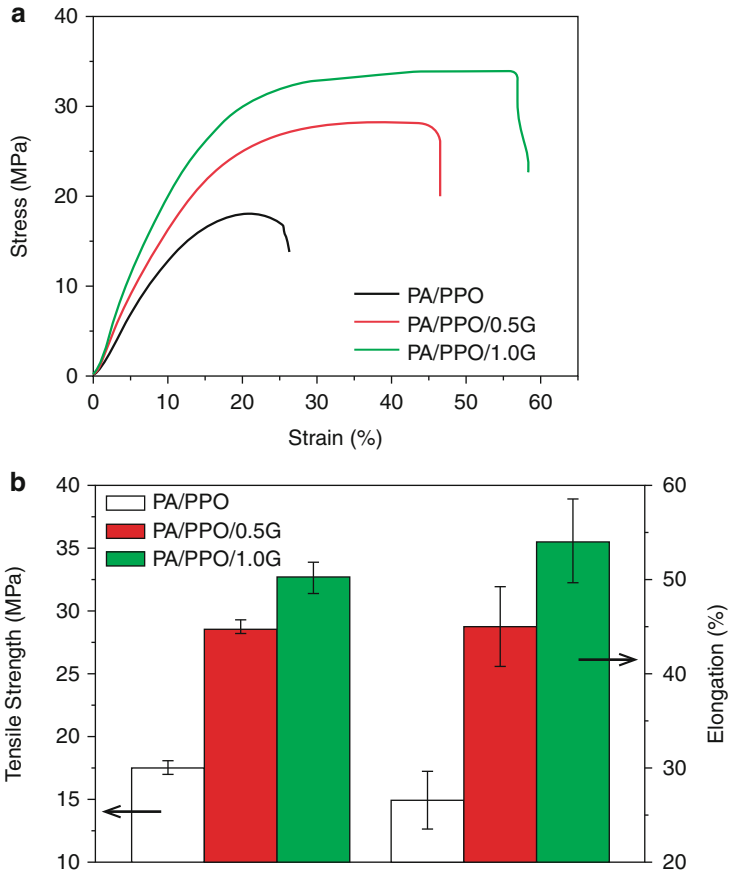

Fig. 10.49 (**a**) Stress–strain curve and (**b**) tensile strength and elongation data of uncompatibilized and GOS compatibilized PA/PPO blend (Cao et al. 2011)

10.5 Thermal Properties

10.5.1 Thermal Resistance (R)

For a flat slab, it is calculated as (ASTM C177)

$$R = A\,\frac{(T_1 - T_2)}{Q} = \frac{1}{\Gamma} = \frac{D}{\lambda} \tag{10.25}$$

where R = thermal resistance (Km^2W^{-1}), A = area measured on a selected isothermal surface (m^2), T_1 = temperature of warm surface of specimens (K), T_2 = temperature of cold surface of specimens (K), Q = heat flow rate (W), Γ = thermal conductance ($Wm^{-2}\ K^{-1}$), D = thickness of specimen measured

Table 10.16 Thermal conductivity units (Ives et al. 1971)

Units	Cal/(cm s °C)	W/(cm °C)	W/(m °C)	Kcal/(m h °C)	Btu in/(ft^2 h °F)
Cal cm/(cm^2 s °C) (or) cal/(cm s °C)	1	4.19	419	360	2900
J cm/(cm^2 s °C) (or) W/cm °C	0.230	1	100	86.0421	693
J cm/(m^2 s °C) (or) W/m °C	0.00239	0.01	1	0.860421	6.93
Kcal m/(m^2 h °C) (or) Kcal/m h °C	0.00278	0.0116	1.16	1	8.06
Btu in/ft^2 h °F	0.000345	0.00144	0.144	0.124	1

along a path normal to isothermal surfaces (m), and λ = thermal conductivity, (W/mK). The reciprocal of thermal resistance is known as thermal conductance, Γ.

10.5.2 Thermal Conductivity (λ)

Thermal conductivity of materials can only be defined for homogeneous materials, where the thickness is greater than that for which the apparent thermal resistivity of the material does not change by more than 2 % with further increase in thickness. The thermal resistance must be sufficiently independent of the area of the specimen, and for a flat slab specimen, the thermal resistance must be proportional to the thickness. When all these conditions are met,

$$\lambda = \frac{QD}{A}(T_1 - T_2) = \frac{D}{R} \tag{10.26}$$

where the symbols are the same as in Eq. 10.25. The reciprocal of the thermal conductivity is called thermal resistivity (r).

The most common units for thermal conductivity are cal/cm °C and Btu in/ft^2 h°F. The SI unit for conductivity is W/mK. Since a variety of units has been in practice for thermal properties, the conversion factors are given in Table 10.16.

ASTM C177 and BS 874 recommend guarded plate method for materials of low conductivity. Two different types of guarded hot plate apparatus are described in ASTM C177. The low-temperature guarded hot plate is the most suitable method for determining the thermal conductivity of polymeric solid materials including foams. It is generally used for measurements where the temperature of the heating unit is not above 500 K. The second method is the high-temperature guarded hot plate which is ordinarily used for measurements where the heating unit temperature is greater than 550 K but less than 1,350 K. The schematic arrangement of the apparatus is shown in Fig. 10.50.

Three possible configurations to restrict edge heat flux are illustrated in Fig. 10.51. The apparatus consists of a heating unit, a cooling unit, and edge insulation. The heating and cooling units may be either round or square. The heating unit consists of a central metering section and a guard section.

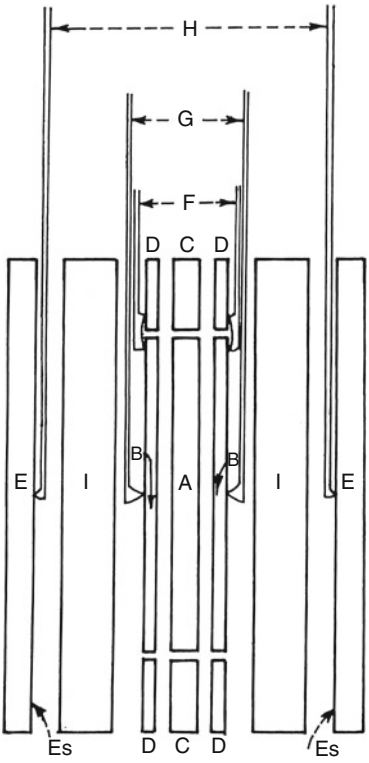

Fig. 10.50 General features of the metal surfaced hot plate apparatus (ASTM C177)

The metering section consists of a metering area heater and metering area surface plates. The guard section consists of one or more guard heaters and the guard surface plates. The working surfaces of the heating unit and cooling plates should be smoothly finished to conform to a true plane.

The heating unit has a separation (or gap) not greater than 4 mm between the surface plates of the metering area and the guard. Two specimens should be selected from each sample with their surfaces made plane. The temperature difference between the hot and cold surfaces of the specimens should be not less than 5 K (De Ponte and Di Filippo 1974).

The central heat source and the guard should have independent power supplies. The cold surface heaters are to be adjusted so that the temperature drops through the two specimens do not differ by more than 1 %. To attain a correct value for properties, the time required should be adjusted – its magnitude depends on the specific apparatus, control system and its operation, the test temperatures, the thermal diffusivity, and thickness of the specimens (Shirtliffe 1974). The conductivity is calculated using the Eq. 10.26. The attainment of equilibrium is important, especially for polymer blends that have low conductivity. The equilibrium times, for example, for cellular materials, are in the order of hours or tens of hours. For this reason, stable over long time period power supplies are necessary.

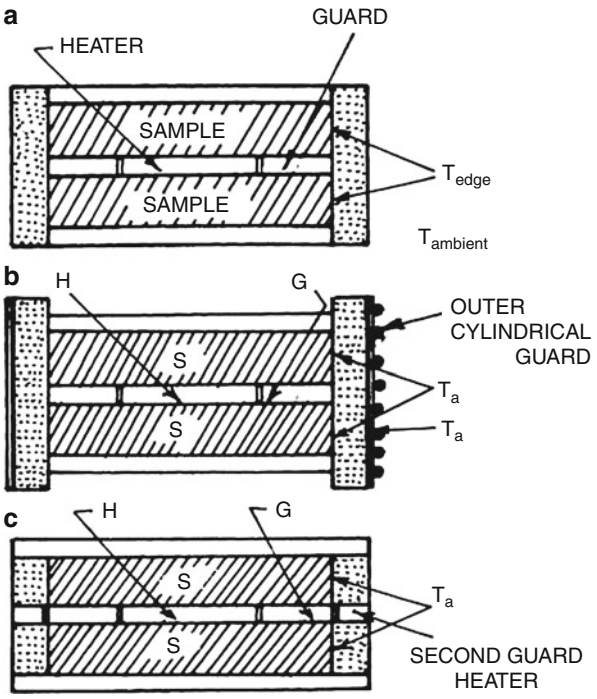

Fig. 10.51 Possible configurations to restrict edge heat loss or gain (ASTM C177)

10.5.3 Heat Capacity

Specific heat of polymer blends is usually measured by differential thermal analysis (DTA) (Slade and Jenkins 1966) or differential scanning calorimetry (DSC) (Strella and Erhardt 1969; Richardson and Burrington 1974). DTA measures the difference in temperature between the sample and a standard for the same rate of heat input, while DSC compares the rate of heat inputs for the same rate of temperature rise. The results of DSC are easier to analyze as they give a direct measure of the rate of heat input.

Measurement of specific heat is made by heating a test specimen at a known and fixed rate (Blaine 1973). Once dynamic heating equilibrium of the specimen is reached, the heat flow is recorded as a function of temperature. This heat flow, normalized to specimen mass and heating rate, is directly proportional to the specimen's specific heat capacity.

In practice, two thermal experiments are required for each measurement. In the first, a baseline run is performed only on the empty pan and lid. In the second run, the test specimen is enclosed in the pan and lid. The specific heat capacity information is derived from the difference between the two resulting thermograms.

Heat flow calibration of the apparatus is also required. This is obtained by running baseline and experimental traces for a material whose specific heat capacity is well known. Sapphire is the calibration material of choice since it is easily available and its specific heat capacity is accurately known.

The relationship for calculation of specific heat capacity is given by

$$C_p = \frac{KEq}{m\beta} \tag{10.27}$$

where C_p is the specific heat capacity (J/kg K), E is the calibration coefficient (dimensionless), q is the heat flow (mW), β is the heating rate (K/min), m is the specimen mass (mg), and K (60,000) is the conversion constant. The calibration coefficient E is expressed as

$$E = \frac{C_p\ (\text{lit})}{C_p\,(\text{obs})} \tag{10.28}$$

where C_p (lit) is the reported literature value of specific heat capacity of the standard sample, while C_p (obs) is its experimentally observed value under the same conditions. The coefficient, E, is to be used for the determination of the unknown.

It is wise to calculate E for several temperatures over the region of interest – E should be constant. If it is not, particularly at low temperatures, it indicates that dynamic temperature equilibrium is not attained at the temperature and that the experimental temperature program needs to be started at a lower temperature. The overall accuracy of the method is found to be ±5.5 %. Precision can be improved with large samples and higher heating rates, provided dynamic temperature equilibrium is achieved.

10.5.4 Heat Distortion Temperature (HDT)

ASTM D648 describes the determination of temperature of deflection under load for plastics and ebonite. ISO 75, BS 2782 Method 121 A and 121 B are equivalent. DIN 53461 is similarly related to the ISO method. Since these standards are similar, only the ASTM method will be described.

The heat distortion temperature (HDT), the deflection temperature under load (DTUL), or the softening temperature is a practical and important parameter of a polymeric material. They denote the upper temperature limit up to which the material can support a load for any appreciable time.

ASTM D648 provides a method for determining DTUL of plastics under flexural load. The method is applicable to molded and sheet materials available in thickness ≥3 mm, which are rigid at room temperature. The specimen is taken in the form of a rectangular bar with the load applied at its center to give maximum fiber stresses of 4.55 or 18.20 kPa (see below). The metal supports (rounded to a radius of mm) for the

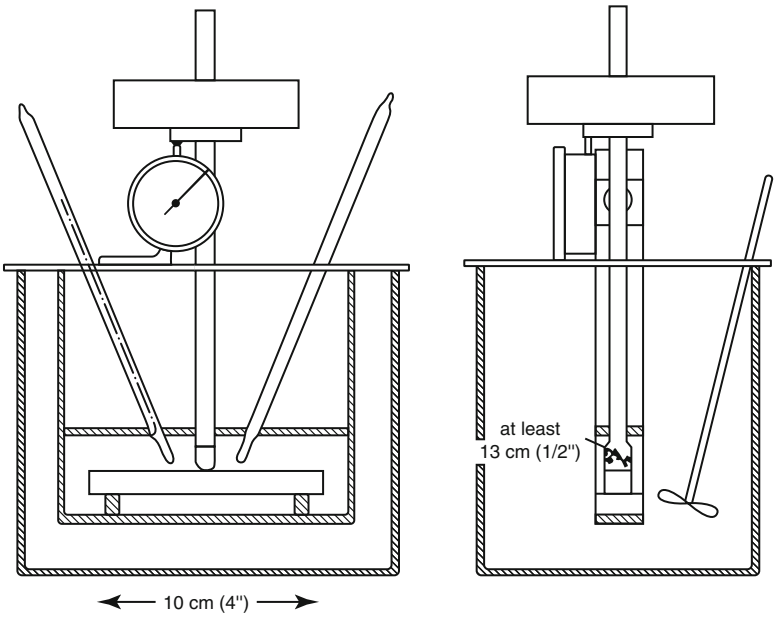

Fig. 10.52 Apparatus for heat deflection temperature test [ASTM D648]

specimen are provided 100 mm apart (see Fig. 10.52) allowing the load to be applied on top of the specimen vertically and midway between the supports. The specimen is immersed under load in a heat-transfer medium. The temperature is raised at 275 ± 0.2 K/min. The load applied on the specimen to obtain a maximum fiber stress of 18.20 kPa ± 2.5 % is calculated using the formula below:

$$P = \frac{2Sbd^2}{3L} \tag{10.29}$$

where P is the load (N), S is the maximum fiber stress in the specimen (18.20 or 4.55 kPa), b is the width of specimen (m), d is the depth of specimen (m), and L (0.1) m is width of span between supports. The load of 18.20 kPa is usually used for rigid polymers (e.g., PS) while 4.55 kPa is used for softer crystalline materials that have $T_g < 298$ K (e.g., PE).

ASTM D1637 provides tensile HDT test for plastic sheets. In this test a load of 345 kPa is applied to a strip, and the temperature is increased at a rate of 2 K/min. The HDT in this case is defined as the temperature at which the elongation becomes 2 %.

ASTM D1525 provides a third type of the softening temperature test. A flat-ended needle of 1 mm circular cross section is pressed into a thick sheet of the polymer with a load of 1.0 kg. The polymer is heated at a rate of either 50 or 120 K/h. The Vicat softening temperature, which is explained in detail below, in Sect. 10.5.5, is the temperature at which the needle has penetrated the polymer to a depth of

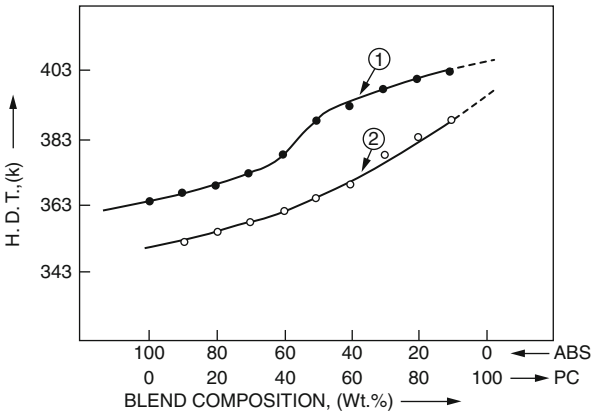

Fig. 10.53 Variation of heat deflection temperature with PC/ABS blend composition (curves 1 and 2 are obtained with loads 4.6 and 18.2 kg.f/cm^2, respectively)

Table 10.17 Variation of HDT with talc concentration in PPCP-EPDM blend (Xavier et al. 1994)

Blend composition	Talc (wt%)	HDT (K)
Neat PPCP	0	353
PPCP + EPDM (10 wt%)	8	355
PPCP + EPDM (10 wt%)	10	356
PPCP + EPDM (10 wt%)	12	359
PPCP + EPDM (10 wt%)	15	360

1 mm. For such a depth of penetration, the material must be very soft; hence, the Vicat softening temperature is higher than other HDT data.

Heat deflection temperature is influenced by (i) blend composition, (ii) fillers/reinforcing agents, (iii) annealing, and (iv) applied stress:

- HDT of a blend is influenced by its composition. Figure 10.53 shows variation of HDT (measured according to ASTM D648) with PC/ABS blend composition (Xavier and Pendyala unpublished). The observed variation is caused by changes in flexural modulus, which is also shown.
- Inorganic fillers (e.g., talc, mica, or $CaCO_3$) or reinforcements (e.g., glass or carbon fibers) increase HDT of neat polymers or blends (Nielsen 1974; Xavier and Sharma 1986). Table 10.17 illustrates the influence of talc concentration on HDT for a blend.
- Annealing of a crystalline polymer, either neat or in a blend, increases the degree of crystallinity, changes the crystallite morphology, and relieves built-in stresses in the amorphous phase. Table 10.18 shows the gradual increase of HDT with annealing time. Flexural modulus also increases. Similar effects were reported for amorphous polymers such as PS (Nielsen 1974).
- Polymer HDT decreases with applied stress. The major cause of this effect is the decrease of modulus with temperature with the consequent greater deformation at the higher temperature for a given load. HDT occurs, by definition, at

Table 10.18 Effect of annealing time on HDT and flexural modulus of PPCP: EPDM (10 wt%) blend (HDT was tested at 4.55 kPa) (Sarcar 1989)

Test	Value obtained after annealing (h)		
	0	3	6
Heat deflection temperature (K)	330.0	343.0	349.4
Flexural modulus (MPa)	805.2	882.2	889.8

Table 10.19 HDT of some alloys with and without reinforcement for car body panels and bumpers (Moro et al. 1988)

No.	Blend	HDT (K); ASTM[a] tests at 455 kPa
1.	PPE/PA (NORYL GTX 900)	456
2.	PBT/Elastomer	348
3.	PBT/Elastomer, Glass Reinforced	421
4.	PP/Elastomer	333
5.	PP/Elastomer, Glass Reinforced	403
6.	PC/PBT	393

[a]ASTM D648-01; see: http://enterprise.astm.org/

a constant deformation. The deformation is proportional to the load and inversely proportional to the modulus. HDT values of some commercial polymer alloys are given in Table 10.19.

10.5.5 Vicat Softening Point

The effect of temperature on the mechanical properties of plastic materials has a fundamental role in the selection of materials. Unlike metals and ceramics, plastics are extremely sensitive to the slightest changes in temperature. The selection of plastics for applications under different temperatures is a complex task. The plastic material must be able to support a stress under operating conditions without getting distorted. The effect of temperature on geometrical stability and mechanical properties in general can be studied following different procedures and methods like at constant temperature or with a temperature ramp.

The Vicat softening temperature (VST) is standardized in ISO 306 and ASTM D 1525. It is very useful as a quality control or development tool (ASTM D1525-2009). (This test method is technically equivalent to ISO 306:1987(E)). The result is a measure of the temperature at which thermoplastics begin to rapidly soften. VST describes the temperature at which a circular indenter with a cross section of 1 mm^2 under a standardized loading of 10 N or 50 N penetrates exactly 1 mm into the specimen. VST was introduced to measurement technology as a substitute value for melting point. VST for some common polymers are presented in Table 10.20.

The apparatus for testing VST consists of a temperature regulated oil bath with a flat-ended needle penetrator so mounted as to register degree of penetration on

Table 10.20 Vicat softening temperatures for some common polymers

	(1 kg load)
Plastics	Measured value (K)
PS	375.5
ABS	375.3
PVC	365.0
PC	429.2
PE	400.3
PP	425.2

Source: Report by Japan Society for Testing Plastics (1972)

Table 10.21 Four different methods used for testing VST

	Load (N)	Heating Rate (K/h)
A50	10	50
B50	50	50
A120	10	120
B120	50	120

a gauge. A specimen is placed with the needle resting on it. The temperature of the bath (preheated to about 323 K lower than anticipated Vicat softening point) is raised at the rate of 323.0 K/h. or 393.0 K/h. The temperature at which the needle penetrates 1 mm is the Vicat softening point. For the Vicat A test, a load of 10 N is used. For the Vicat B test, the load is 50 N. The test conditions are summarized above in Table 10.21.

The test specimen must be between 3 and 6.5 mm thick and at least 10 mm in width and length. No more than three layers may be stacked to achieve minimum thickness.

Traditionally silicone oil has been the most popular medium for performing HDT and VST tests on polymers. They can be used safely only up to a maximum temperature of 553 K.

An alternative medium is required to test high-temperature polymers, such as PEEK, PEI, etc., as they have HDTs and VSTs higher than the temperature at which silicone oil can be used. "CEAST HV500," which utilizes an aluminum oxide fluidized bath, is used to perform a range of HDT and VST tests for both high- and low-temperature applications. Engaging "CEAST HV500" different grades of PEEK, PS, PC, PA, and PPS incorporated with 40 % glass fillers and PP with 15 % glass fillers were tested, at temperature ramps of 323 K/h and 393 K/h:

- VST is a measure of how much a plastic material would soften with increasing temperature. The higher the VST, the higher the temperature necessary for lamination and higher is the service temperature.
- Standard PVC card films (homopolymer) have a VST of 349 K. To achieve high VST values, special blends of PVC/ABS card films (0.25–0.8 mm thick) are engaged. High-VST (364 $\pm$ 2 K) cards are required in environments with high temperatures and stress. Applications include SIM (GSM) cards and pay TV cards.
- Apart from its practical applicability, VST is also used in studying the "miscibility" of polymer blends. Miscibility of PVC/PMMA blends was studied by determining

Table 10.22 Glass transition temperatures of some common polymers

Polymer family	Glass transition temperature (°C) (Approx.)	(K) (Approx.)
PCTFE	120–215	393–488
PTFE	130	403
PS	100	373
PMMA	100	373
PVC	90	363
PET	70	343
PA(nylon)	50	323
ROOM TEMP.	20	293
POM	−15	258
PP	−20	253
PVDF	−45	228
PE-LD	−120 to −100	153–173

the VST of blends. The plot of VST against composition exhibited a continuous curve which revealed miscibility of the blend. This was further confirmed from the study of viscometry, DSC, and FTIR analysis of the blends (Kamira and Naima 2006).

- α-Methylstyrene-acrylonitrile copolymers (AMSAN) are highly compatible with PVC and have a high glass transition temperature. Trials with proportions of AMSAN in the blend confirmed that the Vicat temperature of the blends can be raised by adding this copolymer. For every 10 % by weight of AMSAN added, the Vicat temperature increased by approximately 4 °C (Gottschalk 2006).

10.5.6 Low-Temperature Brittle Point

For most materials low temperatures present a challenging environment and plastics are no exception. Most polymers at room temperature show their familiar properties of flexibility (a low Young's modulus) and high resistance to cracking, but when the temperature decreases, this can change rapidly and many common polymers become brittle with low failure stresses. Low temperatures can be more harmful to plastics than high temperatures. Catastrophic failures can occur if materials selection does not take account of the low-temperature properties of plastics.

Brittle fracture takes place by rapid crack propagation. For most brittle crystalline materials, crack propagation corresponds to the successive and repeated breaking of atomic bonds along specific crystallographic planes, known as cleavage. Cleavage is essentially a low-temperature phenomenon, which can be eliminated if a sufficiently high deformation temperature is used.

The actual value of glass transition temperature (T_g) for real polymers will vary greatly with the specific molecular structure of the base polymer, the molecular weight and the molecular weight distribution of the polymer, the additives incorporated into the mix, and a variety of other factors. Table 10.22 above gives some

typical values of T_g for some common polymers (but these should be regarded as indicative rather than definitive). Polymers that have a T_g greater than room temperature are in glassy state at room temperature, and examples of these are plastics such as PS, PMMA, and PET. These polymers tend to be brittle and easy to break at room temperature. PVC is in the glassy state at room temperature but is a special case because it can be easily modified to be rubbery by the addition of plasticizers (Zeus 2005).

The brittle point test developed by the Bell Telephone Laboratories is simple and sensitive. It is believed that this test may be used to study all cold-resistance problems where damage to the rubber itself and not increase in stiffness is the first consideration.

The "slow-bend brittle point test" does not have the same practical significance as the Bell Telephone Laboratories' brittle point test because most rubber articles which are exposed to low temperatures in service are required to withstand fairly rapid flexing. If the slow-bend brittle point test were used as a criterion of the cold resistance of these rubber articles, it might qualify the rubbers for a lower temperature than they could safely withstand in service (Morris et al. 1944).

ASTM D746-07 describes the Standard Test Method for Brittleness Temperature of Plastics and Elastomers by Impact. It employs three types of specimens. In this method the brittleness temperature is determined by immersing the specimens in a bath containing a heat transfer that is cooled, usually by liquid nitrogen, carbon dioxide, or powdered dry ice, to a predetermined temperature for a period of three minutes. The specimens are then impacted by a device having a striker of a specific geometry, under defined conditions of velocity, distance, and energy. The test temperatures are varied over a range and the brittleness point is defined as that at which 50 % of the specimens fail. This test provides for the evaluation of long term effects, such as crystallization, or the incompatibility of plasticizers incorporated in the material when subjected to subnormal temperatures (ASTM D746-07). This test, however, does not, necessarily, determine the lowest temperature at which the subject material may be used. The results may be used to predict the behavior of plastic and elastomeric materials at low temperatures.

ASTM D1329-08 offers Standard Test Method for Evaluating Rubber Property–Retraction at Lower Temperatures (TR Test). The other related Methods for Temperature Retraction (TR) Test are ISO 2921, BS 903-A29 (UK), and NF T4NF T46-032 (France). This test method describes a temperature-retraction procedure for rapid evaluation of crystallization effects and for comparing viscoelastic properties of rubber and rubberlike materials at low temperatures. This test method is useful when employed in conjunction with other low-temperature tests for selection of materials suitable for low-temperature service (ASTM D1329-08). This is more commonly known as a TR-10; this temperature-retraction test is considered by many within the rubber industry to be the most useful indicator of a material's low-temperature performance. In a nutshell, the TR-10 measures material resilience. Samples are frozen in a stretched state and then gradually warmed until they lose 10 % of this stretch (i.e., retract by 10 %). The results of such tests are believed to provide a good basis for evaluating the effects of crystallization and the impact of low

temperatures on viscoelastic properties. TR-10 results are generally thought to be consistent with the capabilities of most dynamic seals. Static seals can often function at 15 °F/8 °C/281 K below the TR-10 temperature (Hudson 2011).

ASTM D2137-11 provides Standard Test Methods for Rubber Property – Brittleness Point of Flexible Polymers and Coated Fabrics. Related Methods for Brittleness Point Test are ISO 812, DIN ISO 812 (Germany), and BS 903-A25 (UK). These test methods cover the determination of the lowest temperature at which rubber vulcanizates and rubber-coated fabrics will not exhibit fractures or coating cracks when subjected to specified impact conditions (ASTM D2137-11).

Unlike the changes that result from exposure to high temperatures, changes brought about by low-temperature exposure are generally not permanent and can often be reversed once heat returns. For example, extended exposure to low temperatures will increase an elastomer's hardness, but the material will soften again when the temperature rises. Perhaps the most important consideration related to low temperatures involves seals which must also work in a low-pressure environment. Unless the selected seal compound is sufficiently soft and resilient, the combination of low temperature and low service pressure can cause leakage and failure (Hudson 2011).

The brittle–ductile transition temperatures of some commercial polymers, blends, and composites are given in Table 10.23.

10.5.7 Melt and Crystallization Parameters (Using DSC)

Differential scanning calorimeter (DSC) can be used to ascertain melting point, degree of crystallinity, and glass transition temperature or for component quantification of polymeric materials. For some materials – such as crystalline polymers and certain organic chemicals –DSC is used to measure melting points and degree of crystallinity. For amorphous polymers, rubbers, and cross-linked thermoset materials, DSC also provides a fast and accurate measure of the glass transition temperature or the degree of cure.

In a DSC experiment, when a polymer is heated, as it reaches its melting temperature (T_m), the polymer crystals begin to melt. The polymer chains come out of their ordered arrangements and begin to move around. When the polymer crystals melt, they absorb heat in order to do so. Melting is a first-order transition. This means when polymer reaches its melting point, the polymer's temperature does not rise until the crystals melt off. This also means that the furnace has to put up additional heat into polymer in order to melt both the crystals and keep the temperature rising at the same rate as that of the reference pan. This extra heat flow during melting shows up as a large dip in DSC plot as heat is absorbed by the polymer. The temperature at the apex of the peak is taken as the point where the polymer is completely melted. And the area under the peak gives the heat of melting of the polymer. As energy is added to the polymer to make it melt, melting is considered as an endothermic transition (Daniels 1973; Turi 1981).

An understanding of the degree of crystallinity for a polymer is important since crystallinity affects physical properties such as storage modulus, density,

Table 10.23 Low-temperature brittle point of some rubbers (Lindsay 2010)

Properties	Ethylene propylene diene	Nitrile rubber	Poly-chloroprene	Natural rubber	Poly-isoprene	Styrene butadiene rubber	Butyl rubber	Polybutadiene
	EPDM	NBR	CR	NR	IR	SBR	IIR	BR
Tensile strength max, psi (MPa)	2,000 (13.8)	2,500 (17.3)	2,500 (17.3)	3,500 (24.1)	3,000 (20.7)	2,500 (17.3)	2,000 (13.8)	2,000 (13.8)
Low-Temperature brittle point, K	215	222	219	215	215	215	215	200

permeability, and melting point. And melting point in turn influences the processing temperature. While most of these manifestations of crystallinity can be measured, a direct measure of degree of crystallinity provides a fundamental property from which these other physical properties can be predicted.

Polymer crystallinity can be determined with DSC by quantifying the heat associated with melting (fusion) of the polymer. This heat is reported as "% crystallinity" by taking ratio against the heat of fusion for a 100 % crystalline sample of the same material or more commonly by taking ratio against a polymer of known crystallinity to obtain relative values.

If ΔHf is equal to area under the melting peak, then ΔHf is proportional to % crystallinity:

$$\% \text{ Crystallinity} = \left[\frac{\Delta Hf}{\Delta H^{*}\mathrm{f}}\right] \times 100 \tag{10.30}$$

where ΔH*f is ΔHf of 100 % crystalline polymer.

In case of polyethylene, ΔH*f = 68.4 cal/g;

In case of polypropylene, ΔH*f = 209.3 ± 29.9 J/g.

*(These values of ΔH*f are reported to be widely varying from one laboratory to another for the same polymer.)*

An empirical relationship between T_g and T_m of a polymer is given as follows: $T_g/T_m \sim 0.6$

(Here, T_g and Tm are to be taken in Kelvin).

When a semicrystalline polymer, such as polypropylene, cools from melt, the polymer chains begin to form crystals at foreign particles in the melt (Wunderlich 1990). The completely solidified PP part is typically about 60 % crystalline and 40 % amorphous. These crystals exhibit a peak melting temperature (via DSC) of about 438 K. When nucleating agents are incorporated into the PP, the number of sites where crystal growth can start is dramatically increased. This means that the part will crystallize more rapidly in the mold and will also achieve a higher final level of crystallinity. The faster crystallization rate results in faster setup in the mold, and reduced cycle times, while the higher crystallinity results in increased part stiffness.

Another side benefit that accompanies with the use of certain nucleants is improved clarity. Since clarity or transparency is evidently related to the crystalline structure of the polymer and the structure is determined by the conditions of crystallization, parameters characterizing crystallization must be also connected with the optical properties of a PP product. The peak temperature of crystallization (T_c) is one of the quantities often used for the characterization of the crystallization process and efficiency of nucleating agents. With increased crystallization temperature, the thickness of the lamellae increases well. Higher efficiency and concentration of nucleating agent lead to an increase of T_c (as determined by DSC) and decrease of the size of the spherulites.

Figure 10.54a and b illustrate the shift in T_c for polypropylene homopolymer with the addition of a nucleating agent.

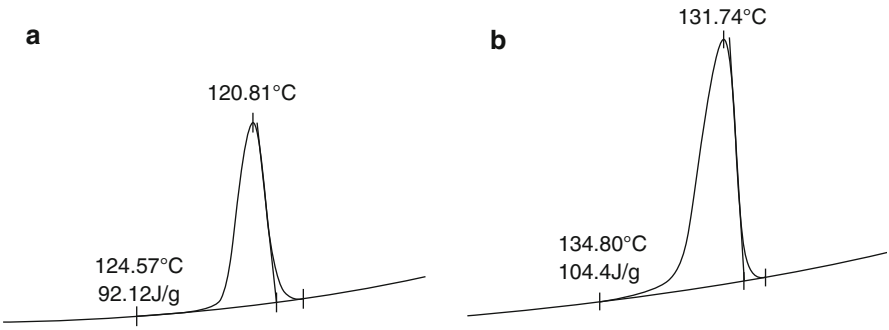

Fig. 10.54 Crystallization exotherm for (**a**) neat PP homopolymer and (**b**) PP with nucleating agent (Xavier 2002)

10.5.7.1 Crystallization of Polypropylene Homopolymer (PPHP) Influence of Nucleating Agent, Millad-3988

Semicrystalline polymers, such as PPHP, display different microstructural features due to the factors like (i) the presence of various additives (Kopp et al. 1994), (ii) depending upon their processing history (Lotz 2003), and (iii) strain in solid (Butler and Donald 1997) as well as melt (Pople et al. 1999) phases. Many methods are being applied to modify the polymers in order to attain high-performance properties. Properties modification by incorporation of additives in polypropylene and its related polymers is observed to be particularly common.

In polypropylene, the crystallization results in large size spherulites, and hence inclusion of heterogeneous nucleating agents is often adopted to improve mechanical properties (Quande Gui and Weiping Zhu 2003) or to reduce optical haze (Gahleitner et al. 1996; Zhao and Dotson 2002). Hence, providing such heterogeneous nucleation is an essential consideration. Creation of various crystallographic phases, differed by the unit cells as well as by the spherulites, is known to be a result of the heterogeneous nucleation (Lotz 2003).

Nucleating efficiency is normally determined isothermally from crystallization half-time, by use of peak crystallization temperature of the nucleated system measured during cooling and compared with that of the neat polymer. The peak crystallization temperature technique is based on a single-point observation. Fillon et al. proposed alternate approach for the evaluation of nucleating efficiency using two dynamic reference points to understand the crystallization behavior of a polymer (Fillon et al. 1993). These two reference points include (i) polymer's crystallization temperature when crystallized normally and (ii) the same when polymer nucleated ideally.

In order to obtain an ideally nucleated polymer, it is heated to just above its melting point so that large number of residual crystal fragments exist in the melt and act as nuclei. This method is referred to as self-seeding or self-nucleation (Blundell 1966). Zhao et al. have evaluated crystallization behavior of propylene/ethylene copolymer by self-seeding approach (Zhao et al. 2001), which was found in good agreement with the earlier published DSC data (Laihonen et al. 1970, 1997).

Millad-3988 is a breakthrough "clarifying agent" for PP. Use of this additive in properly formulated and processed PP gives improved transparency, increased resin throughput, productivity gains, and enhanced physical properties.

DSC investigations were carried out (Fig. 10.55) using PPHP granules as well as fast cooled compression-molded sheets with three different concentrations of Millad-3988 (0.07, 0.14, and 0.21 wt%) in order to see whether the molding conditions would play a role and thus influence the DSC data in comparison to the data obtained using plant supplied granules. The properties of PPHP with different concentrations of Millad-3988 are shown in Table 10.24. From the Table 10.24, it is clear that T_m values for sections cut from the sheets were always less than their corresponding values obtained using granules. In fact, T_c also showed the same trend. The difference between T_m and T_c (i.e., $T_m - T_c$) gradually reduced with increasing concentration of Millad-3988. This behavior is more systematic in case of the sheets. However, T_{onset} which indicates the crystallization "onset" is found to be gradually enhanced with Millad-3988 concentration. The degree of crystallinity, as determined by X-ray diffraction, also gradually increased with increasing concentration of Millad-3988.

The crystallinity (%) of PPHP increases with increasing Millad-3988 concentration, which also influences the surface gloss of polymer sheets to increase (as observed in Haze meter measurements, not presented here). However, the transmission (%) (as measured by the Haze meter) does not undergo the same pattern of change. In fact the transmission (%) was found to be maximum for PPHP sheet with Millad-3988 concentration 0.07 wt% followed by the one with 0.14 and 0.21 wt%. It is interesting to note that the transmission (%) for neat PPHP (87.1 %) is not much different from that with maximum transmission (88.6 %) with Millad-3988 of 0.07 wt%.

10.5.8 Oxidative Induction Time

Oxidative induction time (OIT) provides an index useful in comparing the relative resistance to oxidation of a variety of hydrocarbon materials. The OIT procedure was first developed in 1975 by Gilroy and coworkers at Bell Laboratory as a test procedure to screen polyethylene insulation used in telephone wire and cable for its oxidation resistance. The method first became available as a Western Electric Specification and later as ASTM Test Method for Copper-Induced Oxidative Induction Time of Polyolefins. Polyolefin manufacturers quickly embraced the procedure and began to apply it to other applications including raw resins, finished pipes, wire and cable insulation, and, most recently, geosynthetic waste pit liners (ASTM D3895 2009).

The test consists of heating a specimen to an elevated temperature (often 200 °C) in a DSC. Once temperature equilibrium is established, the specimen atmosphere is changed from inert nitrogen to oxidizing air or oxygen. The time from first oxygen exposure until the onset of oxidation is taken as the OIT value. This general procedure is applied, for example, to polyethylene wire insulation, edible oils, lubricating oils and greases, and geosynthetic barriers. Most materials are tested to measure the

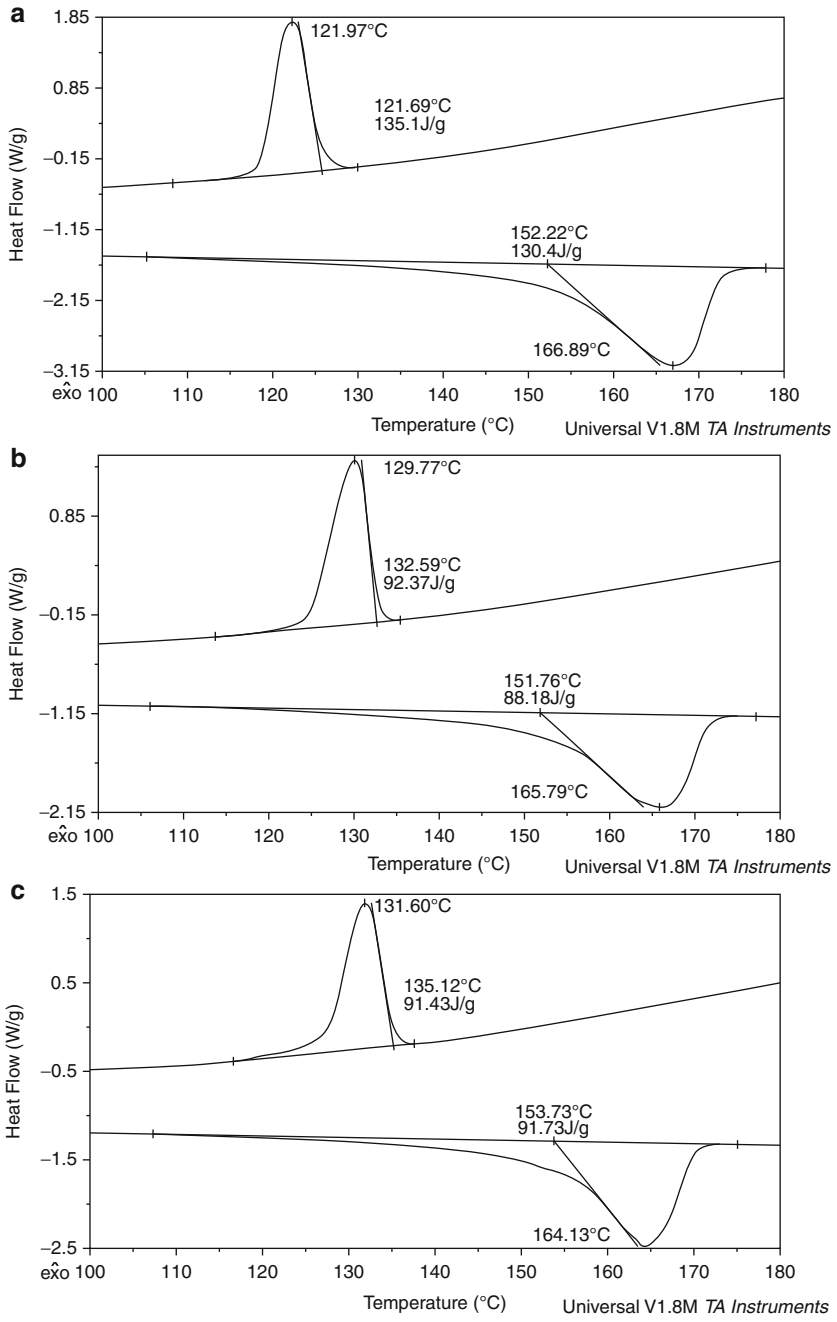

Fig. 10.55 DSC thermograms of PPHP + Millad-3988 at different concentrations (**a**) 0.07 wt%, (**b**) 0.14 wt%, and (**c**) 0.21 wt%, carried out using sections cut from ~0.7 mm thick, fast cooled, compression-molded sheets (Pendyala et al. 2004)

Table 10.24 Properties of polypropylene homopolymer in presence of Millad-3988 (Pendyala et al. 2004)

	PPHP		PPHP + Millad (0.07 %)		PPHP + Millad (0.14 %)		PPHP + Millad (0.21 %)	
	granule	sheet	granule	sheet	granule	sheet	granule	sheet
Melting temp.* (Tm) °C	169.25	167.49	167.30	166.89	167.29	165.79	168.63	164.13
Cryst. temp.* (Tc) °C	120.81	122.11	123.76	121.97	130.59	129.77	131.74	131.60
(T_m–T_c) (°C)	48.44	45.38	43.54	44.92	36.70	36.02	36.89	33.53
T_{onset} (°C)	124.57	125.70	129.75	125.69	136.16	132.59	137.39	135.12
Deg. of cryst.** (%)	–	38.20	–	38.60	–	39.90	–	40.60
Transmission*** (%)	–	87.10	–	88.60	–	88.35	–	86.50

* Tm and Tc were determined from DSC experiments.
** Degree of crystallinity was obtained from X-ray diffractions.
*** Transmission studies were carried out on Haze meter.

effectiveness of the antioxidant package added to improve lifetime, although a few materials (e.g., edible oils) are tested in their natural, non-fortified state.

The onset of oxidation is taken as the endpoint for the OIT measurement. Two means of determining the oxidation onset are in use (Blaine et al. 1997). The most common is the "extrapolated onset" in which the tangents are drawn at the point of maximum rate of oxidation and the baseline prior to oxidation (say 0.05 W/g). The endpoint for the OIT determination is taken at the point where the exothermic event crosses that threshold. If the oxidation exotherm is sharp, these two endpoint indicators produce similar results as seen in Fig. 10.56. However, some materials seem to have a multistaged oxidation, and the endpoint established by the two experimental procedures may be quite different as shown in Fig. 10.57 (Blaine et al. 1997). The selection of the method of determination of the OIT endpoint is the first parameter affecting the comparison of results from one laboratory to another. Apart from this, OIT values are influenced by temperature, oxygen flow rate, oxygen pressure, catalysts (sample pan materials), sample mass and form, and time, which will be discussed below.

10.5.8.1 Parameters Influencing OIT

OIT has been proved to be a useful diagnostic tool in assessing the extent of degradation in the polymer insulation of electric cables. Sample preparation and test conditions are parameters recognized to influence OIT results obtained by DSC. However, quantitative results on the variability of OIT as a function of these parameters have not been presented systematically in the literature.

Factors that influence OIT include test temperature, sample preparation, sample geometry, sample mass, particle size, thermogram interpretation, shelf life, heating rates to reach the isotherm, and oxygen flow. The influence of these parameters was investigated using a two level factorial design using HDPE samples (Rosa et al. 2000). Sample shape, amount of sample, and heating rate were the parameters that showed significant variability.

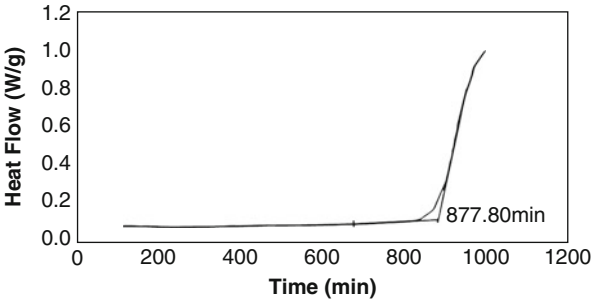

Fig. 10.56 Single stage oxidation endpoint determination (Xavier 2002)

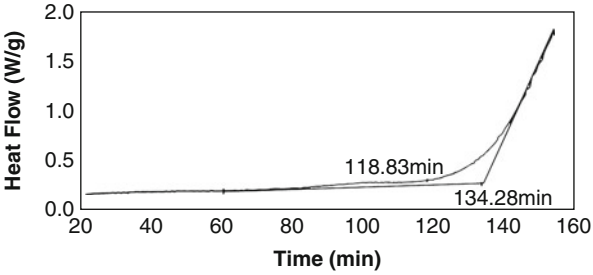

Fig. 10.57 Multistage oxidation endpoint determination (Xavier 2002)

The effects of these parameters and cross-linking in polymer cable insulations, aged in radiation and thermal environments, were investigated. The results were then used to recommend standards for an OIT methodology suited for practical use, including the nuclear power industry. Techniques to estimate error in (O.I.T.) thermograms interpretation and reproducibility were also developed (Mason and Reynolds 1997).

A HDPE film, lightly stabilized with Irganox 1010 and a hindered phenol antioxidant, was proposed as a Standard Reference Material for OIT testing by Blain and Harris of TA Instruments, Inc. The mean OIT values, derived from nine interlaboratory studies and for a number of experimental conditions, were presented (Blaine et al. 1997). The material was found to be statistically homogeneous, a necessary condition for a reference material. The effects of temperature, oxygen pressure, and storage time on the proposed reference material were also explored. As a kinetic parameter, the OIT value appeared to be decreasing with time but in a well behaved and predictable manner. Because the material had been thoroughly tested in a wide variety of OIT conditions, it appeared to be the best available candidate and was offered for consideration as an OIT Reference Material (Blaine et al. 1997).

Oxidation is generally recognized as the key degradation mechanism regarding the long-term durability of HDPE geomembranes. For protection against oxidation during their service lifetime, antioxidants are added. A laboratory accelerated

aging program was conducted to assess the depletion of antioxidant from a Korean HDPE geomembrane subjected to air oven aging followed by incubation in acidic and alkaline buffer solutions at three different temperatures. The changes in OIT were monitored at selected time intervals. The results indicated that for samples subjected to oven aging incubation for 90 days, the OIT results showed that the geomembrane had enough antioxidants to ensure long-term oxidation stability. Immersion in the alkaline buffer solution was found to accelerate the antioxidant depletion rate relative to that observed in the acidic buffer solution. Greater depletion rates were recorded at higher temperature, indicating the temperature dependency of the depletion process. Conservative values of the depletion time ranged from 107 to 9 years depending on temperature and exposure condition. The estimated antioxidant depletion times were longest for exposure to acidic solutions and shortest for exposure to alkaline solutions (Jeon et al. 2008). These studies support the idea to use HDPE as a reference material for studying O.I.T.

10.5.8.2 O.I.T and O.O.T

Two different methods of studying O.I.T. are used in practice: dynamic and isothermal tests. In the dynamic technique, the sample is heated at a defined constant heating rate under oxidizing conditions until the reaction begins. The Oxidation Induction Temperature (O.I.T.) (also called Oxidation Onset Temperature (O.O.T.)) is the same as the extrapolated onset temperature of the exothermal DSC effect which occurs. In isothermal tests, the materials to be investigated are first heated under a protective gas and then held at a constant temperature for several minutes to establish equilibrium and subsequently exposed to an atmosphere of oxygen (or air). The time span from the first contact with oxygen until the beginning of oxidation is called the Oxidation Induction Time (OIT) (NETZSCH).

The procedure for the preparation, implementation, and evaluation of measurements is described in detail in national and international standards such as ASTM D3895 (polyethylene), DIN EN 728 (plastic pipelines), or ISO 11357-6 (plastics). Generally, either open crucibles or crucibles with multiple piercings in the lids are used. For polyolefins like PE or PP, a longer OIT allows one to conclude that the oxidation stability is better and the lifetime therefore longer.

10.5.8.3 OIT Measurements Using TGA

The measurement of OIT based on TGA was used for monitoring the re-stabilization of post-use LDPE samples, subjected to multiple extrusion cycles. This method has abilities and limitations as well which are discussed in literature (Kyriakou et al. 1999). The use of a re-stabilization system improved the oxidative stability of LDPE. A linear calibration curve correlating OIT values to the amount of re-stabilization system was obtained. Nevertheless, limitations concerning quantitative determinations appeared to exist, as a change in the behavior of re-stabilization system during subsequent re-melting cycles was observed.

10.5.8.4 TOIT: A New Method

OIT's oxidation condition is considered as very harsh especially in case of pure and irradiated polymers, particularly PP. PP undergoes pronounced molecular weight degradation in the course of processing and is prone to very fast oxidation and consequently very fast degradation, especially on samples submitted to previous aging and irradiation.

Lugao and his group had introduced a new procedure to determine OIT in non-stabilized, stabilized, irradiated, and nonirradiated PP. The new procedure was based on two main features: (1) starting the oxidation on melted samples at temperatures as low as possible and (2) oxidation under slow heating conditions. Since each sample has a set of two values of time and temperature, it is called as "temperature-dependent oxidative induction time." This new method is found to be reproducible, sensitive (to small changes in additive compositions), simple, and inexpensive (Lugao et al. 2002).

10.5.8.5 High Pressure OIT

A series of high pressure oxidative induction time measurements (HPOIT) were conducted on a PE geomembrane sheet in order to investigate the interaction of the pressure and temperature variables on the induction time. The experiments consisted of determining the HPOIT at constant cell volume employing a wide operational range of pressure and temperature values. The HPOIT test results were found to be inversely related to both variables, with temperature being the predominant factor (Tikuisis et al. 1985).

10.5.9 Thermal Degradation (Using TGA)

Thermogravimetry (or thermogravimetic analysis, TGA) is one of the oldest thermo-analytical procedures and has been used extensively in the study of polymeric systems. The technique involves monitoring the weight loss of the sample in a chosen atmosphere (usually nitrogen or air) as a function of temperature. It is a popular technique for the evaluation of the thermal decomposition kinetics of polymeric materials and hence provides information on thermal stability and shelf life. However, it is well known for its ability to provide information on the bulk composition of polymer compounds.

In the analysis of polymer compounds, the sample is initially heated in a nitrogen atmosphere. Heating under nitrogen ensures that no oxidation reactions take place. Additives are lost first, in order of decreasing volatility, and then the polymer fraction will undergo thermal degradation and volatilizes off. Once the entire polymer has thermally degraded, the species remaining in the TGA pan (which can include, carbon black, inorganic fillers and carbonaceous residue from the breakdown of the polymer) can be examined. This is achieved by changing the atmosphere to air and heating to around 1,273 K. Weight loss events can be

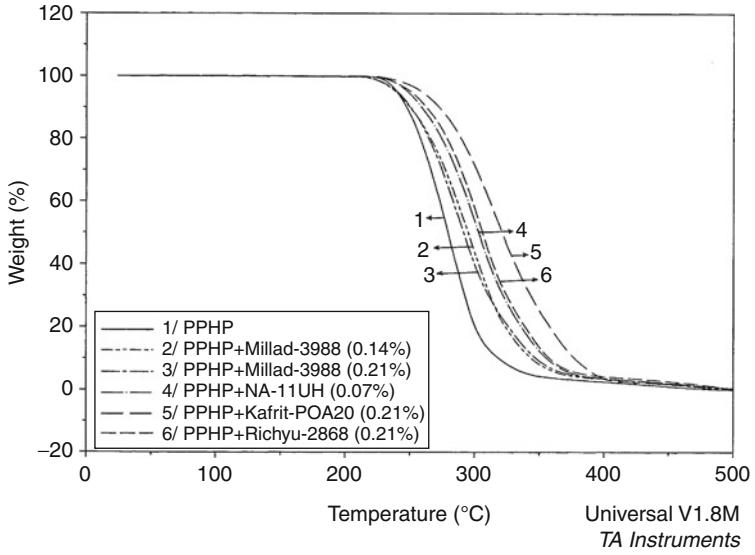

Fig. 10.58 TGA thermograms of ~0.7 mm thick compression-molded specimens of neat PPHP and its compositions with different nucleating agents carried out at a heating rate of 10 K/min in static air (Pendyala et al. 2004)

observed for the oxidation of carbonaceous residues and carbon black and the decomposition of inorganic fillers, such as calcium carbonate. At the end of the analysis an amount of stable inorganic residue will remain. This procedure will enable the amount of plasticizers, polymer, carbon black, and inorganic species to be quantified to an accuracy of at least ~0.5 %.

Although certain additives can be quantified by techniques such as solvent extraction and dry ashing, the advantage of TGA is that only 5–10 mg of sample is required. In recent years the benefits of coupling TGA instruments to either an infrared spectrometer or a mass spectrometer have been appreciated. This enables both qualitative and quantitative data to be obtained in a single analytical experiment. Here, how TGA can be used to evaluate different commercial nucleating agents by studying the thermal stability imparted to the polymer is illustrated below.

10.5.9.1 Thermal Degradation of Polypropylene Homopolymer (PPHP)

TGA of PPHP with and without commercial nucleating agents (Millad-3988 and three other selected nucleating agents) is shown as overlay in Fig. 10.58 and thermal characteristics are shown in Table 10.25. The thermal stability of a polymer is, generally, influenced by various factors such as bond strength, activation energy, cross-linking, presence of low molecular weight/volatile material and weak links, etc.

Table 10.25 Thermal characteristics of PPHP[a] and its compositions with different commercial nucleating agents (Pendyala et al. 2004)

	Composition	Decomposition temp. at K		T_{onset}		$T_{inflection}$	
		10 wt% loss	50 wt% loss	°C	K	°C	K
1	PPHP	247.00	288.20	219.96	492.96	279.01	552.01
2	PPHP + Millad-3988 (0.14 %)	249.70	309.92	213.43	486.43	297.68	570.68
3	PPHP + Millad-3988 (0.21 %)	250.10	303.24	215.00	488.00	297.68	570.68
4	PPHP + NA-11UH (0.07 %)	258.80	304.28	222.66	495.66	301.46	574.46
5	PPHP + Richyu-2868 (0.21 %)	262.60	297.40	221.28	494.28	276.09	549.09
6	PPHP + Kafrit-POA20 (0.21 %)	272.50	311.38	222.73	495.73	312.62	585.62

[a] ~0.7 mm thick compression-molded sheets were used for analysis

The factors influencing thermal stability are to be considered prior to its evaluation. It is observed that the polymer may retain its "usefulness" when half of its strength is retained after one hour of exposure to a specified temperature and that the limit is reached with a weight loss of 10 wt% (Eirich and Mark 1961). This limit is based on many assumptions and it varies with the polymer. Polymer material's decomposition criterion is established by recording the temperatures: (a) at 10 % and 50 % decompositions and (b) at the maximum rate of decomposition (Mark and Gaylord 1971).

From Table 10.25, it is found that neat PPHP indicated loss of 10 % weight at 520 K. The incorporation of Millad-3988 in PPHP, in the concentration range of 0.14–0.21 wt%, showed a marginal increase in the temperatures for 10 % weight loss (~523 K). However, PPHP in presence of the selected commercial nucleating agents (NA-11UH 0.07 %, Richyu-2868 0.21 %, and Kafrit-POA20, 0.21 %) exhibited significant increase in the temperatures (531.80–545.50 K) for 10 % weight loss. Similarly for the 50 % weight loss, PPHP degradation temperatures are found to be enhanced in the presence of Millad-3988 as well as the other selected nucleating agents. From their thermograms shown in Fig. 10.58, it is observed that the decomposition is occurring in single stage for PPHP and a similar behavior is observed in presence of Millad-3988 as well as the other selected commercial nucleating agents.

The onset of thermal decomposition, T_{onset}, of PPHP is found to be 492.96 K (Table 10.25). With the incorporation of commercial nucleating agents, it is observed Millad-3988, in the concentration range of 0.14–0.21 %, reduced the onset temperature of PPHP (~5–7 K) while the other selected nucleating agents enhanced it and that enhancement is higher than that offered by PPHP with the incorporation of Millad-3988. $T_{\mathbf{inflection}}$ temperatures, at which the rate of decomposition is maximum, for PPHP incorporated with Millad-3988 (555.54–570.68 K), are found to be higher than that of neat PPHP (552.01 K); among the selected three commercial nucleating agents, PPHP incorporated with NA-11UH (574.46 K), with Richyu-2868 (549.09 K), and with Kafrit-POA20 (585.62 K) indicated significant improvement in their thermal stability except Richyu-2868. It is observed that Kafrit-POA20 offered the highest improvement of thermal stability for PPHP

among the nucleating agents tried. From the above study, the commercial nucleating agents imparting thermal stability to PPHP is in the following order (Pendyala et al. 2004):

$$Kafrit\ -\ POA20(0.21\,\%) > NA\ -\ 11UH(0.07\,\%) > Millad\ -\ 3988\ (0.21\,\%) > Millad\ -\ 3988(0.14\,\%) > Richyu\ -\ 2868(0.21\,\%).$$

10.5.10 Review of Blends' Thermal Properties

Owing to the absence of electronic effects in most polymers, heat conduction occurs as a result of lattice vibrations, similar to dielectrics. It is known that the thermal conductivity of an amorphous polymer increases to T_g with increasing temperature while it decreases above T_g (Godovsky 1992). Thermal conductivity is a fundamental and important factor in processing polymer blends (Agari 1992).

Influence of miscibility on thermal conductivity and diffusivity was studied (Agari 1993, Agari and Ueda 1994). In the blend of low molecular weight PS with coumarone–indene resin, which showed miscibility over all blend compositions, the thermal conductivity was approximately linearly dependent on composition (Agari 1993). Thermal conductivity, thermal diffusivity, and heat capacity of PMMA/PC blends were studied with respect to temperature and blend composition. The specific heat capacity of the two-phase 50/50 blend was larger than that of the one-phase blend. The thermal diffusivity and the conductivity of the 50/50 blend slightly decreased with the increase of temperature up to 450–460 K (LCST) and then decreased abruptly with increase of temperature (Agari et al. 1997).

Several investigators (Krause et al. 1982; Schultz and Young 1983; Rodriguez-Parada and Percec 1986) had used the specific heat increment (ΔC_p) to investigate the polymer–polymer miscibility by DSC.

The effect of molecular weight of PMMA on the miscibility of PMMA/PS blends was examined by studying the specific heat increment ΔC_p at T_g (Burns and Kim 1988). Using Couchman's equation, C_p for PMMA was calculated and was found to decrease with the composition of PS (Couchman 1978). The C_p for PS similarly decreased with PMMA composition. From these results the authors inferred that some of the PMMA dissolved in the PS phase and vice versa. Thus, the blends were found to be partially miscible. This result was found to be consistent with the polymer–polymer interaction parameter values. The authors also studied the PC/SAN blends miscibility by the thermal analysis (Kim and Burns 1988). The values of the specific heat increment ΔC_p at T_g for PC and SAN in PC/SAN blends were measured. For PC, C_p decreased linearly with addition of SAN. For SAN, C_p also linearly decreased with addition of PC. This suggested that some of the PC dissolved in the SAN-rich phase and *vice versa*.

Thermal studies have become important tools for understanding various basic phenomena in polymer blends and composites all over the world. The changes in crystallization kinetics of polymer blends in comparison to the

parent polymers involved the way a compatibilizing polymer interferes with the crystallization kinetics, and if a reinforcing filler or fiber is introduced into the same system, how the kinetics are getting affected is more a curious situation and it is not easy to make simple predictions without conducting experiments on DSC. The thermal stability of a blend after introducing a compatibilizer needs to be elucidated.

The literature available with such studies is also vast and also several books dedicated to thermal analysis alone are appearing time to time; hence, it is not possible to really justify such a presentation here. Nevertheless, some illustrative examples of such studies are given here in Table 10.26. The reader is advised to go through the desired literature.

10.6 Flammability

10.6.1 Standard Methods of Measurement

There are two types of tests, viz., burning and combustion toxicology tests. The burning tests aim at determining either the burning characteristics or the burning rate. The combustion toxicology tests aim at measuring the types and quantities of toxic gases that evolve during burning and smoldering of plastics and their effects on men and animals. A list of ASTM tests, the specimens, the purpose of each test, etc., is provided in Table 10.27.

Underwriters Laboratories (UL) provide Standards UL 94 Tests for Flammability of Plastic Materials for Parts in Devices and Appliances. The standard is important for classifying polymeric materials (including polymer blends and alloys) for the use in electrical applications. It is widely used and the results are reported in the literature and in company catalogues. However, the requirements are not applicable to polymeric materials used in building construction or finishing. The tests conducted under this standard are summarized below.

10.6.1.1 Horizontal Burning Test for Classifying Materials: 94 HB

The test uses small bar specimens: 127 × 12.7 mm. It is similar to ASTM D635. Materials classified under this test shall not have a burning rate exceeding either 38 or 75 mm/min over a 75 mm span, for specimen's thickness of, respectively, 12.7 or 3 mm. The materials must cease burning before reaching the 100 mm mark.

10.6.1.2 Vertical Burning Test for Classifying Materials: 94 V-0, V-1, V-2

The test specimen (127 × 12.7 mm, with maximum thickness 12.7 mm) is supported vertically by its upper end and is ignited at its lower end for 10 s by Bunsen/Tirril burner, in a draft-free area (see Fig. 10.59). If flaming or glowing combustion stops within 30 s after removal of the flame, the specimen is re-ignited for 10 s. The duration of the flame is again noted. In case the specimen drips flaming particles, they are allowed to fall into a layer of surgical cotton 0.3 m below the sample. The particles are considered significant if the cotton ignites.

Table 10.26 Sources for thermal properties data of polymer blends: examples

Blend	Test	Results	References
HDPE/NA6 with compatibilizers (i) KRATON FG1901X and (ii) KRATON FG1921X	Thermal analysis (DSC), heats of crystallization,	Compatibilizers changed the crystallization kinetics, softened NA6 phase and enhanced impact strength	Chandramouli and Jabarin 1995
PPCP blends with commercial elastomers/ plastomers (EXACT 5371, ENR 7370, ENGAGE 8150, VERSIFY 2300, NORDEL IP 4760P, NORDEL IP 4770P, Chemtura EPDM IM 7565)	DSC, Delta heat of fusion, delta heat of crystallization, T_m, T_c	Charpy impact strength (notched) raised up to 70 kJ/m^2 in case of Engage-8150, Nordel-4760, Nordel-4770, and Chemtura EPDM IM 7565	Xavier 2008
LDPE/DCP	DSC, isothermal studies	Peroxide cross-linking reaction with LDPE studied	Ghasemi et al. 2005
PLLA/PDLLA biodegradable blends	DSC, Glass transition temperature, thermal degradation of blends, TGA	Miscibility of Poly-l-lactic acid (PLLA) and Poly-dl-lactic acid (PDLLA) was studied using DSC and thermal stability using TGA were studied.	Chen et al. 2003
Blends of corn starch with poly(ε-caprolactone), CA, PLA and ethylene-vinyl alcohol copolymer	DSC and TGA	Three degradation mechanisms were identified in the blends	Mano et al. 2003
LDPE/PA6 blends with ethylene-methacrylic acid copolymer Na salt ionomer as compatibilizer	Thermal stability of blends using TGA	TGA measurements demonstrated an improvement in thermal stability when ionomer was added	Lahor et al. 2004
Compatibilized LDPE/ PA6 blends	Thermal stability of blends using TGA	Thermal stability of blends increases in the presence of Escor 5001	Yordanov and Minkova 2003
LDPE/PA6 blends using two different compatibilizers	Isothermal crystallization using DSC	Relative evaluation of compatibilizers used	Minkova et al. 2002
HDPE/PA6 blends with HDPE-g-MAH as a compatibilizer	Thermal properties were studied using TGA and DSC	Thermal behavior of in situ compatibilized blends was studied using TGA and DSC	Hsu et al. 2001
PA6/LDPE blends compatibilized using maleated hydrolyzed ethylene-vinyl acetate copolymer (EVALM)	Crystallinity was studied using DSC	EVALM affected the degree of crystallinity and Tg of PA6 phase	Luo et al. 2001

(*continued*)

Table 10.26 (continued)

Blend	Test	Results	References
NA6/HDPE blends with LDPE-g-GMA (glycidyl methacrylate) as compatibilizer	Crystallization temperature using, and melting point measurements using DSC	Increase in crystallization temperature and a reduction in melting point of nylon phase were observed with addition of the compatibilizers	Wang et al. 1995
PP nanocomposite toughened with poly (ethylene-co-octene) using PP-g-MAH (6 wt%) as compatibilizer	Thermal stability of the rubber-toughened PP nanocomposites was studied	Thermal stability was improved significantly with the addition of small amount of organoclay	Lim et al. 2006
Kinetics of thermal and thermo-oxidative degradation of PS, PE and PP	Thermal degradation of PS, PE, and PP was studied in N_2 and air environments	Activation energies were calculated as a function of extent of degradation	Peterson et al. 2001
LDPE/EPDM and HDPE/EPDM modified with LDPE-g-MAH reinforced with jute fibers	Thermal properties	Influence of compatibilizer on the thermal and mechanical properties of the blends was studied	Sarkhel and Choudhury 2008
PTT/LCP(Vectra A950)	Thermal properties using DSC and TGA	DSC studies revealed the blends are immiscible; and TGA investigations showed that the thermal stabilities of blends were improved	Pisitsak and Magaraphan 2009
XLPE and EPDM cables	OIT measurements using DSC	Assessing the extent of degradation in the polymer insulation of electric cables in nuclear power plants	Mason and Reynolds 1997
Irradiated and nonirradiated PP	Temperature dependant OIT as a new method	A new method more suitable in case irradiated and nonirradiated PP (and other polyolefins) was described	Lugao et al. 2002
Electrochemically aged PP with a dye added	Vicat softening point	Electrochemical aging results (in PP) in decrease in hardness and Vicat softening temperature while increase in water absorptivity and in size of spherulites was noticed	Gnatowski et al. 2010
Polyethylene compositions with improved Vicat softening point	Vicat softening point	A method of selecting materials for polyethylene with improved Vicat softening point has been disclosed	Davis 2008

(*continued*)

Table 10.26 (continued)

Blend	Test	Results	References
Thermal degradation kinetics of LLDPE and Silane cross-linked LLDPE	TGA was employed to study the degradation mechanisms	Silane cross-linked LLDPE was found to be thermally more stable compared to LLDPE	Zong et al. 2005
PE/MMT nanocomposites	Non-isothermal TG experiments	Char formation plays a key role in the mechanism of flame retardation for nanocomposites	Lomarkin et al. 2008
Glycerol modified linseed oil based polyurethane and cardanol based dye	Thermal stability of the blends was investigated using TGA, derivative thermogravimetry (DTG) and other methods	Glycerol modified linseed oil based polyurethane and cardanol based dye are highly cross-linked with high thermal stability and the rate of decomposition of polymer blends depends upon NCO/OH molar ratios and the nature of the dye	Achary et al. 2012
NR/BR rubber blends	Influences of preparation mode and elastomer ratio in blends on thermal degradation using TGA	Degradation of the blends takes place in two steps	Castro et al. 2007
Poly(ester urethane) and poly(ether sulfone) blends with or without poly(urethane sulfone) as a compatibilizer	Thermal degradation of blends using TGA	The presence of polysulfone caused a rise in thermal stability of the blends	Filip and Vlad 2004
Thermal stability of nine polymer systems	Thermal degradation of blends using TG-DTG-DTA etc	Thermal stability, degradation mechanism of organic systems in the presence of inorganic species	Muhammad 2013

Flammability ratings are based on the specimen behavior during the test, materials rated 94 V-0 being the most while those rated 94 V-2 being the least resistant to burning. Table 10.28 summarizes the test requirements.

10.6.1.3 Vertical Burning Test for Classifying Materials: 94 5 V

This test is more stringent than UL 94 V-0, V-1, and V-2. Here, 127 mm ignition flame is applied on specimen bars of dimensions 127 × 12.7 mm, with maximum thickness 12.7 mm. In Method A, a Tirril burner is positioned 20° from the vertical and the overall height of the flame is adjusted to 127 mm. The flame is applied for 5 s and removed for 5 s. The procedure is repeated five times. After the fifth removal of the flame, the duration of flaming and glowing, the distance the specimen burned, the

Table 10.27 Summary of ASTM test methods[a]

No	Test method	Specimen/sample	Purpose of the test	Comments
1.	ASTM D229-96 testing rigid sheet and plate materials used for electrical insulation	Flat sheet or plate form	Relative comparison of the ignition resistance of materials and the extent of burning	
2	ASTM D568 for rate of burning and/or extent of burning of flexible plastics in a vertical position	Flexible thin sheets or films	Relative comparison of rate of burning and/or extent and time of burning (of plastics)	Discontinued in 1991, not replaced
3.	ASTM D635-98 for rate of burning and/or extent of burning of self-supporting plastics in a horizontal position	Bars either molded or cut from sheets, plates, or panels	Relative comparison of average burning rate, average time of burning, and average extent of burning	This method combined with the best features of UL 94 resulted in writing of ASTM D3801
4.	ASTM D757 for incandescence resistance of rigid plastics in a horizontal position	Rigid plastic	Relative resistance to incandescent surface at 1,223 ± 10 K (1,742 ± 18 °F)	Discontinued in 1966, no replacement
5.	ASTM D1433 for rate of burning of flexible thin plastic sheeting supported in a 45° incline	Flexible plastic in the form of film or thin sheeting	Relative rate of burning and/or extent and time of burning	Discontinued in 1987, replaced by D4549
6.	ASTM D1929-96 for ignition properties of plastics (Setchkin technique)		Determination of self-ignition, flash-ignition temperatures, and self-ignition by temporary glow	
7.	ASTM D2843-99 for density of smoke from the burning or decomposition of plastic		To measure smoke density across a 12 in. light path	For materials that excessively drip, auxiliary burner is used
8.	ASTM D2863-97 for measuring the minimum oxygen concentration to support candle-like combustion of plasticThe ratio $O_2/(O_2 + N_2)$ when multiplied by 100 is designated as the oxygen index (Imhof and Steuben 1974)	Various forms such as films, etc	To determine relative flammability of plastic by measuring the minimum concentration of oxygen in a flowing mixture of oxygen and nitrogen that will just support flaming combustion. The apparatus is shown in Fig. 10.60	Useful for determining the "Limiting Oxygen Index" of plastics. It has gone through several modifications

(*continued*)

Table 10.27 (continued)

No	Test method	Specimen/sample	Purpose of the test	Comments
9.	ASTM D3014-99 for flame height, time of burning, and loss of weight of rigid cellular plastics in a vertical position	Rigid cellular plastics	Determining relative extent and time of burning	Revised to accommodate thermosets
10.	ASTM D3713 for measuring response of solid plastic to ignition by a small flame	A set of specimens of identical composition and geometry	To characterize the response of a plastic to a small flame of controlled intensity for quality control	Discontinued in 2000, no replacement
11.	ASTM D3801-96 for measuring the comparative extinguishing characteristics of solid plastics in a vertical position	Solid plastic material. A set of specimens with identical composition and geometry	Determination of comparative extinguishing characteristics	Combination of the best features of UL 94 and ASTM D635
12.	ASTM D3894 for evaluation of fire response of rigid cellular plastics using a small corner configuration	Rigid cellular plastic	Prediction of performance of a Factory Material Full-Scale Corner Wall Test	Discontinued in 1994 and not replaced
13.	ASTM D4100 for gravimetric determination of smoke particulates from combustion of plastic materials	Plastic material in a slab configuration	Gravimetric determination of smoke particulate matter produced from the pyrolysis of plastics	Discontinued in 1997 and not replaced
14.	ASTM E84-00 for surface burning characteristics of building materials	Any building material of dimensions 24 ft. × 20.25 in.	Determination of surface burning characteristics, e.g., of foam insulation	Suffers from several limitations. Also known as Steiner Tunnel Test
15.	ASTM E 119-00 methods of fire tests of building construction and materials	Full-size wall section	Determination of fire resistance of walls, floors, ceilings, roofs, etc	It is similar to UL 263 and NFPA 251
16.	ASTM E136-99 for behavior of materials in a vertical tube furnace at 705 °C	Building material test specimens of size 1.5 × 1.5 × 2 in.	Determination of combustion characteristics of building materials	
17.	ASTM E162-98 for surface flammability of materials using radiant heat energy source (Radiant Panel Test)	Specimen of dimensions 6 × 18 in.	Determination of flame spread index of a material	Intended for research and development only

[a]ASTM standard test methods are available on web: http://enterprise.astm.org/

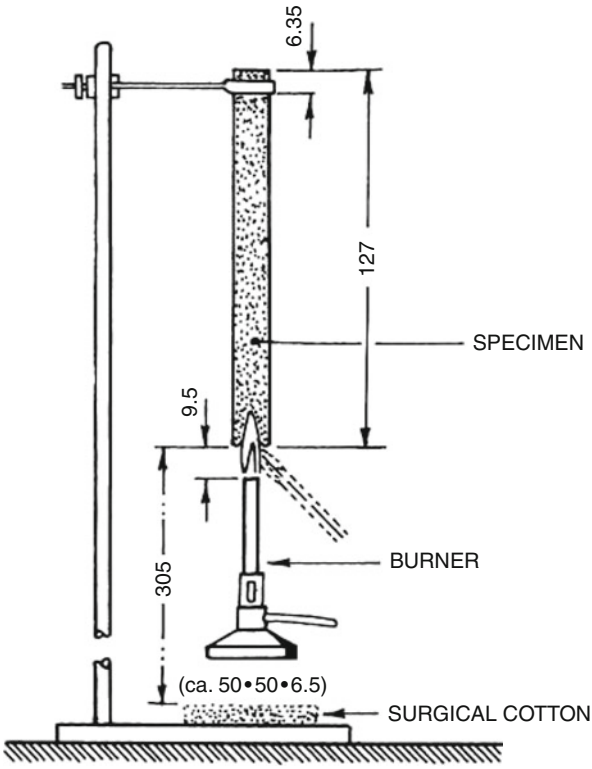

Fig. 10.59 Test layout for classification in 94 V-0, 94 V-1 and 94 V-2 according to UL 94 (Troitzsch 1983)

dripping of particles from the specimen (during the test), and deformation of physical strength of the specimen immediately after burning (and when cooled) are observed.

When the specimen shrinks, elongates, melts, etc., additional tests are carried out using test plaques (152 × 152 mm) under Method B. These tests are conducted in various positions both vertical and horizontal positions of the plaques with flame applied to different places in the plaques, using the procedure as in Method A. The observations focus on the same items as in Method A.

Materials are classified 94-5V when:

- No specimen burns with flaming and/or glowing combustion (after the fifth flame) for more than 60 s.
- None specimen drips particles.

10.6.1.4 Flame Spread Index Test Using Radiant Panels

This test is conducted in accordance with ASTM E162 mentioned in Table 10.28.

10.6.1.5 Vertical Burning Test for Classifying Materials: 94 VTM-0, VTM-1, or VTM-2

Some materials due to their thickness distort, shrink, or get consumed up to the holding clamp, when tested according to the methods described above.

Table 10.28 UL 94 vertical burning test for classifying very thin materials (Landrock 1983)

No.	Requirement	Classification		
		94 V-0 (most severe)	94 V-1 (intermediate)	94 V-2 (least severe)
1.	Total flaming combustion time for 10 ignitions, maximum (sec)	50	250	250
2.	Individual flaming time, maximum (sec)	10	30	30
3.	Glowing combustion time (sec)	30	60	60
4.	Flame drippings	None	None	Allowed if burns briefly

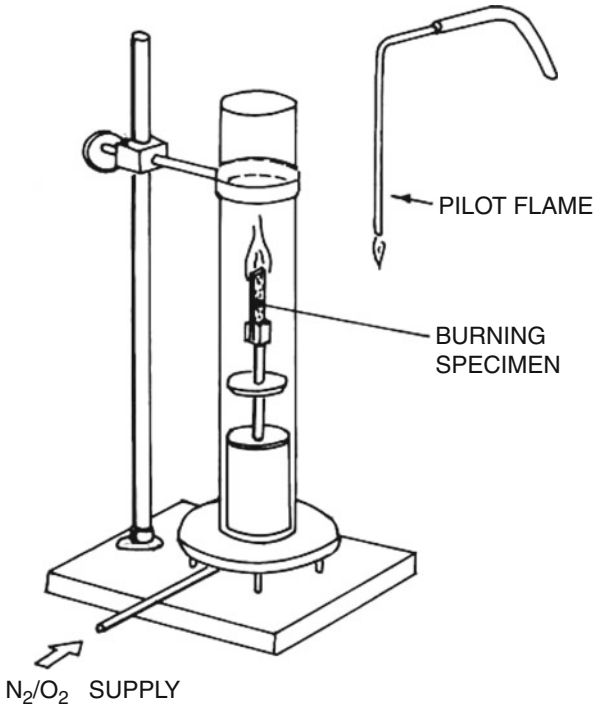

Fig. 10.60 Oxygen index apparatus [Troitzsch, 1983]

VTM means "very thin materials" – test specimens are cut to 200 × 50 mm dimension. Each specimen is supported from the upper 6 mm of its length, with the longitudinal axis vertical using a heavy spring clamp. The lower end of the specimen is placed 9.5 mm above the top of the Bunsen burner tube and 0.3 m above a horizontal layer of dry surgical cotton. The test flame is placed under the lower end of the test specimen for 3 s. Then the flame is taken away from the specimen and the duration of specimen flaming is noted. When flaming of the specimen ceases, the test flame is applied once again for 3 s and then withdrawn.

The deviation of flaming and glowing of the specimen is noted. In case the specimen drips molten or flaming material, the burner may be lighted to angle up to 45°. The following are observed after the removal of the flame:

- Duration of flaming after first flame application
- Duration of flaming after second flame application
- Duration of flaming plus glowing after second flame application
- Whether or not specimens burn up to 127 mm
- Whether or not specimens drip flaming particles that ignite the cotton

94 VTM-0 classifies materials under most severe conditions. Table 10.28 summarizes the test requirements.

10.6.1.6 UL 746A-78 Polymeric Materials' Short-Term Property Evaluations

Test procedures for seven major areas are given in this standard. They are all applied for the determination of resistance of polymeric materials to ignition from electrical sources. The individual tests are Resistance to Hot Wire Ignition, Resistance to High-Current Arc Ignition, Resistance to High-Voltage Arc Ignition, and Resistance to Hot-Bar Ignition.

10.6.1.7 UL 746B-79 Polymeric Material Long-Term Property Evaluations

This standard deals with long-term tests for the evaluation of materials and parts of end products. Along with UL 94, UL 746A, and UL 746C, these tests provide data regarding the physical, electrical, flammability, thermal, and other properties of the materials under consideration.

10.6.1.8 UL 746C-78 Polymeric Materials' Use in Electrical Equipment Evaluations

This is the test procedure, including flammability, for parts of polymeric materials used in electrical equipment. It provides a table of short-term and long-term properties to be considered during evaluation of polymeric materials used in electrical equipment.

10.6.1.9 UL 746D-80 Polymeric Materials' Fabricated Parts

This standard is for blends of polymers, copolymers, terpolymers, and alloys. It considers plastic parts that have been produced under a material identity control system. Molders/fabricators are required not to employ such additives/flame retardants that would adversely affect critical material properties. A detailed discussion on national and international fire protection regulations and test methods for plastics is presented by Troitzsch (1983).

10.6.1.10 ASTM D2863 Measuring the Minimum Oxygen Concentration

The method provides means for the determination of relative flammability of plastics by varying the oxygen to nitrogen concentration. The oxygen indexer is shown in Fig. 10.60.

10.6.2 Factors Affecting Flammability

Application of a heat source, such as flame, raises the temperature of polymer and ultimately causes it to burn. Burning of a solid polymer has been divided into four stages: (i) heating, (ii) decomposition, (iii) ignition, and (iv) combustion (Landrock 1983). In the first stage, a thermoplastic material softens or melts and begins to flow. The temperature at which it melts can have a significant effect. In the second stage, gases or the volatile fragments of degraded polymer are removed. The temperature and the rate at which this occurs depend on the thermal stability of polymer and the chemical reactions occurring under those conditions. Ignition takes place as the flammable gases combine at appropriate ratios with oxygen from the air.

Sustaining the burning depends on the transfer of sufficient heat from the flame to polymer, capable to maintain supply of flammable decomposition byproducts. Supply of oxygen is also essential. If decomposition of the polymer requires more heat than it is supplied by the flame, or if solid nonflammable residues coat the surface and insulate the remainder of the flammable part, a continuous propagating flame will not be obtained. Thus, the last stage of the burning sequence very much depends on the polymer characteristics. It may be correlated with such energy factors as cohesive energy, hydrogen bonding, heat of combustion, and dissociation energy (Einhorn 1972).

An interesting relationship between polymer structure and polymer flammability has been observed. Commercial polymers that possess aromatic groups in the main chain (e.g., PPE, PC, PSF, phenolic resins) undergo char-forming condensed-phase reactions – as a result they have low flammability. Higher oxygen index of PC and PPE was apparently related to their higher charring tendency in comparison to the aliphatic hydrocarbon-type polymers. The greater thermal stability of aromatic-type polymer backbone leads to a higher tendency for condensation into aromatic chars and, therefore, to the less flammable products (Fenimore and Martin 1966).

Van Krevelen had confirmed the empirical relationship between polymer structure, char formation, and polymer flammability. A mathematical formula was proposed that (based on structural units) allows calculation of the oxygen index and char residue values for a wide variety of hydrocarbon polymers. The very existence of such a relationship indicates that pyrolytic condensed-phase process is of primary importance in determining polymer flammability at least in the studied cases (Van Krevelen 1975).

A relationship between the polymer structure and its flammability was related to unsaturation for co-polyterephthalates and co-polycarbonates (Quinn 1977). This work is an excellent illustration of the importance of condensed-phase pyrolytic mechanisms upon polymer flammability.

10.6.3 Prevention Methods

Since a thorough review of fire-retardant methods is beyond the scope of this chapter, only a brief summary is given below. The readers interested in a more

detailed discussion are referred to pertinent reviews (Einhorn 1972; Hilado 1972, 1981; Vandersall 1971). Four general methods for reduction of polymer flammability have been identified (Kuryla and Papa 1978):

- A nonflammable coating that prevents the normal pyrolytic or combustion mechanism is either applied to the polymer surface or produced in the presence of a flame.
- Appropriate chemicals are incorporated during polymer processing. Their role is either to alter the rate of pyrolytic fuel generation or to inhibit the exothermic gas-phase reactions.
- Gas-phase flame reaction can be prevented by the generation of nonflammable gases, which dilute the fuel gases below the flammability limits.
- Incorporated solid components consume sufficient heat during pyrolytic decomposition that they sufficiently cool the substrate to a temperature below the ignition point.

In any given fire retardant, one or more above methods may be used. The effect of a fire retardant strongly depends on the basic chemical structure of the polymeric material. Owing to complexity of the processes and the experimental limitations, it is difficult to predict which mechanism is most important or operative for any system. A list of commercially available fire retardants is given in Appendix 2 (Table 10.37). These materials are classified as organic, inorganic, and reactive types. A fact to be kept in mind is that for blends or alloys, the fire retardancy behavior is usually between those of the base resins; for example, consider Arylon and Kydene (acrylic/PVC) (Landrock 1983).

10.6.4 Review of Fire Retardancy in Polymeric Materials

The concept of fire retardancy is remarkably old. The Greek historian, Herodotus, in 484–431 BC recorded that the Egyptians imparted fire resistance to wood by soaking it in a solution of alum (potassium aluminum sulfate) (Browne 1958). The Romans added vinegar to the alum for the same purpose. Vitruvius in the first century BC described the natural fire-retardant properties of the larch tree and some military applications of fire-retardant materials such as plaster of clay reinforced with hair (Vitruvius 1960). In 1638, Circa recorded that Italian theaters were painted with a mixture of clay and gypsum (potassium aluminum silicate and hydrated calcium sulfate) to protect them from fire. Wild was issued a British patent in 1735 for his process of treating wood with a mixture of alum, ferrous sulfate, and borax (sodium tetraborate decahydrate). And Gay-Lussac in 1821 showed that a solution of ammonium phosphate, ammonium chloride, and borax acts as a fire retardant for wood.

In all these processes the key ingredients are the elements from group III (B and Al) of the periodic table. Now, at the end of the twentieth century, with so much of research activity for better fire retardants, the most effective elements are still found in groups III (B and Al), V (N_2, P, and Sb), and VII (Cl and Br). Research efforts to find new and improved fire-retardant agents for synthetic polymers and their blends have been concentrated on the same three groups of the periodic table, with the same seven elements. The search is for new ways of incorporating them into polymers

(Chamberlain 1978). Certain compounds based on Ba (group II), Zn (group II B), and Sn (group IV) are claimed to be effective in some polymers, especially when used in conjunction with one or more of the seven key elements mentioned above.

The burning or non-burning characteristics of plastics have been given a great deal of attention by the scientific community. After the Federal Trade Commission (FTC) announced inquiry into flammability of plastics in October, 1972, the suppliers started more carefully to describe flammability of their products. ASTM and other standard developing groups have given considerable effort to develop more meaningful tests and have dropped or modified certain tests. Thus, ASTM D1692 was discontinued (Hendersinn 1977).

A theory that certain flame retardants vaporize and produce an effect by acting as free-radical chain stoppers to extinguish the flame or to inhibit the flame speed of the burning gases was proposed. It is based on extensive studies for 30–40 years (Kuryla and Papa 1978). The research efforts devoted to understand the mechanisms of combustion and inhibition for solid materials burning with a diffusion flame in an air environment have multiplied rapidly in the last two decades.

Polymer matrix-based nanocomposites have become a prominent area of current research and development. Exfoliated clay-based nanocomposites have dominated the polymer literature, but there are a large number of other significant areas of current and emerging interest. Increased flammability resistance has been noted as an important property enhancement involving nanoplatelet/nanofiber modification of polymeric matrices. The primary advantage noted with nanofiller incorporation is the reduction in the maximum heat release rate (determined by cone calorimetry) (Morgan 2006; Bourbigot et al. 2006). The majority of the flame retardant studies on nanofiller incorporation in polymers involve exfoliated clay. Studies involving PA6 (Dasari et al. 2007; Kashiwagi et al. 2004) and PP (Qin et al. 2005) yielded similar observations with reduced peak heat release rate but no change in the total heat release with exfoliated clay addition. The primary advantage for nanofiller addition for these tests generally involves reduction in the flame retardant additives that need to be incorporated to pass the specific test (Morgan 2006; Schartel et al. 2006; Nazare et al. 2006). This has been observed in various nanoparticle modified composites including exfoliated clay with halogen-based flame retardants/Sb_2O_3 (Zanetti et al. 2002) and EVA nanocomposites with magnesium hydroxide nanoparticles and microcapsulated red phosphorus (Lv and Liu 2007).

Studies involving carbon nanotubes have also shown decrease in the peak heat release rate with no change in the total heat release (Kashiwagi et al. 2002, 2005) with effectiveness equal to or better than exfoliated clay. The level of dispersion of the carbon nanotubes in the polymer matrix was shown to be an important variable (Kashiwagi et al. 2005). Upon combustion, the surface layer was enriched with a protective nanotube network providing a thermal and structural barrier to the combustion process. Continuity of the network was important to achieve optimum performance as very low levels of nanotube incorporation or poor dispersion did not allow a continuous surface network during the combustion process. It is noted that the incorporation of nanoclay and carbon nanotubes often results in slightly earlier

ignition than the unmodified polymer presumably due to the increased thermal conductivity. However, at the later stages of combustion, the reinforcement of the char layer provides a stable thermal barrier preventing regeneration of polymer at the surface available for rapid combustion (Paul and Robeson 2008).

Fire retardancy behavior of PP/PA66 blends compatibilized with PP-g-MAH and modified with untreated and treated nanoclays was studied (Kouini and Serier 2012). It was found that the intercalation, exfoliation of nanoclays of nanocomposites, and the flame retardancy properties were improved significantly. In addition a good balance of impact strength and flame retardancy was obtained for PP/PA66 nanocomposites in the presence of PP-g-MA compatibilizer. The presence of the clay led to an increase in the flammability time. In addition, the treatment made a more pronounced effect. A 23 % increase was observed only when 4 wt% nanoclay was added and a longer flammability time was noticed with treated clay. This was attributed to the stacking of nanoclay which created a physical protective barrier on the surface of the material. Similar behavior has been reported by earlier workers (Kocsis and Apostolov 2004).

Thermal insulating materials are required to protect structural components of space vehicles during the reentry stage, missile launching systems, and solid rocket motors. A series of review papers were published (Koo et al. 2006, 2007; Ho et al. 2007) on using polymeric composites as ablative thermal protection systems for a variety of military and aerospace applications. Thermal protection materials such as char-forming phenolics and carbon–carbon composites are used for spacecraft heat shields, rocket motor insulation, and rocket nozzle assembly materials. The TPU nanocomposites (TPUNs), with the addition of nanoclays and carbon nanofibers, are prepared, and properties such as density, specific heat capacity, thermal diffusivity, and thermal conductivity of the different TPUN compositions were determined. Cone calorimetry was employed to study the flammability properties of these TPUNs. These novel materials were proposed to replace Kevlar-filled EPDM rubber, the current state-of-the-art solid rocket motor internal insulation (Ho et al. 2010).

10.6.5 Data on Blends

The flame retardancy properties of some commercial polymer blends are given in Table 10.29.

10.7 Electrical Properties

10.7.1 Standard Methods of Measurement

10.7.1.1 Resistivity of Insulating Plastics

Measurements of insulating polymers or polymer blends are usually carried out using a sheet specimen in form of a disc or a square (ASTM D257).

Table 10.29 Data on blends

Blend (trade name, grade, and manufacturer)	UL 94 Flame class			Oxygen index
	HB rating (inch)	V-0 rating (inch)	5 VB rating (inch)	ASTM D 2863-97
PC/ABS **Cycoloy**, GEC	**0.060**	**0.060**	**0.098**	**<21.0**
ASA/PC **Geloy**, XP 1001, XP 2003, XP 4001, GEC	**0.063**	**0.130 V-1**	**0.130 VA**	**–**
PC/PBT **Xenoy**, 6120, 6240, 6123, 6370, 6620, 6380, GEC	**0.061**	**–**	**–**	**–**
PC/ABS **Bayblend**, Miles; FR 1439	**–**	**0.062**	**–**	**28**
FR 1440, FR 1441	**–**	**0.062**	**–**	**30**

Commercially available resistance meters can measure resistance in the range from 10^6 to 10^{15} Ω. In the case of plastics, the method can be applied if the resistance values are of the same order or lower than the volume resistance and if the volume resistivity is $>10^8$ Ω. Flat plate metal electrodes, preferably guarded (Fig. 10.61), are used for testing flexible and compressible materials (at room or elevated temperatures).

Voltmeter–Ammeter Method

The DC voltmeter and the DC amplifier (or electrometers to increase the sensitivity) are connected to the voltage source and the specimen. The applied voltage, V_x, is measured by a DC voltmeter. The current, I_x, is measured in terms of voltage drop across a standard resistance R_s. The voltage drop is amplified by the DC amplifier and read on an indicating meter as V_s. The resistance R_x or the conductance G_x is calculated as

$$R_x = \frac{1}{G_x} = \frac{V_x}{I_x} = \left(\frac{V_x}{V_s}\right) R_s \tag{10.31}$$

The time of electrification, unless otherwise specified, should be 60 s and the applied direct voltage $V_x = 500 \pm 5$ V.

Volume Resistivity or Conductivity

Measure the dimensions of the electrodes and width of the guard gap, g, accurately. Unless otherwise specified, the time of electrification should be 60 s and the applied direct voltage 500 ± 5 V. Volume resistivity is expressed as (Ω-cm)

$$\rho_v = \frac{A}{tR_v} \tag{10.32}$$

where A = the effective area of the measuring electrode (see Fig. 10.61), t = average thickness of the specimen, R_v = measured volume resistance in Ω.

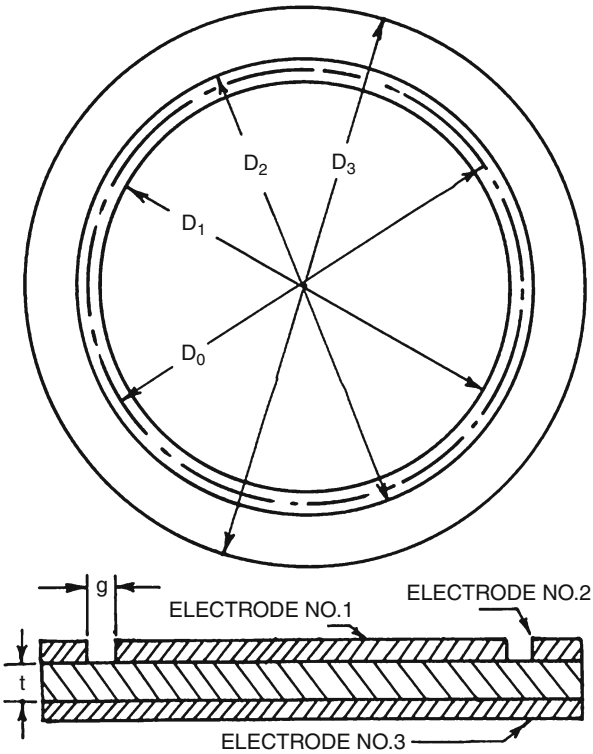

Fig. 10.61 Top view and side view of flat plate guarded metal electrodes [ASTM D257]

Volume conductivity is calculated as (S/cm)

$$\nu_v = \frac{t}{AG_v} \tag{10.33}$$

where G_v = measured volume conductance in Siemens.

Surface Resistivity or Conductivity

The electrode dimensions and the distance between the electrodes, g, are to be measured accurately. The surface resistance or conductance between electrodes No. 1 and 2 is measured with a suitable device (Brown 1981). The time of electrification should be 60 s and the applied direct voltage shall be 500 ± 5 V.

Surface resistivity, per square cm is given by

$$\rho_s = \frac{P}{g\,R_s} \tag{10.34}$$

where P is the effective perimeter of the guarded electrode (see Fig. 10.61), R_s is the measured surface resistance in Ω, and g is as indicated in Fig. 10.61. For specimens of square, rectangular, and tube forms, appropriate electrodes and mathematical relations are given in ASTM D257.

BS 4618 recommends preconditioning of the test specimens at not more than 1 % relative humidity (RH) for the study of effect of temperature. ASTM D257 covers resistivity measurements for insulating materials. Electrode sizes are not stipulated (round, square, and rectangular types are permitted). The gap between guard ring and center electrode is made approximately equal to twice the specimen thickness. The test voltage is usually 500 V applied for 60 s, as in the British test.

DIN 53482 uses methods similar to some of those in IEC 93, using silver or graphite painted electrodes for volume resistivity. A different electrode system was suggested for the measurements of surface and volume resistivity. A narrow guard gap of 1 mm makes it difficult to avoid short-circuiting the electrodes.

Power Factor and Permittivity

Measurements of dielectric constant and loss in polymeric solids and melts over a wide frequency range were described in detail elsewhere (Porter and Boyd 1972). An updated and detailed account of these topics may be found in ▶ Chap. 12, "Broadband Dielectric Spectroscopy on Polymer Blends" of this handbook (Andreas Schonhals 2014).

The measurement of power factor and permittivity and the related parameters such as dissipation factor, phase angle, etc., may need to be carried out over a wide range of frequencies from a few Hz to several tens of GHz. However, most measurements are made between 50 Hz and 100 MHz (Brown 1981).

Insulating materials, such as polymers and polymer blends, are used as dielectrics at commercial frequencies between approximately 50 Hz and 100 GHz. Two different techniques are adopted to study the dielectrics in two ranges, i.e., below and above 100 MHz. Dielectric measurements at ultralow frequencies are of some interest, as they reveal the basic structure of the material (McCrum et al. 1967). Bridge circuits are invariably employed for the measurements of power factor and permittivity.

The test specimen, whose dielectric constant and loss factor are to be measured, is cut or molded to a suitable shape and thickness determined by the material specifications or the test method. The thickness of the specimen must be accurately measured. The electrodes are selected, based on convenience and whether or not the specimen must be conditioned at high temperature and high relative humidity. The test specimen with its attached electrodes is placed in a suitable measuring cell, and its capacitance and a-c loss are measured using a suitable bridge. For routine work when either the highest accuracy is not required, or when neither terminal (of the specimen) is grounded, it is not necessary to place the solid specimen in a test cell.

In the Schering Bridge, one sets the ratio R_1/R_2 (range) and varies C_s and C_1 to obtain a balance (ASTM D150):

$$C_x = \left(\frac{R_1}{R_2}\right) C_s \tag{10.35}$$

$$D_x = W.C_1R_1 \tag{10.36}$$

The test method covers dielectric measurements from 1 Hz to several hundred MHz. It has few recommendations about the procedure or apparatus.

Size of the electrodes is not suggested and it is recommended that the guard gap should be as small as possible and the guard width should be at least twice the thickness of the specimen. An appendix is provided, which describes number of bridges and their circuits. The German standard for dielectric measurements is DIN 53483.

Dielectric Strength

Low-level conduction in insulating materials can originate in a variety of ways. Often it is attributed to impurities that provide small concentrations of charge carriers in the form of ions and/or electrons. At high fields, the electrodes may also inject new carriers into the polymer, causing the current to increase more rapidly with voltage. At very high fields, these and other processes inevitably lead to complete failure of the polymer as a dielectric. This localized, sudden, and catastrophic phenomenon is known as the dielectric breakdown (Ku and Liepins 1987). In many cases the dielectric breakdown or dielectric strength of a material can be the determining factor in the design of an apparatus in which it is to be used.

A method for determination of dielectric strength of solid electrical insulating materials at commercial power frequencies was developed (ASTM D149). The voltage can be applied at a fast uniform rate or step-by-step or at a slow rate of rise. At the dielectric breakdown voltage, an abrupt rupture through the specimen results in a visible puncture and decomposition of the material – the occurrence can be seen and heard. This form of breakdown is irreversible. Dielectric strength is calculated (in terms of KV/mm or V/mil) by noting the gradient at the highest voltage step at which breakdown did not occur. BS 2782 Method 201, deals with plastics breakdown voltage. Other British standards such as BS 3784, BS 3816, BS 3924, and BS 5102 directly invoke BS 2782.

10.7.2 Factors Affecting Electrical Properties

Factors such as improper mixing of polymer blends lead to variations in test specimens. Such compositional and/or structural changes from specimen to specimen often lead to widely divergent data.

10.7.2.1 Effect of Temperature

Resistivity depends on temperature – for nonmetallic materials it invariably decreases with T. Volume resistivity is markedly more sensitive to temperature than surface resistivity. In any measurement it is important to ensure that temperature is maintained constant during the test. Temperature fluctuations produce changes in measured current and lead to significant errors (Brown 1981; ASTM D257). In the case of power factor or permittivity determinations, the effects of temperature and frequency are interrelated. With nonpolar polymeric materials, the changes in properties with temperature and frequency are small, while with polar materials very large changes may take place.

10.7.2.2 Effect of Humidity

The insulation resistance of solid dielectric materials decreases with increasing humidity. Surface resistance is particularly sensitive to humidity changes. Insulation resistance or conductance is a function of both the volume and surface resistance or conductance of the specimen. Surface resistance changes almost instantaneously with a change of RH. Therefore, it is essential to maintain both T and RH within close limits during the conditioning and measuring of the specimens. In a humid environment, absorption of water into the volume of the insulating material as well as the formation of an ionized water film on the specimen surface takes place. These factors lead to significant rise in the insulating materials' permittivity and loss index. The process of dielectric breakdown in the case of neat polymers is not completely understood, and many unknowns are still remaining (Ku and Liepins 1987).

Still many uncertainties exist for polymer blends and alloys. However, it is clear that the chemical structure, the solid-state structure, degree of plasticization, the nature and concentration of filler, molecular weight and morphology of a polymer, etc., influence the electrical properties. For example, the dielectric breakdown of EVAc and its blends was studied in the low-temperature region (193 K) (Nagao et al. 1976, 1977). The dielectric breakdown voltage of EVAc and blends was found to rise with an increase in VAc content. This may be caused by increased electron scattering associated with the decrease of crystallinity and the increase of polar groups.

The process of polymer blending was used for improving the mechanical properties of electric wire insulation, as early as 1968 (Ku and Liepins 1987). In 1978, it was found that the use of a HDPE/LDPE blend enhanced the electrical treeing inception voltage (Nitta and Funayama 1978). This approach to electrical treeing inhibition and some of the experimental results on the use of SB/LDPE and HDPE/LDPE blends are given in Table 10.30 (Wu and Chen 1983).

10.7.3 Review of Blends' Electrical Properties

Most polymers have high electrical resistivity, are inexpensive in comparison to other known insulating materials, and are heat resistant and sufficiently durable. Owing to their sensitivity to oxidation and solvents, they are frequently blended to generate better electrical insulating alloys. In the past two decades, there has been serious effort to modify the electrical properties of polymers and their blends. The electrically conductive polymers can be broadly categorized as (i) electrostatic dissipating polymeric compositions and (ii) electrically conductive polymer blends. Utracki has reviewed evolution of these materials (Utracki 1998).

The electrostatic dissipating polymeric compositions (ESD) are developed to overcome problems related to the accumulation of surface charge and its rapid discharge leading to shocks, fire, explosions, damage to electronic components, etc. These compositions must provide surface resistivity $10^5 < R < 10^{12}$ (Ω cm).

Table 10.30 Effect of polymer blending on tree growth and length (Wu and Chen 1983)

Parameter	LDPE	SBR			HDPE		
Modifier wt%	100	10	20	30	10	15	20
Tl (min)	–	198	127	54	25	70	90
T2 (min)	300	100	200	230	156	170	160
T3 (min)	–	2,180	2,200	–	75	30	2,100
Tl + T2 + T3 (min)	2,300	2,478	2,527	2,284	250	270	2,350
Length §(μm)	1,300	300	600	1,400	450	500	400

T1, induction period for tree initiation in minutes; T2, growth period of the tree in minutes; T3, the saturation period of tree development in minutes; §, The length of the tree after saturation period

The early efforts to achieve the optimum surface resistivity, such as coating the polymeric parts with electrostatic dissipative materials, addition of either graphite, metal particles or fibers, incorporation of low molecular weight antistatic agents, etc., did not yield fruitful results (Kozlowski 1995). Antistatic properties are observed for materials having either -SH or –OH groups (e.g., phenolic, alcoholic, or acidic).

Since the mid-1980, the most frequently used ESD has been a copolymer of ethylene oxide and epichlorohydrin, EO-CHR. Many chemical companies (such as Borg-Warner, B.F. Goodrich, Asahi, and General Electric) came up with several ESD formulations containing EO-CHR for improving the electrostatic properties of PVC, CPC, PC, PEST, epoxy, phenolics, etc. (Federl and Kipouras 1986; Kipouras and Federl 1988; Yu 1988; Lee 1993; Shimamura and Suzuki 1991; Giles and Vilasagar 1994).

The second variety of materials, viz., electrically conducting polymer blends, ECPB, has been known since the early 1980s. These are prepared, in principle, by synthesis of the conducting polymer within the host or by simple blending (Billingham and Calvert 1989). Polyacetylene, PACE, blends were prepared by the polymerization of acetylene in LDPE films doped with Ziegler catalyst (Galvin and Wnek 1982, 1983; Galvin et al. 1984). PACE formed a particulate second phase with a size ranging from 60 to 200 nm. Addition of 7 % PACE LDPE increased the yield point of the latter resin from 7 to 10 MPa, but the extension to break was reduced. The effect was greater in blends produced by polymerization in solid PE.

Acetylene was polymerized in the presence of polybutadiene rubber, and the blends were investigated for their electrical conductivity (Rubner et al. 1983; Sichel and Rubner 1985). The electrical properties of these blends were explained in terms of the morphological features (Tripathy and Rubner 1984). In these investigations, a conductivity of 10 S/cm was achieved at PACE loadings above 30 %. Polymerization of acetylene in EPDM resulted in tough, conductive films (Lee and Jopson 1983, 1984). The conductivity of these films was found to be significantly enhanced by stretching.

Mechanical blending of various conducting polymers with thermoplastics was studied (Wessling and Volk 1987). These materials although processable showed low electrical conductivity ($<10^{-5}$ S/cm). They were prepared by blending an electrically

conductive polymer (such as polyacetylene or polypyrrole) with a polymer having strong anionic group (such as sulfonated PE, sulfonated SEBS, sulfonated PS, or sulfonated polyacrylamidomethylpropane) (Cross and Lines 1995).

Electrically conducting polymer blends are also produced by blending another conducting polymer (e.g., poly-3-octylthiophene) with a matrix polymer (e.g., PP, PVC, PS, PE, EVAc, PVC/ABS, etc.) introducing a dopant (e.g., iodine) (Kokkonen et al. 1994). Several strategies were adopted in preparing ECPBs. In one example, polyaniline was blended with dodecylbenzenesulfonic acid, mixed with PS, PE, or PP and then melt processed. In another case, polyaniline was mixed with protoning acid metallic salt. The conductive material was melt mixed with PE, PS, PP, or ABS (Karna et al. 1994a, b).

ECPBs were prepared by melt blending a matrix polymer (selected from between PE, PP, PB, PIB, PMP, EPR, CPE, CSR, PS, polyalkanes containing styrene, acryl, vinyl, or fluoroethyl groups and their blends) and an electrically conducting thermotropic liquid-crystal polymer, containing either ferric chloride or iodine as a dopant. The blend which could be manufactured into fibers and films was reported to have conductivity as 10^{-12}–10^{2} S/cm (Ho and Levon 1995). Amine-terminated polyaniline was first grafted onto a thermoplastic polymer comprising a functional group capable of reacting with -NH_2, e.g., maleic anhydride. They were further compounded with polymers, fillers, and/or electrically conductive solids (Jongeling 1993). Blends of PVC with "doped" polyaniline and at least one other additive (e.g., impact modifier, plasticizer, acidic surfactant) were developed to give electrically conductive blends.

ECPBs were also prepared compounding polyaniline and a thermoplastic polymer (selected from PA-6, PA-66, PA-11, PA-12, PET, PC TPU, CPE, etc.) and 0–10 wt% carbon black (Kulkarni and Wessling 1992, 1993). Electrically conductive materials were prepared by dispersing pre-blends of aniline to sylate particles and poly(ethylene terephthalate glycol), PETG, and then diluting the pre-blend with PETG. The blends were useful for the manufacture of films, printing inks, and coatings, in shielding, antistatic, and adhesive applications (Shacklette et al. 1993). Curable blends, with good flame retardancy, comprising of fluorine-containing polycyanurates and a thermoplastic polymer (e.g., PSF, PPE, and PEEK) were patented by IBM in 1992. The filled materials were useful in several applications (fabrication of printed circuit boards, semiconductor chip carriers, metal-core boards, chip modules, and multilayer thin film circuits) (Ardakani et al. 1994).

Conducting polymer fibers were prepared by melt mixing and chemical coating on fibers. Different conductive materials were used in order to obtain conductive PP-based fibers with specific electrical and mechanical properties. The electrical conductivity and morphological characteristics of these fibers were investigated (Kim et al. 2004). The conductive fibers are intended for use in creating conductive yarns, conductive fabrics (which can be used as electromagnetic shields), and multifunctional textile structures for novel applications.

Melt-processed immiscible polymer blends of HIPS, LCP, and CB were prepared. Relationships between composition, electrical resistivity, and morphology of the blends produced by adopting different processing methods

were investigated. The LCP phase morphology in the blends was found sensitive to the processing conditions. An important role of the skin region in determining the resistivity of injection-molded samples was found. The study also revealed that shear rate effect on resistivity of capillary rheometer filaments might serve as a predictor of resistivity behavior in real processing procedures (Tchoudakov et al. 2004). Such studies are not frequent. In fact, processing–structure–property relationships in electrical properties of polymeric materials are rarely available.

A two-step method was used to prepare carbon nanotube (CNT)/(EVA)/(PE) and CNT/(PC)/PE composites. First, CNT–EVA and CNT–PC master batches were obtained by solution-phase processing, and second, the CNT master batches were melt mixed with PE. Phase morphological observations revealed decrease in the size of the dispersed particles in the composites (Li et al. 2007).

Pure polyaniline (PANI) and its blends with PVA and PEO were prepared by solution cast method. The blends were characterized by XRD, FTIR, and SEM techniques. The blends were prepared in order to combine the mechanical properties of PVA and PEO with conducting properties of PANI. It was found that the conductivity of pure PANI was more than PANI blends (Subrahmanyam et al. 2012).

Nunoshige et al. developed a novel low-dielectric-loss thermosetting material by blending poly(2-allyl-6-methylphenol-co-2,6-dimethylphenol) (Allyl-PPE) with 1,2-bis(vinylphenyl)ethane (BVPE). BVPE could be used effectively as a cross-linking agent for Allyl-PPE, decreasing the cured temperature to 523 K or lower. The cured products exhibited better thermal and thermomechanical properties. The effect of the composition of the blends on the dielectric constant and the dielectric loss were evaluated (Nunoshige et al. 2007).

Mao et al. had tuned the morphology to improve the electrical properties of graphene filled immiscible polymer blends. PS and PMMA blends filled with octadecylamine-functionalized graphene (GE-ODA) were fabricated to obtain conductive composites with a lower electrical percolation threshold. The dependence of the electrical properties of the composites on the morphology was examined by changing the proportion of PS and PMMA. The electrical conductivity of the composites was optimal when PS and PMMA phases formed a co-continuous structure. For the PS/PMMA blend (50 wt/50 wt), the composites exhibited an extremely low electrical percolation threshold (0.5 wt%) because of the formation of a perfect double percolated structure (Mao et al. 2012).

Advances in nano-material research have opened the door for transparent conductive materials, each with unique properties. These include CNTs, graphene, metal nanowires, and printable metal grids. Transparent electrodes are necessary components in many modern devices such as touch screens, LCDs, OLEDs, and solar cells, all of which are growing in demand. Traditionally, this role has been well served by doped metal oxides, such as indium tin oxide. A review exploring these innovations in transparent conductors and the emerging trends is presented recently (Hecht et al. 2011). Electrical conductivity in PS nanocomposites with ultralow graphene level was found to enhance significantly (Qi et al. 2011).

10.7.4 Data on Blends

Electrical properties of selected commercial polymer blends are listed in Table 10.31.

10.8 Optical Properties

10.8.1 Methods of Measurement

10.8.1.1 Haze and Luminous Transmittance

ASTM D1003 provides two methods for measuring light transmittance and haze in planar sections of transparent plastics. The method making use of a hazemeter is briefly described.

A spherical hazemeter, which is pivotable about a vertical axis through the entrance port (where the specimen is placed), is shown in Fig. 10.62. In the normal position the collimated incident light passes straight through the sphere, leaving through the exit port, which is closed by an absorbent light trap. When light is scattered either by the instrument alone or by the specimen and the instrument (when the specimen is loaded), it is reflected from the region around the edge of the exit port and finally collected by the photocell after multiple reflections from the highly reflecting walls of the sphere.

When the integrating sphere is rotated slightly so that the incident light hits the opposite highly reflecting wall of the sphere adjacent to the exit port, the measurements with and without a specimen give a measure of the total transmittance. The total transmittance, T_t, is given by

$$T_t = \frac{T_2}{T_1} \tag{10.37}$$

where T_2 = the total light transmitted by the specimen and T_1 = the incident light without the specimen. Diffuse transmittance, T_d, and % of haze are calculated as

$$T_d = \frac{\left[T_4 - T_3\left(\frac{T_2}{T_1 1}\right)\right]}{T_1} \tag{10.38}$$

$$\text{Haze } (\%) = 100\left(\frac{T_d}{T_t}\right) \tag{10.39}$$

where T_4 = light scattered by instrument and specimen and T_3 = light scattered by instrument (without specimen). BS 2782 Method 515 A is the British equivalent, which deals with only haze of films.

10.8.1.2 Refractive Index

When a ray of light passes from one isotropic medium into another, the sinus of the angle of incidence makes a constant ratio to the sinus of the angle of refraction (both

Table 10.31 Data on some commercial polymer blends (Martino 1994)

No.	BLEND (trade name, composition, and manufacturer)	Volume resistivity (ohm-m) ASTM D257-99	Surface resistivity (ohm) ASTM D257-99	Dielectric strength oil, 0.125″; V/mil (3.2 mm; kV/mm) ASTM D149-97	Dielectric constant (100 Hz), ASTM D150-98	Dissipation factor (100 Hz), ASTM D150-98
1.	**CYCOLOY** C2950 (PC/ABS) GE Thermoplastics	1.0E15		495 (19.3)	3.0	0.0049
2.	**GELOY** GY1220(ASA/PVC) GE Thermoplastics	1.4E12	1.0E15–1.8E15	476 (19)–490 (17) (in air)	3.4–3.5	0.0007–0.0021
3.	**XENOY**-2230, 2735, 5220, 5230, 5720 (PC/PBT) GEC	2.1E14–9.5E14		705 (28)–1,096 (43) (in air)	2.93–3.60	0.001–0.002
4.	**MAKROBLEND**					
	(PC/PET) UT 1018	>2.6E13		396	3.06 (l MHz)	0.014 (1 MHz)
	UT 400 and UT 403 MILES	>7.4E13		406	3.10 (l MHz)	0.009 (1 MHz)
5.	**BAYBLEND**(PC/ABS) MILES					
	T45MN, T65MN, T44, T64	>1.0E14	>1.0E14	600		0.007 (l MHz)
	T85MN, T84	>1.0E14	>1.0E14	600		0.008 (l MHz)

Note: ASTM standard test methods are available on web: http://enterprise.astm.org/

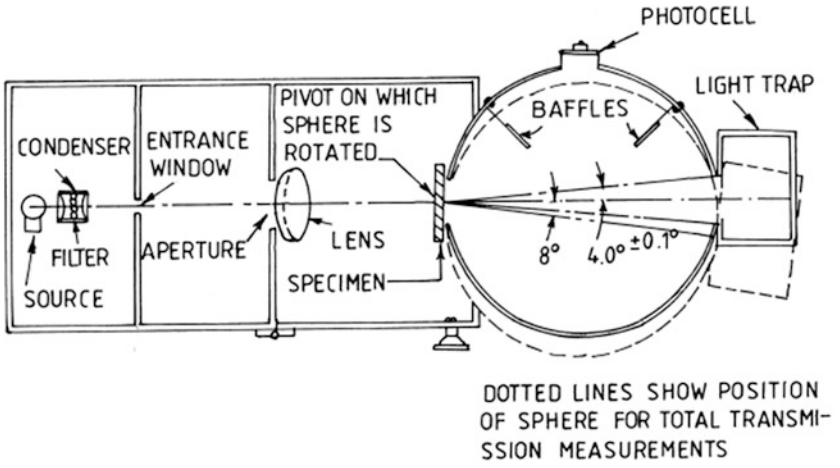

Fig. 10.62 Pivotable-sphere hazemeter [ASTM D1003]

measured with respect to the normal) for all angles of incidence. This dimensionless ratio, while dependent on the wavelength of the light and temperature, characterizes the two media concerned.

ASTM D542 describes two methods, viz., (i) refractometric and (ii) microscopic, for the measurement of refractive index of transparent organic plastics. Both the methods require optically homogeneous specimens of uniform index. The ASTM recommends that refractometric method is to be preferred wherever possible, since it is capable of providing results with greater precision (up to four significant figures). The microscopic method depends on operator's skill, and it yields results accurate up to only three significant figures.

For the refractometric method, the apparatus consists of an Abbe refractometer, a suitable source of white light and a small quantity of suitable contacting liquid. The test specimen for refractometer method should be 12.7 × 6.3 mm, with one flat face and one perpendicular surface. The two surfaces (preferably polished) shall intersect along a sharp line (without a rounded edge). The test specimen is attached to the prism of the refractometer with a drop of liquid of refractive index higher than the test specimen by at least 0.01, and it should not soften or dissolve the specimen. ASTM D542 suggests a list of liquids for a variety of plastics. Measurements are to be carried out at specified conditions, 296 ± 2 K and 50 ± 5 % RH. Temperature is to be accurately controlled. For maximum accuracy, sodium D lines are recommended.

ISO R489 suggests two methods based on Abbe refractometer and the Becke line methods. It does not recommend any specimen conditioning procedure prior to the test. DIN 53491 provides practical details relevant to refractometer measurements. It recommends test temperature as 293 ± 5 K, like ISO R489. For maximum accuracy it suggests the use of sodium light. All these methods provide lists of liquids suitable for different plastics.

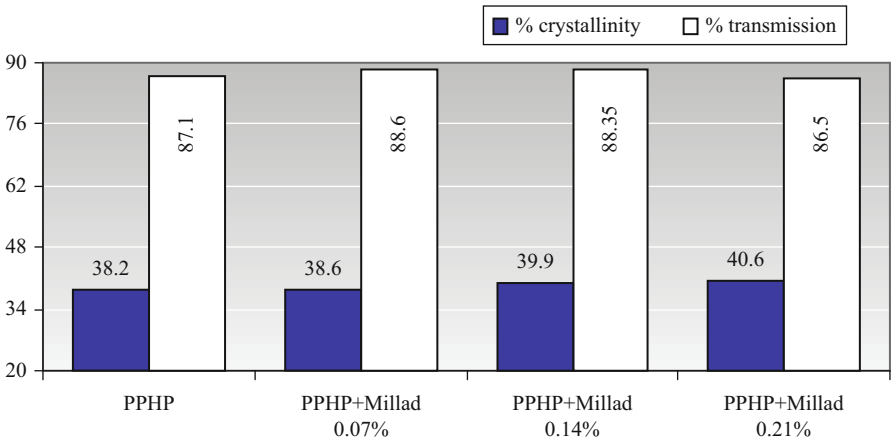

Fig. 10.63 Transmission (%) determined using Haze Meter and crystallinity (%) measured using X-ray diffraction are shown for polypropylene homopolymer mixed with different concentrations (0.07 wt%, 0.14 wt%, and 0.21 wt%) of Millad-3988 (Pendyala et al. 2004)

10.8.2 Transparency in Polypropylene

The degree of crystallinity and regularity of crystallite size have noticeable effects on properties of bulk isotactic polypropylene (PP). Clarity is commonly obtained in PP in two ways. First, resins with lower crystallinity will be clearer than those with higher, but a minimum level of crystallinity is necessary to provide the required strength, stiffness, and resistance to softening at elevated temperature expected of the PP. Second, certain nucleating agents greatly improve the clarity of PP by producing very small crystals in the polymers. These smaller crystals are below the size which scatters visible light that produces haze. Crystallinity vis-à-vis transmission in polypropylene homopolymer with different concentrations of Millad-3988 is illustrated in Fig. 10.63 (Pendyala et al. 2004).

Isotactic polypropylene can crystallize into three different forms: (i) α-phase, (ii) β-phase, and (iii) γ-phase. These spherulites satisfy two requirements to scatter light – they are larger than the wavelength of light and they have a refractive index different from that of the amorphous region. The refractive indices of the crystalline and amorphous regions of a polymer cannot be changed. So, in order to improve clarity, the average spherulites' size must be reduced. Since a spherulite grows until it meets another, their size is dependent on the number of nucleation sites (nucleation density) within the crystallizing polymer.

PP with improved clarity was commercialized in the 1980s by incorporating sorbitol-based clarifying agents by Milliken Chemical Co. and others (Carroll 1984). In PP, the crystallization results in large size spherulites, and hence inclusion of heterogeneous nucleating agents is often adopted to improve mechanical properties (Quande Gui and Weiping Zhu 2003) or to reduce optical haze (Sterzynski et al. 1994; Mannion 1994; Gahleitner et al. 1996; Amos et al. 1999; Zhao and Dotson 2002).

Hence, providing such heterogeneous nucleation is an essential consideration. Creation of various crystallographic phases, differed by the unit cells as well as by the spherulites, is known to be a result of the heterogeneous nucleation (Varga 1992; Lotz 1998).

10.8.3 Review of Blends' Optical Properties

Lack of transparency is a significant drawback in the commercially important toughened polymers such as HIPS or ABS (Manson and Sperling 1981). Transparency in these materials is lost due to the light scattering at the interface between the phases. The degree of light scattering (turbidity) was found to be a function of the amount of dispersed phase present, its particle size, the ratio of refractive indices of the phases, and the wavelength of light. In typical polymer pairs, at a given dispersed phase level, the maximum turbidity was observed in the range of particle sizes considered to be necessary for good impact strength (Conaghan and Rosen 1972). If the refractive indices are matched at a particular temperature, small particle sizes greatly increase the temperature range over which scattering is minimized. In other words, a clear blend can be obtained if both phases have identical refractive indices, regardless of the details of the phase morphology (Rosen 1967). Thus, for example, clarity in ABS and toughened acrylics was achieved by matching refractive indices of the continuous and dispersed phases (Gesner 1967). Impact modifiers for PVC that can impart toughness as well as clarity were described by several workers (Petrich 1972; Souder and Larson 1966; Ryan and Crochowski 1969; Ryan 1972).

Formation of transparent blend films cast from solutions of PVC and $(PC\text{-}PDMS)_n$ multiblock copolymer has created concern (Gorelova et al. 1992). The finding is interesting because the refractive indices of PVC, PC, and PDMS are different, and consequently, transparency of the blend films may suggest miscibility of their constituents, despite the fact that PVC is immiscible with PC and PDMS (Krause 1978). In other words, these blends are pseudo-miscible and their transparency is caused by the very small size of the dispersed block copolymer phase. PVC was also found to form transparent blends with other multiblock copolymers (Papkov et al. 1995). Several examples of the formation of transparent blends were reported. The constituents of these blends are homopolymers of various chemical compositions and flexibility, viz., PS, PMMA, and PVC, and the multiblock copolymers are PC-PDMS, PSF-PDMS, PSF-PB, and polytetramethylene oxide-PB (Papkov et al. 1998). For copolymers and homopolymers of various chemical structures, the composition range for each type of block copolymer, within which the formation of transparent blend film takes place, is relatively narrow.

The phenomenon appears to be similar to the so-called miscibility window in some blends with random copolymers (ten Brinke et al. 1983). Micro phase separation and the evolution of the multiblock copolymer phase in the form of small-sized particles (up to 100 nm in diameter) is the physical basis of their transparency. Thus, these transparent blends are considered microheterogeneous

systems (Papkov et al. 1998). Detailed theoretical and experimental investigations are required to understand details of this phenomenon (Sikora and Karasz 1993).

Blends of transparent polymers are generally hazy. However, transparency is required in many products. The miscible blends, PET/PBT, maintain transparency in almost all cases regardless of the blending ratio, whereas some immiscible blends become hazy. The reason for this haze is the number and size of the dispersed particles. Differences in the refractive indices of various polymers also have a large influence on haze. Stretching makes even the transparent blends hazy, because stretching increases the size of the dispersed particles in the sheet plane and also the difference in the anisotropic refractive indices of the matrix and the dispersed phase is increased by stretching, which is in agreement with the theory of light scattering (Maruhashi and Iida 2001).

The effect of added nanoclays to the morphological characteristics and the macroscopic properties in a blend of isotactic PP and PEO was examined. It was shown that strong interactions between the surfactant used for clay modification and the binary matrix effectively controlled the spatial organization of the suspended polymer droplets. The incorporation of a small amount of organically modified nanoclay induced a dramatic transformation from an opaque to a transparent system (Kelarakis and Yoon 2008).

Several blends of polymers that varied concentrations of PMMA and polyimides based on 2,20-bis(3,4-dicarboxyphenyl)hexafluoropropane dianhydride (6FDA) were prepared in film form by solution casting and using various solvents. The miscibility of the blended films was studied. DSC thermograms revealed two T_gs for specimens using THF as a solvent, indicating immiscibility; on the other hand, samples using methyl chloride and cyclohexanone showed a single T_g, indicating miscibility between the two polymers. The transmittance for 6FDA-6FpDA/PMMA had a value of about 85 % (according to ASTM D1003), in the visual light range. However, 6FDA–6FpDA:DABA 2:1/PMMA showed a low transmittance below wavelengths of 550 nm. For haze, all of the films were clear with values of less than 1 % (Im et al. 2009).

In a separate study immiscible blends were rendered transparent. The components of the immiscible blends were having refractive indices which differ by about 0.006 to about −0.0006. The small difference in the refractive indices enabled the incorporation of regrind into the polymer composition to produce transparent shaped articles (Gilliam et al. 2011; Cliffton et al. 2012).

Interesting advances are taking place in biopolymers with regard to optical transparency. An opaque polylactide/poly(ethylene-co-vinyl alcohol) (PLA/EVOH 90/10 w/w) blend was made transparent by reactive compatibilization. In the presence of a multifunctional epoxy compound and zinc stearate, the dispersed domain size of EVOH in the blend and its distribution decreased significantly. Consequently, the light transmission at 700 nm increased from 9.3 % to 83.5 % for the compatibilized sample. A significant difference in the transparency of the samples can also be confirmed by naked eye (Zhang et al. 2013). In a separate study, binary blends composed of biomass-based cellulose acetate propionate (CAP) and poly(epichlorohydrin) (PECH) were studied. As a result of the interdiffusion, leading to fine

morphology, the blends exhibited high level of optical transparency although the individual pure components had different refractive index. Furthermore, the mechanical toughness of CAP was considerably improved by blending PECH. This will have a great impact on industries because the blend technique widens the application of CAP (Yamaguchi and Masuzava 2013).

10.9 Sound Transmission Properties

Sound retardant (acoustical) assemblies are one of the most commonly used in commercial building. An acoustical assembly is an acoustical door or window that maintains its basic operating function and is at the same time designed to be a significant barrier to the passage of sound. It is called an acoustical assembly because an entire system is involved. A sound retardant assembly encompasses not just the door or window itself but all the components around it. The wall, the frame which surrounds the door, the door itself, the hardware components, and finally the sealing system, whereby the passage of noise is minimized, all combine to create an acoustical assembly.

Sound ratings are typically based off the sound transmission class (STC) scale system, Table 10.32. This single rating system enables a designer to match up architectural products that when combined will create an STC rating for the entire assembly controlling the noise and vibration in room, office, or even an entire building.

10.9.1 Method of Measurement

The preferred method for determining the STC rating of a product is a test called the ASTM E-90, "Standard Method for Laboratory Measurement of Airborne Sound Transmission," which is summarized here below.

ASTM E90-09 provides a method covering the laboratory measurement of airborne sound transmission loss of building partitions such as walls of all kinds, operable partitions, floor–ceiling assemblies, doors, windows, roofs, panels, and other space-dividing elements (ASTM E90 2009). Laboratories are designed so the test specimen constitutes the primary sound transmission path between the two test rooms, and so approximately diffuse sound fields exist in the rooms.

Sound transmission loss refers to the response of specimens exposed to a diffuse incident sound field. The test results are therefore most directly relevant to the performance of similar specimens exposed to similar sound fields. They provide, however, a useful general measure of performance for the variety of sound fields to which a partition or element may typically be exposed. In laboratories designed to satisfy the requirements of this test method, the intent is that only significant path for sound transmission between the rooms is through the test specimen. Laboratories are designed so the test specimen constitutes the primary sound transmission path between the two test rooms and so approximately diffuse sound fields exist in the rooms.

This standard does not purport to address all of the safety concerns.

Table 10.32 Sound transmission class (ZERO International 2001)

Sound Transmission Class (STC) Table		
STC	Performance	Description
50–60	Excellent	Loud sounds heard faintly or not at all
40–50	Very good	Loud speech heard faintly. But not understood
35–40	Good	Loud speech heard but hardly intelligible
30–35	Fair	Loud speech understood fairly well.
25–30	Poor	Normal speech understood easily and distinctly
20–25	Very poor	Low speech audible

It is important to know the sound transmission loss of walls and floors in order to be able to compare different constructions, to calculate acoustic privacy between apartments or noise levels from outdoor sources such as road traffic, and to engineer optimum solutions to noise control problems. Laboratory measurements can be made for many different types of partitions, but it is impractical to test every possible design, and so it is necessary to have reliable methods for predicting the sound transmission loss of typical building constructions.

There are various methods for predicting the sound transmission loss of walls and floors that can be used by noise control engineers. It is important to know how accurate these methods are for typical constructions used in building acoustics (Ballagh 2004). As the standard grows in experience over the years, it reveals the complex variables that must be addressed in order to equalize the conditions that have a potential to affect results.

10.9.2 Factors Affecting Sound Transmission

During an ASTM E-90 test, a test specimen is mounted between a room containing an isolated source of noise and a receiving room. Sound transmission loss, the difference between the sound level in the source room and the receiving room, is measured at specific sound frequencies and used to arrive at the STC rating. The higher the STC rating calculated, the quieter it is in the receiving room.

When sound waves come in contact with a boundary obstacle, such as a wall or door, a portion of the sound wave energy is reflected, a portion is transmitted through the obstacle, and the rest is absorbed by the obstacle. One of the standard methods of measuring the effective sound absorption coefficient of an acoustical material is by finding its effect on the reverberation time, or decay rate, of the sound pressure level in the sound chamber. The total sound absorption in the receiving room is required to determine the noise reduction of the specimen being tested. The key here is to rule out the absorption of sound waves within the chamber that may be attributed to the door being tested.

Because the ASTM standard does not provide a resolution for measuring and standardizing absorption levels from one laboratory to the next, the same product tested in laboratories with different absorption levels can result in different STC ratings. Another variable that the standard does not currently address is the difference between a door and a partition. While the standard makes a provision that a door must be cycled (opened and shut) a number of times, prior to commencing the test, the operating force or the pressure required to release a tightly sealed door is not addressed.

STC values are used to define the performance requirements for achieving a specified reduction in sound transmission from a source room to a receiving room. The STC rating of an installed door also determines how much noise reduction is possible between a given source room and receiving room.

10.9.2.1 Salient Features of Sound Transmission

- Sound waves travel through any opening with very little loss. While the amount of air flowing through a gap increases in proportion with the size of the gap.
- A tiny hole transmits almost as much sound as a much larger gap. For example, a one square inch hole in 100 square feet of gypsum board partition can transmit as much sound as the rest of the partition. Air paths through gaps, cracks, or holes pose serious problems.
- Air trapped in a "sound lock" between a pair of doors, or between layered sets of seals in a gasket, is one of the best sound absorbers.
- It is important to understand that STC values are not proportionate units of measurement. To achieve increasingly higher levels of sound control, each 10 dB increment requires ten times as much improvement as the one before. While door openings rated in the range from STC of 30 to STC of 40 are common, achieving STC of 50 and higher ratings is extraordinarily difficult.
- Acoustical performance depends upon wall design, its thickness and weight, and ultimately cost. Frequently it is not possible to optimize one factor without seriously compromising the others.

10.9.3 Review of Blends in Noise Reduction

Noise has become an environmental issue, and legislation on noise regulation is under review and being drafted in industrialized countries, especially those in Europe. The reduction of noise from machinery, automobiles, and appliances has been studied extensively (Tokairin and Kitada 2005; Zhang et al. 2007; Jiang et al. 2007; Mazeaud and Galland 2007). The techniques using sound absorption and insulation materials to reduce ambient noise have received much attention in this area of research (Zhou et al. 2006; ASTM E413-10).

Traffic noise, which falls within the frequency range of 250 and 4,000 Hz (Lapcik 1998), has been a huge headache for the public, and the common practice to deal with it is to build concrete noise barriers along roads and highways.

The study done by American Acoustical and Insulation Materials Association (1974) showed that these concrete barriers are of very high acoustic reflectivity (95 % and above) and of low sound absorption. This means that concrete barriers are not effective in controlling and reducing traffic noise (Campbell 2000).

In recent years, some notable progress has been made in making non-concrete barriers. It has been reported that a section of polycarbonate noise wall was built in 1996 near Culver City Park in Los Angeles, California, USA. The polycarbonate noise reduction panels are developed by Quilite International (QUILITE Noise Barriers 1997). A jet engine testing shelter was installed by using Lexan (polycarbonate) plastic manufactured by General Electric (Anderson 1997).

Another development is a noise barrier system developed by Carsonite International based in the city of Early Branch, South Carolina, USA, and those noise barriers are lightweight hollow panels made of tongue-and-groove planks of reinforced composite material filled with crumbed tire rubber. A few sections of Carsonite noise barriers have been built in Long Beach, California. Traditional noise barriers have a flat surface. Now new designs are experimenting with nonflat surface textures (Watts and Morgan 1997).

Placing noise reducers on the top of highway noise barriers is another way that aims to reduce traffic noise (Shono et al. 1994). Numerical and/or analytical studies have also been reported on the estimate of noise reduction effect (Alfredson 1990; Tanaka et al. 1990).

These, abovementioned, noise barriers exhibit a much better performance than concrete with sound absorption and transmission loss. But noise reduction is not the only criterion dominating the decision to construct noise barriers. There are other crucial criteria, and they include (1) cost-effectiveness, (2) technology maturity, (3) durability, (4) low cost and convenience in installation, (5) low cost and convenience in maintenance and repair, and (6) aesthetics. Concrete noise barriers meet those criteria very much (Kay et al. 2000). Crumb rubber blends aiming at the application in noise reduction are also developed and are found to yield encouraging results (Han et al. 2008).

The sound insulation efficiency of ABS/carbon nanotube (CNT) composites was increased with an increase in the amount of CNT. Since the sound insulation of ABS/CNT composite was improved with higher stiffness due to CNT, it might be concluded that stiffness is one of principal factors influencing the improvement of transmission loss of polymer/CNT composites (Lee et al. 2008).

Particle boards (PB) from jute stick (JS), date palm leaf, and their blends offered higher sound transmission loss, higher thermal insulation, and lower swelling compared to plywood. Increase of JS in blend with date palm leaf increased sound loss as well as thermal insulation. Sound loss increased with increase in thickness of PB. Relationship between sound loss and thickness is found to be nonlinear. Sound loss reached maximum at board thickness of 19 mm for PB (Ghosh et al. 2010).

Noise inside a motor vehicle arises from various sources. External sources include rain and wind impacting on the vehicle body panels, and internal sources

include the engine of the vehicle. Vibration of the body panels, such as the bonnet, the roof, and door panels, is the source of considerable noise inside the vehicle. Attempts have been made to damp vibration of the body panels and hence reduce the noise inside the vehicle, by attaching layers of damping material to the surfaces of the panels. One traditional method has been to attach press-formed fibrous composite sheets. However, these sheets are prone to rotting when damp, as the material is not water resistant and is very difficult to clean.

More recently, viscoelastic materials have been used. One such material is a copolymer comprising ethylene, vinyl acetate, and acrylic and/or methacrylic acid. Another proposal has been to apply a viscoelastic adhesive composition comprising a polyepoxide, a polyether amine, a hetrocyclic amine, and a phenol, which is said to be useful as a damping material. A yet further proposal has been to use composite comprising an elastomeric butyl polymer sheet bonded to a thin layer of non-elastomeric material on the surface. Furthermore they are not particularly useful in preventing transmission of noise from other sources. Multilayered acoustic tiles for suppressing noise and also reducing its transmission were developed (Gunasekara and Alwis 2004; Bourcier et al. 2009). Improved materials that will not only effectively damp the vibration of the body panels but will also reduce sound transmission through the body panels would be a great advance in the art of vehicle sound proofing which is still evolving.

10.10 Special Test Methods

10.10.1 Aroma Barrier Test

Until the first half of the twentieth century, perishable food articles of daily life, such as meat or cheese, and also non-food articles like detergents or soap were mostly sold in shops and did not use packaging or were just wrapped in paper or cardboard. Glass and metal were the only packaging materials providing high barrier for the few applications which required long shelf life.

Modern lifestyle with self-service supermarkets, plus worldwide and year-round availability of all articles, would not be possible without adequate packaging of those articles. Processing, preservation, and distribution of those articles have created not only a huge growth of traditional packaging materials, e.g., glass, metal, and paper, but also the development of new packaging concepts, especially flexible packaging with plastic materials, for better economy, convenience of packaging, and quick transportation (Kemmer et al. 2008).

The food industry has long depended upon reliable, impermeable packaging materials such as glass and metal. Both suppliers and food manufacturers focus research efforts into lighter-weight, flexible, and semirigid packages, which are typical qualities of plastics. While parameters such as functionality, recyclability, and cost are critical characteristics, the lack of complete impermeability and inertness in these polymer materials can have important effects. Due to their size

and nature, the aroma compounds will interact with packaging materials often consisting of lipophilic hydrocarbons (Johansson 1996).

10.10.1.1 Factors Influencing Aroma Barrier Test

An aroma is a chemical substance sensed by the taste and/or the smell defined by parameters such as its volatility, its polarity, and its aromatic value. The aromas must be protected throughout the retail chain until its use. The conservation of these aromatic contents is mainly based on the packaging (Risch 2000).

Aroma compounds interact with the polymer matrix, leading to polymer structural changes. Plastic packages are made up of polymers that form a matrix of crystalline and amorphous regions, which contain submicroscopic voids. Aromas permeate through packaging by first being adsorbed onto the package's surfaces, diffusing through the voids (absorption), and, without a barrier material, desorbed to the package's exterior. A sorption–diffusion mechanism is thus applied.

The mass transfer phenomenon, commonly described by the sorption, the migration, and the permeation can be determined by three parameters: S, the solubility coefficient; D, the diffusion coefficient; and P, the permeability coefficient. When diffusion is Fickian and sorption follows Henry's law, the relationship $P = DS$ can be used (ASTM F 1769-97).

Literature and knowledge on mass transfer of aroma compounds are few and no standard procedure is recommended. Methods developed for aroma compounds permeability measurements are commonly approached by isostatic or quasi-isostatic methods and depend on the physical state (vapor or liquid) of the aroma compounds (Piringer and Baner 2000).

Aroma barrier is somewhat analogous to flavor barrier. Food products must be protected from outside aromas in the distribution chain, grocery store, and home. Other food and non-food products such as garlic, agricultural chemicals, pesticides, insecticides, or perfumes can be highly aromatic. The desire is to retain the aroma in the package and not let it escape into the surrounding environment (Eval Americas 2007).

Numerous apparatus have been designed, to different degrees of success, to obtain information regarding aroma permeability of packaging films in a reasonable time frame. Experimental setup for studying the permeability through polymeric films is presented in Fig. 10.64 (Vähä-Nissi et al. 2008).

Sensory evaluations of some common aromas packaged in a variety of film structures are presented in Table 10.33. And comparison of permeation rate of different film structures for some common aromas is shown in Table 10.34.

The area of "flavor" and "aroma" barrier is receiving growing attention in the field of plastics packaging. The permeation of flavors is difficult to measure quantitatively because they contain many components. Many times, only a simple component of a flavor is measured if a quantitative value must be determined. Gas chromatography and mass spectrophotometric (GC/MS) techniques have been developed that allow the analysis of complex flavors. However, in most cases, the use of organoleptic testing provides reliable and pertinent data at a greatly reduced cost.

As with flavor permeation, aroma permeation can be determined by sensory evaluation or gas chromatography.

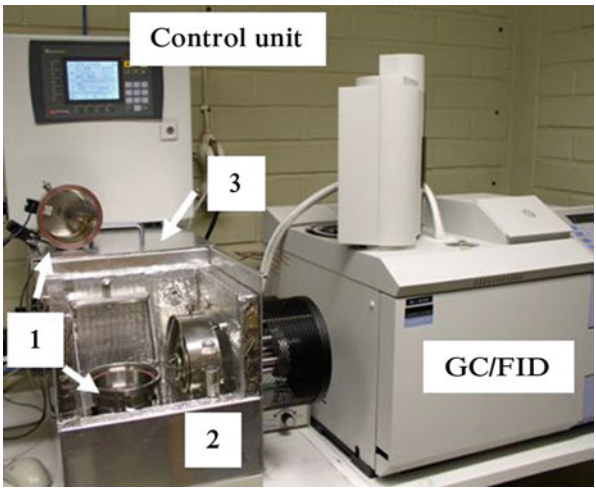

Fig. 10.64 Permeation device with *1*, GC; *2*, test cell; *3*, test cell oven and sample transfer oven (Vähä-Nissi et al. 2008)

Table 10.33 Results of sensory evaluations for various aromas packaged in a variety of film structures. The numbers represent the time it takes the aroma to permeate the package at room temperature (Eval Americas 2007)

Aroma permeation						
PVDC						
Structure thickness (μ)	LDPE (50)	OPP/PE (20/50)	PET/PE (20/50)	Nylon (15)	F Series/ PE (15/50)	EF-XL/PE (15/50)
Orange essence	1	2	3	2	4	5
Strawberry essence	2	2	3	2	3	3
Curry powder	2	3	2	2	3	3
Garlic powder	2	2	2	2	3	3
Coffee powder	2	3	3	3	5	5
Linalol	1	3	3	4	5	5
Geraniol	1	3	3	4	5	5
Prenyl Benzoate	1	2	2	3	5	5
Methyl ionone	2	3	3	3	5	5

Key: 1: <1 h, 2: <1 day, 3: <1 week, 4: <2 weeks, 5: <2 weeks

Diffusion* (D) *and Permeability (P) Coefficients

For different aroma/synthetic material couples, the results of the D and P obtained by the HS-GC/MS and gravimetric methods are compared in the literature (Table 10.35).

D and P for the Limonene/LDPE Couple in Function of Relative Humidity

In view of the previous results, the study of the influence of the relative humidity on the mass transfer of an aroma through a packaging material was realized for the couple limonene/LDPE (Maki and Stevens 2002).

Table 10.34 Comparison of permeation rate of various film structures for common aromas (Eval Americas 2007)

Aroma permeation					
Days to Leakage					
Film construction	Thickness (mils)	Vanillin (Vanilla)	Menthol (Peppermint)	Piperonal (Heliotropin)	Camphor
PET/F Series/ PE	0.5/0.6/2.0	15	25	27	>30
OPP/F Series/ PE	0.7/0.6/2.0	30	>30	27	>30
PET/F Series	0.5/0.6	>30	>30	30	>30
ON/F Series	0.6/0.6	2	>30	27	30
PET/PE	0.5/2.0	2	16	5	>30
ON/PE	0.6/2.0	2	20	5	28
PVDC ct'd PET/PE	0.6/2.0	7	>30	6	30
PVDC ct'd/ OPP/PE	0.7/2.0	6	2	1	13
PVDC ct'd PET	0.9	5	6	1	7

Values in the table above indicate the number of days until leakage through the package is detected. The greater the values, higher the fragrance preservation

Table 10.35 Comparison of the diffusion and permeability coefficients of the HS-GC-MS and gravimetric methods for different relative humidity for the limonene/LDPE couple (Martine and Louvier 2010)

Method	Coefficient at 23 °C	20 % r.h.	50 % r.h.	90 % r.h.
HS-GC/MS	Mean diffusion (**D**) (cm^2/s)	5.34×10^{-9}	7.03×10^{-9}	5.23×10^{-9}
	Permeability (**P**) (g.µm/m2.d.Pa)	14 (n = 3)	20 (n = 7)	7 (n = 3)
		9 → 18	14 → 35	6 → 8
Gravimetry	Mean permeability (**P**) ($g.\mu m/m^2.d.Pa$)	13 (n = 3)	26 (n = 3)	13 (n = 3)
		13	26 → 27	12 → 15

Notice that D and P are lower for 20 % and 90 % relative humidity compared with those for a relative humidity of 50 % whatever the analytical methods used

10.10.1.2 Examples of Polymers as Barrier Films

Nylon 6

Nylon 6 is a good barrier material for nonpolar to slightly polar solvents and smaller organic molecules and a very good barrier to bulky aroma molecules of low to intermediate polarity. For some nonpolar materials, its barrier even exceeds that of EVOH, whereas EVOH has slight advantages for molecules of intermediate polarity. Only for highly polar migrants, as methanol or isopropanol, the barrier of nylon 6 is clearly lower than that of EVOH – a situation well known from oxygen and carbon dioxide permeation.

Due to its moderate price, good processability, and high mechanical and thermal properties, it is found to be a suitable material for packaging of many aroma-containing materials, such as menthol-flavored toothpaste. In case of detergent refill pouches, it further prevents contamination of the environment by the aroma migrating out of the package, an effect that may be undesirable when too many different flavors come together. Another application PA6 that is frequently used for is barrier layer in blow-molded containers as are used for packaging herbicides or pesticides with cyclohexane, xylene, or methyl ethyl ketone solution. Here, nylon provides another advantage over EVOH: nylon 6 may be processed as inner, sealing layer, thereby providing a continuous barrier layer in the container. EVOH however needs to be processed as a core layer, with a PE inner layer which is then in contact to the solvent and also forms the seal. This seal will then be a weak spot in the container for both migration and mechanical strength.

Cyclic Olefin Copolymer (COC)

COC has better aroma barrier than polyethylene and is found to reduce aroma/flavor loss from food when it is utilized as a barrier layer in food packaging. COC is also found to reduce the transmission of objectionable odors to surrounding areas and has utility in disposable food storage bags. Low extractables in COC reduce the possibility of generating an "off-taste" in water or susceptible foods when used as a contact layer or just under a seal layer in packaging (Jester et al. 2005).

10.10.2 Permeability Test for Liquids

There has been a trend to use more plastic-based packaging materials for different applications such as replacements for metal and glass containers. This situation has stimulated the industry to provide new and more efficient barrier solutions. A number of different technologies are being developed and are making their way into the market. Melt processable thermoplastic blends which allow injection molding, blow molding, thermoforming, and other conventional techniques to be applied for making products that are impermeable for diesel, petrol, and other organic liquids while possessing high-performance properties, even after recycling, are being focused.

Following the success story of the plastic bumpers, for automobiles, which commercially replaced the heavy metallic bumpers, the plastic fuel tanks are making inroads to replace metallic fuel tanks. The plastic tanks offer weight reduction, freedom from corrosion, and ease of fabrication.

The principal performance property required for HDPE blend (with polyamide-6) is the reduced permeability for diesel; hence, the morphology of the blends in the final product is extremely important. The morphology of the binary blends and the influence of different compatibilizers in different concentrations were also investigated using scanning electron microscope (SEM). Here, for morphology

studies, the injection-molded flexural bars were allowed to soak in liquid nitrogen and were fractured quickly after taking them out. The fractured surfaces were carefully cut and were studied under SEM, after making their surfaces conducting by depositing gold vapors in an ion sputtering unit.

The blends disclosed dispersed domains of polyamide within a continuous phase of HDPE. Since HDPE and polyamide are incompatible, use of a compatibilizer is essential. There are three main factors governing compatibilization and interfacial interactions, viz., reduction of the interfacial tension, increased interfacial adhesion, and achievement of a viscosity ratio conducive to efficient dispersion.

10.10.2.1 Factors Influencing Permeability Test

Permeation is a mass transport phenomenon in which molecules transfer through the polymer from one environment to another through diffusive processes. Mass transport proceeds through a combination of three factors in case of polymers. They are (1) dissolution of molecules in polymer (following absorption at the surface), (2) diffusion of molecules through the material, and (3) desorption from the surface of the material (Crank and Park 1968; Kumins and Kwei 1968).

In case of polymers, mass transport of small molecules can take place, as there is intrinsic porosity in the polymer matrix. Even solid homogeneous polymers are likely to be porous to some degree owing to defects, inclusions and different phases, which leave pores, voids, and crazes capable of accommodating small molecules. For molecules to undergo transport within a polymer, they must dissolve in the solid polymer. If the molecules do not dissolve, in the polymer, then diffusion is irrelevant. The basic mechanism for diffusion is occupation of the free volume between the polymer chains. Dissolution is a thermodynamic process, where the solubility is determined by enthalpy change on dissolution of the molecule in the polymer matrix and the volume available. And diffusion is the net transport of matter in a system, which acts to nullify the potential differences in order to bring in a state of equilibrium. Here, the rate of diffusion is proportional to the concentration gradient of the diffusant.

The factors, which influence the permeability or mass transport, are the following: chemical composition of the polymer matrix and its free volume. In fact, crystallinity, molecular orientation, and physical aging in turn influence the free volume of a polymer matrix. In addition, porosity and voids, like free volume, offer sites into which molecules can absorb and are far less of a barrier to transport than solid polymer. Temperature also affects permeability and diffusion properties of small molecules in polymers. With increased temperature, the mobility of molecular chains (in polymer) increases and thermal expansion leads to reduced density; therefore, the free volume in the system will increase. External tensile stress applied is expected to increase free volume and open up internal voids or crazes, providing additional sites into which molecules can absorb. Of course, there may be unquantified internal residual stresses, arising from processing, present in the polymers. It is well established that the properties of materials

Fig. 10.65 HDPE–polyamide-6 (20 wt%) blend. Injection-molded flexural bar in the skin zone as viewed under SEM (Xavier and Pendyala 2008)

near the interphase are different from those of the bulk material. Thus, the diffusion properties in the interfacial region are likely to be different from those of the bulk material.

10.10.2.2 Permeability and Polymer Blend Morphology

Morphology of HDPE-Polyamide-6 Compatibilized Blends

PE and PA-6 are incompatible with an unstable morphology when blended. To stabilize PE/PA-6 blends, many compatibilizers have been used (Yeh et al. 1995; Chen et al. 1988; Kouloori et al. 1997; Gadekar et al. 1998; Raval et al. 1991; Willis and Favis 1988; Halldén et al. 2001), e.g., copolymers or adducts of maleic anhydride (Chen et al. 1988; Gadekar et al. 1998), acrylate copolymers such as poly(ethylene-*g*-butyl acrylate) (Raval et al. 1991) and ethylene/methacrylic acid/isobutyl acrylate terpolymer (Willis and Favis 1988), poly(ethylene-*g*-ethylene oxide) and poly(ethylene-*co*-acrylic acid) (Halldén, and Wesslen 1996; Serpe et al. 1988), and succinic anhydride functional groups (Padwa 1992; Sánchez-Valdes et al. 1998; Kudva et al. 1999; Kelar and Jurkowski 2000; Pan et al. 2001; Jurkowski et al. 2002; Filippi et al. 2002).

The morphology of the cryogenic fracture surfaces of HDPE blends with polyamide-6 (PA-6) are presented in Figs. 10.65 and 10.66. PA-6 distributed in a matrix of HDPE is clearly visible in Fig. 10.65. Here, as no compatibilizer was engaged, the protruding strips of PA-6 do not show any interaction with the matrix material. But when a compatibilizer, ethylene-methacrylic acid copolymer, was engaged, the fracture morphology has altered (Fig. 10.66) and the PA-6 dispersion is rather more uniform and does not show such protruding strips. The dispersion of PA-6 (35 wt%) as viewed from optical microscope (Fig. 10.67) also exhibits good dispersion of the same (Xavier and Pendyala 2008).

Morphology of HDPE-Polyamide-66 Compatibilized Blends

Poor interfacial interactions between polyamide-66 and matrix material are responsible for considerable pulling out of the dispersed phase as revealed in Fig. 10.68.

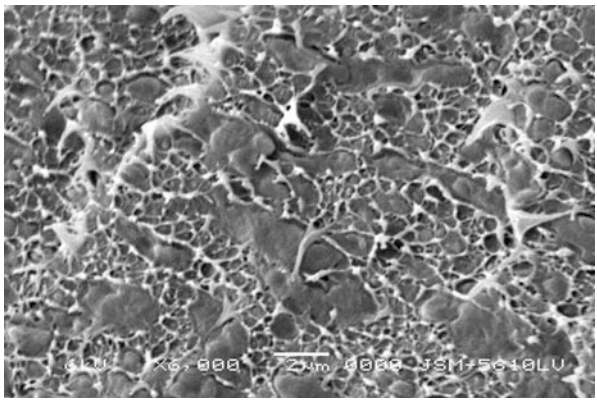

Fig. 10.66 HDPE–polyamide-6 (20 wt%) blend with compatibilizer ethylene–methacrylic acid copolymer neutralized with metal ions (5 wt%). Injection-molded flexural bar in the skin zone as viewed under SEM (Xavier and Pendyala 2008)

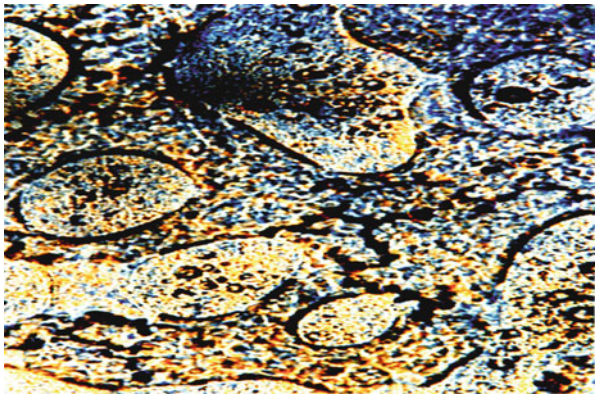

Fig. 10.67 Optical micrograph of HDPE–polyamide-6 (35 wt%) at 20X with polarizers crossed. Microtomed section of injection-molded flexural bar in the core region (Xavier and Pendyala 2008)

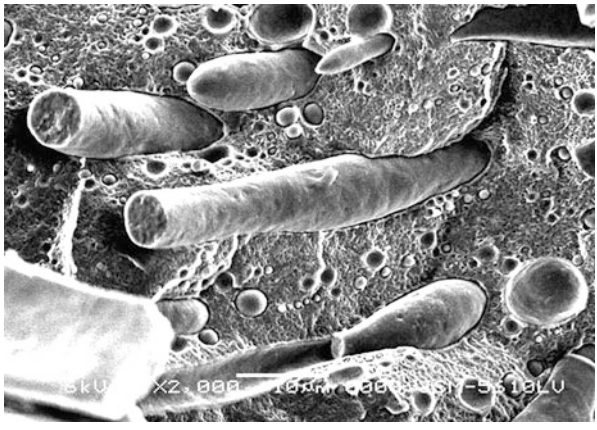

Fig. 10.68 HDPE–polyamide-66 (30 wt%) blend. Injection-molded flexural bar in the core zone as viewed under SEM (Joshi et al. 2005)

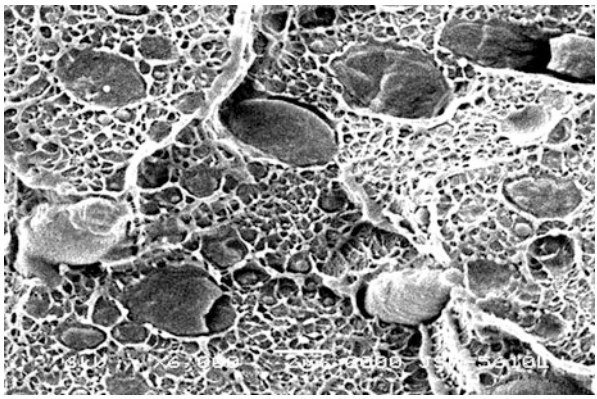

Fig. 10.69 HDPE–polyamide-66 (23.75 wt%) with compatibilizer ethylene–methacrylic acid copolymer neutralized with metal ions (5 wt%). Injection-molded flexural bar in the core zone as viewed under SEM (Joshi et al. 2005)

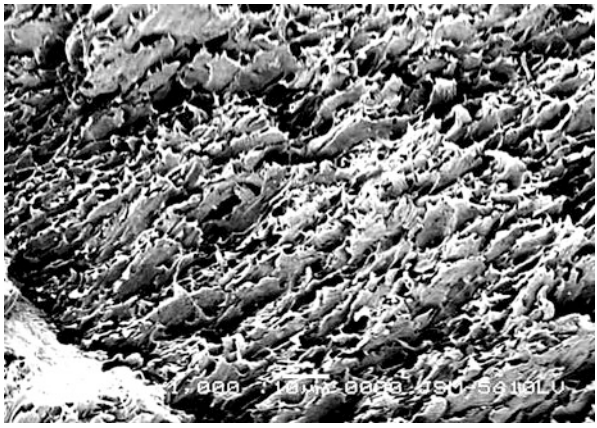

Fig. 10.70 Lamellar morphology in fractured bottle wall of HDPE–polyamide-6 compatibilized blend with good barrier properties for diesel as viewed under SEM (Xavier and Pendyala 2008)

String and bead type of morphology is observed at many locations. However, as compatibilizer ethylene–methacrylic acid copolymer is introduced, the fracture has taken place in flat plane and no protrusions of polyamide-66 are observed (Joshi et al. 2005). The presence of the compatibilizer has altered the fracture propagation mechanism (Fig. 10.69).

The blow-molded bottle of HDPE blend with polyamide-6, after testing for permeability of diesel, was also tested for its morphology, using SEM. The bottle wall was cut into strips and the strip was fractured after soaking in liquid nitrogen. The morphology of the fractured surface revealed lamellae formed by the dispersed phase and oriented in the melt flow direction, parallel to the wall surface of the bottle (Fig. 10.70). These lamellae are responsible for restricting the permeation of diesel through the bottle. The wall of the bottle as well as the bottom of the cylindrical-shaped bottle was cut, and morphology

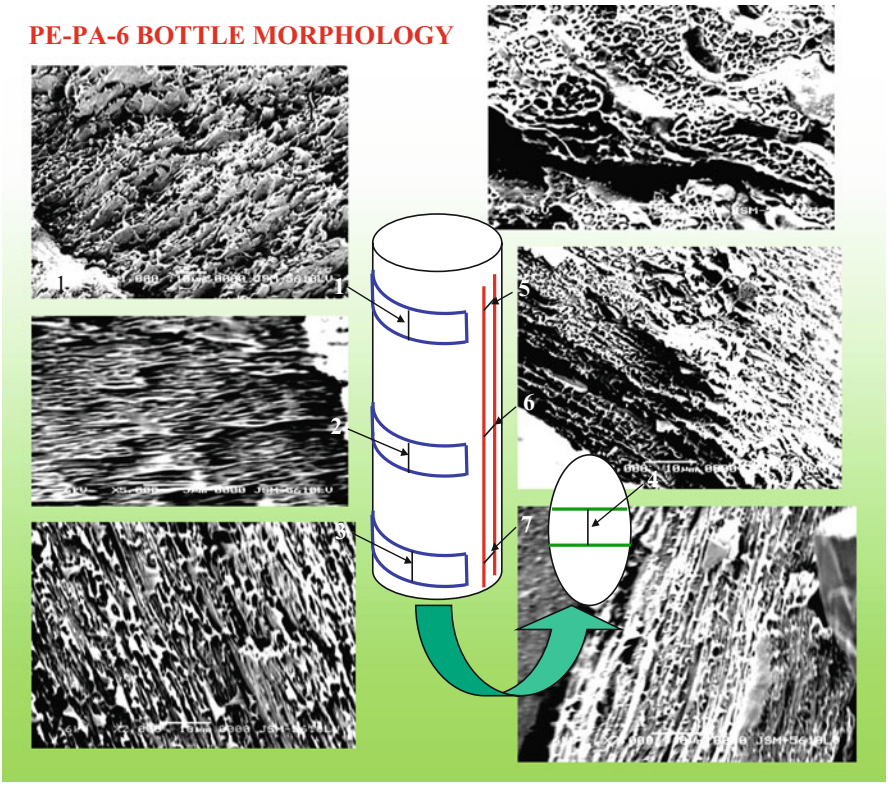

Fig. 10.71 PE–PA-6 bottle wall morphologies at different locations (Xavier and Pendyala 2008)

was studied at different locations. The lamellar morphology (as viewed in Fig. 10.70) was found to be present at all the locations of the bottle investigated (Fig. 10.71).

10.10.2.3 Permeability Tests for Diesel and Petrol

Permeation tests by pouring liquids in bottles and monitoring the weights of the bottles with regard to time have been practiced in many laboratories (Armstrong 1968a, b; Mesrobian et al. 1968; Subramanian 1983, 1984, 1985, 1987; Jen-Taut 1997; Xavier and Pendyala 2008).

Bottles of 250 ml capacity were prepared out of the dried granules of HDPE as well as compatibilized blend (with PA-6) having high mechanical properties; preferably with high notched Izod impact strength along with suitable melt flow characteristics. The injection molding was carried out in a Windsor Machine, SP-110, in a temperature range, 513–573 K, with injection pressure, 50–60 kg/cm^2, locking pressure around 70 t, injection time, 4.0–6.0 s, and cooling time, 5.0–7.0 s.

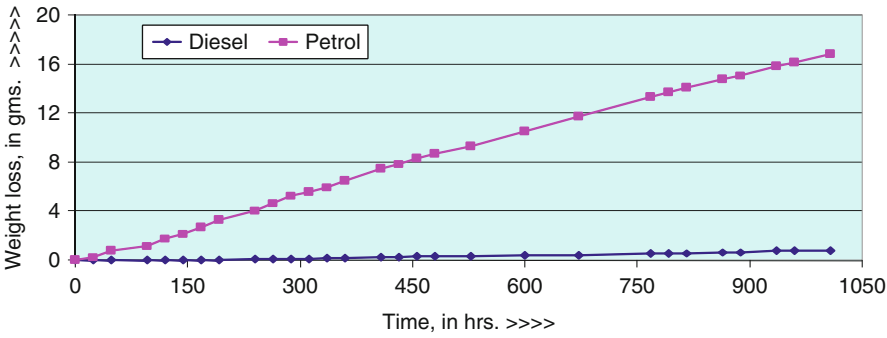

Fig. 10.72 Weight loss in bottles filled with Petrol and Diesel with regard to time in hours. Each point on the graph is an average weight of three bottles kept under investigation (Xavier and Pendyala 2008)

Diesel, as well as petrol, was poured separately into bottles of neat HDPE (control) and the selected blend bottles, at least three bottles for each case, covered with aluminum foil using a silicone sealant that cured at room temperature. It was further covered with molded plastic lid and was sealed with the same sealant. After the adhesive is cured, diesel/petrol permeation is tested and recorded at regular intervals by measuring the weight of each bottle.

Bottles with Petrol had shown a loss of 7 wt% in 25 days (600 h). Bottles filled with diesel had shown a marginal loss of 0.2 wt% in 25 days (600 h) or a weight loss of 0.8 g in about 1,000 h. See Fig. 10.72 (Xavier and Pendyala 2008).

10.10.3 Environmental Stress Cracking

Environmental stress cracking (ESC) in plastics means the failure of the plastic involved at about room temperature due to continuously acting external and/or internal stresses in the presence of surface-active substances (known as stress-cracking agents), which are normally liquids, such as alcohols, soaps, dyes, and agents containing moisture (Scheirs 2000; Wright 1996; Lagaron and Dixon 1998; Lagaron et al. 1999). ESC is a major problem in the long-term service behavior of plastic products. It can lead to quite expensive failures during warehouse storage, shipping, or during long-time applications. ESC of polymers is analogous to the stress corrosion problem in metals. It takes place after a certain period of time: the lower the stress, the longer the durability.

ESC occurs, in general, in amorphous polymers such as PC, PMMA, PS, PVC, SAN, and ABS as well as in semicrystalline thermoplastics like PE, PP, PA, and PB (Wright 1996). Amorphous polymers exhibit a higher tendency for this type of failure because their loose structure facilitates fluid permeation into the polymer. Amorphous polymers show enhanced sensitivity to ESC at temperatures close to

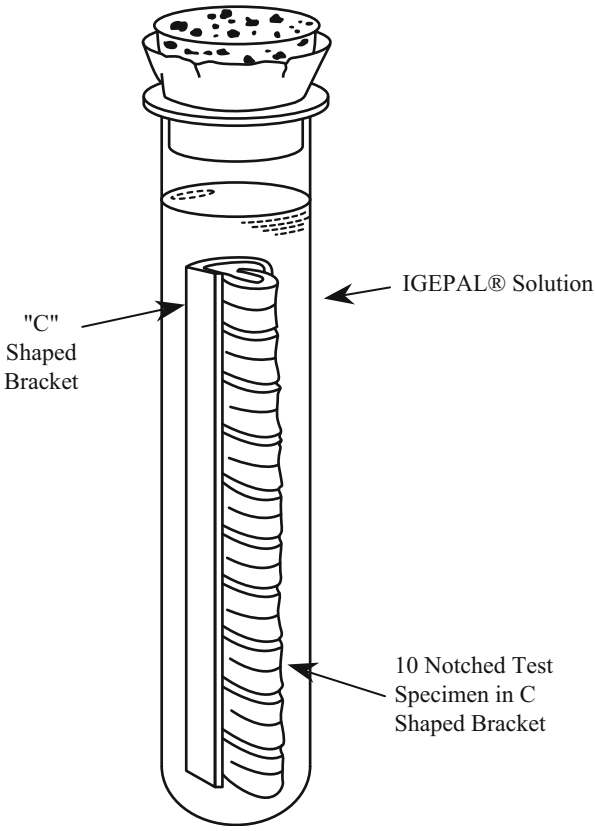

Fig. 10.73 Bent Strip ESCR Test (ASTM D1693-12)

their T_g values due to the increased free volume as T_g is approached, which facilitates fluid permeation into the polymer. The solvent then becomes locally dissolved and promotes crazing which is a fore runner for cracking. Several molecular mechanisms have been proposed to explain ESC over the past few years (Lagaron et al. 2000). Lustiger and Ishikawa have proposed "interlamellar failure" as the controlling mechanism of ESC (Lustiger and Ishikawa 1991).

10.10.3.1 Test Methods for ESC

ASTM D 1693: Bent Strip ESC Test

This is a well-known original ESC test developed by Bell Labs in the late 1940s. Ten rectangular-shaped specimens are cut from a molded plaque prepared using standard methods. A controlled notch is cut horizontally across each specimen, which serves as a crack initiation point. The specimens are bent and inserted into a "C"-shaped bracket, creating a stress in the specimen. A diagram of this test method is shown in Fig. 10.73. The specimens and bracket are inserted into a tube filled with Igepal® solution. The tube is then placed into a heated environment

and monitored for cracking (failures). Solution concentration, environment temperature, and sample dimensions vary with the test condition mentioned in the method.

The various test conditions suggested in the method introduce different stresses and strains and allow testing of different polymers and still obtain results in a timely manner.

ASTM D 1693 is not used popularly, today, for it is not sufficiently aggressive towards modern resins. This test is a constant strain test, but polyethylene, like many polymers, relaxes when strained. This stress relaxation allows testing to run without failure for very long time periods (>1,500 h), even under severe conditions of temperature and *Igepal*® concentrations.

ASTM F 1248: Notched Pipe Ring ESCR Test

This method has been used in the United States for many years to measure ESC on finished pipe up to 12 in. diameter that is notched using a razor blade in a special notching device.

ASTM D 5397-99 Standard Test Method for Evaluation of Stress Crack Resistance of Polyolefin Geomembranes Using Notched Constant Tensile Load Test

This test is typically used in the United States to test Geomembrane materials. But other PE materials, including some pipe resins, have been tested to gauge slow crack growth performance. Typical test conditions are 50 °C in a 10 % *Igepal*® *solution*, and the applied load is 30 % of the sample's yield stress. The depth of the notch is 20 % of the thickness of the sample (ASTM D 5397-99).

The Full Notch Creep Test (FNCT)

This method is being accepted throughout Europe as the standard method to test PE pipe grade materials that exhibit very high environment stress crack resistance (ESCR) values. The FNCT test has been preferred in Europe, as it leads to shorter failure times, due to its particular specimen design and to the presence of a surface-active environment.

ASTM F 1473: The Polyethylene Notch Tensile (PENT) Test (Constant Load)

The PENT test is being used in the United States to test PE pipe grade materials that exhibit high ESCR values (ASTM F1473-11). A parallel test method is also being developed in Europe under the ISO protocol. Typical test conditions are 80 °C air and 2.4 MPa stress.

ISO 13479: Notch Pipe Pressure Test

This method is accepted as the standard method to test PE pipes throughout Europe. The specific performance levels are detailed in the respective pipe standards (i.e., ISO 4427 for water and ISO 4437 for gas). Typically a minimum of 165 h is set for PE pipe materials.

10.10.3.2 Factors Influencing ESC

The ESC behavior of a polymer is strongly influenced by (a) the concentration of the stress-cracking agent (liquid chemical), (b) exposure temperature, (c) exposure time, and, most of all, (d) the level of strain on/in the polymer.

The absorption of a stress-cracking agent into a micro-yielded or stress-dilated zone of a polymer ultimately leads to ESC. This process locally reduces yield strength of the polymer and leads to fracture. The fracture may be either ductile or brittle depending on stress and time considerations. Diffusion of detergent molecules into the polymer due to stress might result in increased chain mobility and therefore in a reduction of the activation energy (plasticizing effect) of the deformation process (Lagaron et al. 1999). Stress-cracking agents act to lower the cohesive forces which maintain the tie molecules in the crystallites, thus facilitating their "pullout" and disentanglement from the lamellae (Scheirs 2000). The stress-cracking agents accelerate the brittle-failure process. Any stress-cracking agent will lubricate the tie molecules and that will facilitate their pullout from the lamellae.

The effect of temperature is complex. It has been shown that the higher the test environment temperature, the faster the ESC onset. The transition to brittle behavior is accelerated to shorter times by increasing temperature, cyclic loading, dilational stress, and stress concentrations. Localized concentration of the stress due to local geometrical features as notches, voids, and inclusions will increase the stress and modify the nature of the stress field. Craze initiation is accelerated by stress fields with high dilational stress and retarded under hydrostatic pressure (Wright 1996).

In addition, there are critical polymer properties and variables which affect ESCR significantly. The higher the molar mass the longer the polymer chains, which results in more tie molecules and increased ESCR (Huang and Brown 1988). ESCR is directly influenced by the type, length, and complexity of chain branching. For polyethylenes, density is a convenient, if not wholly accurate, measure of short chain branching. As a general rule of thumb, as branching increases, so does ESCR. Thus, as density decreases, ESCR generally increases. ESCR appears to be particularly sensitive to subtle variations in crystal structure and thus to differences in short chain branching. ESCR decreases with increasing the degree of crystallinity (Huang and Brown 1988; Lagaron et al. 1998). Higher comonomer content and longer comonomer short chain branches (higher α–olefins) provide better ESCR of LLDPE (Lustiger 1998; Soares et al. 2000). Increased pigment content usually decreases the ESCR (Kendall and Sherliker 1980; Lustiger 1986). The thermal history of the material and the processing conditions are also important factors for the ESCR behavior of the polymers (Roe and Gieniewski 1975; Lu and Brown 1987; Wang et al. 2003).

10.10.3.3 ESC in Polymers and Blends: Examples

Polycarbonate

Polycarbonate is tough, strong, high-performance amorphous engineering thermoplastic which is finding widespread use in industry. It has applications where high

impact resistance and its ability to maintain its shape and size even under great stresses over a wide range of temperatures are desired. It is an ideal engineering plastic since it can be injection molded or extruded. Due to its excellent properties, it is often used in the appliance industry for vacuum cleaner bases, cord hooks, impellers and blender, and food processor housings. Motorcycle windshields, police shields, and headlight covers are other typical high stress applications that use polycarbonate.

A detailed investigation of environmental stress cracking was conducted with both monoethanolamine and surfactants. The detailed investigation (Faulkner 1985) included determinations of cracking strains for polycarbonate upon exposure to the fluid's components and several nonionic surfactants. Critical strain determinations for polycarbonate exposed to the liquid components indicate that both monoethanolamine and surfactants are stress-cracking agents for polycarbonate. Cracking strains were also determined for a polycarbonate/acrylic blend upon exposure to the same fluid and were shown to be significantly greater than those obtained for pure polycarbonate. However, both the materials stress crack in splash tests. Plastics with even moderate amounts of designed-in stress are at risk under prolonged exposure to certain chemicals, which makes design and manufacturing of such parts a challenge (Krishna and Berg 2011).

The synergistic effects of photodegradation on ESC of PC were also investigated. Injection-molded samples were exposed to the ultraviolet light for various times in the laboratory prior to solvent contact. The bars were then stressed with two different loads in a tensile testing machine under the presence of ethanol. During this period, the stress relaxation was monitored, and, after unloading, the ultimate properties were evaluated. The results indicated that ethanol causes significant modification in PC, with extensive surface crazing as well as reduction in mechanical properties. The synergist action of photodegradation and stress cracking in PC may be a consequence of the chemical changes caused by oxidation (Timoteo et al. 2008).

High-Density Polyethylene

Considering the fact that the slow crack resistance of polyethylene is usually assessed by tedious and time-consuming testing methods performed on the notched samples in contact with specific fluids, the findings of Kurelec et al. offer a possibility to assess the information on slow crack propagation in much simpler and faster way (Kurelec et al. 2005; Jansen 2004). It is shown that the average strain hardening slope <G> correlates with the data obtained by a classical accelerated ESCR test. The results provide experimental evidence for the existence of the unique strain–stress–strain rate surface by offering a simple way to predict long-term performance. The resistance to slow crack propagation in polyethylene can be predicted from a simple tensile measurement performed at 80 °C and for different types of polyethylene homopolymers and copolymers the slope of a tensile curve above its natural draw ratio (i.e., strain hardening) correlates well with the measured stress crack resistance.

The investigations confirm that the slow crack resistance in polyethylene is determined by the failure of the fibrils within the craze, which is shown to be determined by the strain hardening of a tensile curve. A material with a strong strain hardening will reduce the strain rate and consequently the time to failure will be strongly increased (ASTM D2561-12).

Polymethyl Methacrylate (PMMA)

The deterioration of polymer properties by ESC has been studied for several decades. But the actual mechanism is not certainly established (Hansen 2002). It is believed that in the presence of the stress, the active fluid causes local plasticization that generates crazes and eventually catastrophic cracks. The ultimate result in many cases is brittle fracture, even in normal ductile polymers like polyethylene, ABS, and polycarbonate. Since failure by ESC can be induced by environmental fluids like cleaning agents and lubricants and the mechanical stress can be the residual (molded-in) stresses, it was considered to be a "silent killer" (Sepe 1999).

The effects of environmental stress cracking in injection-molded PMMA samples were studied by Sousa et al. They used both γ-radiation and ethanol as stress-cracking agents. The combination of gamma degradation and the contact with ethanol intensifies the action of stress-cracking in PMMA (Sousa 2007).

Alex and Janice studied the resistance to crack and craze growth in PC and PMMA in the presence of several surface-active solvents including a component of the universal chemical warfare decontaminant, DS2 (Alex and Janice 1989). A static dead weight-loading apparatus is used for experimentation, and LEFM is used to interpret craze initiation and crack propagation via compact tension specimens. Results reflect relationships based on solubility parameters of the solvents and the polymers.

Acrylonitrile Butadiene Styrene (ABS)

The evaluation of the resistance of plastics to ESC is very important in material selection. ABS is widely used in a variety of fields owing to favorable cost/performance ratio. The advantages of ABS are its luster and resistance to impact. ABS is, therefore, used mainly for housings of appliances. However, ABS is vulnerable to certain chemical agents such as organic solvents and surfactants (Faulkner 1984; Woshinis 1994). ESC of ABS caused by a nonionic surfactant was investigated by creep tests and edge crack tension (ECT) tests. It was found that the results of the creep tests performed in the nonionic surfactant were very different from those conducted in air. The results showed that the change in the mechanism of fracture was attributable to the change of morphology at the crack tip (Kawaguchi et al. 2002).

An investigation was carried out by Wang et al. to determine the appropriate values of strain to be exerted in the test for environmental stress cracking of different kinds of polymeric materials (Wang et al. 2003). It was found that for

the brittle plastics the elastic region on the stress–strain curve is the best selection; for toughened plastics the strain should be selected in the plastic region; for polycarbonate, which can crack easily in a chemical medium, a strain below the yield point is Suitable.

10.10.3.4 Predicting ESC

The phenomenon of ESC has been known for several decades. And many researchers have been focusing their attention in understanding the phenomenon. However, research has not yet enabled prediction of this type of failure for all environments and for every type of polymer. Some scenarios are well known and documented and are able to be predicted. But there is no complete or comprehensive reference for all combinations of stress, polymer, and environment. The rate of ESC is dependent on many factors including the polymer's chemical structure, bonding, crystallinity, surface roughness, molecular weight, and residual stress. It also depends on the liquid reagent's chemical nature and concentration, the temperature of the system and the strain rate. Theoretical studies with computer-assisted modeling and practical confirmations may enable researchers to predict ESC with reasonable accuracy. And one may look forward for such attempts in research in years to come.

10.11 Outlook on the Future of Polymer Blends

This chapter is focused on the characteristic properties of polymer blends. Their measurements have reached a mature stage, both in terms of necessary theories and the methods of testing. However, efforts made in enhancing one property are often mitigated by the loss of another property. Intensive study of interrelations between processing, microstructure, and properties would certainly enable one to have a good control on performance of an ultimate product. Looking at the likely advances in understanding of these materials and their integration with developing technology, polymer blends will continue to receive increasing acceptance for a variety of applications.

Acknowledgments S. F. Xavier gratefully acknowledges the guidance and encouragement given by late Dr. L. A. Utracki, to whom this chapter has been dedicated. He is also thankful for the support and motivation given by Dr. Devanshu J. Patel and Dr. Geetika Madan Patel, Managing Trustees of Parul Arogya Seva Mandal.

10.12 Cross-References

► Applications of Polymer Blends
► Commercial Polymer Blends

- ▶ Compounding Polymer Blends
- ▶ Crystallization, Micro- and Nano-structure, and Melting Behavior of Polymer Blends
- ▶ Degradation, Stabilization, and Flammability of Polymer Blends
- ▶ Interphase and Compatibilization by Addition of a Compatibilizer
- ▶ Mechanical Properties of Polymer Blends
- ▶ Miscible Polymer Blends
- ▶ Morphology of Polymer Blends
- ▶ Reactive Compatibilization
- ▶ Rheology of Polymer Alloys and Blends
- ▶ Thermodynamics of Polymer Blends

Notations and Abbreviations Used

ABS Poly(acrylonitrile-co-butadiene styrene)
ASTM American Standard Test Method
BS British Standard
CAB Cellulose acetate butyrate
DGEBA Diglycidyl ether of bisphenol A
DSC Differential scanning calorimetry
ENR Epoxidized natural rubber
EVA Ethylene-co-vinylacetate
EPDM Ethylene propylene diene monomer
ESC Environmental stress cracking
HDT Heat deflection/distortion temperature
HDPE High-density polyethylene
HIPS High-impact polystyrene
HTBN Hydroxyl terminated poly(butadiene/acrylonitrile)
IGC Inverse gas chromatography
LCST Lower critical solution temperature
LEFM Linear elastic fracture mechanics
LLDPE Linear low-density polyethylene
OIT Oxidative induction time
PA-6 Polyamide-6
PA-66 Polyamide-66
PBMA Poly(butyl methacrylate)
PBT Polybutylene terephthalate
PC Polycarbonate
PCL Poly(ε-caprolactone)
PE Polyethylene
PEEK Polyether ether ketone

PEI Polyetherimide
PEO Polyethylene oxide
PEOx Poly(ethyl oxazoline)
PES Polyethylene sulphide
PET Poly ethylene terephthalate
PLLA Poly(L-lactic acid)
PMMA Poly(methyl methacrylate)
POM Polyoxymethylene
PPBC Polypropylene block copolymer
PPHP Polypropylene homopolymer
PPS Polyphenylene sulphide
PPO Polyphenylene oxide
PS Poly styrene
PSMA Poly(styrene-*co*-maleic anhydride)
PTFE Poly tetra fluoro ethylene
PTT Poly(trimethylene terephthalate)
PVAc Polyvinyl acetate
PVB Polyvinyl butyral
PVC Polyvinyl chloride
PVDF Polyvinylidene fluoride
PVME Poly(vinyl methyl ether)
PVP Polyvinyl pyrrolidone
PVPh Poly(4-vinylphenol)
SAN Poly(styrene-co-acrylonitrile)
SANS Small-angle neutron scattering
SAXS Small-angle X-ray scattering
SF Silk fibroin
SMA Styrene-co-maleic anhydride
SPEEK Sulfonated poly(ether ether ketone)
TGA Thermogravimetric analyzer
TMOS Tetramethyl bisphenol A oligosulfones
UCST Upper critical solution temperature

Appendix 1

See Table 10.36.

Appendix 2

See Table 10.37.

Table 10.36 Definition of terms used in this chapter

Autoignition	Ignition caused solely by heat without application of a flame (also called self-ignition)
Autoignition temperature	The minimum temperature to which a substance must be heated, without application of a flame, in order to cause that substance to ignite
Burning behavior	The physical and chemical changes that take place when materials, products, or structures burn and/or exposed to fire
Char	Carbonaceous material formed by pyrolysis or incomplete combustion (ASTM E 176-81a)
Chemical resistance	The ability of a material to resist chemical attack (the attack is dependent on the method of test and its severity and is measured by determining the changes in physical properties (ASTM 1982)
Combustion	Reaction of a substance with oxygen with release of heat, generally accompanied by flaming and/or emission of smoke. Any chemical process that produces light and heat, either as glow or flame
Decomposition temperature	This is the temperature range associated with the decomposition of the polymer in the presence of oxygen
Dielectric breakdown voltage	The voltage at which electrical failure or breakdown of a dielectric occurs when energized between two electrodes under prescribed test conditions
Dielectric constant	For a given configuration of electrodes, the ratio of the capacitance with the material as the dielectric to the capacitance with vacuum
Dielectric strength	The average voltage gradient at which electric breakdown occurs under specific conditions of test
Dissipation factor	The ratio of the loss index to its relative permittivity, the tangent of its loss angle, δ or the cotangent of its phase angle, Θ
Elongation	The strain produced in the test specimen by a tensile stress, expressed as a percentage with respect to the gauge length
Elongation at break	The percentage elongation produced in the gauge length of the test specimen at the break point
Elongation at yield	The percentage elongation produced in the gauge length of the test specimen at the yield stress
Fatigue	The process of progressive localized permanent structural change occurring in a material subjected to conditions that produce fluctuating stresses and strains at some point or points that may culminate in cracks, complete fracture, or thermal softening after sufficient number of fluctuations (Borders et al. 1946)
Fatigue crack growth rate	Crack extension caused by constant amplitude fatigue loading and expressed in terms of crack extension per cycle of fatigue, da/dN (Borders et al. 1946)
Fire	A process of combustion characterized by the emission of heat, accompanied by smoke and/or flame (Mark et al. 1975)
Fire resistance	The property of a material or an assembly to withstand fire or give protection from it

(*continued*)

Table 10.36 (continued)

Fire retardant (flame retardant)	The quality of a substance of suppressing, reducing, or delaying markedly the combustion of certain materials. A fire retardant causes a material to resist burning when exposed to a high-energy source (Sanders 1978)
Flexural deflection	The distance over which the top or the bottom surface of the test piece at mid-span has deviated during flexure from its original position
Flexural stress (at conventional deflection)	The flexural stress at a deflection equal to 1.5 times the thickness of the test piece
Flexural stress at maximum load	The flexural stress developed when the load reaches the first maximum
Flexural stress at rupture	The flexural stress developed at the moment of rupture
Fracture	A break in the mechanical continuity of a material caused by stress exceeding the strength of the material, including joints and faults
Fracture toughness	A conventional fracture mechanics strength parameter indicating the resistance of a material to crack extension
Gauge length	The original length between two marks on the test piece over which the change in length is determined
Haze	Percentage of transmitted light that passes through the specimen deviates from the incident beam by forward scattering (ASTM D 1003)
Haze reflection	The scattering of reflected light in directions near that of specular reflection by a specimen having a glossy surface
Haze transmission	The scattering of light within a specimen or at its surface responsible for the cloudy appearance of objects observed through the specimen
Homogeneous specimen	A specimen in which every geometrically identical portion has the same apparent thermal conductivity
Impact strength	The property to resist physical breakdown when subjected to a rapidly increasing applied force (ASTM Standard Definitions 1982)
Layered specimen	A specimen that if sliced parallel to the faces has one or more slices with a significantly different apparent thermal conductivity than the other slices
Limiting oxygen index (LOI)	This is a measure of the minimum concentration of oxygen in an oxygen–nitrogen atmosphere that is necessary to support a flame for at least 3 min under specified test conditions (Mark et al. 1975)
Refraction	Change in the direction of propagation of radiation determined by change in the velocity of propagation in passing from one medium to another
Refractive index	The ratio of the velocity of light (of specified wavelength) in air to its velocity in the substance under examination
Rockwell hardness	A number derived from the net increase in the depth of impression as the load on a penetrator is increased from a fixed minor load to a major load and then returned to the minor load (ASTM D 785)

(*continued*)

Table 10.36 (continued)

Secant modulus	The ratio of stress to strain, in general, at any given point on the stress–strain curve
Smoldering	Combustion of a solid without flame. The combustion of a material without light being visible and generally evidenced by smoke and an increase in temperature (ASTM E 176-81a)
Specific heat	The heat capacity, C, per unit mass or per unit volume; usually the term refers to mass specific heat (Brown 1981)
Strain	The change in length per unit original length of the measured gauge length of the test specimen. It is expressed as a dimensionless ratio
Surface resistance (R_s)	Resistance between two electrodes that are on the surface of a specimen is the ratio of the direct voltage applied to the electrodes to that portion of the current between them which is primarily in a thin layer of moisture or other semiconducting material that may be deposited on the surface
Surface resistivity	The ratio of the potential gradient parallel to the current along its surface to the current per unit width of the surface
Tensile modulus (also elastic modulus in tension or Young's modulus)	The ratio of tensile stress to corresponding strain below the proportional limit. Many polymers/blends do not obey Hooke's law through out the elastic range but deviate therefrom even at stresses well below the yield stress. However, stress–strain curves almost always show a linear region at low stresses, and a straight line drawn tangent to this portion of the curve permits calculation of tensile modulus
Tensile strength (nominal)	The maximum tensile stress (nominal) sustained by a test piece during a tension test
Tensile stress (nominal)	The tensile force per unit area of the original cross section within the gauge length carried by the test piece at any given moment. The standard unit is mega-Pascal (MPa = MN/m)
Tensile stress at break	The tensile stress at which break of the test specimen occurs
Tensile stress at yield	The tensile stress at which the first marked inflection of the stress–strain curve occurs. Where any increase in strain occurs without any increase in stress, this point is taken as the tensile stress at yield or yield stress
Thermal conductance, (Γ)	The reciprocal of thermal resistance
Thermal Conductivity, (λ)	The heat flux per unit temperature gradient in the direction perpendicular to an isothermal surface, under steady-state conditions
Thermal resistance, R	The temperature difference required to produce a unit of heat flux through the specimens under steady state conditions (ASTM C 177)
Thermal resistivity (r)	The reciprocal of the thermal conductivity
Toughness	That property of a material by virtue of which it can absorb work

(*continued*)

Table 10.36 (continued)

Toxicity	The amount of a substance that produces detrimental effects in an animal. It is expressed as a dose divided by the body weight of the animal, i.e., in mg/kg (Chamberlain 1978)
Transmittance (of light)	That fraction of the incident light of a given wavelength which is not reflected or absorbed, but passes through a substance
Volume resistance, (R_v)	The volume resistance between two electrodes that are in contact with or embedded in a specimen is the ratio of the direct voltage applied to the electrodes to that portion of the current between them that is distributed through the volume of the specimen (ASTM Standard Definitions 1982)
Volume resistivity	The volume resistance (in ohm-cm) between opposite faces of one centimeter cube of the material

Table 10.37 Principal flame retardants, their trade names, and suppliers (Agranoff 1993)

No.	Name	Recommended for	Supplier	Trade name
A. Organic				
1.	Phosphate esters	A, CA, CAB, CN, E, EC, N, P, PE, PP, PS, PVA, PVC, UF, UR	Akzo, Harwick	Lindol, Phosflex TPP 362, 370, 387, 390, 710
			Albright and Wilson	Pliabrac TCP, TXP, 521, 519, 524.
			FMC	Kronitex 50, 100, 200, 3600, 100B, 20OB; TCP, TXP25
			Monsanto	Santicizer 141, 143, 148, 154, TPPa
2.	Decabromodiphenyl oxide	ABS, A, E, P, PET, PE, PP, PS, PVA, UF, UR, PBT, N, (EPDM)	Ameribrom	FR-1210
			Elf Atochem	Thermoguard 505
			Ethyl	Saytex 102E
			Great Lakes Chem.	Great Lakes DE – 83R
3.	Tricresyl phosphate	A, CN, E, EC, PET, PS, PVA, PVC	Akzo, Harwick	Lindol, Lindol XP Plus
			Albright and Wilson	Pilabrac TCP
			FMC	Kronitex TCP
			Miles	Disflamoll TKP
4.	Tributyl phosphate	CA, CAB, CN, EC, PVC	Akzo, Harwick	Phosflex 4
			Albright and Wilson	Albrite TBPO
			FMC	TBP
			Focus Chem.	TEP
5.	Tributoxy ethyl phosphate	A, CA, CAB	Akzo, Harwick.	Phosflex TBEP
			Albright and Wilson	Amgard TBEP
			FMC	KP-140
			Focus Chem.	TBEP

(*continued*)

Table 10.37 (continued)

No.	Name	Recommended for	Supplier	Trade name
6.	Halogenated hydrocarbons	A, E, EC, N, PVA, PVC, UF	Argus	Flexchlor, CPP, FLX
			Elf Atochem	Electrofine S-70
			Dover	Chlorez, Paroil
			Ferro	Kloro series
			Harwick	Plastichlor, CPW100
			Occidental	Chlorowax
7.	Trioctyl phosphate	PVC	Albright and Wilson	Amgard TOF
			FMC	TOF
			Miles	Disflamoli TOF
			Rhone-Poulenc	TOF
8.	Triphenyl phosphate	CA, CAB, CN, PVA, PVC	Akzo	Phosflex TPP
			FMC	Kronitex TPP
			Miles	Disflamoli TP
9.	Halogenated organic phosphate	A, CA, CAB, CN	Akzo	Fyrol CEF, DMMP, EFF 38, 25, 6, FR2, PCF 99, 51
			Albright and Wilson	Antiblaze 78, 80, 100, 125, 150, 175, 190
			Great Lakes Chem.	Firemaster 836, 642, HP 36
10.	Halogenated organics	ABS, A, CA, E, EC, N, PET, PA, PE, PP, PS, PVA, PVC, UR, UF, (PBT, EVA, TPR)	Argus	Flexchlor CPF, FLX, Fyarestor 100, 102, 205, 104
			Elf Atochem	Electrofine S-70 and Thermoguard XS 70T
			Dover	Chlorez and Paroil
			Ferro	Kloro-check series
			Harwick	Plastichlor, CPW 100
			Occidental	Chlorowax and Dechlorane Plus
			Quantum, USI.	Spectratech
			Stanchem.	Cereclor 42, 545, 562, 70
11.	Nonhalogenated organics	PE, PP, UF, UR, PBT, EVA, TPU, PET	Great Lakes Chem.	NH-1511, CN-1197
			Hoechst Celanese	Exolit IFR
			Monsanto	Spin-Flam MF-82
			3-V Chem.	Plastisan B
12.	Chlorinated paraffin	ABS, A, CA, E, EC, N, PET, PS, PVA, PVC, UF, UR	Elf Atochem	Electroline S-70, Thermoguard XS-70-T
			Argus	Flexchlor CPF, FLX
			Dover	Chlorez solids and Paroli liquids
			Ferro	Keil CW Series.
			Harwick	Plastichlor Series, CPW 100

(*continued*)

Table 10.37 (continued)

No.	Name	Recommended for	Supplier	Trade name
			Occidental	Chlorowax
			Quantum USI	Spectratech
13.	Chlorinated hydrocarbon	ABS, A, CA, E, EC, N, PET, PS, PVA, PVC, UF, UR (Polybutylene)	Elf Atochem	Electrofine S-70, Thermoguard XS-70-T
			Argus	Flexchlor, CPF, FLX
			Dover	Chlorez solids and Paroli liquids
			Ferro	Kloro 6001
			Harwick	Plastichlor series CPW 100
			Occidental	Chlorowax
			Stanchem	Cereclor 42, 545, 552, 70
14.	Brominated organic	ABSI E, PC, PA, PS (PBT, PET)	Ameribrom	FR-1034, FR-1025, FR-913
			Argus	Fycerestor series
			Elf Atochem	Thermoguard 200 series, BBH 44, Pyronil series
			Dover	DD 8426, DD 8133, DD 8207, DG 8410
			Ethyl	Saytex: BN-451, BCL-462, BT-93, BT-93 W, 120, 8010
			FMC	Kronitex PB-460, PB-370
			Ferro	Bromoklor 50/70 Pyro-chek
			Great Lakes Chem.	BC-52, BC-58, FF-680, PE-68, PO-64P, DP-45, FR-756, FB-72, PDBS-10 and 80
			Quantum, USI	Spectratech
			Santech	Santechem 17-184
15.	Chlorinated organics	ABS, A, CA, CAB, CN, E, EC, N, P, PET, PE, PP, PS, PVA, PVC, UF, UR	Akzo	Fyrol PCF, CEF, Fr-2, 38
			Albright and Wilson	Antiblaze 80, 100, 125, 150, 175, 195
			Argus	Flexchlor, CPF, FLX
			Elf Atochem.	Electrofine S-70, Thermoguard XS-70-T
			Ferro	Kloro 3000, 3100
			Dover	Chlorez solid and Paroil liquids
			Harwick	Plastichlor series, CPW 100
			Occidental	Chlorwax, Dechlorane Plus
			Quantum, USI	Spectratech
B. Inorganic additives				
1.	Alumina trihydrate	ABS, A, E, N, P, PC, PET, PE, PP, PS, PVA, PVC, UF, UR	Alcan	H, FRF, SF and UF series
			Alcoa	C-series, Hydral series
			AluChem.	AC-series
			Climax	Hydrax ATH series

(*continued*)

Table 10.37 (continued)

No.	Name	Recommended for	Supplier	Trade name
			Custom Grinders	Polyfil series Custom grinds
			Franklin Industrial	H-series Custom grinds of hydrate and carbonate
			Georgia Marble	KC-series
			R. J. Marshall	A-100 series, A-200 series
			Solem, Harwick	SB-series surface-modified aluminas. Micral series
2.	Antimony oxide	ABS, A, CA, CAB, CN, E, EC, N, P, PC, PET, PE, PP, PS, PVA, PVC, UF, UR	Amspec	Amstar HP, KR-High and LTS-Low Tint
			Anzon	TMS, Oncor 75 RA and 55, TMS-HP Trutint 50 Microfine, Trutint 80
			Asarco	Very high, high, and low tint, ultra pure
			Elf Atochem.	Thermoguard S.L., CPA, Low Dust Series, Antimony Halogen Series
			Harwick, Laurel Ind.	Fire shield H-L and Ultrafine grades; LSFR, Pentoxide TP2, TPL
			Miljac	Regular, Red and White, Treated
			Quantum, USI	Spectratech
			Holtrachem	Montana high tint, low tint, Micropure treated blends
3.	Antimony oxide dispersions	ABS, A, CA, CAB, CN, E, EC, N, P, PC, PET, PE, PP, PS,PVA, PVC, UF, UR	Amspec	Amsperse
			Anzon	Environstrand, Fyrebloc
			Elf Atochem	Thermoguard S, L, NF
			Holtrachem.	Montana DIDP treated, high, low, tints, Micro pure
4.	Magnesium hydroxide	ABS, A, E, P, PE, PP, PS, PVC, UF, UR (TPE, EPR, EVA)	Aluchem	ACM-MW, ACM-MH 93
			Climax	Hydramax HM-B8, HM-B8S, HM-C9, HM-C9S
			D. J. Enterprises	ACM-MW, ACM-MH93
			Solem	Zerogen
5.	Organic–inorganic additive	ABS, A, CA, CAB, CN, E, R, EC, N, P, PC, PA, PE, PP, PS, PVA, PVC, UFF, UFR.(EVA, PBT, SAN, TPE)	Anzon	F.R.C. Enviro- strands, Fyrebloc
			D. J. Enterprises	Micro P, Sillum 200, PL-200, Q/P
6.	Sodium antimonate	ABS, A, CN, E, N, PET, PE, PP, PS, PVC, UFF, UFR	Amspec.	S. A. 100
			Anzon	Pyrobloc SAP
			Elf Atochem	Thermoguard FR
			Holtrachem	Montana

(*continued*)

Table 10.37 (continued)

No.	Name	Recommended for	Supplier	Trade name
7.	Tin compounds	ABS, El N, P, PC, PA, PET, PE, PP, PS, PVA, PVC, UFF, UFR	Alcan	Flamtard H.S
8.	Zinc Borate	ABS, A, E, N, P, PC, PET, PE, PP, PS, PVA, PVC, UFF, UFR	Climax	ZB-112, 325, 237, 233, 467
			Harwick	Firebrake ZB,
			U.S – Borax	Zb-Fine, Fire brake 500, Fire brake 415
Reactive types				
1.	Tribromoneopentyl alcohol	A, CA, CN, PET, UFF, UFR	Ameribrom	FR-513
2.	Di-(polyoxyethylene) hydromethyl phosphonate	CN, P, PET, UFF, UFR	Akzo	Victastab HMP
3.	Tribromophenyl maleimide	ABS, PE, PP, PS	Ameribrom	FR-1033
4.	Dibromoneopentyl glycol	A, CA, E, PET, UFF, UFR	Ameribrom Ethyl	FR-522
				FR-1138
5.	Tetrabromobisphenol A	ABS, E, P, PC, PET, UFF, UFR	Ameribrom Ethyl	1524 Saytex RB-100
			Great Lakes Chem.	Great Lakes BA-59P
6.	Ethylene oxide adduct of TBBPA	ABS, E, PET, UFF, UFR	Ameribrom	FR-1525
7.	Phosphorus-containing polyol	E, P, UFF, UFR	Albright and Wilson	Vircol 82
8.	Tetrachlorophthalic anhydride	E, P, PET, UFR	Monsanto	Tetrathal
9.	Hexa-chloro cyclopentadiene	CA, CAB, CN, EC	Velsicol	PCL

Note: *A* = acrylic; *CA* = cellulose acetate; *CAB* = cellulose acetate butyrate; *CN* = cellulose nitrate; *E* = epoxy; *EC* = ethyl cellulose; *N* = nitrile; *P* = phenolic; *PC* = polycarbonate; *PA* = polyamide; *PE* = polyethylene; *PET* = polyester, thermoset; *PP* = polypropylene; *PS* = polystyrene; *PVA* = polyvinyl acetate; *PVC* = polyvinyl chloride; *UFF* = urethane flexible foam; *UFR* = urethane rigid foam

References

P.G.R. Achary, N. Mohanty, B.N. Guru, N.C. Pal, J. Chem. Pharm. Res. **4**, 1475 (2012)
Y. Agari, A. Ueda, J. Polym. Sci. Polym. Phys. Ed. **32**, 59 (1994)
Y. Agari, A. Ueda, S. Nagai, J. Appl. Polym. Sci. **45**, 1957 (1992)
Y. Agari, A. Ueda, S. Nagai, J. Appl. Polym. Sci. **47**, 331 (1993)
Y. Agari, A. Ueda, Y. Omura, S. Nagai, Polymer **38**, 801 (1997)
J. Agranoff (ed.), *Modern plastics encyclopedia* (McGraw-Hill, New York, 1993)
Y.A. Akpalu, P. Ping, Mater Manuf Process **23**, 269 (2005)

R.J. Alfredson, *Vibration and Noise-Measurement Prediction and Control* (Melbourne, 1990), pp. 16–19. Preprints of Papers, Barton, ACT: Institution of Engineers, Australia
M. Amano, K. Nakagawa, Polymer **28**, 263 (1987)
S.E. Amos, K.E. Nielson, C. McRoberts, M.A. Wicki, U.S. Patent 5,981,636 to 3M Innovative Properties Company, 1999
L. An, Z. Wang, D. Yu, J. Jing, Y. Jiang, R. Ma, X. Kou, J. Appl. Polym. Sci. **59**, 1843 (1996a)
L. An, Z. Wang, D. Yu, J. Jing, Y. Jiang, R. Ma, X. Kou, Angew. Makromol. Chem. **243**, 1 (1996b)
K.M. Anderson, Wall J. **31**, 5 (1997)
E.H. Andrews, in *Testing of Polymers*, ed. by W.E. Brown, vol. 4 (Wiley-Interscience, New York, 1969), p. 237
T. Aouak, A.S. Alarifi, J. Saudi Chem. Soc. **13**, 227 (2009)
A.A. Ardakani, J.T. Gotro, J.C. Hedrick, K. Papathomas, N.M. Patel, J.M. Show, A. Vichleck, European Patent Applications, 581,314, 2 Feb 1994; Jpn. Pat., 6,107,958, 19 Apr, Appl. 31 July 1992, to IBM Corp.
A.S. Argon, R.E. Cohen, in *Advances in Polymer Science 91/92*, ed. by H.H. Kausch (Springer, Berlin, 1990)
R.G. Armstrong, US Patent 3,373,222, 1968a
R.G. Armstrong, US Patent 3,373,223, 1968b
ASTM F 1769-97, *Standard Test Method for Measurement of Diffusivity, Solubility, and Permeability of Organic Vapor Barriers Using a Flame Ionization Detector* (Philadelphia, 1997)
ASTM C177-93, *Steady-State Thermal Transmission Properties by Means of the Guarded Hot Plate* (Philadelphia, 1993)
ASTM D1003-92, *Standard Test Method for Haze and Luminous Transmittance of Transparent Plastics* (Philadelphia, 1992)
ASTM D1329-08, *Standard Test Method for Evaluating Rubber Property – Retraction at Lower Temperatures (TR Test)* (Philadelphia, 2008)
ASTM D149-93, *Standard Test Method for Dielectric Breakdown Voltage and Dielectric Strength of Solid Electrical Insulating Materials at commercial Power Frequencies* (Philadelphia, 1993)
ASTM D150-93, *Standard Test Methods for A–C Loss Characteristics and Permittivity (Dielectric Constant) of Solid Electrical Insulating Materials* (Philadelphia, 1993)
ASTM D1525-09, *Standard Test Method for Vicat Softening Temperature of Plastics* (Philadelphia, 2009)
ASTM D1525-91, *Test for Vicat Softening Point of Plastics* (Philadelphia, 1992)
ASTM D1637-61, *Test for Tensile Heat Distortion Temperature of Plastic Sheeting* (Philadelphia, 1970; discontinued in 1990)
ASTM D1693-12, *Standard Test Method for Environmental Stress-Cracking of Ethylene Plastics* (Philadelphia, 2012)
ASTM D2137-11, *Standard Test Methods for Rubber Property – Brittleness Point of Flexible Polymers and Coated Fabrics* (Philadelphia, 2011)
ASTM D256-00, *Impact Resistance of Plastics and Electrical Insulating Materials* (Philadelphia, 1993)
ASTM D2561-12, *Standard Test Method for Environmental Stress-Crack Resistance of Blow-Molded Polyethylene Containers* (Philadelphia, 2012)
ASTM D257-93, *Standard Test Method for D–C Resistance or Conductance of Insulating Materials* (Philadelphia, 1993)
ASTM D2583-95, *Standard Test Method for Indentation Hardness of Rigid Plastics by Means of a Barcol Impressor* (Philadelphia, 1996)
ASTM D3895-09, *Standard Test Method for Oxidative-Induction Time of Polyolefins by Differential Scanning Calorimetry* (American Society for Testing and Materials, Philadelphia, 2009)
ASTM D542-90, *Standard Test Methods for Index of Refraction of Transparent Organic Plastics* (Philadelphia, 1990)

ASTM D635-91, *Test Method for Rate of Burning and/or Extent of Burning of self-supporting Plastics in a Horizontal Position* (Philadelphia, 1991)
ASTM D638-95, *Standard Test Method for Tensile Properties of Plastics* (Philadelphia, 1996)
ASTM D648-82, *Deflection Temperature of Plastics Under Flexural Load* (Philadelphia, 1988)
ASTM D671-93, *Flexural Fatigue of Plastics by Constant Amplitude of Force* (Philadelphia, 1993)
ASTM D695-91, *Compressive Properties of Rigid Plastics* (Philadelphia, 1992)
ASTM D746-07, *Standard Test Method for Brittleness Temperature of Plastics and Elastomers by Impact* (Philadelphia, 2007)
ASTM D785-93, *Rockwell Hardness of Plastics and Electrical Insulating Materials* (Philadelphia, 1993)
ASTM D790-92, *Flexural Properties of Plastics and Electrical Insulating Materials* (Philadelphia, 1992)
ASTM E162-94, *Method for Surface Flammability of Materials Using a Radiant Heat Energy Source* (Philadelphia, 1994)
ASTM E399-90, *Standard Test Method for Plane-Strain Fracture Toughness of Metallic Materials* (Philadelphia, 1991)
ASTM E413-10, *Standard Classification for Rating Sound Insulation* (Phildelpheia, 2010)
ASTM E813, *Standard Test Method for J_{IC}, A Measure of Fracture Toughness*, in 1997 was replaced by E1737, which in turn was discontinued in 1998, Annual Book of ASTM Standards, Part 10 (American Society for Testing and Materials, Philadelphia, 1981)
ASTM E813-89, *Standard Test Method for J_c, a Measure of Fracture Toughness* (Philadelphia, 1990)
ASTM E90-09, *Standard Method for Laboratory Measurement of Airborne Sound Transmission* (Philadelphia, 2009)
ASTM F1473-11, *Standard Test Method for Notch Tensile Test to Measure the Resistance to Slow Crack Growth of Polyethylene Pipes and Resins* (Philadelphia, 2011)
ASTM, *Standard Definitions, Compilation of* (Philadelphia, 1982)
K.O. Ballagh, in *The 33rd International Congress and Exposition on Noise Control Engineering*, August 22–25 (Prague, 2004)
P. Beahan, A. Thomas, M. Bevis, J. Mater. Sci. **11**, 1207 (1976)
J.A. Begley, J.D. Landes, *ASTM STP 514* (1972)
N.C. Billingham, P.D. Calvert, Adv. Polym. Sci., 90 (Springer, Berlin, 1989)
R.L. Blaine, E-53865, Brief #88, *Du Pont Thermal Analysis Technical Literature* (Wilmington, DE, 1973)
R.L. Blaine, C.J. Lundgren, M.B. Harris, in *Oxidative Induction Time – A Review of DSC Experimental Effects*, ed. by A.T. Riga, G.H. Patterson, ASTM STP 1326 (American Society for Testing and Materials, Philadelphia, 1997)
K.G. Blizard, D.G. Baird, Polym. News **12**, 44 (1986a)
K.G. Blizard, D.G. Baird, SPE Techn. Pap. **44**, 311 (1986b)
K.G. Blizard, D.G. Baird, Polym. Eng. Sci. **27**, 653 (1987)
K.G. Blizard, C. Federici, O. Federico, L. Chhapoy, Polym. Eng. Sci. **30**, 1442 (1990)
D.J. Blundell, A. Keller, A.J. Kovacs, J. Polym. Sci. Part B Polym. Lett. **4**, 481 (1966)
A.M. Borders, R.D. Juve, L.D. Hess, Ind. Eng. Chem. **38**, 955 (1946)
S. Bourbigot, S. Duquesne, C. Jama, Macromol. Symp. **233**, 180 (2006)
D.P. Bourcier, J.J. D'Errico, J-P. Etienne, G. Matis, V.J. Yacovone, U.S. Patent Pub. No. US 2009/0286046 A1, 2009
M. Bramuzzo, Polym. Eng. Sci. **29**, 1077 (1989)
H. Breuer, F. Haaf, J. Stabenow, J. Macromol. Sci. Phys. B. **14**, 387 (1977)
K.B. Broberg, J. Mech. Phys. Solids **19**, 407 (1971)
K.B. Broberg, J. Mech. Phys. Solids **23**, 215 (1975)
D. Broek, *Elementary Engineering Fracture Mechanics*, 4th edn. (Nijhoff, Dordrecht, 1986)
W. Brostow, R.D. Corneliussen (eds.), *Failure of Plastics* (Hanser, Munich, 1986)

W. Brostow, R.S. Dziemianowicz, J. Romanski, W. Werber, Polym. Eng. Sci. **28**, 785 (1988)
H.R. Brown, J. Mater. Sci. **8**, 941 (1973)
R.P. Brown (ed.), *Handbook of Plastics Test Methods* (George Godwin, London, 1981)
H.R. Brown, E.J. Kramer, J. Macromol. Sci. Phys. **19B**, 487 (1981)
F.L. Browne, *Theories of the Combustion of Wood and its Control*, Report No. 2136, Forest Products Laboratory, Forest Service (U.S. Department Agriculture, Madison, Wisconsin, 1958)
BS 2782 Method 1001, *Measurement of Hardness by Means of a Barcol Impressor* (London, 1977).
BS 2782 Method 306A, *Impact Strength (Pendulum Method)* (London, 1970)
BS 2782 Method 365A, *Determination of Softness Number of Flexible Plastics Materials* (London, 1976)
BS 2782 Method 365D, *Determination of Hardness by Ball Indentation Method* (London, 1978)
BS 2782, *Methods of Testing Plastics* (London, 1970)
BS 2782, Method 335A, *Determination of Flexural Properties of Rigid Plastics* (London, 1978)
BS 2782, Method 336B, *Determination of Deflection in Bend Under an Applied Force* (London, 1978)
BS 2782, Method 345A, *Determination of Compressive Properties by Deformation at Constant Rate* (London, 1979)
BS 2782, Method 351A, *Determination of Charpy Impact Resistance of Rigid Plastics and Ebonite* (London, 1977)
BS 2782, Method 515A, *Haze of Film* (London, 1970)
BS 2782, Methods 121A and 121B, *Determination of Temperature of Deflection under a Specified Bending Stress of Plastics and Ebonite* (London, 1976)
BS 2782, Methods 320 A to F, *Plastics-Tensile Strength, Elongation and Elastic Modulus* (London, 1976)
BS 3784, *Polytetrafluoroethylene Sheet* (London, 1973)
BS 3816, *Cast Epoxide Resin Insulating Material for Electrical Applications at Power Frequencies* (London, 1964)
BS 3924, *Specification for Pressure Sensitive Adhesive Tapes for Electrical Insulating Purposes* (London, 1978)
BS 4618, *Recommendations for the Presentation of Plastics Design Data. Part 2. Electrical Properties, Section 2. 3 Volume Resistivity; Section 2. 4 Surface Resistivity* (London, 1975)
BS 5102, *Phenolic Resin Bonded Paper Laminated Sheets for Electrical Applications* (London, 1974)
BS 5762, *Methods for Crack Opening Displacement Testing* (British Standards Institution, London, 1979)
BS 874, *Methods for Determining Thermal Insulating Properties* (London, 1973)
C.B. Bucknall, *Toughened Plastics* (Applied Science Publishers, London, 1977)
C.B. Bucknall, in *Comprehensive Polymer Science*, ed. by C. Booth, C. Price, vol. 2 (Pergamon Press, New York, 1988)
C.B. Bucknall, A. Marchetti, J. Appl. Polym. Sci. **28**, 2689 (1983)
C.B. Bucknall, W.W. Stevens, J. Mater. Sci. **15**, 2950 (1980)
C.B. Bucknall, K.V. Gotham, P.I. Vincent, in *Polymer Science*, ed. by A.D. Jenkings (North-Holland, Amsterdam, 1972)
C.B. Bucknall, in *Advances in Polymer Science*, vol. 27 Ed. J. D. Ferry (Springer, New York, 1978)
C.M. Burns, W.N. Kim, Polym. Eng. Sci. **28**, 1362 (1988)
M.F. Butler, A.M. Donald, J. Mater. Sci. **32**, 3675 (1997)
F. Cakar, O. Cankurtaran, F. Karaman, Chromatographia **75**, 1157 (2012)
N. Cameron, Eur. Polym. J. **38**, 597 (2002)
K. Campbell, Wall J. **41**, 12 (2000)
L. Canfora, S. Fillippi, F.P. La Mantia, Polym. Eng. Sci. **44**, 1732 (2004)
Y. Cao, J. Zhang, J. Feng, P. Wu, www.acsnano.org (2011)
C.C. Carroll, *Modern Plastics* (1984)
D.F. Castro, R.C.R. Nunes, L.L.Y. Visconte, G.M. Silva, Int. J. Polym. Mater. Polym. Biomater. **56**, 1127 (2007)

C.M. Chaleat, Polym. Degrad. Stabil. **97**, 1930 (2012)
D.L. Chamberlain, in *Flame Retardancy in Polymeric Materials*, ed. by W.C. Kuryla, A.J. Papa, vol. 4 (Marcel Dekker, New York, 1978)
M.K.V. Chan, J.G. Williams, Polym. Eng. Sci **21**, 1019 (1981)
M.K.V. Chan, J.G. Williams, Polym. Eng. Sci. **19**, 145 (1983)
W.Y.F. Chan, J.G. Williams, Polymer **35**, 1666 (1994)
K. Chandramouli, S.A. Jabarin, Adv. Polym. Tech. **14**, 35 (1995), Published Online: 8 Apr 2003
L.L. Chang, E.M. Woo, Macromol. Chem. Phys. **5**, 202 (2001)
J.-M. Charrier, R.J.P. Ranchouse, Polym. Eng. Sci. **11**, 381 (1971)
H.Y. Chen, Polymer **42**, 7819 (2001)
C.C. Chen, E. Fontan, K. Min, J.L. White, Polym. Eng. Sci **28**, 69 (1988)
C.C. Chen, J.Y. Chueh, H. Tseng, H.M. Huang, S.Y. Lee, Biomaterials **24**, 1167 (2003)
J. Chen, G. Wang, X. Zeng, H. Zhao, D. Cao, J. Yun, C.K. Tan, J. Appl. Polym. Sci. **94**, 796 (2004)
C.P. Cherepynov, Appl. Math. Mech. **31**, 503 (1967)
W.-Y. Chiang, D.-S. Hwung, Polym. Eng. Sci. **27**, 632 (1987)
H.K. Chuang, C.D. Han, Adv. Chem. Ser. **206**, 171 (1984)
H.K. Chuang, C.D. Han, J. Appl. Polym. Sci. **30**, 2457 (1985)
J.H. Chun, S. Ki-Maeng, K.S. Suh, J. Mater. Sci. **26**, 5347 (1991)
M.D. Cliffton, S.A. Gilliam, W.R. Hale, T.J. Pecorini, M.E. Rogers, M.D. Shelby, M.E. Stewart, U.S. Patent 8,133,417, 13 Mar 2012, Appl. 29 Apr 2011, to Eastman Chem. Co.
F.N. Cogswell, B.P. Griffin, J.B. Rose, Eur. Pat. Appl. **30**, 417 (1981)
M.M. Coleman, J.T. Graf, P.C. Painter, *Specific Interactions and the Miscibility of Polymer Blends* (Technomic, Lancaster, 1991)
B.F. Conaghan, S.L. Rosen, Polym. Eng. Sci. **12**, 134 (1972)
P.R. Couchman, Macromolecules **11**, 1156 (1978)
J. Crank, G.S. Park, in *Diffusion of Polymers*, ed. by J. Crank, G.S. Park (Academic, New York, 1968). Chapter 1
M.G. Cross, R. Lines, U.S. Patent 5,378,402, 3 Jan 1995, Appl. 21 July 1983, Br. Appl. 2 Aug 1982, to Raychem Ltd.
T. Daniels, *Thermal Analysis* (Kogan Page, London, 1973)
K.C. Dao, J. Appl. Polym. Sci. **27**, 4799 (1982)
N.A. Darwish, A.B.. Shehata, A.A. Abd El-Megeed, S.F. Halim, A. Mounir, Polym. Plast. Tech. Eng. **44**, 1297 (2005)
A. Dasari, Z.Z. Yu, Y.W. Mai, S. Liu, Nanotechnology **18**, 445602 (2007)
D.S. Davis, U.S. Patent 7,439,306, 2008 to ExxonMobil Chemical Patents Inc.
F. De Ponte, P. Di Filippo, *Design Criteria for Guarded Hot Plate Apparatus, Heat Transmission Measurements in Thermal Insulations* (ASTM STP 544, Am. Soc. Testing Mats., Philadelphia, 1974)
R.D. Deanin, M.F. Sansone, Polym. Symp. **19**, 211 (1978)
D.D. Deshpande, D. Patterson, H.P. Schreiber, C.S. Su, Macromolecules **7**, 530 (1974)
DIN 53435, *Testing of Plastics Determination of Flexural Properties and Impact Resistance with Dynstat Test Specimens* (1977)
DIN 53442, *Testing of Plastics: Fatigue Test in the Field of Bending Strain of Flat Specimens* (1975)
DIN 53452, *Testing of Plastics Bending Test* (1977)
DIN 53453, *Testing of Plastics; Determination of Impact Resistance* (1975)
DIN 53454, *Testing of Plastics Compression Test* (1971)
DIN 53456, *Testing of Plastics Indentation Hardness* (1979)
DIN 53461, *Testing of Plastics-Determination of Temperature of Deflection Under Load* According to ISO 75 (1979)
DIN 53482, *Methods for Determination of Electrical Resistance Values* (1967)
DIN 53483, *Determination of Dielectric Properties* (1969)
DIN 53491, *Testing of Plastics Determination of Refractive Index and Dispersion* (1955)

A.M. Donald, E.J. Kramer, J. Mater. Sci. **17**, 1765 (1982)
L. D'orazio, R. Greco, E. Martuscelli, G. Ragosta, Polym. Eng. Sci. **23**, 489 (1983)
G. Dreezen, G. Groeninck, S. Swier, B. Van Mele, Polymer **42**, 1449 (2001)
M. Du, Q. Wu, M. Zuo, Q. Zheng, Eur. Polym. J. http://dx.doi.org/10.1016/j.eurpolymj.2013.06.006 (2013)
D.S. Dugdale, J. Mech. Phys. Solids **8**, 100 (1960)
W.H. Dukes, *Unresolved Problems in Brittle Material Design*, U.S. Govt. Report, AD 654119 (1966)
M.M. Dumoulin, Ph.D. Thesis, Ecole Polytech., Montreal 1988
I.N. Einhorn, in *Fire Retardance in Polymeric Materials*, ed. by I. Skeist. Reviews in Polymer Technology, vol. 1 (Marcel Dekker, New York, 1972), pp. 113–184
F.R. Eirich, H.F. Mark, *Thermal Degradation of Polymers*. Monograph No. 13 (Society of Chemical Industry, London, 1961), p. 43
Eval Americas, Technical Bulletin No. 190, *Flavor and Aroma Barrier Properties of EVAL Resins* (2007); www.evalca.com
G. Fairley, R.E. Prud'homme, Polym. Eng. Sci. **27**, 1495 (1987)
G. Fairley,Ph. D Thesis, Laval University, Quebec 1990
A.M. Farooque, D.D. Deshpande, Polymer **33**, 5005 (1992)
D.L. Faulkner, Polym. Eng. Sci. **24**, 1174 (1984)
D. Faulkner, *Environmental Stress Cracking of Polycarbonate and a Polycarbonate/Acrylic Blend by Windshield Washer Fluids*. SAE Technical Paper 851628 (1985). doi:10.4271/851628
A.R. Federl, G. Kipouras, U.S. Patent 4,588,773, 13 May 1986, Appl. 21 Dec 1984, to Borg-Warner Chemicals Inc.
E. Fekete, E. Foldes, B. Pukanszky, Eur. Polym. J. **41**, 727 (2005)
C.P. Fenimore, F.J. Martin, Mod. Plast. **44**, 141 (1966)
R.J. Ferguson, G.P. Marshall, J.G. Williams, Polymer **14**, 451 (1973)
T. Fett, Mater. Prüfung **14**, 151 (1972)
D. Filip, S. Vlad, High Perform. Polym. **16**, 101 (2004)
S. Filippi, V. Chiono, G. Polacco, M. Paci, L. Minkova, P. Magagnini, Macromol. Chem. Phys. **203**, 1512 (2002)
B. Fillon, J.C. Williams, B. Lotz, A. Thierry, J. Polym. Sci. Polym. Phys. Ed. **31**, 1383 (1993)
B. Fisa, SPE Techn. Pap. **37**, 1135 (1991)
R. Gadekar, A. Kulkarni, J.P. Jog, J. Appl. Polym. Sci. **69**, 161 (1998)
M. Gahleitner, J. Wolfschwenger, C. Bachner, K. Bernreitner, W. Neissl, J. Appl. Polym. Sci. **61**, 649 (1996)
M.E. Galvin, G.E. Wnek, Polym. Commun. **23**, 795 (1982)
M.E. Galvin, G.E. Wnek, J. Polym. Sci. Chem. **21**, 2727 (1983)
M.E. Galvin, G.F. Dandreaux, G.E. Wnek, Am. Chem. Soc. Ser. **242**, 40 (1984)
J. Gao, Polymer **53**, 1772 (2012)
O.S. Gebizlioglu, H.W. Beckham, A.S. Argon, R.E. Cohen, H.R. Brown, Macromolecules **23**, 3968–3975 (1990)
B.D. Gesner, J. Appl. Polym. Sci. **11**, 2499 (1967)
I. Ghasemi, H.K. Rasmussen, P. Szabo, J. Morshedian, Iranian Polym. J. **14**, 715 (2005)
S.K. Ghosh, S. Sengupta, M. Naskar, J. Sci. Indus. Res. **69**, 396 (2010)
B.S. Giles, S. Vilasagar, European Patent Applications 596,704, 11 May 1994, Appl. 2 Nov 1993, U.S. Appl. 4 Nov 1992, to GE Co.
S.A. Gilliam, W.R. Hale, T.J. Pecorini, M.D. Shelby, U.S. Patent 7,968,164, 28 June 2011, Appl. 27 Feb 2006, to Eastman Chem. Co.
V.V. Ginzburg, Macromolecules **38**, 2362 (2005)
A. Gnatowski, J. Wawrzyniak, T. Jaruga, Arch. Mater. Sci. Eng. **41**, 37 (2010)
Y.K. Godovsky, *Thermophysical Properties of Polymers* (Springer, New York, 1992)
M.M. Gorelova, A.J. Pertsin, V.Y. Levin, L.I. Makarova, L.V. Filimonova, J. Appl. Polym. Sci. **45**, 2075 (1992)

A. Gottschalk, M. Breulmann, E. Fetter, K. Kretschmer, M. Bastian, Kunststoffe Int. **7**, (2006)
Gouveia, Rev. Latin Am. Metal. Mat. **31**(1), 26 (2011)
R. Greco, G. Mucciariello, G. Rogasta, E. Martuscelli, J. Mater. Sci. **15**, 845 (1980)
H.W. Greensmith, J. Appl. Polym. Sci. **7**, 993 (1963)
B.L. Gregory, A. Siegmann, J. Im, E. Bear, J. Mater. Sci. **22**, 532 (1987)
A.A. Griffith, Philos. Trans. R. Soc. London Ser. A. **221**, 163 (1920)
E.A. Grulke, J. Brandrup, E.H. Immergut (eds), *Polymer Handbook*, 4th edn. Wiley, New York (1999), p. 675
D.A. Gunasekara, M.D. Alwis, U.S. Patent App. Pub. No. 2004/0168853, 2004
C.S. Ha, W.J. Cho, Polym. Test. **21**, 123 (2002)
Å. Halldén, B. Wesslén, J. Appl. Polym. Sci. **60**, 2495 (1996)
Å. Halldén, M.J. Deriss, B. Wesslén, Polymer **42**, 8743 (2001)
C.D. Han, H.K. Chuang, J. Appl. Polym. Sci. **30**, 2431 (1985)
Z. Han, L. Chunsheng, T. Kombe, Mater. Struct. **41**, 383 (2008)
C.M. Hansen, Polym. Stab. Degrad. **77**, 43 (2002)
S. Hashemi, J. Mater. Sci. **20**, 229 (1993a)
S. Hashemi, J. Plast. Rubber Compos. Proc. Appl. **20**, 229 (1993b)
S. Hashemi, Polym. Eng. Sci. **37**, 912 (1997)
S. Hashemi, J.G. Williams, Polym. Eng. Sci. **26**, 760 (1985)
S. Hashemi, J.G. Williams, Polymer **27**, 85 (1986)
S. Hashemi, Z. Yuan, J. Plast. Rubber Compos. Proc. Appl. **21**, 151 (1994)
S. Havriliak Jr., C.A. Cruz Jr., S.E. Slavin, Polym. Eng. Sci. **36**, 2327 (1996)
R.N. Haward, C.B. Bucknall, Pure Appl. Chem. **46**, 227 (1976)
C. He, A.M. Donald, M.F. Butler, O. Diat, Polymer **39**, 659 (1998)
D.S. Hecht, L. Hu, G. Irvin, Adv. Mater. 23, 1482 (2011). (doi:10.1002/adma.201003188. Epub 2011 Feb 15)
R. Hendersinn, Fire retardancy (survey), in *Encyclopedia of Polymer Science and Technology*, ed. by N.B. Bikales, vol. 2 (Wiley-Interscience, New York, 1977), pp. 270–339. Supplement
R.W. Hertzberg, J.A. Manson, *Fracture of Engineering Plastics* (Academic, New York, 1980)
C.J. Hilado, Chem. Tech. **2**, 32 (1972)
C.J. Hilado, J. Combustion Toxicol. **8**, 121 (1981)
J.H. Hildebrand, R.L. Scott, *The Solubility of Non-Electrolytes* (Dover, New York, 1964)
K.-S. Ho, K. Levon, U.S. Patent 5,391,622, 21 Feb 1995, Appl. 3 May 1994, U.S. Appl. 20 May 1992, to Neste Oy
D.W.K. Ho, J.H. Koo, M.C. Bruns, O.A. Ezekoye, in *Proceedings of the 43rd AIAA/ASME/SAE/ASEE Joint Propulsion Conference*, 8, 7524, AIAA, Reston, (2007), AIAA Paper 2007–5773
W.K. Ho, J.H. Koo, O.A. Ezekoye, J. Nanomater. 2010 (2010), Article ID 583234, 11 pp. doi:10.1155/2010/583234
G. Holden, E.T. Bishop, N.R. Legge, J. Polym. Sci. **C26**, 37 (1969)
Y. Hong, X. Zhang, C. Qu, B. Li, L. Zhang, Q. Zhang, Q. Fu, Polymer **48**, 860 (2007)
D.V. Howe, M.D. Wolkowicz, Polym. Eng. Sci. **27**, 1582 (1987)
A.J. Hsieh, J.J. Vanselow, U.S. Army Materials Technology Laboratory Watertown, Massachusetts 02172-0001 AMCMS Code 612105.H840011, SLCMT-EMP, Report No.: MTL TR 89-12, (1989)
H. Hsu, D.-J. Lin, L.-P. Cheng, J.-T. Yeh, K.-N. Chen, J. Polym. Res. **8**, 209 (2001)
D.D. Huang, Polym. Mater. Sci. Eng. **63**, 578 (1990)
J.M. Huang, Polymer **46**, 8068 (2005)
Y. Huang, N. Brown, J. Mater. Sci. **23**, 3648 (1988)
J.C. Huang, M.S. Wang, Adv. Polym. Technol. **9**, 239 (1989)
D.D. Huang, J.G. Williams, J. Mater. Sci. **22**, 2503 (1987)
D.D. Huang, J.G. Williams, Polym. Eng. Sci. **30**, 1341 (1990)

D.D. Huang, in *Proceedings, Seventh International Conference on Deformation, Yield and Fracture of Polymers* (The Plastics and Rubber Institute, London, 1988)
R.L. Hudson, *The ChemGuide App*. 2011 info@rlhudson.com
H. Im, H. Kim, J. Kim, Mater. Trans. **50**, 1730 (2009)
L.G. Imhof, K.C. Steuben, Polym. Eng. Sci. **13**, 146 (1974)
ZERO International, Website: www.zerointernational.com, (2001)
A.I. Isayev, M.J. Modic, Polym. Comp. **8**, 158 (1987)
ISO 2039, *Plastics and Ebonite Determination of Hardness by Ball Indentation Method* (Switzerland, 1973)
ISO 178, *Plastics Determination of Flexural Properties of Rigid Plastics* (Switzerland, 1975)
ISO 604, *Plastics Determination of Compressive Properties* (Switzerland, 1973)
ISO 75, *Plastics and Ebonite Determination of the Temperature of Deflection Under Load* (Switzerland, 1974)
ISO R1184, *Plastics-Determination of Tensile Properties of Films* (Switzerland, 1970)
ISO R179, *Determination of the Charpy Impact Resistance of Rigid Plastics* (Switzerland, 1961)
ISO R180, *Determination of the Izod Impact Resistance of Rigid Plastics* (Switzerland, 1961)
ISO R489, *Plastics, Determination of the Refractive Index of Transparent Plastics* (Switzerland, 1966)
ISO/DIS 527, *Plastics-Determination of Tensile Properties* (Switzerland, 1968)
G.C. Ives, J.A. Mead, M.M. Riley, *Handbook of Plastics Test Methods* (Butterworth Group, London, 1971)
B.Z. Jang, D.R. Uhlmann, J.B. Van der Sande, J. Appl. Polym. Sci. **30**, 2485 (1985a)
B.Z. Jang, D.R. Uhlmann, J.B. Van der Sande, Polym. Eng. Sci. **25**, 643 (1985b)
J.A. Jansen, Adv. Mater. Process., June 2004, 50–53
G. Jeffrey, M.S. Weiss, J. Polym. Sci. Part B Polym. Phys. **44**, 2253 (2006)
Y. Jen-Taut, C.–.C. Fan-Chiang, S.-S. Yang, J. Appl. Polym. Sci. **64**, 1531 (1997)
H.-Y. Jeon, A. Bouazza, K.-Y. Lee, Polym. Test **27**, 434 (2008)
R. Jester, et al. *2005 PLACE Conference*, Las Vegas, Nevada, September 27–29, (2005)
M. Jiang, H. Xie, Prog. Polym. Sci. **16**, 977 (1991)
Y.Y. Jiang, S. Yoshimura, R. Imai, H. Katsura, T. Yoshida, C. Kato, J. Fluid. Struct **23**, 531 (2007)
F. Johansson, *Food and Packaging Interactions Affecting Food Quality*, Doctoral Dissertation and SIK-Rapport no. 628, (Chalmers University of Technology, Gothenburgh, 1996)
L. Jong, E.M. Pearce, T.K. Kwei, Polymer **34**, 48 (1993)
T.J.M. Jongeling, European Patent Applications 538,939, 28 Apr 1993 Appl. 21 Oct 1991, to DSM NV
E.G. Joseph, G.L. Wilkes, D.G. Baird, Polym. Prepr. **25**, 94 (1984)
C. Joshi, S. Dabke, V.N.S. Pendyala, K.V. Rao, S.F. Xavier, *Chemcon-2005* (Department of Chem. Engg., I.I.T., Delhi, 2005)
R. Juana, A. Etxberria, M. Cortazar, J.J. Iruin, Macromolecules **27**, 1395 (1994)
B. Jurkowski, Y.A. Olkhov, K. Kelar, O.M. Olkhova, Eur. Polym. J. **38**, 1229 (2002)
R.P. Kambour, Polym. Sci. Macromol. Rev. **7**, 1 (1973)
R.P. Kambour, in *Encyclopedia of Polymer Science and Engineering*, ed. by H.F. Mark, N.M. Bikales, C.G. Overberger, G. Menges, J.I. Kroschwitz (Wiley, New York, 1986), p. 299
A. Kamira, B.-B. Naima, Polym. Test. **25**, 1101 (2006)
J. Karger-Kocsis, T. Czigany, Polymer **37**, 2433 (1996)
J. Karger-Kocsis, J. Varga, J. Appl. Polym. Sci. **62**, 291 (1996)
J. Karger-Kocsis, A. Kallo, V.N. Kuleznev, Plaste Kautsch **28**, 629 (1981)
J. Karger-Kocsis, A. Kallo, V.N. Kuleznev, Polymer **25**, 279 (1984)
T. Karna, J. Laakso, K. Levon, E. Savolainen, U.S. Patent 5,346,649, 13 Sep 1994a, US Appl. 4 Dec 1992, Fin. Appl. 5 Dec 1991, to Neste Oy
T. Karna, J. Laakso, T. Niemi, H. Ruohonen, E. Savolainen, H. Lindstrona, E. Virtanon, O. Ikkale, A. Andreatta, U.S. Patent 5,340,499, 23 Aug 1994b, US Appl. 11 Aug 1992, to Neste Oy
T. Kashiwagi, E. Grulke, J. Hilding, R. Harris, W. Awad, J. Douglas, Macromol. Rapid. Commun. **23**, 761 (2002)

T. Kashiwagi, R.H. Harris Jr., X. Zhang, R.M. Briber, B.H. Cipriano, S.R. Raghavan, Polymer **45**, 881 (2004)
T. Kashiwagi, F. Du, K.I. Winey, K.M. Groth, J.R. Shields, S.P. Bellayer, Polymer **46**, 471 (2005)
K. Kato, Kolloid-Z. Z. Polym. **220**, 24 (1967a)
K. Kato, Polym. Eng. Sci. **7**, 38 (1967b)
H.H. Kausch, (ed.), Adv. Polym. Sci. **52/53** (Springer, Berlin, 1983)
H.D. Kay, S.M. Morgan, S.N. Bodapati, Wall J. **41**, 24 (2000)
J.D. Keitz, J.W. Barlow, D.R. Paul, J. Appl. Polym. Sci. **29**, 3131 (1984)
K. Kelar, B. Jurkowski, Polymer **41**, 1055 (2000)
A. Kelarakis, K. Yoon, Eur. Polym. J. **44**, 3941 (2008)
I. Kelnar, J. Kotek, L. Kapralkova, J. Hromadkova, J. Kratochvil, J. Appl. Polym. Sci. **100**, 1571 (2006)
D. Kemmer, S. Smolic, R. Franz1, V. Coma, *Poster presentation at the 4th International Symposium on Food Packaging*, Prague, November 19–21 (2008)
K. Kendall, F.R. Sherliker, Brit. Polym. J. **12**, 111 (1980)
W.N. Kim, C.M. Burns, Polym. Eng. Sci. **28**, 1115 (1988)
K.J. Kim, T. Kyu, Polymer **40**, 6125 (1999)
B. Kim, V. Koncar, E. Devaux, AUTEX Res. J. **4**, 9 (2004)
A.J. Kinloch, in *Polymer Blends and Mixtures*, ed. by D.J. Walsh, J.S. Higgins, A. Maconnachie (Nijhoff, Dordrecht, 1985)
A.J. Kinloch, R.J. Young, *Fracture Behavior of Polymers* (Applied Science Publishers, New York, 1983)
G. Kipouras, A.R. Federl, U.S. Patent 4,755,716, 4 Oct 1988, Appl. 12 May 1986, to Borg-Warner Chemicals Inc.
E. Kiran, J. Supercritical Fluid. **47**, 466 (2009)
G. Kiss, Polym. Eng. Sci. **27**, 410 (1987)
J. Kocsis, A.A. Apostolov, J. Appl. Polym. Sci. **91**, 175 (2004)
T. Kokkonen, T. Karna, J. Laakso, P. Nuholm, J.-E. Sterholm, H. Stubb, U.S. Patent 5,279,769, 18 Jan 1994, US Appl. 2 Dec 1991, Fin. Appl. 30 Mar 1990, to Neste Oy
J. Kolarík, J. Macromol. Sci. Part B Phys. **39**, 53 (2000)
J. Kolarik, G.C. Locati, L. Fambri, A. Penati, Polym. Netw. Blend. **7**, 103 (1997)
K. Koo, T. Inoue, K. Miyasaka, Polym. Eng. Sci. **25**, 741 (1985)
J.H. Koo, D.W.H. Ho, O.A. Ezekoye, in *Proceedings of the 42nd AIAA/ASME/SAE/ASEE Joint Propulsion Conference*, 8, 5895, AIAA, Reston, (2006), AIAA Paper 2006-4936
J.H. Koo, D.W.H. Ho, M.C. Bruns, O.A. Ezekoye, in *Proceedings of the AIAA/ASME/ASCE/AHS/ASC Structures, Structural Dynamics and Materials Conference*, 5136–5175, AIAA, Reston, (2007), AIAA Paper 2007–2131
S. Kopp, J.C. Wittmann, B. Lotz, Polymer **35**, 908 (1994)
B. Kouini, A. Serier, Mater. Design **34**, 313 (2012)
E.G. Kouloori, A.X. Georgaki, J.K. Kallitsis, Polymer **38**, 4185 (1997)
M. Kozlowski, Polym. Netw. Blend. **5**, 163 (1995)
E.J. Kramer, J. Macromol. Sci. Phys. **B10**, 191 (1974)
E.J. Kramer, J. Polym. Sci. Phys. **13**, 509 (1975)
E.J. Kramer, in *Crazing in Polymers, Advances in Polymer Science*, ed. by H.H. Kausch, vol. 52/53 (Springer, Berlin, 1983)
S. Krause, J. Macromol. Sci. Revs. Macromol. Chem. **C7**, 251 (1972)
S. Krause, in *Polymer Blends*, ed. by D.R. Paul, S. Newman, vol. 1 (Academic, New York, 1978). Chapter 2
S. Krause, M. Iskandar, M. Iqbal, Macromolecules **15**, 105 (1982)
A. Krishna, E. Berg, *Stress Cracking of Polycarbonate Exposed to Sunscreen* (Delphi Automotive LLP, 2011-01-0037, 2011)

C.C. Ku, R. Liepins, *Electrical Properties of Polymers, Chemical Principles* (Hanser, Munich, 1987)
R.A. Kudva, H. Keskkula, D.R. Paul, Polymer **40**, 6003 (1999)
V.G. Kulkarni, B. Wessling, European Patent Applications 497,514, 5 Aug 1992, U.S. Appl 31 Jan 1991. U.S. Patent 5,290, 483, 2 Mar 1994, Appl. 22 June 1993
V.G. Kulkarni, B. Wessling, European Patent Applications 536, 915, 14 Apr 1993, U.S. Appl. 8 Oct 1991, to Americhem Inc.
A.K. Kulshreshtha, G.C. Pandey, S.F. Xavier, J.S. Anand, Eur. Polym. J. **25**, 925 (1989)
C.A. Kumins, T.K. Kwei, in *Diffusion of Polymers*, ed. by J. Crank, G.S. Park (Academic, New York, 1968). Chapter 4
T. Kunori, P.H. Geil, J. Macromol. Sci. Phys. **B18**, 93–135 (1980)
T. Kurauchi, T. Ohta, J. Mater. Sci. **19**, 1699 (1984)
L. Kureleca, M. Teeuwenb, H. Schoffeleersb, R. Deblieckb, Polymer **46**, 6369 (2005)
W.C. Kuryla, A.J. Papa (eds.), *Flame Retardancy of Polymeric Materials*, vol. 4 (Marcel Dekker, New York, 1978)
S.A. Kyriakou, M. Statherpoulos, G.K. Parissakis, C.D. Papaspyrides, C.N. Kartalis, Polym. Degrad. Stab. **66**, 49 (1999)
F.P. La Mantia, A. Valenza, M. Paci, P.L. Magagnini, J. Appl. Polym. Sci. **38**, 583 (1989)
J. Lagaron, N.M. Dixon, B.J. Kip, Macromolecules **31**, 5845 (1998)
J. Lagaron, J. Pastor, B. Kip, Polymer **40**, 1629 (1999)
J. Lagaron, G. Capaccio, L.J. Rose, B.J. Kip, J. Appl. Polym. Sci. **77**, 283 (2000)
A. Lahor, M. Nithitanakul, B.P. Grady, Eur. Polym. J. **40**, 2409 (2004)
S.-M. Lai, Y.-C. Liao, T.-W. Chaen, J. Appl. Polym. Sci. **100**, 1364 (2006)
S. Laihonen, U.W. Gedde, P.E. Werner, M. Westdahl, P. Jääskeläinen, G.J. Lake, *Conference Proceedings of the Physical Institute. The Yield Deformation and Fracture of Polymers* (Cambridge, 1970)
S. Laihonen, U.W. Gedde, P.E. Werner, J. Martinez-Salazar, Polymer **38**, 361 (1997)
G.J. Lake, P.B. Lindley, A.G. Thomas, in *Fracture*, ed. by L. Averbach (Chapman & Hall, London, 1979)
J.D. Landes, J.A. Begley, in *Post-Yield Fracture Mechanics*, ed. by D.G.H. Latzko (Applied Science Pubishers, London, 1979)
A.H. Landrock (ed.), *Handbook of Plastics Flammability and Combustion Toxicology* (Noyes Pub, New Jersey, 1983)
L. Lapcik Jr., in *Proceedings of Fifth International Conference on Composites Engineering* (Chicago, 1998), pp. 515–521
A. Lazzeri, M. Malanima, M. Pracella, J. Appl. Polym. Sci. **74**, 3455 (1999)
B.-L. Lee, Polym. Eng. Sci. **28**, 1107 (1988)
C.B. Lee, F.C. Chang, Polym. Eng. Sci. **32**, 792 (1992)
K.I. Lee, H. Jopson, Makromol. Chem. Rapid Commun. **4**, 375 (1983)
K.I. Lee, H. Jopson, Am. Chem. Soc. Symp. Ser. **242**, 39 (1984)
B.L. Lee, U.S. Patent 5,237,009, 17 Aug 1993, Appl. 24 Apr 1991, to B.F. Goodrich Co.
C.B. Lee, M.L. Lu, F.C. Chang, J. Chinese Inst. Chem. Eng. **23**, 305 (1992a)
C.B. Lee, M.L. Lu, F.C. Chang, Polym. Mater. Sci. Eng. **64**, 510 (1992b)
C.B. Lee, M.L. Lu, F.C. Chang, J. Appl. Polym. Sci. **47**, 1867 (1993)
J.-C. Lee, Y.-S. Hong, R.-G. Nan, M.-K. Jang, C.S. Lee, S.-H. Ahn, Y.-J. Kang, J. Mech. Sci. Technol. **22**, 1468 (2008)
J.D. Lendes, J.A. Begley, ASTM STP **560**, 170 (1974)
W. Lethersich, *Technical Report L/T 186 – Impact Testing Critical Resume* (British Electrical and Allied Industries Research Association, London, 1948)
E.G. Lezcano, C. Salom Coll, M.G. Prolongo, Macromolecules **25**, 6849 (1992)
E.G. Lezcano, M.G. Prolongo, C. Salom Coll, Polymer **36**, 565 (1995)
E.G. Lezcano, C. Salom Coll, M.G. Prolongo, Polymer **37**, 3603 (1996)
E.G. Lezcano, R. de Arellano, M.G. Prolongo, C. Salom Coll, Polymer **39**, 1583 (1998)
Z.-M. Li, S.-N. Li, X.-B. Xu, Polym-Plast. Tech. Eng. **46**, 129 (2007)

T. Lian, W. Xu, P. Liu, H. Ren, Polym. Plast. Tech. Eng. **43**, 31 (2004)
J.W. Lim, A. Hassan, A.R. Rahmat, M.U. Wahit, Polym. Intnl. **55**, 204 (2006)
Lindsay Rubber Products, Best *Type of Rubber* (2010)
Liu, X., Jiang, Z., and Zhu, W., *e-Polymers* (2007) Europ. Polym. Fed., CODEN: EPOLCI J. 7, 675 (1999)
S.M. Lomarkin, I.L. Dubnikova, A.N. Shchegolikhin, G.E. Zaikov, R. Kozlowski, G.-M. Kim, G.H. Michler, J. Therm. Anal. Calorim. **94**, 719 (2008)
C. Lotti, A.C. Carlos, V.C. Sebastiao, Mater. Res. **3**, 1 (2000)
B. Lotz, Polymer **39**, 4562 (1998)
B. Lotz, J. Macromol. Sci. Part B-Phys. **41**, 685 (2003)
X. Lu, N. Brown, Polymer **28**, 1505 (1987)
M.L. Lu, F.C. Chang, Polymer **36**, 2541–4639 (1995)
M.L. Lu, C.B. Lee, F.C. Chang, Polym. Eng. Sci. **35**, 1433 (1995)
M.L. Lu, K.C. Chiou, F.C. Chang, Polym. Eng. Sci. **36**, 2289 (1996)
A.B. Lugao, E.C.L. Cardoso, B. Hutzler, L.D.B. Machado, R.N. Conceicao, Radiat. Phys. Chem. **63**, 489 (2002)
A. Lustiger, Environmental stress cracking: the phenomenon and its utility, in *Failure of Plastics*, ed. by W. Brostow, R. Corneliussen (Hanser, Munich, 1986), pp. 305–329
A. Lustiger, N.J. Ishikawa, J. Polym. Sci. Polym. Phys. **29**, 1047 (1991)
A. Lustiger, Understanding Environmental Stress Cracking in Polyethylene, in *Medical Plastics: Degradation, Resistance & Failure Analysis* ed. R.C. Portnoy (SPE, Plastic Design Library, Rice RC, Tritsch DE, 1998), pp. 66–71
J.P. Lv, W.H. Liu, J. Appl. Polym. Sci. **105**, 333 (2007)
W.J. MacKnight, R.W. Lenz, P.V. Musto, R.J. Somani, Polym. Eng. Sci. **25**, 1124 (1985)
Y.W. Mai, Int. J. Mech. Sci. **35**, 995 (1993)
Y.W. Mai, B. Cotterell, Int. J. Fract. **32**, 105 (1986a)
Y.W. Mai, B. Cotterell, Int. J. Fract. **30**, R37 (1986b)
Y.W. Mai, P. Powell, J. Polym. Sci. Part B. Polym. Phys. **29**, 785 (1991)
Y.W. Mai, B. Cotterell, R. Horlyck, G. Vigna, Polym. Eng. Sci. **27**, 804 (1987)
D. Maki, M. Stevens, *Calculation of Effective Diffusion and Solubility Coefficients in Non-Fickian Materials*, in TAPPI 2002 PLACE Conference, p. 5 (2002)
T.M. Malik, P.J. Carreau, N. Chapleau, Polym. Eng. Sci. **29**, 600 (1989)
B.M. Mandal, C. Bhattacharya, S.N. Bhattacharya, J. Macromol. Sci. Chem. A, **26**, 175 (1989)
M.J. Mannion, U.S. Patent 5,310,950, 1994 to Milliken Research Corporation
J.F. Mano, D. Koniarova, R.L. Reis, J. Mater. Sci. Mater. Medic. **14**, 127 (2003)
J.A. Manson, L.H. Sperling, *Polymer Blends and Composites* (Plenum Press, New York, 1981)
C. Mao, Y. Zhu, W. Jiang, ACS Appl. Mater. Interfaces **24**, 5281 (2012). doi:10.1021/am301230q. Epub 2012 Sep 18
H.F. Mark, N.G. Gaylord (eds.), *Encyclopedia of Polymer Science and Technology*, vol. 14 (Interscience Publishers, New York, 1971), p. 24
H.F. Mark, S.M. Atlas, S.W. Shalaby, E.M. Pearce, in *Flame-Retardant Polymeric Materials*, ed. by M. Lewin, S.M. Atlas, E.M. Pearche (Plenum Press, New York, 1975)
G.P. Marshall, J.G. Williams, C.E. Turner, J. Mater. Sci. **8**, 949 (1973)
E. Martine, D. Louvier, *HEIG-VD/LEC, Analytical Method for the Determination of the Aroma Permeation Through Packaging Materials* (Switzerland, 2010)
R.J. Martino, (ed.), *Modern Plastics Encyclopedia '93*, (McGraw-Hill, New York, 1994)
M.A. Martins, C.G. Mothe, Polym. Test. **15**, 91 (1996)
Y. Maruhashi, S. Iida, Polym. Eng. Sci. 41, 1987 (2001), Article first published online: 7 APR 2004. doi:10.1002/pen.10895
L.R. Mason, A.B.. Reynolds, J. Appl. Polym. Sci. **66**, 1691 (1997)
B. Mazeaud, M.A. Galland, Mech. Syst. Signal Process. **21**, 2880 (2007)
N.G. McCrum, B.E. Read, G. Williams, *Anelastic and Dielectric Effects in Polymeric Solids* (Wiley, London, 1967)
E. Meaurio, E. Zuza, J.R. Sarasua, Macromolecules **38**, 1207 (2005)

A. Mehta, A.I. Isayev, Polym. Eng. Sci. **31**, 971 (1991)
R.B. Mesrobian, P.E. Hinsdale, O.F. Sellers, A. Domas, U.S. Patent 3,373,224, 1968
R.A. Mickiewicz, E. Ntoukas, A. Avgeropoulos, E.L. Thomas, Macromolecules **41**, 5785 (2008)
L. Minkova, H. Yordanov, S. Filippi, Polymer **43**, 6195 (2002)
M-j. Luo, Y-x. Lu, Q-q. Chen, Z. Deng, D-q. Chen, W-b. Xie, L. M-j. Fu, Gaofenzi Cailiao Kexue Yu Gongcheng **17**, 71–79 (2001)
A.B.. Morgan, Polym. Adv. Technol. **17**, 206 (2006)
A. Moro, A. Chiolle, L. Credali, G. Foschcini, Makromol. Chem. Macromol Symp. **16**, 137 (1988)
R.E. Morris, R.R. James, T.A. Werkenthin, Rubber Chem. Tech. **17**, 92 (1944)
E.J. Moskala, M.R. Tant, Polym. Mater. Sci. Eng. **63**, 63 (1990)
A. Muhammad, Ph.D. Thesis, Mechanistic Studies Of Thermal Behavior Of Certain Polymeric Systems With Additives, Bahauddin Zakariya University, Multan, 01 Apr 2013
M. Nagao, G. Sawa, M. Ied, Trans. Inst. Elect. Eng. Japan **96-A**, 605 (1976)
M. Nagao, S. Toyoshima, G. Sawa, M. Ieda, Trans. Inst. Elect. Eng. Japan **97-A**, 617 (1977)
L. Narisawa, Polym. Eng. Sci. **27**, 41 (1987)
I. Narisawa, M.T. Takemori, Polym. Eng. Sci. **29**, 671 (1989)
I. Narisawa, M.T. Takemori, Polym. Eng. Sci. **30**, 1345 (1990)
S. Nazare, B.K. Kandola, A.R. Horrocks, Polym. Adv. Technol. **17**, 294 (2006)
NETZSCH, G:\O I T\Determination of the Oxidation Induction Time or Temperature O_I_T_ and O_O_T_ – NETZSCH Analyzing & Testing.mht
L.V. Newmann, J.G. Williams, Polym. Eng. Sci. **18**, 893 (1978)
L.E. Nielsen, *Mechanical Properties of Polymers and Composites*, vol. 2 (Marcel Dekker, New York, 1974)
T. Nishi, T.T. Wang, Macromolecules **8**, 909 (1975)
T. Nishi, T.T. Wang, Macromolecules **10**, 421 (1977)
Y. Nitta, M. Funayama, IEEE Trans. Electr. Insul. **EI-13**, 130 (1978)
M.R. Nobile, D. Acierno, L. Incarnato, E. Amendola, L. Nicolais, C. Carfagna, J. Appl. Polym. Sci. **41**, 2723 (1990)
QUILITE Noise Barriers, *QUILITE International* (California, 1997)
E. Nolley, J.W. Barlow, D.R. Paul, Polym. Eng. Sci. **20**, 364 (1980)
J. Nunoshige, H. Akahoshi, Y. Liao, S. Horiuchi, Y. Shibasaki, M. Ueda, Polym. J. **39**, 828 (2007). doi:10.1295/polymj.PJ2006280
O. Olabisi, Macromolecules **8**, 316 (1975)
O. Olabisi, L.E. Robeson, M.T. Shaw, *Polymer-Polymer Miscibility* (Academic, New York, 1979)
E. Orowan, Rep. Prog. Phys. **12**, 185 (1948)
R.M. Ottenbrite, L.A. Utracki, S. Inoue (eds.), *Rheology and Polymer Processing, Multiphase Systems*. Current Topics in Polymer Science, vol. 2 (Hanser, Munich, 1987)
C. Ozdilek, Polymer **52**, 4480 (2011)
A.R. Padwa, Polym. Eng. Sci. **32**(22), 1703 (1992)
P. Pakeyangkoon, M. Nithiitanakul, B.P Grady, *World Congress of Chemical Engineering, 7th,* Glasgow, UK, July 10–14, (2005)
L. Pan, T. Chiba, T. Inoue, Polymer **42**, 8825 (2001)
V.S. Papakov, G.G. Nikiforova, I.M. Raygorodsky, I.P. Storozhuk, J. Polym. Sci. **37B**, 428 (1995)
V.S. Papakov, G.G. Nikiforova, V.G. Nikolsky, I.A. Krasotkina, E.S. Obolonkova, Polymer **39**, 631 (1998)
E. Paredes, E.W. Fischer, Macromol. Chemie **180**, 2707 (1979)
K.J. Pascoe, in *Failure of Plastics*, ed. by W. Brostow, R.D. Corneliussen (Hanser, Munich, 1986). Chapter 7
D.R. Paul, J.W. Barlow, J. Macromol. Sci. -Rev. Macromol. Chem. **C18**, 109 (1980)
D.R. Paul, L.M. Robeson, Polymer **49**, 3187 (2008)
D.R. Paul, in *Polymer Compatibility and Incompatibility Principles and Practice*, vol. 2, ed. by K. Solc, MMI Press Symposium Series (1982)

V.N.S. Pendyala, K.V. Rao, S.F. Xavier, A.K. Kulshreshtha, *Evaluation of Commercial Nucleating Agents' Efficiency in Polypropylene Homopolymer*, R.I.L., Report No. RD/MSG/153, Feb 21, (2004)
J.D. Peterson, S. Vyazovkin, C.A. Wight, Macromol. Chem. Phys. **202**, 775 (2001)
R.P. Petrich, *Impact Reinforcement of Polyvinylchloride*, presented at SPE RETEC meeting, Cleveland, 7 March 1972
D. Pfefferkorn, Eur. Polym. J. **48**, 200 (2012)
O.-G. Piringer, A.L. Baner, in *Plastic Packaging Materials for Food: Barrier Function, Mass Transport, Quality Assurance, and Legislation* (Wiley-VCH, 2000), p. 576
P. Pisitsak, R. Magaraphan, Polym. Test. **28**, 116 (2009)
E. Plati, J.G. Williams, Polym. Eng. Sci. **15**, 470 (1975)
A.P. Plochocki, Polym. Eng. Sci. **23**, 618 (1983)
G. Poli, M. Paci, P. Magagnini, R. Scaffaro, F.P. La Mantia, Polym. Eng. Sci. **36**, 1244 (1996)
I. Polios, Macromolecules **30**, 4470 (1997)
J.A. Pople, G.R. Mitchell, S.J. Sutton, A.S. Vaughan, C.K. Chai, Polymer **40**, 2769 (1999)
C.H. Porter, R.H. Boyd, in *Dielectric Properties of Polymers*, ed. by F.E. Karasz (Plenum Press, New York, 1972)
K. Premphet, W. Paecharoenchai, J. Appl. Polym. Sci. **85**, 2412 (2002)
B. Pukanszky, F. Tudos, Makromol. Chem., Macromol. Symp. **38**, 221 (1990)
B. Pukanszky, F. Tudos, A. Kallo, G. Bodor, Polymer **30**, 1399–1407 (1989)
X.Y. Qi, D. Yan, Z. Jiang, Y.K. Cao, Z.Z. Yu, F. Yavari, N. Koratkar, ACS Appl. Mater. Interfaces **3**, 3130 (2011). doi:10.1021/am200628c. Epub 2011 July 20
H. Qin, S. Zhang, C. Zhao, G. Hu, M. Yang, Polymer **46**, 8386 (2005)
Z.X. Quande Gui, G.D. Weiping Zhu, J. Appl. Polym. Sci. **88**, 297 (2003)
C.B. Quinn, J. Polym. Sci. Polym. Chem. **15**, 2587 (1977)
D. Quintens, G. Groeninckx, Polym. Eng. Sci. **30**, 1474 (1990)
S. Radhakrishnan, P.D. Venkatachalapathy, Polymer **37**, 3749 (1996)
J.C. Radon, Int. J. Fracture **16**, 533 (1980)
R. Ramanathan, K. Blizard, D. Baird, SPE Techn. Papers **33**, 1399 (1987)
R. Ramanathan, K. Blizard, D. Baird, SPE Techn. Papers **34**, 1123 (1988)
H. Raval, S. Devi, Y.P. Singh, M.H. Mehta, Polymer **32**, 493 (1991)
P.E. Reed, in *Developments in Polymer Fracture*, ed. by E.H. Andrews (Applied Science Publishers, London, 1979)
J.R. Rice, in *Fracture, An Advanced Treatise*, ed. by H. Liebowitz, vol. 2 (Academic, New York, 1968)
M.J. Richardson, P. Burrington, J. Thermal Anal. **6**, 345 (1974)
C.M. Rimnac, T.M. Wright, R.W. Klein, Polym. Eng. Sci. **28**, 1586 (1988)
M. Rink, T. Ricco, W. Lubert, A. Pavan, J. Appl. Polym. Sci. **22**, 429 (1978)
S.J. Risch, *ACS Symposium series-756* (2000), p. 94
S. Ritzenthaler, E. Girard-Reydet, J.P. Pascault, Polymer **41**, 6375 (2000)
R.S. Rivlin, A.G. Thomas, J. Polym. Sci. **10**, 291 (1953)
R.E. Robertson, D.R. Paul, J. Appl. Polym. Sci. **17**, 2579 (1973)
J.M. Rodriguez-Parada, V. Percec, J. Polym. Sci., (A) Polym. Chem. **24**, 579 (1986a)
J.M. Rodriguez-Parada, V. Percec, Macromolecules **19**, 55 (1986b)
R.J. Roe, C. Gieniewski, Polym. Eng. Sci. **15**, 421 (1975)
D.S. Rosa, J. Sarti, L.H.I. Mei, M.M. Filho, S. Silveira, Polym. Test. **19**, 523 (2000)
S.L. Rosen, Polym. Eng. Sci. **7**, 115 (1967)
M.R. Rubner, S.K. Tripathy, J. George Jr., P. Chlewa, Macromolecules **16**, 870 (1983)
C.F. Ryan, U.S. Patent 3,678,133, 1972
C.F. Ryan, R.J. Crochowski, U.S. Patent 3,426,101, 1969
S.F. Xavier, V.N.S. Pendyala, Unpublished results
S. Saha, Eur. Polym. J. **37**, 2513 (2001)
S. Sánchez-Valdes, I.Y. Flores, R. de Valle LF, O.S. Rodriguez-Fernandez, F. Orona-Villarreal, M.L. Quintanilla, Polym. Eng. Sci. **38**(1), 127 (1998)

K. Sandeep, B.V. Ramanaiah, A.R. Ray, Polym.-Plast Tech. Eng. **45**, 1039 (2006)
M.J. Sanders, *Flame Retardants Special Report*, Chem. Eng. News, 56, 22–28 (Apr 24) 1978
M.C. Sarkar, M. Tech., Dissertation, Delhi College of Engineering, Delhi, 1989
G. Sarkhel, A. Choudhury, J. Appl. Polym. Sci. **108**, 3442 (2008)
K. Satake, J. Appl. Polym. Sci. **14**, 1007 (1970)
J.A. Sauer, C.C. Chen, in *Crazing in Polymers*, ed. by H.H. Kausch (Springer, Heidelberg, 1983)
J.A. Sauer, C.C. Chen, Polym. Eng. Sci. **24**, 786 (1984)
J.A. Sauer, G.C. Richardson, Int. J. Fract. **16**, 499 (1980)
A. Savadori, Mater. Technik **4**, 212 (1985)
B. Schartel, M. Bartholmai, U. Knoll, Polym. Adv. Technol. **17**, 772 (2006)
J. Scheirs, *Compositional and Failure Analysis of Polymers* (Wiley, Chichester, 2000)
A.R. Schultz, A.L. Young, J. Appl. Polym. Sci. **28**, 1677 (1983)
B. Selvakumar, Ind. J. Chem. Tech. **15**, 547 (2008)
M.C. Senake Perera, U.S. Ishiaku, Z.A. Mohd. Ishak, Eur. Polym. J. **37**, 167 (2001)
M. Sepe, Stress cracking: how to avoid this silent killer (part 1). *IMM Magazine*, (1999)
J. Seppala, M. Heino, C. Kapanen, J. Appl. Polym. Sci. **44**, 1051 (1992)
G. Serpe, J. Jarrin, F. Dawans, Polym. Eng. Sci. **28**(21), 1416 (1988)
R.J. Seward, J. Appl. Polym. Sci. **14**, 852 (1970)
L.W. Shacklette, G.G. Miller, C.C. Han, R.L. Elsenbaumer, PCT Int. Appl., WO 93 024,555, 9 Dec 1993, Appl. 3 June 1992, to Allied Signal Inc.
S.D. Sharma, B.Tech. Dissertation, University of Calcutta, Calcutta, 1988
Y.N. Sharma, J.S. Anand, A.K. Kulshreshtha, S.F. Xavier, S. Chakrapani, Int. J. Polym. Mater. **12**, 165 (1988b)
K. Shimamura, Y. Suzuki, Jpn. Patent 0,324,153, 1 Feb 1991, to Asahi Chemical Co. Ltd.
B.Y. Shin, I.J. Chung, Polym. J. **21**, 851 (1989)
C.J. Shirtliffe, *Heat Transmission Measurements in Thermal Insulation* (ASTM STP 544, Am. Soc. Testing Mats., Philadelphia, 1974)
Y. Shono, Y. Yoshida, K. Yamamoto, in *Proceedings of the Japan Society of Civil Engineers* (Tokyo, 1994), pp. 81–89
E.K. Sichel, M.F. Rubner, J. Polym. Sci. Phys. **23**, 1616–1629 (1985)
A. Siegmann, A. Dagan, S. Kenig, Polymer **26**, 1325 (1985)
A. Sikora, F.E. Karasz, Macromolecules **26**, 3438 (1993)
R.E. Skochdopole, C.R. Finch, J. Marshall, Polym. Eng. Sci. **27**, 627 (1987)
P.E. Slade Jr., L.T. Jenkins (eds.), *Techniques and Methods of Polymer Evaluation*. Thermal Analysis, vol. 1 (Dekker, New York, 1966)
P.K. So, L.J. Broutman, Polym. Eng. Sci. **26**, 1173 (1986)
J. Soares, R. Abbott, J. Kim, J. Polym. Sci. Polym. Phys. **38**, 1267 (2000)
K.C. Šolc (ed.), *Polymer Compatibility and Incompatibility* (Harwood Academic, New York, 1982)
L.C. Souder, B.E. Larson, U.S. Patent 3,251,904, 1966
A.R. Sousa, E.S. Arau'jo, A.L. Carvalho, M.S. Rabello, J.R. White, Polym. Degrad. Stab. **92**, 1465 (2007)
W.M. Speri, G.R. Patrick, Polym. Eng. Sci. **15**, 668 (1975)
F.C. Stehling, T. Huff, C.S. Speed, G. Wissler, J. Appl. Polym. Sci. **26**, 2693 (1981)
T. Sterzynski, M. Lambla, H. Crozier, M. Thomas, Adv. Polym. Technol. **3**, 25 (1994)
S. Strella, P.F. Erhardt, J. Appl. Polym. Sci. **13**, 1373 (1969)
H. Suarez, J.W. Barlow, D.R. Paul, J. Appl. Polym. Sci. **29**, 3253 (1984)
A.R. Subrahmanyam, V. Geetha, A. Kumar, A. Alakanandana, J. Siva Kumar, Int. J. Mater. Sci. **2**, 27 (2012)
P.M. Subramanian, Polym. Eng. Sci. **25**, 483 (1985)
P.M. Subramanian, Polym. Eng. Sci. **27**, 663 (1987)
P.M. Subramanian, U.S. Patent 4,410,482, 1983
P.M. Subramanian, U.S. Patent 4,444,817, 1984
A.M. Sukhadia, D. Done, D.G. Baird, Polym. Eng. Sci. **30**, 519 (1990)

H. Swei, B. Crist, S.H. Carr, Polymer **32**, 1140 (1991)
T. Kawaguchi, H. Nishimura, F. Miwa, K. Abe, T. Kuriyama, I. Narisawa, *Environmental Stress Cracking (ESC) of ABS*, Web Page, 6/21/2002
M.T. Takemori, Ann. Rev. Mater. Sci. **14**, 171 (1984)
M.T. Takemori, I. Narisawa, in *Advances in Fracture Research*, ed. by K. Salama (Pergamon Press, New York, 1989)
T. Tanaka, T. Masuda, T. Yoshimura, S. Noguchi, R&D, Research Develop (Kobe Steel, Ltd) **40**, 53 (1990)
M. Tasdemir, M. Topsakaloglu, J. Appl. Polym. Sci. **104**, 3895 (2007)
R. Tchoudakov, M. Narkis, A. Siegmann, Polym. Eng. Sci. **44**, 528 (2004)
G. ten Brinke, R.E. Karsz, W.J. MacKnight, Macromolecules **16**, 1827 (1983)
T. Theuer, A. Cornee, J. Krey, K. Friedrich, in *Proceedings, 7th International Conference on Deformation, Yield and Fracture of Polymers* (The Plastics and Rubber Institute, London, 1988)
A.G. Thomas, J. Appl. Polym. Sci. **3**, 168 (1960)
T. Tikuisis, P. Lam, M. Cossar, *High Pressure Oxidative Induction Time Analysis By Differential Scanning Calorimetry* (TA Instruments Inc., TA085, 1985)
G.A.V. Timoteo, G.J.M. Fechine, M.S. Rabello, Stress cracking and photodegradation behavior of polycarbonate. Polym. Eng. Sci. **48**, 2003–2010 (2008)
S.C. Tjong, S.P. Bao, J. Polym. Sci. Part B. Polym. Phys. **43**, 585 (2005)
T. Tokairin, T. Kitada, Environ. Monit. Assess. **105**, 121 (2005)
J.S. Trent, J.I. Scheinbeim, P.R. Couchman, J. Polym. Sci. Polym. Lett. Ed. **19**, 315 (1981)
J.S. Trent, J.I. Scheinbeim, P.R. Couchman, Macromolecules **16**, 589 (1983)
S.K. Tripathy, M.F. Rubner, Am. Chem. Soc. Symp. Ser. **242**, 38 (1984)
J. Troitzsch, *International Plastics Flammability Handbook* (Hanser, Münich, 1983)
M. Tsuburaya, H. Saito, Polymer **45**, 1027 (2004)
E.A. Turi, *Thermal Characterization of Polymeric Materials* (Academic, New York, 1981)
S. Turner, *Mechanical Testing of Plastics* (The Butterworth Group, London, 1973). ASTM D 638-95 *Standard Test Method for Tensile Properties of Plastics* (Philadelphia, 1996)
I.C. Um, Y.H. Park, Fib. Polym. **8**, 6 (2007)
L.A. Utracki, *Polymer Alloys and Blends, Thermodynamics and Rheology* (Hanser, Munich, 1989)
L.A. Utracki (ed.), *Encyclopaedic Dictionary of Commercial Polymer Blends* (ChemTec Pub, Toronto, 1994)
L.A. Utracki, in *Polypropylene: Structure, Blends, and Composites*, ed. by J. Karger-Kocsis (Chapman & Hall, London, 1995)
L.A. Utracki, *Commercial Polymer Blends* (Chapman & Hall, London, 1998)
M. Vähä-Nissi, T. Hjelt, M. Jokio, R. Kokkonen, J. Kukkonen, A. Mikkelson, Packag. Technol. 4464 Sci. 425 (2008)
B. van Eerdebbrugh, L.S. Taylor, Pharm. Res. **29**, 2754 (2012)
D.W. Van Krevelen, Polymer **16**, 615 (1975)
H.L. Vandersall, J. Fire Flammability **2**, 97 (1971)
J. Varga, J. Mater. Sci. **27**, 2557 (1992)
P.I. Vincent, *Impact Tests and Service Performance of Thermoplastics* (Plastics Institute, London, 1971)
Vitruvius, *The Ten Books on Architecture* (M.H. Morgann, Tr.) (Dover, New York, 1960). (Original Pub., Howard University Press, 1914)
D.J. Walsh, S. Rostami, *Advances in Polymer Science*, vol. 72 (Springer, Berlin, 1985)
Wang, Polym.Test. **31**, 39 (2012)
J. Wang, S. Velankar, Rheol. Acta **45**, 741 (2006)
L. Wang, W. Ma, R.A. Gross, S.P. McCarthy, Polym. Degr. Stab. **57**, 161 (1998)
J. Wang, M.K. Cheung, Y. Mi, Polymer **42**, 2077 (2001)
H.T. Wang, B.R. Pan, Q.G. Du, Y.Q. Li, Polym. Test. **22**, 125 (2003)
H-H. Wang, W-C. Lee, D-T. Su, W-J. Cheng, B-Y. Lin, *Annual Technical Conference-Society of Plastics Engineers*, 53rd **2**, 2105 (1995); Pub., Society of Plastics Engineers

I.M. Ward, *Mechanical Properties of Solid Polymers*, 2nd edn. (Wiley, New York, 1983)
G.R. Watts, P.A. Morgan, Noise Vib Worldw **49**, 18 (1997)
G. Weber, J. Schoeps, Angew. Makromol. Chemie **136**, 45 (1985)
Y. Wei, R. Li, C. Zhou, Polymer **52**, 2693 (2011)
R.A. Weiss, N. Chung, A. Kohli, Polym. Eng. Sci. **29**, 573 (1989)
W.W. Werring, Proc. ASTM II **26**, 634 (1926)
B. Wessling, H. Volk, Synth. Met. **18**, 671 (1987)
B.S. Westerlind, J.A. Carlsson, Y.M. Andersson, J. Mater. Sci. **26**, 2630 (1991)
J.G. Williams, Trans. Plast. Inst. **35**, 505 (1964)
J.G. Williams, *Fracture Mechanics of Polymers* (Ellis Horwood, Chichester, 1984)
J.G. Williams, H. Ford, J. Mech. Eng. Sci. **6**, 405 (1964)
J.M. Willis, B.D. Favis, Polym. Eng. Sci. **28**, 1416 (1988)
L. Wong, Polym. Test. **21**, 691 (2002)
W.A. Woshinis, D.C. Wright, Advan. Mat. Proc. **12**, 39 (1994)
D. Wright, *Environmental Stress Cracking of Plastics* (RAPRA Technology, Shawbury, 1996)
S. Wu, Polym. Eng. Sci. **27**, 335 (1987)
J. Wu, S. Chen, J. Xian Jiao Tong Univ. **17**, 79 (1983)
J. Wu, Y.W. Mai, Polym. Eng. Sci. **36**, 2275 (1996)
W.B. Wu, W.Y. Chiu, W.B. Liauwu, J. Appl. Polym. Sci. **64**, 411 (1997)
B. Wunderlich, *Thermal Analysis*, (Academic, New York, 1990)
S.F. Xavier, in *Two Phase Polymer Systems*, ed. by L.A. Utracki (Hanser Pub, Munich, 1991)
S.F. Xavier, Y.N. Sharma, Polym. Comp. **7**, 42 (1986)
S.F. Xavier, *Thermal Analysis in Polymer Science* presented in 'Work-Shop on Thermal Analysis' (Vadodara, 2002)
S.F. Xavier, V.N.S. Pendyala, I.S. Bhardwaj, in *Encyclopaedic Dictionary of Commercial Polymer Blends*, ed. by L.A. Utracki (ChemTec Publishing, Toronto, 1994)
S.F. Xavier, V.N.S. Pendyala, *Impermeable Polyolefin Blends for Storing Diesel, other Organic Liquids and an Improved Process for the Preparation Thereof* (RIL Technical Report, Vadodara, 2008)
S.F. Xavier, *RIL Management Information Report, Key Result Area* (India, 2008)
L. Xue et al., Progr. Polym. Sci. **37**, 564 (2012)
M. Yamaguchi, K. Masuzava, *Transparent Polymer Blends Composed of Cellulose Acetate Propionate and Poly(epichlorohydrin)*, ResearchGate, 2013, (2013researchgate.net)
K. Yamaoka, T. Harada, K. Tomari, S. Tonogai, S. Nagai, *The Fifth Annual Meeting, PPS*, April 11–14, Kyoto, Japan (1989)
O.F. Yap, W.W. Mai, B. Cotterell, J. Mat. Sci. **18**, 657 (1983)
F. Yazaki, A. Kohara, R. Yosomiya, Polym. Eng. Sci. **34**, 1129 (1994)
A.F. Yee, R.A. Pearson, J. Mater. Sci. **21**, 2462–2475 (1986)
J.T. Yeh, C.C. Fanchiang, M.F. Cho, Poly. Bull. **35**, 371 (1995)
H. Yordanov, L. Minkova, Europ. Polym. J. **39**, 951 (2003)
R.J. Young, in *Comprehensive Polymer Science*, ed. by C. Colin Booth, C. Price, vol. 2 (Pergamon Press, New York, 1988)
S.H.P. Yu, European Patent Applications 282,985, 21 Sept 1988;Jpn. Patent 63 314,261, 22 Dec 1988; U.S. Appl. 20 Mar 1987, to B.F. Goodrich Co.
M. Zanetti, G. Camino, D. Canavese, A.B.. Morgan, F.J. Lamelas, C.A. Wilkie, Chem. Mater. **14**, 189 (2002)
Zeus Industrial Products, Inc., Technical White Paper, *Low Temperature Properties of Polymers*, 2005, http://www.zeusinc.com
J. Zhang, H. Zhang, Y. Yang, J. Appl. Polym. Sci. **72**, 59 (1999)
L. Zhang, C. Li, R. Huang, J. Polym. Sci. Part B. Polym. Phys. **42**, 1656 (2004)
Y. Zhang, L. Wang, Y. Gao, J. Chen, X. Shi, Med. Eng. Phys. **29**, 699 (2007)
W. Zhang, Z. Gui, C. Lu, S. Cheng, D. Cai, Y. Gao, Mater. Lett. **92**, 68 (2013)
Z. Zhao, H. Ma, Suliao **34**, 57–100 (2005)

Y. Zhao, A.S. Vaughan, S.J. Sutton, S.G. Swingler, Polymer **42**, l6599 (2001)
X.E. Zhao, D.L. Dotson, U.S. Patent 6,465,551 to Milliken & Co, 2002
S. Zheng, K. Nie, Q. Guo, Thermochim. Acta **419**, 267 (2004)
Z. Zhong, Q. Guo, Polymer **39**, 517 (1998)
H. Zhou, B. Li, G.S. Huang, Mater. Lett. **60**, 3451 (2006)
P. Zhuang, T. Kyu, J.L. White, Polym. Eng. Sci. **28**, 1095 (1988)
R. Zong, Z. Wang, N. Liu, Y. Hu, G. Liao, J. Appl. Polym. Sci. **98**, 1172 (2005)

Sources of Additional Information

International Patent Office Sites
European Patent Office: http://ep.espacenet.com/
Indian Patent Office: al_2007.htm: http://www.patentoffice.nic.in/ipr/patent/journal_archieve/journal_2007/patent_journal
Japanese Patent Office: http://ipdl.inpit.go.jp/homepg_e.ipdl (Select PAJ – Patent Abstract of Japan)
USPTO Patent Office: http://www.uspto.gov/ptft/index.html
World Intellectual Property Office (WIPO): http://www.wipo.int/pctdb/en
Free Online Patent Databases
Freepatentsonline: http://www.freepatentsonline.com
Freshpatents: http://www.freshpatents.com
Google Patent Search: http://www.google.com/patents
Patentstorm: http://www.patentstorm.us/, www.patentstorm.us/
Free Open Literature Databases
http://scholar.google.com
www.alltheweb.com
www.research.com
www.vivisimo.com